Understanding Proton Shuttling with Pendent Bases in Catalyzing the Interconversion of Dioxygen and Water

Tristan Andrew Tronic

A dissertation
submitted in partial fulfillment of
the requirements for the degree of

Doctor of Philosophy

University of Washington
2012

Reading committee:
James M. Mayer, Chair
Dennis M. Heinekey
Julia A. Kovacs

Program Authorized to Offer Degree:
Department of Chemistry

University of Washington

Abstract

Understanding Proton Shuttling with Pendent Bases in Catalyzing the Interconversion of Dioxygen and Water

Tristan Andrew Tronic

Chair of the Supervisory Committee:
Professor James M. Mayer
Department of Chemistry

The electrocatalyzed interconversion of dioxygen and water is critical to the development of non-carbon based renewable fuels, because these are half-reactions in hydrogen fuel cells/water electrolyzers. These reactions require the coordinated transfer of four protons and electrons. Transition metal complexes are known to catalyze these reactions by facilitating electron transfer, but methods to facilitate proton transfer have not been explored. In this work, model systems with pendent bases are studied, in order to understand the ability of pendent bases to improve catalyst efficiency by acting as proton shuttles. In Chapters 2 and 3, the oxidation of phenols with pendent pyridines is explored. These molecules are models for the oxidation of Tyr 161 in photosystem II, the protein responsible for biological catalytic water oxidation. Oxidation of these phenols is coupled to concerted transfer of the phenolic proton to the pendent pyridine. In Chapter 1, the basicity of the pendent pyridine is tuned synthetically to determine the critical parameters in predicting the kinetics of oxidation. The contribution of the driving force for oxidation, determined by the basicity of the pendent pyridine, is found to far outweigh other parameters in determining oxidation rates. In Chapter 2, a model system is synthesized with an alcohol positioned between the phenol and pyridine in an effort to observe oxidation-coupled proton transfer through a hydrogen-bonding chain. Chapters

4-6 are concerned with developing transition metal complexes with pendent bases in the second coordination sphere of the metal and studying how these bases affect catalysis of oxygen reduction. In Chapter 4, cobalt complexes with tetraazamacrocyclic ligands with pendent bases are synthesized. These ligands are found to be difficult to synthesize and insufficiently rigid, failing to restrict the pendent bases from binding to the cobalt. In Chapters 5 and 6, ruthenium complexes with more rigid diazadiphosphine ligands are synthesized. These complexes are found by X-ray diffraction and NMR spectroscopy to bind dioxygen, and their pendent amines direct protons in a hydrogen bonding interaction towards the dioxygen. Electrochemical studies indicate that the pendent bases facilitate reduction, but these complexes do not catalyze four-electron reduction to water.

TABLE OF CONTENTS

LIST OF FIGURES

LIST OF TABLES

ACKNOWLEDGMENTS

I would first like to gratefully acknowledge my advisor, Jim Mayer, without whom none of this work would be possible. Jim has been an excellent teacher, and like all great teachers, has known when to guide me and when to let me make mistakes on my own. He has challenged me intellectually, and always treated me as a respected colleague. I am privileged to count him as a friend. In short, Jim is rad.

Secondly, I must acknowledge the numerous students and post-docs who have contributed to this work and to my training. Todd Markle, who did much of the preliminary work for chapters 1 and 2, patiently trained me in organic synthesis and electronic structure calculations, despite my having no prior experience in these fields, such that I have occasionally been the group expert on these subjects. Attaining Todd's quiet but razor-sharp intellect has been my goal as a grad student. I credit Todd with giving me the skills to be chemist, and I am forever indebted. I would also like to acknowledge Virginia Manner, Chris Waidmann, and Lisa Park-Gehrke. They have been like a family to me while I've been so far from home. Without their friendship and guidance, getting to the point of writing this thesis surely would not have been possible. Jeff Warren has been a great friend and scientific partner. He has reminded me continuously that science can and probably should be fun. Despite Jeff's many jokes, especially his "old HAT" joke, he is an intellectual force who has shaped my understanding of PCET, and it has been the great honor of my career to have worked with him on his review of PCET thermodynamics. Rebecca Hayoun has been a great friend, supporting me at the times I have needed the most help, and I have valued her friendship more than she probably knows. I have had the pleasure of sitting uncomfortably close to Mauricio Catteneo and Adam Tenderholt, both of whom have contributed intellectually to this work. They have been kind enough to share their wisdom about chemistry and life whenever I have swiveled around in my chair, for which I am deeply grateful. Colin Carver has helped me to take on a completely new area of research within our lab, a challenge I could not have faced on my own. Finally, Brian Cochran has assisted in attempting to tackle the challenges presented in Chapter 2.

I would next like to acknowledge current members of the Mayer lab for their contributions. Johanna Blacqueire has been my partner in oxygen reduction, and any success I have achieved in this regard is thanks to her. She has been a great friend, and has helped me through some of my biggest challenges in science and life with a profound kindness and patience. Carolyn Valdez has helped me to think clearly about difficult problems, and has provided me with the baked goods my brain needs to tackle those problems. I have been lucky to have been able to sit next to her. David Lao has assisted me in maintaining the lab, and I am grateful for his calm, careful approach to science and ability to keep myself and the group focused. Tom Porter has been great to talk science with, and has challenged me to think of new approaches to problems. Alex Miller has provided me with numerous invaluably helpful suggestions along the way, thanks to his combination of professorial knowledge of the literature and grad student practicality. He has been a good friend, and I have been lucky to have him in our lab. I am thankful for the assistance of Shoshanna Barnett, Jessica Wittman, and Miles Braten, who have provided me with help, scientific and otherwise, along the way. Joel Schrauben and Caroline Saouma have shared their wisdom with myself and the lab, albeit with very different styles, and we are better for it. Caroline has spent a significant amount of time discussing the finer details of my work with me, and has greatly improved the quality of my work. Sophia Tran and Ben Leipzig (honorary group members) have also helped me along the way. I am grateful for their friendship, and am excited for the future of UW chemistry.

I would like to thank my collaborators at Pacific Northwest National Lab, who have contributed significantly to this work. In particular, Mary Rakowski DuBois is responsible for performing the preliminary experiments on which Chapters 4 and 5 are based, and kindly allowed me to work with her in this area. Dan DuBois and Morris Bullock have provided valuable guidance and insight during my career, and have been incredibly invested in my success even though I am not their student. John Roberts, Michael Mock, Molly O'Hagan, and Jenny Yang have assisted me experimentally, trained me, and have been great to work with.

I could not have completed this work without the assistance of the excellent staff of the UW Chemistry Department. In particular, I need to thank Werner Kaminsky and

Michael Coggins for their tireless work obtaining X-ray structures, and Rajan Paranji and Paul Miller for their NMR assistance. Additionally, Michael Coggins has been an ally in understanding oxygen chemistry, and I have learned a tremendous amount from discussions with him.

I wish to acknowledge my thesis committee, Michael Heinekey, Julie Kovacs, Munira Khalil, Brandi Cossairt, and James Pfaendtner for the time they have committed to helping me and for their invaluable guidance over the years.

Finally, I need to thank my wife and family. Without their love and support none of this would have been possible. This document is the product of the love and support of my parents Debbie and Sid, including weekends spent at the Maryland Science Center, non-fiction bedtime stories about space travel, letting me take the family computer apart in high school, college tuition, and so much more. I hope that it is a source of pride for you. Trying to capture what my wife Elaine has meant to me in a few sentences has been the hardest part of writing this document. Her love is the best thing in my life, and I am forever thankful for it.

Chapter 1

Introduction

1.1 Importance of Oxygen Reduction/Water Oxidation

The efficient electrocatalytic reduction of dioxygen (O_2) to water (H_2O) (equation 1.1) and the oxidation of water to dioxygen (the reverse of equation 1.1) are considered among the current "grand challenges" of science.[1] These reactions are critical to the development of renewable solar fuels. Because of abundance and benign environmental impact of oxygen and water, oxygen reduction to water is the best candidate for the cathodic half-reaction in mobile fuel cell applications, particular hydrogen PEM fuel cells. [2,3] For the same reasons, water is an ideal source of protons for solar driven production of fuels such as hydrogen from proton reduction or methanol from proton coupled reduction of CO_2.[1,4] Generating protons and reducing equivalents from water at one half of a photo or electrochemical cell requires oxidation of water to O_2 at the other half-cell electrode.

$$O_2 + 4e^- + 4H^+ \rightarrow 2H_2O \qquad (1.1)$$

1.2 Challenges of Oxygen Reduction/Water Oxidation

Controlled, efficient catalytic interconversion of dioxygen and water presents several substantial challenges. The overall thermodynamic standard potential of this half-reaction is +1.23 V vs NHE.[5] This high potential is attractive for fuel cell applications because higher potentials allow for greater power output of the fuel cell, but many molecules that might be used in electrode materials are not stable at this high potential. Additionally, dioxygen/water interconversion requires the coordinated movement of four electrons as well as four protons. These eight particles cannot move in a single step. Instead, the reaction potentially proceeds through a series of high energy intermediates (Figure 1.1),[6] necessitating the use of a catalyst that can stabilize these intermediates and flatten the potential energy surface. A partial reduction/oxidation that releases one of these intermediates can be quite detrimental to the fuel production/consumption process. One significant detriment is that energy is wasted. For instance, partial two-electron

reduction of dioxygen to hydrogen peroxide has a standard potential of +0.70 V vs. NHE,[5] meaning that a hydrogen fuel cell that reduced oxygen to hydrogen peroxide at the cathode would be wasting almost half of the energy of the hydrogen. The other major detriment of partial conversion is the destruction of the molecules of the fuel cell/photochemical cell by reactive intermediates. Both catalyst materials as well as other components, such as proton conducting membranes, can be irreversibly oxidized by these intermediates. In particular, hydroxyl radical ($HO^{\bullet}$) from the one electron oxidation of water and hydroxyl radical ($HOO^{\bullet}$) from the one electron reduction of oxygen at low pH are potent hydrogen atom abstractors from organic molecules, with hydrogen atom bond-dissociation free energies (BDFE) of +123 kcal/mol and +91 kcal/mol in water, respectively.[6] These BDFEs are high, with hydroperoxyl capable of H-atom abstraction from weaker C-H bonds such as allylic C-H bonds, and hydroxyl capable of H-atom abstraction from essentially all aliphatic C-H bonds,[6] and so stabilization of these species is absolutely critical.

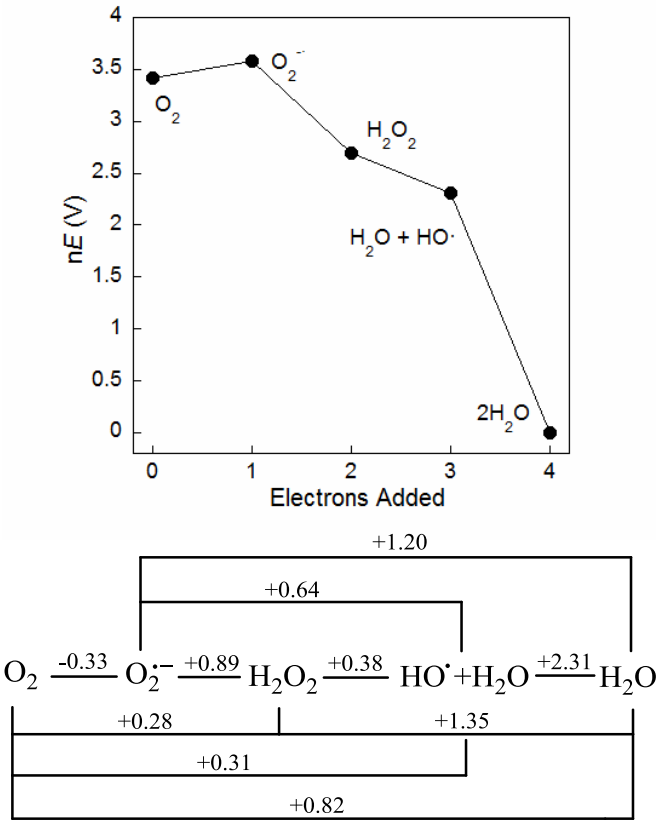

Figure 1.1: Frost and Latimer diagram for O_2/H_2O in water at pH 7 from Ref. 6.

1.3 Catalysts for Oxygen Reduction

A number of transition metal catalysts for oxygen reduction have been explored. The state of the art technology for this reaction used in fuel cells is platinum particles on a carbon support.[7,8] Platinum on carbon has many characteristics of an effective catalyst. It is not degraded by reactive intermediates, produces less than 1% H_2O_2, and under typical fuel cell conditions operates with a moderate overpotential of 500-600 mV.[7] However, there are several drawbacks to the use of platinum. Platinum is a rare and expensive metal, prohibiting its widespread deployment. The estimated cost of the platinum required for a transportation fuel cell is $5000-$10000, with the majority of the platinum loading on the O_2 side to make up for the much slower kinetics of O_2 reduction relative to H_2 oxidation.[7] The platinum deposited on carbon also slowly dissolves under fuel cell operating conditions.[3] Additionally, the mechanism for oxygen reduction at platinum is still unknown,[7,9,10] making it difficult to improve the efficiency of this system. Other heterogeneous catalysts made of iron/cobalt/copper, carbon, and nitrogen have recently emerged as low-cost, earth abundant alternatives to platinum.[11-13] However, these technologies suffer from high overpotentials, relatively low stabilities, and modest selectivity for four-electron reduction. Like platinum, the mechanism of reduction with these catalysts remains unknown, making it difficult to improve on these systems.[14,15]

Because of the challenges of characterizing and improving heterogeneous systems, there has been considerable focus on developing molecular, homogeneous catalysts for O_2 reduction. Many of these draw their inspiration from the natural oxidase and oxygenase enzymes that catalyze O_2 reduction to water and which utilize earth-abundant iron and copper in their active sites,[16] such as cytochrome *c* oxidase,[17] cytochrome P450 (which generates one equivalent of water per O_2 and an oxidizing ferryl heme),[18] and laccase.[19] The heme-iron active site of enzymes like cytochrome *c* oxidase and cytochrome P450 has served as the inspiration for a number of iron and cobalt porphyrinoid molecular catalysts,[20-23] and laccase inspired copper catalysts have also been demonstrated.[24-27] These molecular catalysts have revealed many of the important factors in controlling electron delivery in oxygen reduction,[28] and in some cases product selectivity of essentially 100% H_2O has been achieved under electrocatalytic

conditions.[26] Still, these catalysts suffer from very high overpotentials and low turn-over frequencies that make them impractical.

1.4 Oxygen Reduction Catalysts with Positioned Proton Relays

While considerable attention has been paid to electron delivery during oxygen reduction, only recently has an effort been made to control the delivery of protons during oxygen reduction catalysis. However, control of proton delivery may be as or more important than control of electron delivery in determining catalyst stability and overpotential as well as product selectivity. There are numerous biological examples of enzymes with hydrogen bonding or proton donating amino acids in the second coordination sphere of the active site metal that play a key role in O_2 binding or reduction. These amino acids stabilize reactive intermediates, preventing "uncoupling", or the release of partially reduced, reactive oxygen species.[17,18,29-33] Many of the steps in O_2 reduction must be proton-coupled electron transfer (PCET) reactions to avoid high energy charge separated species. PCET reaction kinetics are quite sensitive to the basicity of the proton donor and acceptor,[6,34] and are also sensitive to the proton transfer coordinate,[35] in part because of the much steeper distance dependence for proton transfer versus electron transfer.[36] Controlling these factors could have a significant effect on catalyst overpotential, though to date this has not been clearly demonstrated in a synthetic system. In the related proton-coupled redox process of reducing protons to dihydrogen, it has been extensively demonstrated that positioned amine bases in the second coordination sphere of a transition metal catalyst can act as proton shuttles or relays, lowering barriers to proton delivery and stabilizing intermediates, dramatically improving catalyst overpotential and turn-over frequency.[37-39]

Recent work from the DuBois group has shown that by adding amines to the second coordination sphere of a nickel(II) bis-diphosphine complex, they are able to observe electrocatalytic O_2 reduction, while without these amines catalytic reduction is not observed.[40] The effect of pendent amines in this case was dramatic, but even with the amines the catalyst operated at an overpotential of greater than 1 V, and was unstable to oxidation of the phosphine ligands. Unfortunately, no information about the catalytic mechanism could be determined for this system to learn the role of the pendent amines.

One of many possibilities is that this catalyst functions as an O_2 hydrogenation catalyst, first forming a nickel hydride, followed by O_2 insertion into the Ni-H bond. Similar chemistry has been proposed for the formation of water by the reaction of O_2 with a Noyori-type hydrogenation catalyst.[41]

Nocera and Mayer have each demonstrated dramatic improvements in selectivity for H_2O over H_2O_2 by incorporating pendent carboxylic acids into porphyrinoid ligand frameworks. Nocera and coworkers have synthesized a series of "hangman" porphyrins[42] and corroles[43] that position a single carboxylic acid over the metal center through a xanthene linker. They have shown that by positioning this carboxylic acid in a position to hydrogen bond to the distal O atom of a bound oxygen, they can increase selectivity for H_2O production from 48% to 71% in electronically similar complexes.[42] Mayer and coworkers have built on this concept by demonstrating very high selectivity for H_2O production by including four positioned carboxylic acids.[44] They showed that iron(III) (*meso*-tetra(2-carboxyphenyl))porphine could reduce O_2 without producing any detectable H_2O_2, while the 4-carboxylphenyl derivative of this complex, with its carboxylates positioned away from the metal, produced ~9% H_2O_2. These systems have been quite successful at demonstrating the dramatic effect that positioned proton shuttles can have on O_2 reduction, but many questions remain. None of the previous studies of electrocatalysts with proton shuttles have identified the catalytic pathway or any of the reductive intermediates, so the role of the proton shuttles can only be speculated on. In Chapters 4-6 of this work, new complexes of cobalt and ruthenium are synthesized with pendent bases in an effort to learn more about the role of pendent proton shuttles in oxygen reduction. In Chapter 4, cobalt cyclam (1,4,8,11-tetrazacyclotetradecane) derivatives are synthesized so that their oxygen binding and reductive electrochemistry may be compared to that of the parent complex, for which many intermediates have been identified via cyclic voltammetry and rotating ring disk voltammetry.[45,46] In Chapters 5 and 6, ruthenium complexes with diazadiphosphine ligands are synthesized and their reactivity compared to complexes with alkyl diphosphine ligands. The interaction of protons and O_2 in these complexes are observed by X-ray crystallography and NMR.

1.5 Catalysts for Water Oxidation

Catalytic water oxidation presents an additional challenge over oxygen reduction, because additional overpotentials for this process exceed +1.23 V vs RHE.[6] There are few materials that are not degraded at these very high potentials, and for the most part electrocatalysts have been limited to heterogeneous oxides of precious metals.[47-50] Recently oxides of non-precious metals cobalt,[51,52] nickel,[53,54] and manganese[55-57] have gained attention as possible lower cost alternatives, though their performance does not match that of the precious metals. In biology, water oxidation is accomplished with a tetramanganese oxide cluster called the Oxygen Evolving Complex (OEC), located within the Photosystem II protein,[58] at a modest overpotential of *ca.* 0.3 V.[59] A number of molecular homogeneous transition metal catalysts have been synthesized. Many of these catalysts consist of metal oxide or hydroxide clusters or dimers inspired by the OEC. There are numerous examples of manganese oxide clusters and dimers[60,61] and ruthenium dimers,[61,62] as well as a few recent examples of cobalt[63,64] clusters and dimers. Water oxidation has also been demonstrated for molecular complexes with only one metal site. A number of polypyridyl ruthenium complexes have been synthesized that are capable catalysts,[61,62,65,66] and recently there have been examples of single metal catalysts with earth-abundant iron, [67,68] cobalt,[69,70] and copper[71] centers. Still, overpotentials for known water oxidation catalysts for all but the platinum group metal oxides are quite high, and so there remains substantial room for improvement in these catalysts if practical electrocatalytic water oxidation is to be realized.

1.6 Water Oxidation Catalysts with Positioned Proton Relays

As with O_2 reduction, control of proton removal during water oxidation has received little focus. This is likely due in part to the fact that bases that might shuttle proton, by having energetically accessible pairs of electrons, are often readily oxidized under water oxidation conditions. However, there is some evidence that proton transfer is important in determining catalytic efficiency. Meyer has found that water oxidation with a molecular polypyridyl ruthenium complex is more efficient at a given pH as the concentration of phosphate or acetate buffer is increased.[72] Nocera has found that for a "hangman" cobalt corrole with a carboxylic acid positioned over the metal, water

oxidation with this complex occurs with an overpotential that is reduced by ~0.1 V versus the complex without the positioned carboxylic acid.[73] This effect is observed even from pH 1-14, so it is not clear in this case what role the pendent carboxylate is playing, though it is speculated that it serves to pre-order the water molecules around the metal center in some way. It should be noted that improving water oxidation catalysis through control of proton movement is not as straightforward as simply adding a basic site to the second coordination sphere of the metal. Thummel and Fujita have incorporated a 2-(pyrid-2′-yl)-1,8-naphthyridine ligand into Ru polypyridyl water oxidation catalyst in place of a 2,2'-bipyridine ligand, such that the naphthyridine positions a pyridine ring with the nitrogen adjacent to the water binding site of the complex.[74] This complex with a positioned pendent base does not act as a water oxidation catalyst, while the nearly identical isomer with the naphthyridyl nitrogen not positioned near the water site is an active catalyst for water oxidation.

The biological OEC is able to achieve water oxidation at modest overpotential without a platinum group metal, and more impressively, is able to accomplish this reaction within the organic framework of a protein.[58,75,76] For this reason, we have decided to study in detail proton motion in this species. One key reaction that we have focused on is the oxidation of Tyr161 by a P680 chlorophyll radical. This oxidation produces a tyrosyl radical which then oxidizes the tetramanganese cluster. Oxidation of the tyrosine is coupled to proton transfer from the phenolic oxygen to the hydrogen-bonded His190 residue. This proton transfer accelerates the rate of tyrosine oxidation,[77,78] and may play a role in shuttling protons out of the enzyme active site.[79] In Chapters 2 and 3, model systems of this tyrosine-histidine complex are synthesized, and their chemical and electrochemical oxidation is studied. These model compounds are 2,4-di-*t*-butyl phenols with pendent pyridines in the 6 position, and modifications are made to the proton transfer coordinate. In chapter 2, the pK_a of the pendent base is varied, which affects the proton transfer distance and strength of the hydrogen bonding interaction between the phenol and the base. In Chapter 3 an alcohol is inserted synthetically between the phenol and pyridine to test the effect of a proton transfer chain on phenol oxidation. The kinetics of the oxidation of these model phenols is studied in order to better understand the important parameters in determining the rates of these

PCET reactions. While these results will help further elucidate the catalytic mechanism of the OEC, they also build a general understanding of PCET reactions of this type, in which the proton and electron are transferred to different acceptors. This type of reaction is important in almost any scheme for O_2/H_2O interconversion in which electrons are moved to or from an electrode and protons move to or from the solution.

1.7 Notes to Chapter 1

(1) Eisenberg, R.; Gray, H. B. *Inorg. Chem.* **2008**, *47*, 1697.

(2) Winter, M.; Broad, R. J. *Chem. Rev.* **2004**, *104*, 4245.

(3) Borup, R.; Meyers, J.; Pivovar, B.; Kim, Y. S.; Mukundan, R.; Garland, N.; Myers, D.; Wilson, M.; Garzon, F.; Wood, D.; Zelenay, P.; More, K.; Stroh, K.; Zawodzinski, T.; Boncella, J.; McGrath, J. E.; Inaba, M.; Miyatake, K.; Hori, M.; Ota, K.; Ogumi, Z.; Miyata, S.; Nishikata, A.; Siroma, Z.; Uchimoto, Y.; Yasuda, K.; Kimijima, K.-I.; Iwishita, N. *Chem. Rev.* **2007**, 107, 3904.

(4) Kumar, B.; Llorente, M.; Froehlich, J.; Dang, T.; Sathrum, A.; Kubiak, C. P. *Annu. Rev. Phys. Chem.* **2012**, *63*, 541.

(5) Sawyer, D. T. *Oxygen Chemistry*. New York: Oxford University Press, 1991.

(6) Warren, J. J.; Tronic, T. A.; Mayer, J. M. *Chem. Rev.* **2010**, *110*, 6961.

(7) Gasteiger, H. A.; Kocha, S. S.; Sompalli, B.; Wagner, F. T. *App. Catal. B* **2005**, *56*, 9.

(8) Gewirth, A. A.; Thorum, M. S. *Inorg. Chem.* **2010**, *49*, 3557.

(9) Nørskov, J. K.; Rossmeisl, J.; Logadottir, A.; Lindqvist, L.; Kitchin, J. R.; Bligaard, T.; Jónsson, H. *J. Phys. Chem. B* **2004**, *108*, 17886.

(10) Song, C.; Zhang, J. in *PEM Fuel Cell Electrocatalysts and Catalyst Layers Fundamentals and Applications* Zhang, J. (ed.) **2008**, *12*, 110-114.

(11) Bezerra, C. W. B.; Zhang, L.; Lee, K. C.; Liu, H. S.; Marques, A. L. B.; Marques, E. P.; Wang, H. J.; Zhang, J. J. *Electrochim. Acta* **2008**, 53, 4937.

(12) Nallthambi, V.; Lee, J-W.; Kumaraguru, S. P.; Wu. G.; Popov, B. N. *J. Power Sources* **2008**, *183*, 34.

(13) Lefevre, M.; Proietti, E.; Jaouen, F.; Dodelet, J. P. *Science* **2009**, *324*, 71.

(14) Jain, M.; Chou, S-H.; Siedle, A. *J. Phys. Chem. B* **2006**, *110*, 4179.

(15) Thorum, M. S.; Hankett, J. M.; Gewirth, A. A. *J. Phys. Chem. Lett.* **2011**, *2*, 295.

(16) Cracknell, J. A.; Vincent, K. A.; Armstrong, F. A. *Chem. Rev.* **2008**, *108*, 2439.

(17) Kaila, V. R. I.; Verkhovsky, M. I.; Wikström, M. *Chem. Rev.* **2010**, *110*, 7062.

(18) Meunier, B.; de Visser, S. P.; Shaik, S. *Chem. Rev.* **2004**, *104*, 3947.

(19) Solomon, E. I.; Chen, P.; Metz. M.; Lee, S.-K.; Palmer, A. E. *Angew. Chem. Int. Ed.* **2001**, *40*, 4570.

(20) Collman, J. P.; Boulatov, R.; Sunderland, C. J.; Fu, L. *Chem. Rev.* **2004**, *104*, 561.

(21) Shigehara, K; Anson F. C. *J. Phys. Chem.* **1982**, *86*, 2776.

(22) Wisener, K.; Ohms, D.; Neumann, V.; Franke, R. *Mater. Chem. Phys.* **1989**, *22*, 457.

(23) Fukuzumi, S.; Okamoto, K.; Gros, C. P.; Guilard, R. *J. Am. Chem. Soc.* **2004**, *126*, 10441.

(24) McCrory, C. C. L.; Ottenwaelder, X.; Stack, T. D. P.; Chidsey, C. E. D. *J. Phys. Chem. A* **2007**, *111*, 12641.

(25) McCrory, C. C. L.; Devadoss, A.; Ottenwaelder, X.; Lowe, R. D.; Stack, T. D. P.; Chidsey, C. E. D. *J. Am. Chem. Soc.* **2011**, *133*, 3696.

(26) Ward, A. L.; Elbaz, L.; Kerr, J. B.; Arnold, J. *Inorg. Chem.* **2012**, *51*, 4694.

(27) Fukuzumi, S.; Kotani, H.; Lucas, H. R.; Doi, K.; Suenobu, T.; Peterson, R. L.; Karlin, K. D. *J. Am. Chem. Soc.* **2010**, *132*, 6874.

(28) Shi, Z.; Zhang, J. *J. Phys. Chem. C* **2007**, *111*, 7084.

(29) Rodriguez-Lopez, J. N.; Smith, A. T.; Thorneley, R. N. F. *J. Biol. Chem.* **1997,** *272*, 389.

(30) Proshlyakov, D. A.; Pressler, M. A.; Babcock, G. T. *Proc. Nat. Acad. Sci. USA* **1998,** *95*, 8020.

(31) Hamdane, D.; Zhang, H.; Hollenberg, P. *Photosynth. Res.* **2008,** *98*, 657.

(32) Song, W. J.; McCormick, M. S.; Behan, R. K.; Sazinsky, M. H.; Jiang, W.; Lin, J.; Krebs, C.; Lippard, S. J. *J. Am. Chem. Soc.* **2010,** *132*, 13582.

(33) Nagano, S.; Poulos, T. L. *J. Biol. Chem.* **2005**, *280*, 31659.

(34) Huynh, M. H. V.; Meyer, T. J. *Chem. Rev.* **2007**, *107*, 5004.

(35) Hammes-Schiffer, S.; Stuchebrukhov, A. A. *Chem. Rev.* **2010**, *110*, 6939.

(36) Krishtalik, L. I. *Biochim. Biophys. Acta.* **2000**, *1458*, 6.

(37) Small, Y. A.; DuBois, D. L.; Fujita, E.; Muckerman, J. T. *Energy Environ. Sci.* **2011**, *4*, 3008.

(38) DuBois, M. R.; DuBois, D. L. *Chem. Soc. Rev.* **2009**, *38*, 62.

(39) DuBois, D. L.; Bullock, R. M. *Eur. J. Inorg. Chem.* **2011**, *1017.*

(40) Yang, J. Y.; Bullock, R. M.; Dougherty, W. G.; Kassel, W. S.; Twamley, B.; DuBois, D. L.; Rakowski DuBois, M. *Dalton Trans.* **2010,** *39*, 3001.

(41) Heiden, Z. M.; Rauchfuss, T. B. *J. Am. Chem. Soc.* **2007**, *129*, 14303.

(42) McGuire, R.; Dogutan, D. K.; Teets, T. S.; Suntivich, J.; Shao-Horn, Y.; Nocera, D. G. *Chem. Sci.* **2010**, *1*, 411.

(43) Dogutan, D. K.; Stoian, S. A.; McGuire, R.; Schwalbe, M.; Teets, T. S.; Nocera, D. G. *J. Am. Chem. Soc.* **2011**, *133*, 131.

(44) Carver, C. T.; Matson, B. D.; Mayer, J. M. *J. Am. Chem. Soc.* **2012**, *134*, 5444.

(45) Geiger, T.; Anson, F. C. *Inorg. Chem.* **1981**, *103*, 7489.

(46) Kang, C.; Anson, F. C. *Inorg. Chem.* **1995**, *34*, 2771.

(47) Song, S.; Zhang, H.; Ma, X.; Shao, Z.; Baker, R. T.; Yi, B. *Int. J. Hydrogen Energy* **2008**, *33*, 4955.

(48) Nakagawa, T.; Bjorge, N. S.; Murray, R. W. *J. Am. Chem. Soc.* **2009**, *131*, 15578.

(49) Chen, X.; Chen, G.; Yue, P. L. *J. Phys. Chem. B*, 2001, **105**, 4623.

(50) Blakemore, J. D.; Schley, N. D.; Olack, G. W.; Incarvito, C. D.; Brudvig, G. W.; Crabtree, R. H. *Chem. Sci.* **2011**, *2*, 94.

(51) Kanan, M. W.; Nocera, D. G. *Science* **2008**, *321*, 1072.

(52) Esswein, A. J.; McMurdo, M. J.; Ross, P. N.; Bell, A. T.; Tilley, T. D. *J. Phys. Chem. C* **2009**, *113*, 15068.

(53) Wang, X.; Luo, H.; Yang, H.; Sebastian, P. J.; Gamboa, S. A. *Int. J. Hydrogen Energy* **2004**, *29*, 967.

(54) Dincă, M.; Surendranath, Y.; Nocera, D. G. *Proc. Nat. Acad. Sci. USA* **2010**, *107*, 10337.

(55) Morita, M.; Iwakura, C.; Tamura, H. *Electrochim. Acta* **1979**, *24*, 357.

(56) Najafpour, M. M.; Ehrenberg, T.; Wiechen, M.; Kurz, P. *Angew. Chem. Int. Ed.* **2010**, *49*, 2233.

(57) Gorlin, Y.; Jaramillo, T. F. *J. Am. Chem. Soc.* **2010**, *132*, 13612.

(58) McEvoy, J. P.; Brudvig, G. W. *Chem. Rev.* **2006**, *106*, 4455.

(59) Dau, H.; Zaharieva, I. *Acc. Chem. Res.* **2009**, *42*, 1861.

(60) Cady, C. W.; Crabtree, R. H.; Brudvig, G. W. *Coord. Chem. Rev.* **2008**, *252*, 444.

(61) Liu, X.; Wang, F. *Coord. Chem. Rev.* **2012**, *256*, 1115.

(62) Concepcion, J. J.; Jurss, J. W.; Brennaman, M. K.; Hoertz, P. G.; Patrocinio, A. O. T.; Iha, N. Y. M.; Templeton, J. L.; Meyer, T. J. *Acc. Chem. Res.* **2009**, *42*, 1954.

(63) Symes, M. D.; Surendranath, Y.; Lutterman, D. A.; Nocera, D. G. *J. Am. Chem. Soc.* **2011**, *133*, 5174.

(64) McCool, N. S.; Robinson, D. M.; Sheats, J. E.; Dismukes, G. C. *J. Am. Chem. Soc.* **2011**, *133*, 11446.

(65) Duan, L.; Bozoglian, F.; Mandal, S.; Stewart, B.; Privolov, T.; Llobet, A.; Sun, L. *Nature Chem.* **2012**, *4*, 418.

(66) Concepcion, J. J.; Jurss, J. W.; Templeton, J. L.; Meyer, T. J. *J. Am. Chem. Soc.* **2008**, *130*, 16462.

(67) Ellis, W. C.; McDaniel, N. D.; Bernhard, S.; Collins, T. J. *J. Am. Chem. Soc.* **2010**, *132*, 1077

(68) Fillol, J. L.; Codolà, Z.; Garcia-Bosch, I.; Gómez, L.; Pla, J. J.; Costas, M. *Nature Chem.* **2011**, *3*, 807.

(69) Dogutan, D. K.; McGuire, R.; Nocera, D. G. *J. Am. Chem. Soc.* **2011**, *133*, 9178.

(70) Wasylenko, D. J.; Palmer, R. D.; Schott, E.; Berlinguette, C. P. *Chem. Commun.* **2012**, *48*, 2107.

(71) Barnett, S. M.; Goldberg, K. I.; Mayer, J. M. *Nature Chem.* DOI: 10.1038/NCHEM.1350

(72) Chen, Z.; Concepcion, J. J.; Hu, X.; Yang, W.; Hoertz, P. G.; Meyer, T. J. *Proc. Nat. Acad. Sci. USA* **2010**, *107*, 7225.

(73) Dogutan, D. K.; McGuire, R.; Nocera, D. G. *J. Am. Chem. Soc.* **2011**, *133*, 9178.

(74) Boyer, J. L.; Polyansky, D. E.; Szalda, D. J.; Zong, R.; Thummel, R. P.; Fujita, E. *Angew. Chem. Int. Ed.* **2011**, *50*, 12600.

(75) Tommos, C. ; Babcock, G. T. *Acc. Chem. Res.* **1998,** *31*, 18.

(76) Renger, G. *Biochim. Biophys. Acta* **2012** DOI: 10.1016/j.bbabio.2012.02.005

(77) Hays, A-M. A.; Vassiliev, I. R.; Golbeck, J. H.; Debus, R. J. *Biochemistry* **1998**, *37*, 11352.

(78) Meyer, T. J.; Huynh, M. H. V.; Thorp, H. H. *Angew. Chem. Int. Ed.* **2007**, *46*, 5284.

(79) Umena, Y.; Kawakami, K.; Shen, J.-R.; Kamiya, N. *Nature* **2011**, *473*, 55.

Chapter 2

Effect of Basic Site Substituents on Concerted Proton-Electron Transfer in Hydrogen Bonded-Pyridyl Phenols

2.1 Introduction

Proton-coupled electron transfer (PCET) reactions are of considerable current interest, due to their importance in fundamental biological processes, energy transduction, and other chemical reactions.[1-6] Of particular importance is developing an understanding of the parameters that affect PCET reactivity. This report is focused on one class of PCET reactions, in which a proton and an electron are transferred to different sites in a single kinetic step, termed separated concerted proton-electron transfer (sCPET)[7,8] or alternatively multiple site electron-proton transfer (MS-EPT).[2] Such reactions play important roles in a variety of chemical and biological processes, from energy conversion to the generation of reactive oxygen species.[1] One important example is the oxidation of tyrosine to a neutral tyrosyl radical,[9,10] as in the Oxygen Evolving Complex of the Photosystem II protein of photosynthetic organisms.[11-15] Water oxidation involves oxidation of tyrosine-160 by long-range electron transfer to an oxidized chlorophyll P680 molecule concomitantly with transfer of the phenolic proton to a near-by hydrogen-bonded histidyl imidazole.[16,17]

The understanding of separated CPET reactions is being developed through both experimental and theoretical studies. One of the goals of work reported here is to build stronger connections between experiment and theory, which is challenging because of the complexity of the theoretical formulations.[5,18-23] Many of these formulations view sCPET as an outgrowth of the non-adiabatic form of the Marcus theory of electron transfer.[24,25] Marcus theory relates the rate constant to a pre-exponential electronic coupling term V_{el} and exponentially to a free energy barrier ΔG^* that is related to the thermodynamic reaction driving force ($\Delta G°$) and an intrinsic barrier or reorganization energy λ (eq 2.2). Extending this formalism to sCPET requires taking into account the a proton tunneling probability, which can be done with a Franck-Condon (FC) term describing the overlap between proton vibrational wavefunctions in the reactants and

products. The rate expression in equations 2.1 and 2.2 is a simplistic version of this formalism, and provides a framework with which to interpret experimental results.

$$k \propto (FC)(V_{el})^2 e^{-\Delta G^*/k_B T} \quad (2.1)$$

$$\Delta G^* = (\Delta G^\circ + \lambda)^2/4\lambda \quad (2.2)$$

Phenol oxidations have been a focus of experimental studies of sCPET, apparently starting with Linschitz *et al.*'s study of photoexcited C_{60} oxidizing a hydrogen-bonded adduct between phenol and pyridine.[26,27] More recent studies by the groups of Hammarström, Meyer, Thorp, Nocera, Savéant and others have used photochemical and electrochemical approaches to study sCPET.[28-36] These studies have primarily been performed in buffered aqueous solution with external proton acceptors. However, these studies are complicated by trimolecular kinetics and a lack of definition of the proton transfer coordinate. Our approach has used stopped flow kinetic studies of phenols with well-defined intramolecular hydrogen bonds, using model systems consisting of a di-*tert*-butyl phenol with a base attached *ortho* to the phenolic oxygen.[7,37-39] When an electron is removed by an outer-sphere oxidant in aprotic media, the phenolic proton is transferred intramolecularly to the basic site, yielding a distonic radical cation (Scheme 2.1). The use of a pendent basic site in aprotic media is advantageous for studying the effect of various parameters on sCPET reactivity because the free energy change, ΔG°_{CPET} is readily and unambiguously determined using cyclic voltammetry or chemical equilibration experiments. Also, the chemical environment of the transferring proton within the relatively strong O-H···N hydrogen bond can be probed experimentally and computationally.

In previous studies of phenol-pyridines, our laboratory has found that changing the pendent base can substantially affect the sCPET reactivity, and that rate constants (k_{sCPET}) do not always show a simple variation with driving force.[7,37] Specifically, phenols with pendent pyridyl and imidazolyl basic sites in conjugation with the phenol undergo CPET with substantially higher rate constants than phenols with unconjugated pyridyl and primary amine basic sites, even at the same driving force. This effect was initially attributed to a lowering of λ in the conjugated systems due to stronger hydrogen

bonding between the phenol and the basic site,[37] and recent results indicate that differences in the exponential prefactor vibrational and electronic overlap terms also contribute.[40]

Scheme 2.1: sCPET reactivity of phenols with pendent bases, and the phenols with pendent pyridines used in this study, **HOAr-pyX** and **HOArCH$_2$pyX**.

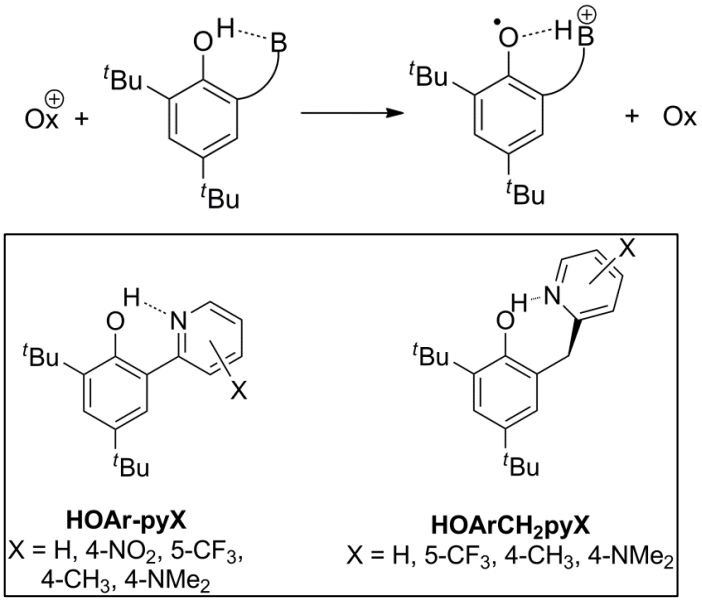

Herein, the properties of the phenol-pyridine molecules that affect their sCPET reactivity are examined in more detail. As shown in Scheme 2.1, two series of di-*tert*-butyl phenols with pendent substituted pyridine bases have been synthesized and studied. The **HOAr-pyX** compounds (X = 4-NMe_2, 4-CH_3, 5-CF_3, 4-NO_2) have a substituted pyridine attached directly to the phenol, while the **HOArCH$_2$pyX** series (X = 5-CF_3, 4-CH_3, 4-NMe_2) have the pyridine attached to the phenol through a methylene linker. A preliminary account has described the chemistry of the unsubstituted compounds (X = H).[37] In this study, the substituents allow systematic variation of the sCPET driving force, the strength of the OH···N hydrogen bond, the proton transfer distance (d_{ON}), the X–H vibrational frequencies, and other parameters relevant to sCPET kinetics. There is a strong contrast between the behaviors of the conjugated (**HOAr-pyX**) *vs.* the non-

conjugated (**HOArCH$_2$pyX**) compounds, in terms of how their reactivity depends on $\Delta G°_{CPET}$ and how their intrinsic reactivity (at $\Delta G°_{CPET}$ = 0) is modulated by the substituents. Much of the work in this chapter, particularly the analysis of **HOAr-pyX** compounds, was performed by or with the assistance of Dr. Todd Markle, and some of it has been reported previously in his doctoral thesis, Ref. 41.

2.2 Results and Discussion

2.2.1 Synthesis and Characterization

The non-conjugated pyridyl-methyl-phenols **HOArCH$_2$pyX** were synthesized by a modification of the previously reported method for the parent **HOArCH$_2$py**.[37] *Ortho*-lithiated substituted pyridines were prepared *in situ* from *n*-butyllithium and the corresponding substituted 2-bromopyridine (except for X = 4-NMe$_2$) were added to benzyl-ether protected 3,5-di-tert-butylsalicylaldehyde. This method gives improved yields with respect to the aldehyde compared to the pyridyl Grignard reagent used in the initial synthesis of the parent compound **HOArCH$_2$py** (X = H).[37] The resulting alcohol was acylated, and catalytic hydrogenation removed both the acetate and the benzyl protecting group. The substituted pyridyl phenols **HOAr-pyX** were prepared via Suzuki couplings of 2,4-di-*tert*-butyl-methoxyphenyl-6-boronic acid with the appropriate halo-pyridine, followed by deprotection of the phenol. All the **HOArCH$_2$pyX** and **HOAr-pyX** compounds were characterized by ^{1}H and ^{13}C NMR spectroscopy and mass spectrometry. The full procedures are given in the experimental section chapter 2.4.

The substituents have a substantial effect on the ^{1}H NMR chemical shift of the phenolic proton (δO*H*) in 'dry' CD_3CN. In the pyridylmethyl series **HOArCH$_2$pyX**, this proton appears as a singlet with δO*H* from 10.19 ppm for the nitro derivative (X = NO$_2$) to 12.06 ppm for X = NMe$_2$. This singlet is far downfield from δO*H* for phenols without pendent basic sites, such as tri-*tert*-butyl phenol (δO*H* = 5.3 in this solvent). The phenolic resonances for **HOAr-pyX** are even further downfield, ranging from δ14.01 to 15.45 ppm (Table 2.1).[41]

These large differences in chemical shift reflect differences in the OH···py hydrogen bonding. In general, stronger hydrogen bonding leads to more downfield δO*H*

resonances,[42] and the hydrogen bond strength increases as the pK_a of the donor and [protonated] acceptor are more closely matched.[43] Determining the effective base strength of the pyridine in these strongly H-bonded compounds is problematic, so we use the pK_a of the free pyridine as a measure of the substituent effect. The substituted pyridines **pyX** vary in basicity by nearly ten orders of magnitude, as the protonated pyridinium ions in acetonitrile solution have estimated pK_as ranging from 8.7 for 4-nitropyridinium to 18.5 for 4-dimethylaminopyridinium.[44-50] The more electron donating substituents raise the pK_a of the pyridinium, bringing it closer to the pK_a of the phenol (pK_a of phenol = 27 in MeCN),[51] and thereby leading to stronger hydrogen bonding and more downfield resonances. Given the large range of basicity, there should be notable differences in the hydrogen bonding environment of the phenolic proton, so the variation in δO*H* is not surprising. Within each series of compounds, δO*H* varies roughly linearly with the pK_a of the pyridinium (Figure 2.1a), and for the same substituent the chemical shift for ***H*OAr-pyX** is almost 4 ppm downfield of ***H*OArCH$_2$pyX**.

Table 2.1: Structural and spectroscopic properties of **HOArCH$_2$pyX** and **HOAr-pyX**.

	X	pK_a[a]	δOH[b]	d_{ON} (X-ray)[c]	d_{ON}(DFT)[c]	νOH$_{DFT}$[d]
-CH$_2$pyX	4-NMe$_2$	18.5	12.06	-	2.726	3053
	4-CH$_3$	14.1	11.31	2.724(3)	2.753	3137
	H[e]	12.9	11.15[e]	2.6914(13)[e]	2.761	3160
	5-CF$_3$	9.5	10.19	[2.778(5), 2.766(5)][f]	2.782	3224
-pyX	4-NMe$_2$[h]	18.5	15.45	2.500(4)	2.551	2838
	4-CH$_3$[h]	14.1	14.95	2.531(3)	2.560	2897
	H[g]	12.9	14.83	[2.561(3), 2.567(3), 2.573(3)][f]	2.565	2918
	5-CF$_3$[h]	9.5	14.26	[2.565(4), 2.547(4), 2.570(4)][f]	2.569	2958
	4-NO$_2$[h]	8.7	14.01	2.548(3)	2.578	2999

[a] Estimated, from Ref. 44. [b] In ppm, in CD$_3$CN. [c] In Å. [d] In cm^{-1}, corrected following to Ref. 52. [e] Ref. 37. [f] multiple independent molecules in the unit cell. [g] Ref. 7. [h] Ref 41.

Another key parameter of the OH···N hydrogen bond is the donor-acceptor distance between the phenol oxygen and the pyridyl nitrogen, d_{ON}. X-ray crystal structures were obtained for all of the **HOAr-pyX** compounds and for all **HOArCH$_2$pyX** derivatives except for X = NMe_2 (Table 2.1). ORTEP drawings are given are given in Figure 2.2. The d_{ON} values are ca. 0.2 Å longer for the **HOArCH$_2$pyX** vs. the **HOAr-pyX** compounds, because of the larger ring size for the **HOArCH$_2$pyX** derivatives. In most cases, smaller d_{ON} distances are found for compounds with more electron donating substituents, but the range of distances is small. A number of the structures have multiple independent molecules in the unit cell, which differ in their d_{ON} values by more than 0.01 Å, indicating that crystal packing plays a significant role in the observed d_{ON}.

Computed structures may give a better indication of the d_{ON} in solution, avoiding the influence of crystal packing forces. Density functional theory gas-phase B3LYP/6-31G(d,p) optimized geometries (Table 2.1) correlate more strongly with the pK_a of the pyridyl group (Figure 2.1b). Calculated values of d_{ON} for **HOArCH$_2$pyX** vary by 0.056 Å, and for **HOAr-pyX** they vary by 0.026 Å. Calculated gas phase OH stretching frequencies (νOH_{DFT}), another measure of hydrogen bond strength, also correlate with the pK_a of the base. These values are calculated from the second derivative of the potential energy surface at the minimum, and therefore do not capture the anharmonicity and mode mixing that strongly affect the experimental spectra.[53] The calculated νOH_{DFT} are *ca.* 250 cm^{-1} higher for the **HOArCH$_2$pyX** compounds, and the values are higher with more electron withdrawing substituents (from 3053 cm^{-1} for X = NMe_2 to 3224 cm^{-1} for X = CF_3 for **HOArCH$_2$pyX**; Table 2.1).

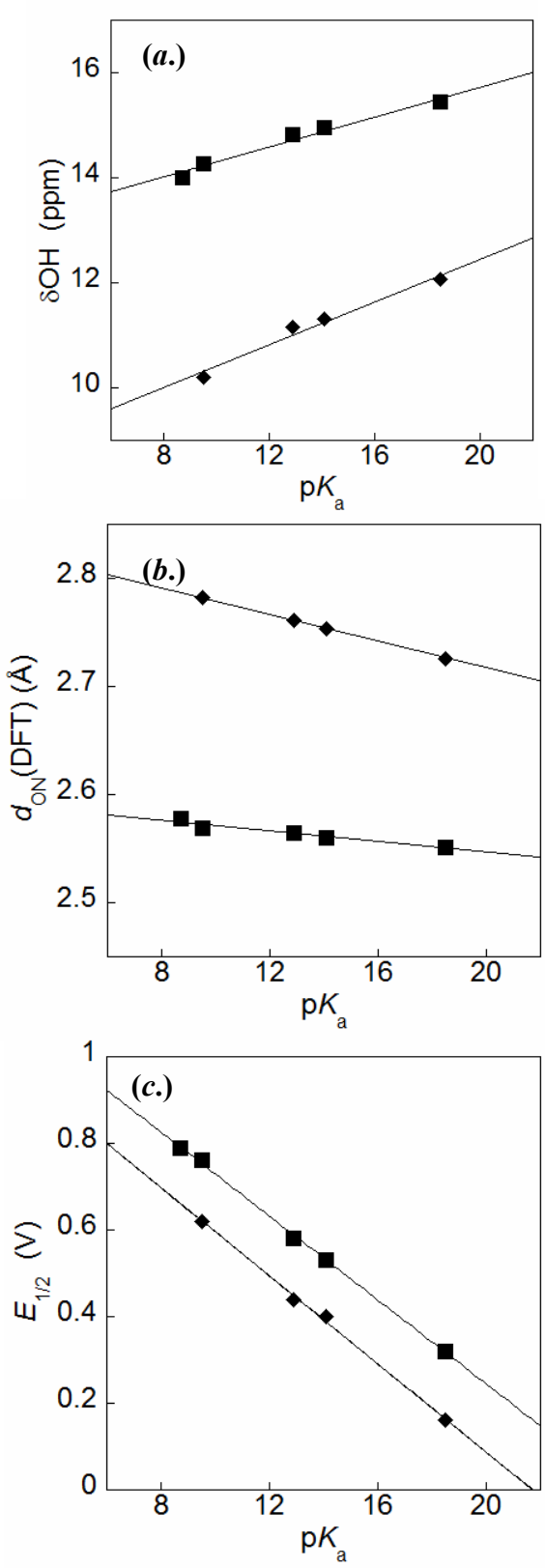

Figure 2.1: . Variation of thermochemical and structural parameters in **HOArCH$_2$pyX** (♦) and **HOAr-pyX** (■) versus the estimated pK_a of the pyridinium (see Ref. 44).

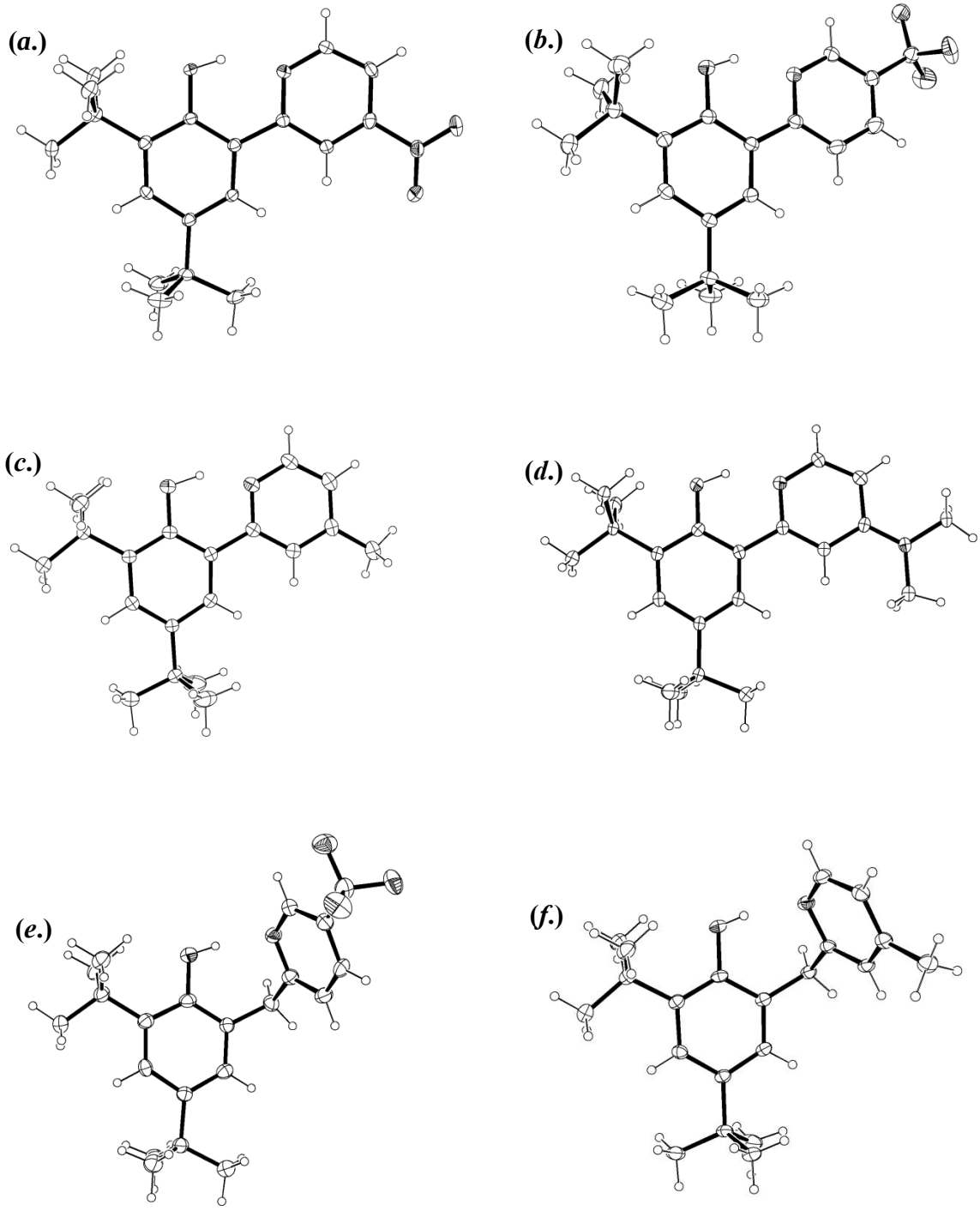

Figure 2.2: ORTEP diagrams of (*a.*) **HOAr-pyNO$_2$**, (*b.*) **HOAr-pyCF$_3$**, (*c.*) **HOAr-pyCH$_3$**, (*d.*) **HOAr-pyNMe$_2$**, (*e.*) **HOArCH$_2$pyCF$_3$**, (*f.*) **HOArCH$_2$pyCH$_3$**. Thermal ellipsoids are shown at 30% probability. For clarity, only one independent molecule from the unit cell is shown. Crystallographic data are given in Table 2.2. **HOAr-pyNO$_2$**, **HOAr-pyCH$_3$**, and **HOAr-pyNMe$_2$** from Ref. 41.

Table 2.2: Crystallographic data for **HOAr-pyX** and **HOArCH$_2$pyX**

	HOAr-pyNO_2	**HOAr-pyCF_3**	**HOAr-pyCH_3**
Formula	$C_{19}H_{24}N_2O_3$	$C_{20}H_{24}F_3NO$	$C_{20}H_{27}NO$
T (K)	208(2)	130(2)	130(2)
Wavelength	0.71073 Å	0.71073 Å	0.71073 Å
Size (mm)	0.20 x 0.15 x 0.10	0.59 x 0.48 x 0.36	0.48 x 0.05 x 0.05
Cryst. Syst	Triclinic	Triclinic	Orthorhombic
Space group	P-1	P-1	P b c m
a (Å)	6.0430(17)	10.9713(6)	9.6250(3)
b (Å)	10.138(3)	12.6281(7)	26.7940(4)
c (Å)	15.059(5)	14.4453(11)	6.9060(14)
α (deg)	79.706(5)	89.791(2)	90
β (deg)	81.949(6)	97.735(3)	90
γ (deg)	76.489(5)	112.271(5)	90
V (Å^3)	877.9(4)	1832.8	1781.0(4)
Z	2	4	4
D_{calc} (g/cm^3)	1.242	1.274	1.109
Abs. coeff. (mm^{-1})	0.084	0.099	0.067
Refl. total	6375	11749	1925
Refl. uniq. (R_{int})	3069 [R(int) = 0.0295]	6595 [R(int) = 0.0761]	1925 [R(int) = 0.0980]
Data/restraints/ parameters	3069 / 0 / 226	6595 / 36 / 492	1925 / 0 / 133
GOF	1.208	1.037	0.999
R1/wR2 ([I>2σ(I)])	0.079 / 0.1589	0.0650 / 0.1581	0.0607 / 0.1300
R1/wR2 (all data)	0.0965 / 0.1663	0.1131 / 0.1825	0.1252 / 0.1520

Table 2.2 (*continued)*: Crystallographic data for **HOAr-pyX** and **HOArCH$_2$pyX**

	HOAr-pyNMe$_2$	**HOArCH$_2$pyCF$_3$**	**HOArCH$_2$pyCH$_3$**
Formula	$C_{21}H_{32}N_2O$	$C_{21}H_{26}F_3NO$	$C_{21}H_{29}NO$
T (K)	130(2)	130(2)	130(2)
Wavelength	0.71073 Å	0.71073 Å	0.71073 Å
Size (mm)	0.24 x 0.24 x 0.12	0.26 x 0.20 x 0.12	0.59 x 0.58 x 0.17
Cryst. Syst	Monoclinic	Orthorhombic	Monoclinic
Space group	C 2/m	P c c n	P 21/a
a (Å)	18.83960(140)	14.6043(5)	10.0062(10)
b (Å)	6.95260(59)	22.5308(10)	11.1917(9)
c (Å)	14.93540(150)	23.7796(8)	16.7970(15)
α (deg)	90	90	90
β (deg)	107.2190(32)	90	102.784(4)
γ (deg)	90	90	90
V (Å^3)	1868.621(285)	7824.6	1834.4
Z	4	16	4
D_{calc} (g/cm^3)	1.160	1.241	1.128
Abs. coeff. (mm^{-1})	0.071	0.095	0.068
Refl. total	2958	13098	10520
Refl. uniq. (R_{int})	1796 [R(int) = 0.0673]	6957 [R(int) =0.1592]	3290 [R(int) = 0.1314]
Data/restraints/ parameters	1796 / 0 / 148	6957 / 0 / 492	3290 / 0 / 216
GOF	0.975	0.918	1.020
R1/wR2 ([I>2σ(I)])	0.0698 / 0.1687	0.0766 / 0.1623	0.024 / 0.1416
R1/wR2 (all data)	0.1318 / 0.1965	0.2265 / 0.2286	0.1114 / 0.1693

Taken together, the d_{ON}, νOH_{DFT}, and $\delta O\mathit{H}$ values indicate that there is weaker hydrogen bonding for the **HOArCH$_2$pyX** compounds, and weaker hydrogen bonding with more electron-withdrawing X groups. The changes in these parameters across each series are somewhat smaller than the differences *between* the two series: *i.e.*, **HOAr-pyNO$_2$** has a shorter d_{ON}, lower νOH, and higher δO*H* than does **HOArCH$_2$pyNMe$_2$**. Figures 2.1a and 2.1b also show the more subtle effect that the changes with substituent are more pronounced for the **HOArCH$_2$pyX** compounds than for **HOAr-pyX**. This

could be due to the **HOArCH$_2$pyX** compounds having greater flexibility of their seven-membered rings, more linear O-H···N angles, or because the conjugation in **HOAr-pyX** allows for compensatory effects of the substituent on the pK_a of the phenol, as discussed below.

2.2.2 Thermodynamics of HOArCH$_2$pyX and HOAr-pyX Oxidation

The potentials for the oxidation of **HOArCH$_2$pyX** and **HOAr-pyX** were determined by cyclic voltammetry (CV). Cyclic voltammograms of **HOArCH$_2$pyX** (Figure 2.3) and **HOAr-pyX**[41] in acetonitrile containing 0.1 M [*n*-Bu$_4$N][PF$_6$] are chemically reversible, with roughly equal anodic and cathodic currents. The separations between the anodic and cathodic peaks (ΔE_p) are somewhat larger than the theoretical value of 0.059 V, as has been observed in related systems.[6,7,37-3839]. These quasi-reversible CVs indicate that electrochemical oxidation is coupled to proton transfer to the pyridyl moiety. Reversible cyclic voltammograms have been observed for a variety of phenols with pendent bases in aprotic media,[7,37-39,54] while the CVs of phenols without pendent bases in aprotic media are irreversible,[55] in part due to proton transfer to the bulk solution upon oxidation. Proton transfer from the phenol is energetically favorable because the phenol radical cation is very acidic, with a pK_a in acetonitrile of ~0.[55] CVs of **HOAr-pyNO$_2$**, **HOAr-pyCF$_3$**,[41] and **HOArCH$_2$pyCF$_3$** show decreased cathodic current at a scan rates of 0.1 V/s, indicating instability of the oxidized product on the timescale of the experiment. This instability may be due to deprotonation of the weakly basic pendent pyridines on the timescale of the CV experiment.

The measured redox potentials ($E_{1/2}$) for **HOArCH$_2$pyX** vary with substituent, ranging from 0.16 V (X = NMe$_2$) to 0.62 V (X = CF$_3$) (Table 2.3). The redox potentials vary linearly with the estimated pK_a of the pyridyl moiety (Figure 2.1c), indicating that the thermodynamics of oxidation depend on the energy to transfer the proton to the basic site. The slope of this relationship is –0.051(2) V/pK_a, just slightly lower than the predicted value of –0.059 V/pK_a. This result underscores a key advantage of this system in the study of sCPET, as the thermodynamics of the proton transfer are varied in a systematic and well-defined way. The redox potentials of **HOAr-pyX** also vary linearly

the pK_a of the pyridyl moiety (Table 2.3 and Figure 2.1c).[41] The slope of this relationship, –0.048(1) V/pK_a, is further from the predicted value than for **HOArCH$_2$pyX**. This somewhat greater deviation from the predicted value is likely be due to the increased electronic communication between the phenol and the basic site substituent in the conjugated compounds, which allows the substituent to affect both the acidity and oxidizability of the phenol.

Table 2.3: Thermochemical properties of **HOArCH$_2$pyX** and **HOAr-pyX**.

	X	pK_a(pyX)[a]	$E_{1/2}$[b] (ΔE_p)[c]
-CH$_2$pyX	4-NMe$_2$	18.5	0.16 (0.12)[d]
	4-CH$_3$	14.1	0.40 (0.21)[d]
	H[e]	12.9	0.44 (0.22)
	5-CF$_3$	9.5	0.62 (0.12)[d]
-pyX	4-NMe$_2$	18.5	0.32 (0.09)
	4-CH$_3$	14.1	0.53 (0.11)
	H[f]	12.9	0.58 (0.10)
	5-CF$_3$	9.5	0.76 (0.08)
	4-NO$_2$	8.7	0.79 (0.09)

[a] Estimated, from Ref. 44. [b] vs. $Cp_2Fe^{+/0}$ in MeCN, estimated error is ± 0.02 V. [c] In V, scan rate = 0.2 V/s. [d] Scan rate = 0.1 V/s. [e] Ref. 37. [f] Ref 7.

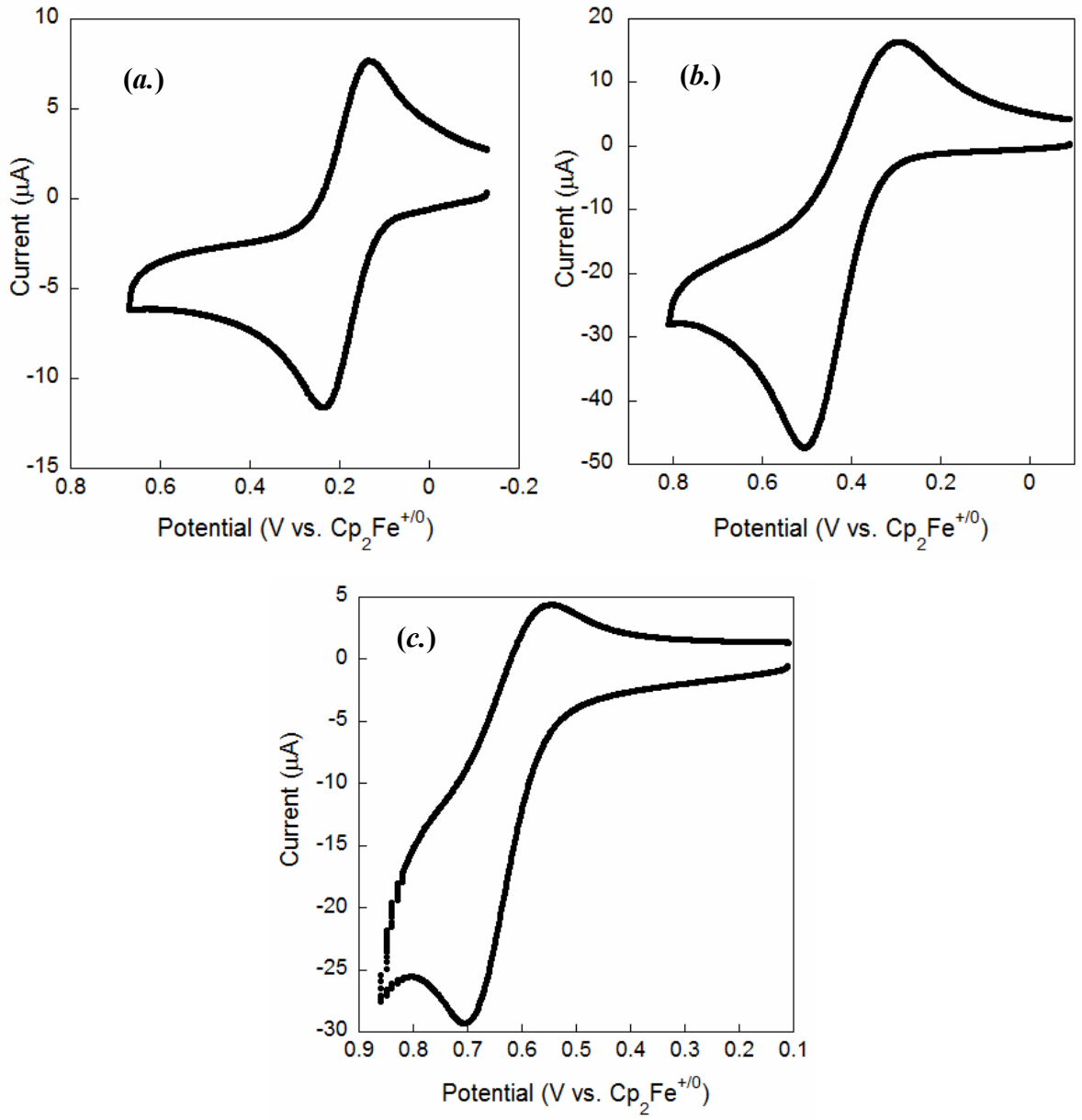

Figure 2.3: Oxidizing cyclic voltammograms of (*a.*) **HOArCH$_2$pyNMe$_2$**, (*b.*) **HOArCH$_2$pyCH$_3$**, and (*c.*) **HOArCH$_2$pyCF$_3$**. CVs were recorded in anaerobic acetonitrile (0.1 M [*n*-Bu$_4$N][PF$_6$]) at a scan rate of 0.1 V/s.

2.2.3 Kinetics of sCPET Oxidations of HOArCH$_2$pyX and HOAr-pyX

The kinetics of the reactions of **HOArCH$_2$pyX** and **HOAr-pyX** with one-electron chemical oxidants in acetonitrile at 295(2) K were measured by stopped-flow UV/Vis spectroscopy. The one-electron oxidants used were the hexafluorophosphate salts of a variety of *para*-substituted triarylamminium cations, $[N(C_6H_4X)_3]^{+\cdot}$, and substituted tris(bipyridyl) and tris(phenanthroline) iron(III) complexes, $[Fe(R_2bpy)_3]^{3+}$ and $[Fe(Me_xphen)_3]^{3+}$. Reactions performed with $[N(C_6H_4X)_3]^{+\bullet}$ were monitored by following the disappearance of the blue amminium, and reactions performed with $[Fe(R_2bpy)_3]^{3+}$ and $[Fe(Me_xphen)_3]^{3+}$ were monitored by following the appearance of the red Fe^{II} species and the disappearance of the blue Fe^{III} species. Typical reactions were performed with *ca.* 0.01 mM oxidant and the phenol concentration varied from *ca.* 3 – 30 equivalents. Bimolecular rate constants were obtained by fitting to opposing second order kinetics using SpecFit^{TM} global analysis software.[56] The results are summarized in Table 2.4.

2.2.3.1 Substituent and driving force effects on CPET kinetics of HOArCH$_2$pyX

Bimolecular rate constants have been determined for nine CPET reactions of the substituted **HOArCH$_2$pyX** compounds with various $[N(C_6H_4X)_3]^{+\bullet}$ oxidants. These rate constants span three orders of magnitude, while the $\Delta G°$ (from CV data) varies such that K_{eq} spans 10^6, depending both on the choice of oxidant and internal base. A Brønsted plot, log(k) vs log(K_{eq}) (Figure 2.4a), of this data gives a strong linear correlation (R^2 = 0.92) with a slope of $\alpha = 0.54(5)$. This value of α, which is equivalent to $\partial\Delta G^*/\partial\Delta G°$, is within error of the value of 0.5 predicted for CPET reactions in the limit where $\Delta G° << 2\lambda$ (eq. 2.2). Thus the rate constants for CPET reactions of **HOArCH$_2$pyX** depend primarily of the driving force of the reaction, despite the changes in proton transfer coordinate discussed above. A similar result was obtained in our related studies of phenol-imidazoles ($\alpha = 0.55$)[39] and for a phenol-amine with oxidants of varying potential ($\alpha = 0.53$).[7] Fecenko, Thorp, and Meyer have reported a slope of ~0.6 for oxidation of tyrosine in aqueous buffers.[29] Such a dependence of the rate on driving force has previously been shown to indicate a concerted proton-coupled mechanism rather than stepwise electron transfer/proton transfer or proton transfer/electron transfer.[7,29,57]

Table 2.4: Kinetic data for oxidations of **HOArCH$_2$pyX** and **HOAr-pyX**.

Phenol	Oxidant	E_{rxn}(V)	k (M^{-1} s^{-1})	$k°$ (M^{-1} s^{-1})[a]
-CH_2pyNMe_2	$[N(C_6H_4OMe)_3]^{+\bullet}$	0.00	$5.4 \pm 0.5 \times 10^5$	5.4×10^5
-CH_2pyCH_3	$[N(C_6H_4OMe)(C_6H_4Br)_2]^{+\bullet}$	0.08	$8.0 \pm 0.9 \times 10^5$	1.7×10^5
	$[N(C_6H_4Me)_3]^{+\bullet}$	-0.02	$1.4 \pm 0.2 \times 10^5$	2.2×10^5
	$[N(C_6H_4OMe)_2(C_6H_4Br)]^{+\bullet}$	-0.08	$4.4 \pm 0.5 \times 10^4$	2.2×10^5
	$[Fe(4,7\text{-}Me_2phen)_3]^{3+}$	0.13	$5.0 \pm 0.5 \times 10^5$	4.0×10^4
-CH_2py	$[N(C_6H_4OMe)(C_6H_4Br)_2]^{+\bullet}$ [b]	0.04	$5.3 \pm 0.5 \times 10^5$	2.4×10^5
	$[N(C_6H_4Me)_3]^{+\bullet}$ [b]	-0.06	$1.2 \pm 0.1 \times 10^5$	3.9×10^5
	$[N(C_6H_4OMe)_3]^{+\bullet}$ [b]	-0.28	$8 \pm 2 \times 10^2$	1.9×10^5
	$[Fe(4,7\text{-}Me_2phen)_3]^{3+}$ [c]	0.09	$2.5 \pm 0.3 \times 10^5$	4.3×10^4
CH_2pyCF_3	$[N(C_6H_4Br)_3]^{+\bullet}$	0.05	$7.5 \pm 1.5 \times 10^5$	2.8×10^5
	$[N(C_6H_4OMe)(C_6H_4Br)_2]^{+\cdot}$	-0.14	$7.6 \pm 0.8 \times 10^3$	1.2×10^5
	$[Fe(4,7\text{-}Me_2phen)_3]^{3+}$	-0.09	$3.4 \pm 0.3 \times 10^3$	2.0×10^4
-pyCH_3	$[Fe(5,5'\text{-}Me_2bpy)_3]^{3+}$ [c]	0.05	$2.2 \pm 0.2 \times 10^6$	8.3×10^5
-py	$[Fe(bpy)_3]^{3+}$ [d]	0.12	$5.2 \pm 0.8 \times 10^6$	5.0×10^5
	$[Fe(5,5'\text{-}Me_2bpy)_3]^{3+}$ [d]	0.00	$5.8 \pm 0.9 \times 10^5$	5.8×10^5
	$[Fe(4,4'\text{-}Me_2bpy)_3]^{3+}$ [c]	-0.07	$4.5 \pm 0.9 \times 10^5$	1.8×10^6
	$[Fe(4,7\text{-}Me_2phen)_3]^{3+}$ [d]	-0.05	$1.9 \pm 0.4 \times 10^6$	5.0×10^6
	$[Fe(3,4,7,8\text{-}Me_4phen)_3]^{3+}$ [d]	-0.12	$3.3 \pm 0.6 \times 10^5$	3.4×10^6
	$[Fe(4,4'\text{-}^tBu_2bpy)_3]^{3+}$ [c]	-0.06	$4.6 \pm 0.5 \times 10^4$	1.5×10^5
-pyCF_3	$[Fe(bpy)_3]^{3+}$ [c]	-0.06	$3.7 \pm 0.4 \times 10^4$	1.2×10^5
	$[Fe(phen)_3]^{3+}$ [c]	-0.07	$1.6 \pm 0.2 \times 10^5$	6.3×10^5
-pyNO_2	$[Fe(bpy)_3]^{3+}$ [c]	-0.09	$2.1 \pm 0.2 \times 10^4$	1.2×10^5
	$[Fe(phen)_3]^{3+}$ [c]	-0.10	$7.5 \pm 1.5 \times 10^4$	5.3×10^5

[a] Intrinsic rate constants, corrected to $\Delta G° = 0$ (see text). [b] Ref. 37. [c] Ref. 41. [d] Ref. 7.

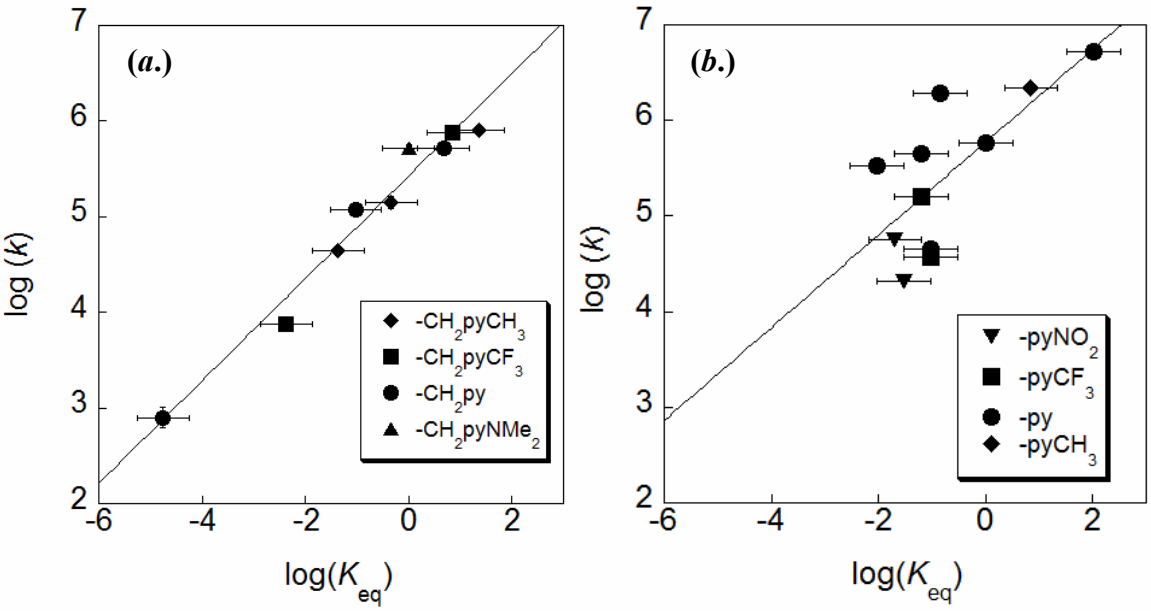

Figure 2.4: Brønsted plots for (*a.*) reactions of **HOArCH$_2$pyX** with $[N(C_6H_4X)_3]^{+\cdot}$, and (*b.*) reactions of **HOAr-pyX** with $[Fe(R_2bpy)_3]^{3+}$ and $[Fe(Me_xphen)_3]^{3+}$ (Ref. 41).

While the correlation of rate constants with driving force in Figure 2.4a is quite strong, there are some modest deviations. These deviations could indicate whether the rate constants are affected differently when $\Delta G°$ is varied through the proton-transfer *vs.* electron transfer coordinate. In the reactions of **HOArCH$_2$pyCH$_3$** and **HOArCH$_2$py**, the ET component of $\Delta G°$ has been varied by changing the triarylamminium oxidant, $[N(C_6H_4X)_3]^{+\bullet}$, as shown in the Brønsted plots of Figures 2.5a and 2.5b. These plots are linear (R^2 = 0.99 for both) with α = 0.46(5) and 0.49(6), respectively. Alternatively, $\Delta G°$ can also be varied by the substituent on the pyridine. This affects primarily the proton transfer coordinate through well-defined changes in the pK_a of the pyridine base (as indicated by the slope of the experimental $E_{1/2}$ vs. estimated pK_a). Figure 2.5c shows Brønsted plots for the oxidations of **HOArCH$_2$pyX** (X = CF_3, H, and Me) by $[N(C_6H_4OMe)(C_6H_4Br)_2]^{+\bullet}$ (points on dashed line) or by $[Fe(Me_2phen)_3]^{3+}$ (points on solid line). Both of these plots are linear, with α = 0.57(6) (R^2 = 0.99) for the amminium reactions and α = 0.59(6) (R^2 = 0.99) for the iron reactions. At the same driving force, the amminium reactions have rate constants roughly ten times larger than the i reactions,

due to the smaller ET intrinsic barrier for the $[N(C_6H_4X)_3]^{+\cdot}$ reagents.[7] The agreement between the two values of α indicates that the effect causing α to be larger than ½ is independent of the outersphere oxidant.

The Brønsted slopes are larger when $\Delta G°$ is varied by changing the pyridine substituent [α = 0.57(6), 0.59(6)] than varying the oxidant [α = 0.46(5), 0.49(6)]. This conclusion is tentative because the plots each involve only three points, and the uncertainties are significant (due primarily to the large estimated uncertainties in the redox potentials and K_{eq} values). However, the confidence level is raised by the agreement between the two series where the oxidant is varied (α = 0.48), and between the two series where the substituent is varied (α = 0.58). This result is in contrast to the previous study by Meyer *et al.*, in which α ~ 0.6 was observed both when changing the oxidant potential and when changing the pK_a of the buffer.[29] The rate constants being more sensitive to changes in $\Delta G°_{sCPET}$ from changes in the proton transfer coordinate vs. the ET coordinate could arise from various effects. In a purely classical picture, this could reflect an asymmetry in the reaction coordinate, with the transition structure involving more proton transfer.[58] In the context of PCET theory (eq 2.1), changing the pyridine substituent could affect k_{sCPET} via changes in the intrinsic barriers λ or quantum mechanical pre-factor terms V_{el} and FC. This is discussed in more detail below. The net result is that more electron withdrawing substituents result in smaller rate constants than would be predicted if the substituent affected only $\Delta G°_{sCPET}$.

2.2.3.2 Substituent and driving force effects on CPET kinetics of HOAr-pyX

The reactions of the conjugated **HOAr-pyX** compounds are significantly faster than those of **HOArCH$_2$pyX** at the same driving force, as was observed for the parent X = H compounds.[37] This results in the reactions of **HOAr-pyX** with triarylamminiums being too fast to measure with our approach, because they are complete within the mixing time of the stopped-flow instrument even at the lowest practical concentrations. Still, the kinetics for ten reactions with $[Fe(N\text{-}N)_3]^{3+}$ oxidants have been measured (Table 2.4), with values of E_{rxn} which vary by 0.24 V (or 10^4 in K_{eq}) and rate constants that vary by a factor of 250. The majority of these are slightly uphill reactions ($\Delta G°_{CPET} > 0$), and have

been measured with approach-to-equilibrium kinetics. Overall, substituents have a smaller effect on the rate constants for **HOAr-pyX** reactions than they do for the

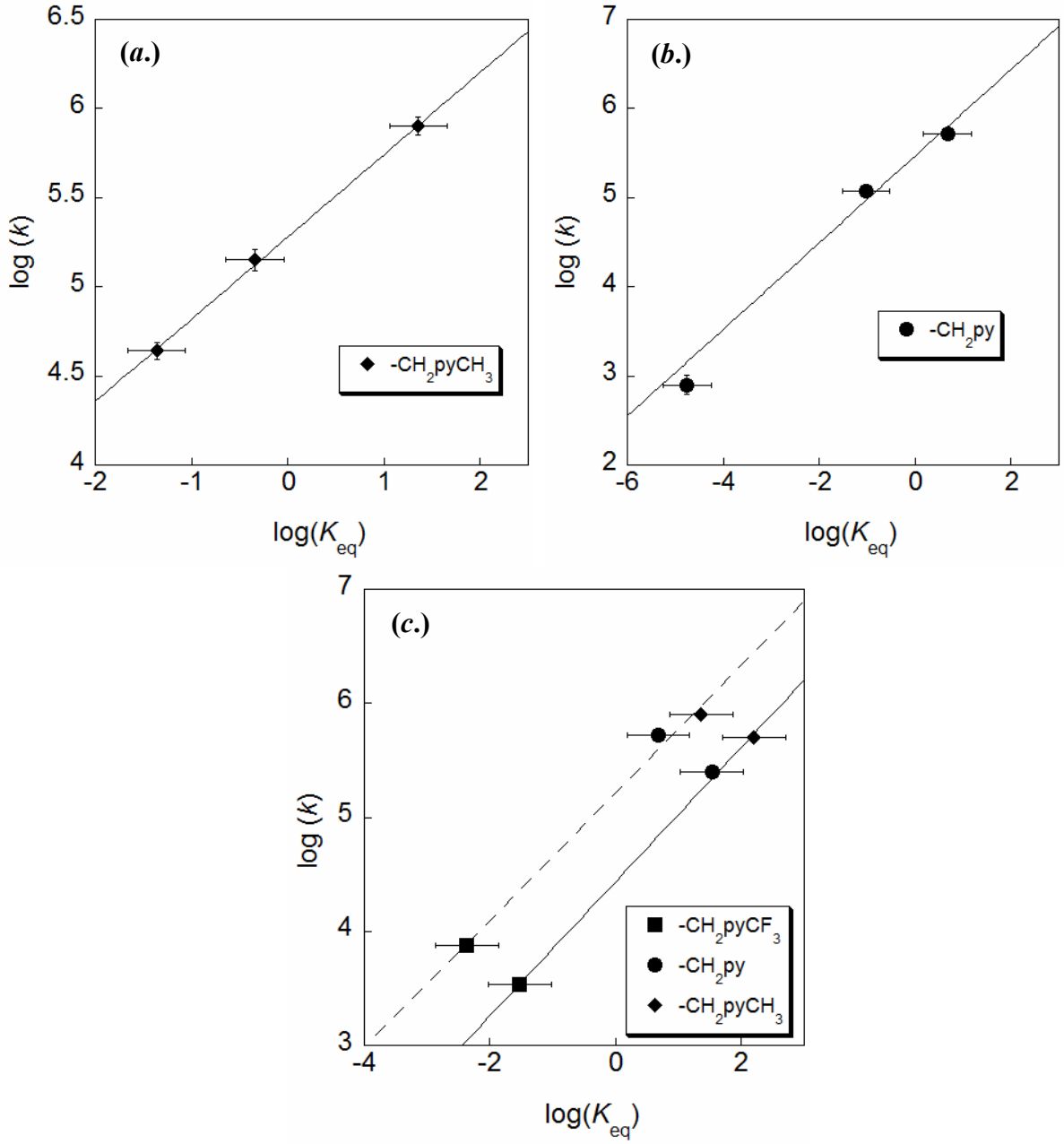

Figure 2.5: Brønsted plots for (*a.*) reactions of **HOArCH$_2$pyCH$_3$** with $[N(C_6H_4X)_3]^{+\cdot}$, (*b.*) reactions of **HOArCH$_2$pyH** with $[N(C_6H_4X)_3]^{+\cdot}$, and (*c.*) reactions of **HOArCH$_2$pyX** with $[N(C_6H_4OMe)(C_6H_4Br)_2]^{+\cdot}$ (points on dashed line) and $[Fe(Me_2phen)_3]^{3+}$ (points on solid line).

HOArCH$_2$pyX compounds. This is in part due to the smaller dependence of $\Delta G°_{CPET}$ on the substituent noted above, with the redox potential varying only –0.048(1) V per unit change in pyridine pK_a, *vs.* a –0.051(2) V/pK_a shift for **HOArCH$_2$pyX**. This effect parallels the smaller influence of substituents in the **HOAr-pyX** series on the phenolic ^{1}H NMR chemical shifts and the calculated O–H stretching frequencies and O···N distances (Table 2.1 and Figure 2.1).

The Brønsted plot of log(k) *vs.* log(K_{eq}) for oxidations of **HOAr-pyX** shows substantial scatter, as shown in Figure 2.4b above. The linear fit is very poor, with R^2 = 0.53. For example, the reactions of **HOAr-py** + $[Fe(4,7\text{-}Me_2phen)_3]^{3+}$ and **HOAr-pyCF$_3$** + $[Fe(bpy)_3]^{3+}$ have very similar driving forces (E_{rxn} = –0.05 and –0.06 V) but their rate constants differ by a factor of 50. Thus for the **HOAr-pyX** series, other parameters besides the thermodynamic driving force play an important role in determining the sCPET rate. This contrasts with the non-conjugated **HOArCH$_2$pyX** system, as well as the previous reports of sCPET phenol oxidations mentioned above.[28-31,36,37,39]

Examining the rate constants in Table 2.4, including the intrinsic rate constants $k°$ described in the next section, it is apparent that the oxidation reactions with $[Fe(Me_xphen)_3]^{3+}$ are significantly faster than the reactions with $[Fe(R_2bpy)_3]^{3+}$. For instance, the reactions of **HOAr-pyCF$_3$** and **HOAr-pyNO$_2$** with $[Fe(bpy)_3]^{3+}$ and $[Fe(phen)_3]^{3+}$ show that the $[Fe(phen)_3]^{3+}$ reactions are 4.3 and 3.6 times faster even though they are 10 mV less favorable. A small part of this is the *ca.* three-times larger electron transfer self-exchange reaction rate constants for $[Fe(Me_xphen)_3]^{3+}$ *vs.* $[Fe(R_2bpy)_3]^{3+}$.[59] However, this should only account for a factor of about 1.7 (using the Marcus cross relation),[24] which is almost exactly counterbalanced by the difference in driving force (accounting for a factor of 0.7 with α = ½). This effect was noted previously for of **HOAr-py**,[7] but it is not observed in the reactions of **HOArCH$_2$pyX**. In the context of Marcus models for CPET such as equation 2.1 above, the observation of a pyridyl-phenol reacting faster with $[Fe(Me_xphen)_3]^{3+}$ than with $[Fe(R_2bpy)_3]^{3+}$ at essentially the same driving force must be an effect of the electronic coupling V_{el} (called H_{AB} in ET theory). The other parameters that affect CPET rates are the Frank-Condon factors (*FC*) and the intrinsic barrier λ. The *FC* term is a property of the pyridyl-phenol,

independent of the oxidant, and the ET intrinsic barriers of the two oxidants are very similar based on the self-exchange rate constants given above.

The electronic coupling V_{el} is probably larger for the phenanthroline compounds than the bipyridine ones because the larger conjugated π system of phenanthroline provides a better conduit for electron transfer. The reason that this effect is seen for **HOAr-pyX** and not for **HOArCH$_2$pyX** is most likely related to the conjugation of the phenol and substituted pyridine rings in **HOAr-pyX**. The optimal electron transfer pathway from the phenol to the oxidant could be via the pyridine since the phenol has two sterically protecting tertiary butyl groups. The significant interaction between the pyridyl and phenol groups in the **HOAr-pyX** compounds is indicated by the dependence of the CPET redox potential on the basicity of the pyridine, –0.048(2) V/pK_a, which is lower than the 0.059 V/pK_a predicted for non-interacting fragments (see above). In addition, the hydrogen bonds are significantly stronger for the **HOAr-pyX** compounds, as indicated by the O···N distances being *ca.* 0.2 Å shorter, the stretching frequencies being ~ 200 cm^{-1} lower, and the δOH being 3-4 ppm lower.

2.2.4 Understanding the substituent effect on sCPET kinetics

2.2.4.1 Intrinsic rate constants *k*°

To understand the effects of pyridine substitution on k_{sCPET}, it is helpful to separate the thermodynamic contribution from other factors. The reactions described here all have $|\Delta G°| << 2\lambda$,[7] so the barrier ΔG^* becomes linear with $\Delta G°$ and equation 2.1 reduces to equation 2.3. Separating out the thermochemical driving force from the intrinsic kinetic terms yields an "intrinsic rate constant" $k°$ (eqs 2.4, 2.5). In essence, $k°$ is the rate constant extrapolated to $\Delta G° = 0$. This analysis is analogous to the derivation of the standard electrochemical rate constant, which is extrapolated to zero driving force using the Tafel slope, which is equivalent to the Brønsted α and is typically taken as ½, as in equations 2.3 and 2.4.

$$k \propto (FC)(V_{el})^2 e^{-(\Delta G^\circ/2 + \lambda/4)/k_B T} \quad (2.3)$$

$$k = k^\circ e^{-\Delta G^\circ/2k_B T} \quad (2.4)$$

$$k^\circ \propto (FC)(V_{el})^2 e^{-\lambda/4k_B T} \quad (2.5)$$

Plotting k^0 *vs.* the pK_a of the pyridyl moiety (Figure 2.6) illustrates clearly the difference between the **HOArCH$_2$pyX** and **HOAr-pyX** reactions. For the oxidations of **HOArCH$_2$pyX** by amminium ions, changing the pyridine substituent has almost no effect on k°. The slope of a linear fit is within error of zero [0.04 (4), R^2 = 0.34] and the values of k° vary by a factor of 4.5 (Table 2.4) while the rate constants for these same reactions vary by a factor of 10^3. This indicates that the *FC*, V_{el}, and λ change only slightly with the pyridine substituent, so that all of the rate constants are well predicted by a single value of k° and the ΔG°_{CPET}. This is consistent with the tightness of the Brønsted plot in Figure 2.4 above. For the three reactions of **HOArCH$_2$pyX** with [Fe(4,7-Me$_2$phen)$_3$]$^{3+}$, there appears to be a small increase in k^0 with the pK_a of the base [slope = 0.07(5), R^2 = 0.88].

In contrast, there is a strong dependence of k° on pK_a for the reactions of **HOAr-pyX** with iron oxidants. First, it is immediately apparent that the reactions of [Fe(Me$_x$phen)$_3$]$^{3+}$ have four-to-ten times greater k° values of than reactions with [Fe(R$_2$bpy)$_3$]$^{3+}$, as discussed above. Once the two iron oxidants are plotted separately, as in Figure 2.6, it is evident that k° depends strongly on the electron donating character of the substituent. The apparent scatter in the Brønsted plot is due to this variation. The values of k° vary by a factor of approximately seven over the *ca.* five orders of magnitude in pyridine pK_a. Plots of log(k°) versus the pK_a of the pendent base for oxidations of **HOAr-pyX** are better fit by a linear trend, with slopes of 0.19(10) (R^2 = 0.79) and 0.24(4) (R^2 = 0.98) for the bpy and phen reactions, respectively. Substituent effects on k° account for as much as 50% of the variation in rate constants for the reactions of **HOAr-pyX** with [Fe(4,7-Me$_2$phen)$_3$]$^{3+}$, while changes in k° account for at most 5% of the variation in reactions of **HOArCH$_2$pyX** with the same oxidant.

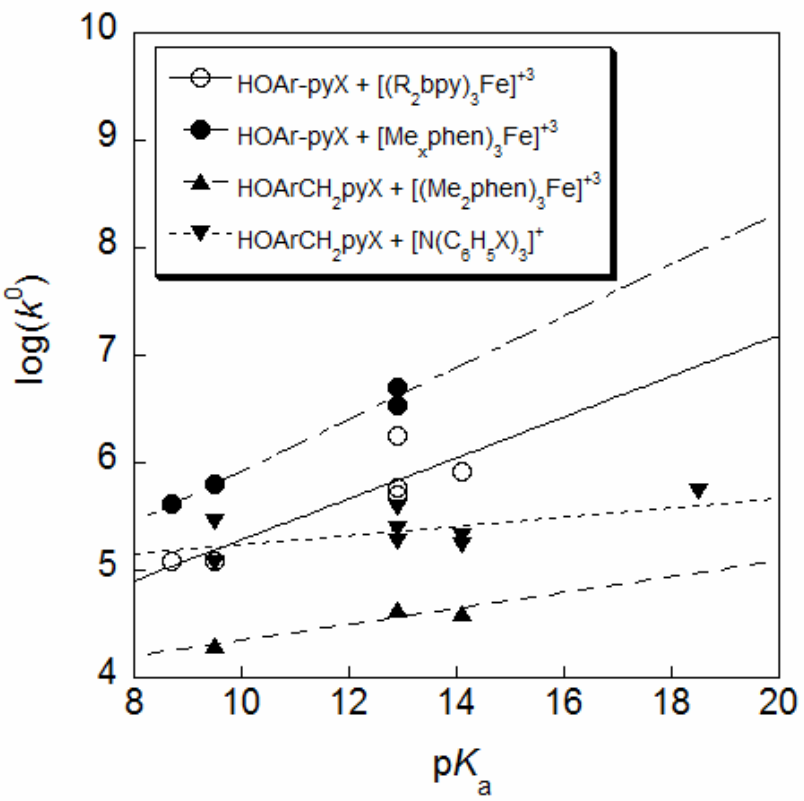

Figure 2.6: Intrinsic kinetic rate constants $k°$ (Table 2.4) plotted vs. the estimated pK_a of the pyridine (Table 2.1), for reactions of **HOArCH$_2$pyX** and **HOAr-pyX** with different oxidants. Values of log($k°$) are in M^{-1} s^{-1}; the estimated error on log($k°$) is ± 0.3.

2.2.4.2 Analysis of the origin of the substituent effects

Experimental values for the intrinsic barriers λ, the electronic couplings V_{el}, and Franck-Condon proton transfer terms *FC* are not readily accessible. However, insight may be gained by looking for correlations of $k°$ and computed values of λ with the available parameters d_{ON}, ν_{OH}, and δO*H* (Table 2.1).

For the series of reactions of the **HOAr-pyX** compounds, the $k°$ values are smaller for the more electron withdrawing substituents which have longer calculated d_{ON} and weaker hydrogen bonds as indicated by δO*H*. This is consistent with the expected trends for both the *FC* and λ parameters. The Franck-Condon term describes the overlap of initial and final proton vibrational wavefunctions, the proton tunneling component of the CPET process. It is known to be smaller for longer proton-donor acceptor tunneling

distances,[5,18,19] so the *FC* term would be expected to be smaller for molecules with longer ground state O···N distances d_{ON}. This is only an approximate argument, however, because the proton actually tunnels at configurations of the molecules that have smaller d_{ON} than the ground state.[5,19,21,60] Still, molecules with longer ground state d_{ON} should have higher reorganization energies to reach good tunneling configurations, so they should still have smaller $k°$.

Thus, for the **HOAr-pyX** compounds, there is an overall trend of smaller $k°$ values for compounds with weaker hydrogen bonds with their longer d_{ON} distances, stiffer O–H modes, and lower chemical shift hydroxyl protons. However, there is very little variation of $k°$ values for the non-conjugated **HOArCH$_2$pyX** compounds, despite the fact that their ranges of these parameters are larger than the ranges for the conjugated **HOAr-pyX** analogs. The ranges, for **HOArCH$_2$pyX** *vs.* **HOAr-pyX**, are 0.056 *vs.* 0.026 Å for d_{ON}, 171 *vs.* 120 cm^{-1} for ν_{OH}, and 1.87 *vs.* 1.44 for δOH. Thus the simple correlations of sCPET rates with structure and spectroscopy do not hold across all of the compounds discussed here. The **HOArCH$_2$pyX** compounds may behave differently because they have a hydrogen bond in a seven-membered ring, which is more flexible and allows a more linear OH···N structure. Calculations show that the energy to distort d_{ON} is smaller for **HOArCH$_2$pyX** than for **HOAr-pyX**.[53]

We have previously shown that DFT calculations of the inner-sphere reorganization energies λ_i qualitatively explained the two-order of magnitude faster sCPET reactions of **HOAr-py** versus **HOArCH$_2$py**.[37] Both inner-sphere and solvent reorganizations are involved in the intrinsic barrier λ, which is the energy to move the reactants into the geometry of the products. The solvent contributions are expected to be similar for all the reactions analyzed here because of the similar size of the phenol-pyridines. The calculations of λ_i(sCPET) followed Nelson's four-point method for ET reorganization energies,[61,62] with the proton transfer included in the reorganization energy, as we[37] and others[63] have done previously. The energies of the neutral molecule and radical cation (denoted E^0 and E^+, respectively) are calculated at the optimized neutral and cation geometries (denoted ng and cg, respectively), and λ_i(sCPET) is taken as the sum of the neutral and cation relaxation energies (denoted $E_{relax}{}^0$ and $E_{relax}{}^+$, repectively).[61] While quantitative accuracy is not achieved from this simple model,

which ignores the quantum mechanical character of the proton and the dynamic effects of promoting vibrations, its success for the parent compounds (X = H)[37] encouraged us to apply it to the substituted derivatives. DFT (B3LYP/6-311+G(d,p)) was used to calculate the four needed energies for each of **HOArCH$_2$pyX**, X = 4-CH_3, 5-CF_3, 4-NMe_2, and **HOAr-pyX**, X = 4-NO_2, 4-NMe_2 using a polarizable continuum solvent model (PCM) for acetonitrile (Table 2.5). The λ_i(sCPET) values for **HOAr-pyX** are calculated to be *ca.* 10 kcal mol^{-1} lower than those for **HOArCH$_2$pyX** (20-23 *vs.* 31-32 kcal mol^{-1}), corresponding to a difference in $k°$ of a factor of 70 ($k°$ is proportional to $\lambda/4k_BT$, eq. 2.5). The calculated λ_i(sCPET) do not vary significantly with substituent for either the **HOAr-pyX** or the **HOArCH$_2$pyX** series of compounds. This is consistent with the constant $k°$ for the **HOArCH$_2$pyX** series. The trend of slightly larger λ_i(sCPET) with more electron-donating substituents is also consistent with the observed trend in $k°$, but only accounts for variation in $k°$ of a factor of ~3, not the full difference of a factor of ~10 observed, so differences in λ_i(sCPET) with substituent appear to be only part of the origin of the substituent effect.

Table 2.5: Calculation of λ_i(sCPET) by four-point method.[a]

	X	E_{ng}^{0}	E_{ng}^{+}	E_{cg}^{0}	E_{cg}^{+}	E_{relax}^{0}	E_{relax}^{+}	λ_i
HOArCH$_2$pyX	4-NMe_2	0	134	9	111	9	23	32
	4-CH_3	0	135	13	117	13	18	31
	5-CF_3	0	137	17	123	17	14	31
HOAr-pyX[c]	4-NMe_2	0	133	6	116	6	17	23
	4-CH_3	0	135	8	121	8	14	22
	4-NO_2	0	139	10	129	10	10	20

[a]Energies in kcal/mol relative to E_{ng}^{0}, from calculations at the B3LYP/6-311+G(d,p)//B3LYP/6-31G(d,p) level of theory.

The DFT calculations show one other substantial difference between the **HOAr-pyX** and **HOArCH$_2$pyX** series of compounds. The HOMOs of **HOAr-pyX** and **HOArCH$_2$pyX**, and SOMOs of the corresponding radical cations, have most of their density in the π system of the phenol, but for **HOAr-pyX** significant electron density is

located on the pyridine. This is because the pyridine is in conjugation with the phenol. More electron donating substituents may slightly increase the density of the HOMO and SOMO on the pyridine ring. For instance, the HOMO of **HOAr-pyNMe$_2$** has 8.8% pyridine contribution by Mulliken population analysis, compared to 7.3% for **HOAr-pyNO$_2$** (Figure 2.7).[64] If the pathway for electron transfer is *via* the pyridine, this suggests that more electron donating substituents would be expected to lead to increased electronic coupling (larger V_{el}), and thereby increase $k°$ as is observed experimentally. In contrast, the DFT calculated HOMO and SOMO orbitals for **HOArCH$_2$pyX** (X = 4-CH$_3$, 5-CF$_3$, 4-NMe$_2$) have relatively little density on the pyridine ring. Changing the substituent on the pyridine ring in **HOArCH$_2$pyX** has almost no effect on the HOMO or SOMO, which are localized on the phenol ring. For example, even with X = 4-NMe$_2$, only 1.5% of the electron density of the HOMO is on the pyridine (Figure 2.7). This would be expected to lead to small differences in V_{el} with substituent and therefore small differences in $k°$, consistent with experiment. While accurate calculations of V_{el} would require a more thorough theoretical analysis, the substituent effects on the phenol molecular orbitals seem likely to be a part of the origin of the differences between the conjugated and non-conjugated systems. However, the differences in orbital character with substituents are subtle, and it seems unlikely that these differences entirely account for the observed substituent effect. There is also likely a substituent effect on the proton transfer coordinate that has not been captured by these calculations.

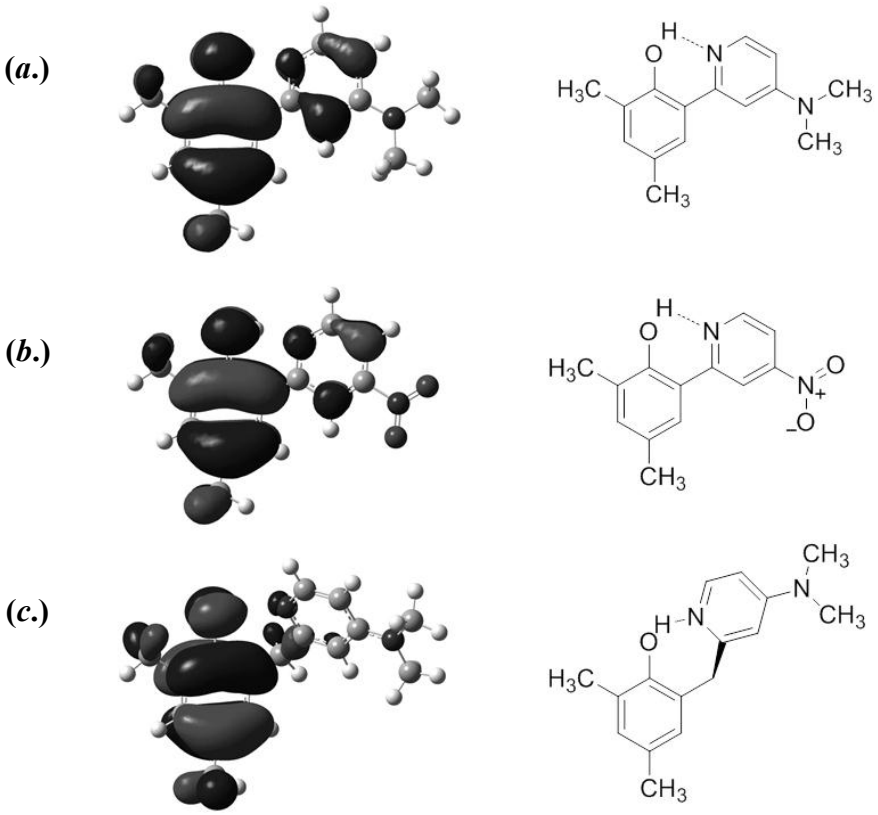

Figure 2.7: Kohn-Sham molecular orbital diagrams for the HOMOs of (*a.*) **HOAr-pyNMe$_2$**, (*b.*) **HOAr-pyNO$_2$**, and (*b.*) **HOArCH$_2$pyNMe$_2$**.

2.3 Conclusions

Studies of phenols with pendent substituted pyridines and –CH$_2$pyridines, including the kinetics of their oxidations, reveal new features of separated concerted proton-electron transfer (sCPET). The substituent groups vary the pK_a's of the pyridinyl groups by almost 10 pK_a units, causing substantial differences in the phenol-pyridine hydrogen bond strength, the proton transfer distance, and the proton-coupled oxidation potential. With the methylene linker between the phenol and the pyridine, there is little electronic communication between the two sites and they act almost as separate molecules, as evidenced by the –51(2) mV per unit change in the estimated pK_a of the substituted pyridine. The rate constants for oxidation of **HOArCH$_2$pyX** vary primarily with the changes in ΔG^o, as has been found in related studies of phenol-imidazoles[39] and

aqueous phenol oxidations.[29] There are, however, small differences in the effects of varying $\Delta G°$ via changes in the oxidant *vs.* the base, as indicated by different slopes in Brønsted plots of $\log(k_{sCPET})$ *vs.* $\log(K_{sCPET})$. Much larger substituent effects are observed for the **HOAr-pyX** series of compounds, in which the pyridine and phenol are in conjugation. The importance of this conjugation is evident in the smaller dependence of oxidation potential on pyridyl pK_a (–48(1) mV/pK_a), the stronger hydrogen bonds, and the nature of the frontier molecular orbitals. Extracting an intrinsic rate constant $k°$ by extrapolating to $\Delta G° = 0$ shows that substituents have a substantial effect on the intrinsic reactivity, with electron donating groups leading to faster reactions. Surprisingly, while the **HOAr-pyX** compounds show greater sensitivity of their intrinsic sCPET rate constants to substituents, the **HOArCH$_2$pyX** series shows a greater effect of substituents on ground state properties such as the proton-donor acceptor distance and the phenol proton chemical shift. The substituent effects in the two systems have been analyzed in the context of sCPET rate theory. Variations in electronic couplings V_{el} with substituent appear to be significant for reactions of the **HOAr-pyX** compounds.

2.4 Experimental

2.4.1 General Considerations

Unless otherwise noted, reagents were purchased from Aldrich, solvents from Fischer, and deuterated solvents from Cambridge. Acetonitrile was purchased from Burdick and Jackson (low-water brand) and stored in an argon-pressurized stainless steel drum plumbed directly into a glovebox. *n*-BuLi (1.6M in hexanes) was purchased from Acros. CD_3CN was dried by stirring over CaH_2 overnight, then distilled onto P_2O_5, followed by another distillation from CaH_2, and was stored in a glove box. The **HOAr-pyX** compounds were prepared as described previously.[7,41] The iron-bipyridyl and phenanthroline complexes were synthesized according to literature procedures[65] and were used as PF_6^- salts. 3,5-Di-tert-butyl-2-(benzyloxymethyl)benzaldehyde[66] and 2-bromo-5-trifluoromethylpyridine[67] were synthesized according to literature procedures. Triarylamminium hexafluorophosphate salts were prepared from the corresponding amines as described previously.[7] ^{1}H NMR and ^{13}C NMR spectra were recorded on Bruker AV300 or AV500 spectrometers at ambient temperatures; chemical shifts are

reported relative to TMS in ppm by referencing to the residual solvent signals. Column chromatography used silica gel as the stationary phase. Mass spectrometry was performed on a Bruker Esquire Ion Trap Mass Spectrometer using electrospray ionization and on a Hewlett Packard 5971A Gas Chromatograph/Mass Spectrometer using electron impact ionization, and are reported as m/z with relative abundance in parentheses when multiple peaks were observed.

2.4.2 Synthesis

2.4.2.1 BnOArCH(OH)pyCH$_3$

(2-(benzyloxy)-3,5-di-tert-butylphenyl)(4-methylpyridin-2-yl)methanol

n-Butyllithium (1.6 M in hexanes, 0.78 mL, 1.3 mmol) was added dropwise to a solution containing 2-bromo-4-methylpyridine (0.14 mL, 1.6 g/mL, 1.3 mmol) in anhydrous toluene (1 mL) at -78°C in an oven-dried round bottom flask. The yellow-brown reaction mixture was stirred at this temperature for 2 hr, after which a solution of 2-(benzyloxy)-3,5-di-tert-butylbenzaldehyde (0.41 g, 1.3 mmol) in anhydrous toluene (1 mL) was added dropwise with stirring at -78°C. The reaction mixture was stirred at -78°C for 1 hr, then warmed to 0°C and stirred for 1 hr, turning a deep red-brown on warming. After 1 hr, the reaction was quenched with H_2O (10 mL), and CH_2Cl_2 (20 mL) was added yielding a biphasic mixture. The organic layer was washed with H_2O (3 x 20 mL), followed by brine, and dried over $MgSO_4$. The solvent was removed on the rotavap, leaving a yellow oil. Column chromatography (3/1 v/v hexanes/ethyl acetate) yielded (2-(benzyloxy)-3,5-di-tert-butylphenyl)(4-methylpyridin-2-yl)methanol (0.16 g, 0.37 mmol, 28% yield) as a white solid. ^{1}H NMR ($CDCl_3$): δ 8.39 (d, *J* = 6 Hz, 1 H), 7.56-6.87 (m, 9 H), 6.15 (s, 1 H), 5.52 (br s, 1 H), 5.26 (d, *J* = 12 Hz, 1 H), 5.20 (d, *J* = 12 Hz, 1 H), 2.24 (s, 3 H), 1.48 (s, 9 H), 1.20 (s, 9 H). ^{13}C{^{1}H} NMR ($CDCl_3$): δ 161.1, 154.2, 147.8, 146.9, 146.2, 141.9, 138.0, 136.4, 128.4, 127.5, 127.0, 124.2, 124.1, 123.3, 122.3, 77.2, 68.5, 35.5, 34.6, 31.4, 21.1 (the two *t*-Bu methyl resonances are overlapping). MS (ESI, *m/z*) 418 (M+H).

2.4.2.2 BnOArCH(OAc)pyCH$_3$

(2-(benzyloxy)-3,5-di-tert-butylphenyl)(4-methylpyridin-2-yl)methylacetate

The alcohol **BnOArCH(OH)pyCH$_3$** (0.16 g, 0.37 mmol) was dissolved in 5 mL of pyridine and acetic anhydride (1:1) and heated to 100 °C under N_2 for 30 min. The volatiles were removed under vacuum yielding a yellow oil. This oil was dissolved in hexane, and the remaining volatiles were removed on the rotavap, yielding the product (2-(benzyloxy)-3,5-di-tert-butylphenyl)(4-methylpyridin-2-yl)methyl acetate (0.17g, 0.37 mmol, 100% yield) as a white solid. ^{1}H NMR ($CDCl_3$): δ 8.43 (d, *J* = 6 Hz, 1 H), 7.55-6.95 (m, 9 H) 5.18 (d, *J* = 12 Hz, 1 H), 5.10 (d, *J* = 12 Hz, 1 H), 2.26 (s, 3 H), 2.19 (s, 3 H) 1.43 (s, 9 H), 1.28 (s, 9 H). ^{13}C{^{1}H} NMR ($CDCl_3$): δ 170.2 (O*C*(O)CH_3), 158.9, 153.7, 149.1, 147.5, 146.1, 142.2, 137.7, 132.1, 128.4 , 127.6, 127.2, 125.0, 124.7, 123.4, 122.5, 77.2, 72.7, 35.6, 34.6, 31.4, 21.3, 21.1 (the two *t*-Bu methyl resonances are overlapping). MS (ESI, *m/z*) 461 (M+H).

2.4.2.3 HOArCH$_2$pyCH$_3$

2,4-di-*tert*-butyl-6((4-methylpyridin-2-yl)methyl)phenol

A solution **BnOArCH(OAc)pyCH$_3$** (0.16 g, 0.37 mmol) in EtOH (30 mL) containing Et_3N (0.10 mL, 0.68 mmol) was agitated in a Parr apparatus under H_2 (50 psi) in the presence of Pd(C) (10 mol%). After 24 hr the reaction was filtered through Celite, and volatiles were removed on the rotavap. Column chromatography (3/1 v/v hexanes/ethyl acetate) yielded 2,4-di-*tert*-butyl-6((4-methylpyridin-2-yl)methyl)phenol (0.10 g, 0.32 mmol, 86% yield) as a white solid. ^{1}H NMR (CD_3CN): δ 11.31 (s, 1 H), 8.30 (d, *J* = 6 Hz, 1 H), 7.29-7.09 (m, 4 H,), 4.00 (s, 2 H), 2.35 (s, 3 H), 1.39 (s, 9 H), 1.26 (s, 9 H). ^{13}C{^{1}H} NMR (CD_3CN): δ 160.9, 152.8, 149.5, 147.1, 141.8, 127.4, 126.4, 124.7, 123.5, 122.7, 122.6, 41.8, 35.0, 34.0, 31.5, 29.7, 21.0. MS (ESI, *m/z*) 312 (M+H).

2.4.2.4 BnOArCH(OH)pyCF$_3$

(2-(benzyloxy)-3,5-di-tert-butylphenyl)(5-trifluoromethylpyridin-2-l)-methanol

n-Butyllithium (1.6 M in hexanes, 0.63 mL) was added dropwise to a solution containing 2-bromo-5-trifluoromethylpyridine (0.250 g, 1.1 mmol) in anhydrous toluene (1 mL) at -78°C in an oven-dried round bottom flask. The yellow-brown reaction mixture was stirred at this temperature for 2 hr, after which a solution of 2-(benzyloxy)-3,5-di-tert-butylbenzaldehyde (0.32 g, 1.0 mmol) in anhydrous toluene (1 mL) was added dropwise with stirring at -78°C. The reaction mixture was stirred at -78°C for 1 hr, then warmed to 0°C and stirred for 1 hr, turning a deep red-brown on warming. After 1 hr, the reaction was quenched with H_2O (10 mL), and CH_2Cl_2 (20 mL) was added yielding a biphasic mixture. The organic layer was washed with H_2O (3 x 20 mL), followed by brine, and dried over $MgSO_4$. The solvent was removed on the rotavap, leaving a yellow oil. Removal of volatiles under reduced pressure yielded the desired product as an orange solid (0.36 g, 76% yield). ^{1}H NMR ($CDCl_3$): δ 8.80 (s, 1 H), 7.82-7.20 (m, 10 H), 5.18 (d, *J* = 12 Hz, 1 H), 5.10 (d, *J* = 12 Hz, 1 H), 1.47 (s, 9 H), 1.22 (s, 9 H), ^{13}C{^{1}H} NMR ($CDCl_3$): δ 165.3, 154.0, 146.7, 144.5 (q, *J* = 4 Hz), 142.4, 137.7, 135.3, 133.8 (q, *J* = 4 Hz), 128.5, 127.6, 126.7, 125.3 (q, *J* = 33 Hz), 124.7, 123.9, 121.5, 77.2, 69.4, 35.6, 34.6, 31.4 (the two *t*-Bu methyl resonances are overlapping, *C*F_3 not visible due to ^{19}F coupling).

2.4.2.5 BnOArCH(OAc)pyCF$_3$

(2-(benzyloxy)-3,5-di-tert-butylphenyl)(5-trifluoromethylpyridin-2-yl)methylacetate

The alcohol **BnOArCH(OH)pyCF$_3$** (0.36 g, 0.76 mmol)was dissolved in 5 mL of pyridine and acetic anhydride (1:1) and heated to 100 °C under N_2 for 30 min. The volatiles were removed under vacuum yielding a yellow oil. This oil was dissolved in hexane, and the remaining volatiles were removed on the rotavap. Column chromatography (6/1 v/v hexanes/ethyl acetate) yielded (2-(benzyloxy)-3,5-di-tert-butylphenyl)(5-trifluoromethylpyridin-2-yl)methylacetate as a white solid (0.24 g, 55% yield). ^{1}H NMR ($CDCl_3$): δ 8.78 (s, 1 H), 7.85-7.05 (m, 9 H), 6.26 (s, 1 H), 5.23 (d, *J* = 12 Hz, 1 H), 5.15(d, *J* = 12 Hz, 1 H), 2.20 (s, 3 H), 1.44 (s, 9 H), 1.28 (s, 9 H), ^{13}C{^{1}H}

NMR ($CDCl_3$): δ 170.1, 163.1, 153.7, 146.5, 146.2 (q, *J* = 4 Hz), 142.7, 137.4, 133.7 (q, *J* = 4 Hz), 131.3, 128.5, 127.8, 127.1, 124.4, 121.0 (one aryl *C* not visible), 77.2, 72.4, 35.7, 34.7, 31.4, 21.2 (the two *t*-Bu methyl resonances are overlapping, *C*F_3 not visible due to ^{19}F coupling).

2.4.2.6 HOArCH$_2$pyCF$_3$

2,4-di-*tert*-butyl-6((5-trifluoromethylpyridin-2-yl)methyl)phenol

A solution **BnOArCH(OAc)pyCF$_3$** (0.85 g, 0.17 mmol) in EtOH (30 mL) containing Et_3N (0.05 mL, 0.3 mmol) was agitated in a Parr apparatus under H_2 (50 psi) in the presence of Pd(C) (10 mol%). After 24 hr the reaction was filtered through Celite, and volatiles were removed on the rotavap. Column chromatography (5% ethyl acetate/hexanes) yielded 2,4-di-*tert*-butyl-6((5-trifluoromethylpyridin-2-l)methyl)phenol as a yellow solid (0.60 mg, 100% yield). ^1H NMR (CD_3CN): δ 10.19 (s, 1 H), 8.82 (s, 1 H), 8.08 (d, *J* = 6 Hz, 1 H), 7.64 (d, *J* = 6 Hz, 1 H), 7.19 (d, *J* = 9 Hz, 1 H), 7.16 (d, *J* = 9 Hz, 1 H), 4.16 (s, 2 H), 1.40 (s, 9 H), 1.26 (s, 9 H). $^{13}C\{^1H\}$ NMR (CD_3CN): δ 166.7, 153.1, 146.1 (q, *J* = 4 Hz), 143.3, 138.6 (q, *J* = 4 Hz), 127.1, 126.1, 125.5 (q, *J* = 33 Hz), 123.9, 123.8, 123.5, 41.6, 35.7, 34.8, 31.8, 30.0, (*C*F_3 not visible due to ^{19}F coupling). MS (ESI, *m/z*) 366(M+H).

2.4.2.7 BnOArCH(OH)pyNMe$_2$

(2-(benzyloxy)-3,5-di-tert-butylphenyl)(4-dimethylaminopyridin-2-yl)methanol

4-dimethylaminopyridine was used rather than 2-bromo-4-dimethylaminopyridine, which is not readily available. *n*-butyllithium (1.6 M in hexanes, 1.25 mL, 2.0 mmol) was added dropwise to a solution containing dimethylaminoethanol (0.100 mL, 0.88 g/mL, 1.0 mmol) in anhydrous toluene (1 mL) at -5°C and stirred for 20 min. 4-dimethylaminopyridine (0.061 g, 0.5 mmol) was added as a solid, and stirred at -5°C for 1 hour to generate the *ortho*-lithiated 4-dimethylaminopyridine. A solution of 2-(benzyloxy)-3,5-di-tert-butylbenzaldehyde (0.32 g, 1.0 mmol) in anhydrous toluene (1 mL) was added dropwise with stirring at -78°C. The reaction mixture was stirred at -78°C for 1 hr, then warmed to 0°C and stirred for 1 hr, turning a deep red-brown on

warming. After 1 hr, the reaction was quenched with H_2O (10 mL), and CH_2Cl_2 (20 mL) was added yielding a biphasic mixture. The organic layer was washed with H_2O (3 x 20 mL), followed by brine, and dried over $MgSO_4$. The solvent was removed on the rotavap, leaving a yellow oil. Column chromatography (5% methanol/DCM) yielded 2-(benzyloxy)-3,5-di-tert-butylphenyl)(4-dimethylaminopyridin-2-yl)methanol as a tan solid (0.084 g, 38% yield) ^{1}H NMR ($CDCl_3$): δ 8.14 (d, *J* = 8 Hz, 1 H), 7.56-7.22 (m, 8 H) 6.37, (s, 1H), 6.10 (s, 1 H), 5.29 (d, *J* = 12 Hz, 1 H,), 5.21 (d, *J* = 12 Hz, 1 H), 2.88 (s, 6 H), 1.47 (s, 9 H), 1.24 (s, 9 H,).

2.4.2.8 BnOArCH(OAc)pyNMe$_2$

(2-(benzyloxy)-3,5-di-tert-butylphenyl)(4-dimethylaminopyridin-2-yl)methylacetate

The alcohol **BnOArCH(OH)pyNMe$_2$** (0.038 g, 0.85 mmol) was dissolved in 5 mL of pyridine and acetic anhydride (1:1) and heated to 100 °C under N_2 for 30 min. The volatiles were removed under vacuum yielding a yellow oil. This oil was dissolved in hexane, and the remaining volatiles were removed on the rotavap, yielding **(2-**(benzyloxy)-3,5-di-tert-butylphenyl)(4-dimethylaminopyridin-2-yl)methylacetate as an amber oil (0.042 g, 100% yield). ^{1}H NMR ($CDCl_3$): δ 8.20 (d, *J* = 6 Hz, 1 H), 7.57-7.21 (m, 8 H), 6.38 (s, 1H), 5.17 (d, *J* = 12 Hz, 1 H), 5.09 (d, *J* = 12 Hz, 1 H), 2.85 (s, 6 H), 2.19 (s, 3 H) 1.43 (s, 9 H), 1.30 (s, 9 H).

2.4.2.9 HOArCH$_2$pyNMe$_2$

2,4-di-*tert*-butyl-6((4-dimethylaminopyridin-2-yl)methyl)phenol

A solution **BnOArCH(OAc)pyNMe$_2$** (0.042 g, 0.085 mmol) in EtOH (30 mL) containing Et_3N (0.22 mL, 1.5 mmol) was agitated in a Parr apparatus under H_2 (50 psi) in the presence of Pd(C) (10 mol%). After 24 hr the reaction was filtered through Celite, and volatiles were removed on the rotavap. Column chromatography (3/1 v/v hexanes/ethyl acetate) yielded 2,4-di-*tert*-butyl-6((4-dimethylaminopyridin-2-yl)methyl)phenol as a white solid (0.022 g, 76% yield). ^{1}H NMR (CD_3CN): δ 12.06 (s, 1 H), 7.98 (d, *J* = 4 Hz, 1 H), 7.14 (d, *J* = 2 Hz, 1 H), 7.10 (d, *J* = 2 Hz, 1 H), 6.63 (d, *J* = 2 Hz, 1 H), 6.43 (dd, *J* = 4, 2 Hz, 1 H), 3.89 (s, 2 H), 2.98 (s, 6 H), 1.39 (s, 9 H), 1.26 (s, 9

H). $^{13}C\{^{1}H\}$ NMR (CD_3CN): δ 162.1, 156.6, 154.2, 147.8, 142.0, 138.2, 128.4, 125.8, 123.1, 105.5, 105.3, 42.5, 39.4, 35.6, 34.7, 31.8, 30.0. MS (ESI, *m/z*) 419(M+H).

2.4.3 X-ray Crystallography

X-ray quality crystals were grown by slow evaporation of hexane solvent. Crystals were mounted on glass capillaries with Paratone-N oil (Hampton Research) and frozen immediately in a cold nitrogen gas stream at 130 K (208 K for **HOAr-pyNO$_2$**). Data were collected on an Enraf-Nonius KappaCCD diffractometer (Bruker Kappa APEXII CCD for **HOAr-pyNO$_2$**) with Mo-Kα radiation (λ = 0.71073 Å) utilizing both Φ and Ω scans. Crystal-to-detector distance was 30 mm (60 mm for **HOAr-pyNO$_2$**). The data were integrated and scaled with hkl-2000 or hkl-SCALEPACK[68] (Bruker SAINT and SADABS for **HOAr-pyNO$_2$**).[69] These programs apply a multiplicative correction factor (*S*) to the observed intensities (*I*) and has the following form: $S = (e^{-2B(\sin^2\theta)/\lambda^2})/\text{scale}$. *S* is calculated from the scale and B factor, which is determined for each frame and is then applied to *I* to give the corrected intensity (I_{corr}). Solution by direct methods (SIR97)[70] produced a complete heavy atom phasing model consistent with the proposed structure and refined by full-matrix least-squares based on F^2 (SHELXL-97).[71,72] All nonhydrogen atoms were refined anisotropically. All hydrogen atoms were placed by using a riding model, except for hydroxyl hydrogen atoms in the structures of **HOAr-pyNO$_2$**, **HOAr-pyNMe$_2$,** and **HOAr-pyCH$_3$**. Hydroxyl hydrogen atoms for these compounds were located from the Fourier difference map and their positions were refined isotropically. Collection and refinement data are given in Table 2.2.

2.4.4 Electrochemistry

Cyclic voltammetry (CV) was performed under N_2 using an E2 Epsilon apparatus (BASi) equipped with Pt disc or glassy carbon working electrode (3.0 mm dia), platinum wire auxiliary electrode, and $Ag/Ag(NO)_3$ (0.01 M) reference electrode. CV was carried out in acetonitrile with 0.1 M [*n*-Bu_4N][PF_6] as supporting electrolyte with *ca.* 5 mM substrate. [*n*-Bu_4N][PF_6] was recrystallized three times from EtOH and dried *in vacuo* for two days at 110 °C prior to use. Ferrocene was added as an internal standard and all potentials are reported vs. the $Cp_2Fe^{+/0}$ couple.

2.4.5 Kinetics

All kinetics experiments were performed at room temperature in low-water acetonitrile using an OLIS USA stopped-flow instrument with an OLIS rapid scanning monochromator and UV-vis detector. Kinetic data were analyzed using SpecFit^{TM} global analysis software,[56] and were fit to opposing second order kinetics. Kinetic experiments using the iron oxidants were run in MeCN with 0.1 M NBu_4PF_6 because the potentials of these compounds vary with ionic strength.[73-75]

2.4.6 DFT Calculations

All calculations were performed with *Gaussian03*.[76] In all cases, *tert*-butyl groups were replaced with methyl groups to save computational time. All optimized geometries were confirmed to be local minima by vibrational analysis (NImag = 0). Four-point analysis of λ was performed following reference.[61] Optimizations of the neutral and cation geometries of **HOArCH$_2$pyX** and **HOAr-pyX** were performed at the B3LYP/6-31G(d,p) level of theory. Single point energies calculated for determination of λ on these geometries were performed at the B3LYP/6-311+G(d,p) level of theory with acetonitrile solvent modeled by a polarizable continuum model (PCM). In all cases, geometries corresponding to the non-proton-transferred radical cations ($[HOAr\text{-}B]^{\bullet+}$) or the zwitterions ($^{-}OAr\text{-}BH^{+}$) are not local minima. Energies are not corrected for zero-point vibrational energy.

2.5 Notes to Chapter 2

(1) Hammes-Schiffer, S. *Chem. Rev.* **2010**, *110*, 6937.

(2) Huynh, M. H. V.; Meyer, T. J. *Chem. Rev.* **2007**, *107*, 5004.

(3) Mayer, J. M. *Annu. Rev. Phys. Chem.* **2004**, *55*, 363.

(4) Hodgkiss, J. M.; Rosenthal, J.; Nocera, D. G.; In *Hydrogen Transfer Reactions*, Hynes, J. T.; Klinman, J. P.; Limbach, H. -H.; Schowen, R. L., Eds.; Wiley-VCH: Weinheim, 2007, pp. 503.

(5) Cukier, R. I.; Nocera, D. G. *Annu. Rev. Phys. Chem.* **1998**, *49*, 337.

(6) Costentin, C. *Chem. Rev.* **2008**, *108*, 2145.

(7) Rhile I. J.; Markle T. F.; Nagao H.; DiPasquale A. G.; Lam O. P.; Lockwood M. A.; Rotter K.; Mayer J. M. *J. Am. Chem. Soc.* **2006**, *128*, 6075.

(8) The term 'separated CPET' emphasizes that these reactions are distinct from hydrogen atom transfer reactions (HAT) because of the separation of the e^- and H^+. Mayer, J. M. *Acc. Chem. Res.* **2011**, *44*, 36.

(9) Stubbe, J.; van der Donk, W. *Chem. Rev.* **1998,** *98*, 705.

(10) Pesavento, R. P.; van der Donk, W. A. *Adv. Prot. Chem.* **2001**, *58*, 317.

(11) Kuhne, H. ; Brudvig, G. W. *J. Phys. Chem. B* **2002**, *106*, 8189.

(12) Umena, Y.; Kawakami, K.; Shen, J.-R.; Kamiya, N. *Nature* **2011**, *473*, 55.

(13) McEvoy, J. P.; Brudvig, G. W. *Chem. Rev.* **2006**, *106*, 4455.

(14) Tommos, C. ; Babcock, G. T. *Acc. Chem. Res.* **1998,** *31*, 18.

(15) Renger, G. *Biochim. Biophys. Acta* **2012** DOI: 10.1016/j.bbabio.2012.02.005

(16) Hays, A-M. A.; Vassiliev, I. R.; Golbeck, J. H.; Debus, R. J. *Biochemistry* **1998**, *37*, 11352.

(17) Meyer, T. J.; Huynh, M. H. V.; Thorp, H. H. *Angew. Chem. Int. Ed.* **2007**, *46*, 5284.

(18) Cukier, R. I. *J. Phys. Chem. B* **2002**, *106*, 1746.

(19) Hammes-Schiffer, S.; Stuchebrukhov, A. A. *Chem. Rev.* **2010**, *110*, 6939.

(20) Hammes-Schiffer, S. *Acc. Chem. Res.* **2001**, *34*, 273.

(21) Kuznetsov, A. M.; Ulstrup, J. *Can. J. Chem.* **1999**, *77*, 1085.

(22) Tishchenko, O.; Truhlar, D. G.; Ceulemans, A.; Nguyen, M. T. *J. Am. Chem. Soc.* **2008**, *130*, 7000.

(23) Stuchebrukhov, A. A. "Electron transfer reactions coupled to proton translocation in proteins. Computational studies or redox driven proton pumps, cytochrome c oxidase, and biological energy transduction," in: *Energy, Heat and Signal Flows in Proteins*, D. Leitner and J. Straub Eds., Taylor and Francis/CRC Press, 2009, Chapter 4, 71-106.

(24) Marcus, R. A.; Sutin, N. *Biochim. Biophys. Acta* **1985**, *811*, 265.

(25) Barbara, P. F.; Meyer, T. J.; Ratner, M. A. *J. Phys. Chem.* **1996**, *100*, 13148.

(26) Bíczók, L.; Gupta, N.; Linschitz, H. *J. Am. Chem. Soc.* **1997**, *119*, 12601.

(27) Bíczók, L.; Linschitz, H. *J. Phys. Chem.* **1995**, *99*, 1843–1845.

(28) Irebo T.; Reece S. Y.; Sjödin M.; Nocera D.G.; Hammarström L. *J. Am. Chem. Soc.* **2007,** *129*, 15462.

(29) Fecenko, C. J.; Thorp, H. H.; Meyer, T. J. *J. Am. Chem. Soc.* **2007**, *129*, 15098.

(30) Irebo, T.; Johansson, O.; Hammarström, L. *J. Am. Chem. Soc.* **2008**, *130*, 9194.

(31) Costentin, C.; Robert, M.; Savéant, J. -M. *J. Am. Chem. Soc.* **2007**, *129*, 5870.

(32) Ishikita, H.; Soudackov, A. V.; Hammes-Schiffer, S. *J. Am. Chem. Soc.* **2007**, *129*, 11146.

(33) Song, N.; Stanbury, D. M. *Inorg. Chem.* **2008**, *47*, 11458.

(34) Sjödin, M.; Irebo, T.; Utlas, T. E.; Lind, J.; Merényi, G.; Åkermark, B.; Hammarström, L. *J. Am. Chem. Soc.* **2006**, *128*, 13076.

(35) Sjödin, M.; Styring, S.; Wolpher, H.; Xu, Y.; Sun, L.; Hammarström, L. *J. Am. Chem. Soc.* **2005**, *127*, 3855.

(36) Reece, S. Y.; Nocera, D. G. *J. Am. Chem. Soc.* **2005**, *127*, 9448.

(37) Markle, T. F.; Mayer, J. M. *Angew. Chem. Int. Ed.* **2008**, *47*, 738.

(38) Markle, T. F.; Rhile, I. J.; Mayer, J. M. *J. Am. Chem. Soc.* **2011**, *133*, 17341.

(39) Markle, T. F.; Rhile, I. J.; Mayer, J. M.; DiPasquale, A. G. *Proc. Nat. Acad. Sci. USA* **2008**, *105*, 8185.

(40) Schrauben, J. N.; Cattaneo, M.; Day, T. C.; Tenderholdt, A. L.; Mayer, J. M. *unpublished results.*

(41) Markle, T. F. *Concerted Proton-Electron Transfers in the Oxidation of Hydrogen Bonded Phenol-Base Compounds* Ph.D. Thesis, University of Washington, Seattle, Washington, **2009**.

(42) Jeffrey, G. A. in *An Introduction to Hydrogen Bonding*; Oxford Univ Press: NewYork, 1997, pp 12, 228.

(43) Shan, S.-O.; Loh, S.; Herschlag, D. *Science* **1996**, *272*, 97.

(44) Not all of the pK_as of the pyridines in this study are known in acetonitrile. For consistency, we have estimated the acetonitrile pK_as using the values of the aqueous pK_as from ref. 45-50 and correcting them according to the correlational relationship pK_a(MeCN) = 1.25 × pK_a(H2O) + 6.34 derived in Ref. 45. The values estimated by this method are in good agreement with the experimental acetonitrile pK_a values available in Ref. 45, 46, and 51.

(45) Augustin-Nowacka, D.; Chmurzyñski, L. *Anal. Chim. Acta* **1999**, *381*, 215.

(46) Kaljurand, K.; Kütt, A.; Sooväli, L.; Rodima, T.; Mäemets, V.; Leito, I.; Koppel, I. A. *J. Org. Chem.* **2005**, *70*, 1019.

(47) Perrin, D. D.; Dempsey, B.; Serjeant, E. P. *pKa Prediction for Organic Acids and Bases.* Chapman and Hall: New York, 1981, pp. 108-139.

(48) Chrystiuk, E.; Williams, A. *J. Am. Chem. Soc.* **1987**, *109*, 3040.

(49) Perrin, D. D. *Dissociation Constants of Organic Bases in Aqueous Solution.* Butterworths: London, 1965.

(50) The pK_a of 3-trifluomethylpyridinium is estimated as 2.5 from the Hammet parameter, following Clark, J.; Perrin, D. D. *Quart. Rev. (London)* **1964**, *18*, 295.

(51) Izutsu, K. *Acid-Base Dissociation Constants in Dipolar Aprotic Solvents*, IUPAC Chemical Data Series No. 35; Blackwell Scientific Publications: Boston, MA, 1990, pp 17-35.

(52) ν(OH)DFT, corr = [ν(OH)DFT – 159.5] × 0.9904 from Korth, H.-G.; de Heer, M. I.; Mulder, P. J. *J. Phys. Chem. A* **2002**, *106*, 8779.

(53) Markle, T. F.; Tenderholt, A. L.; Mayer. J. M. *J. Phys. Chem. B* **2012**, *116*, 571.

(54) Costentin, C.; Robert, M.; Savéant, J. -M. *J. Am. Chem. Soc.* **2007**, *129*, 9953.

(55) Bordwell, F. G.; Cheng, J. P. *J. Am. Chem. Soc.* **1991**, *113*, 1736.

(56) Binstead, R. A.; Zuberbühler, A.D.; Jung, B. *Specfit™,* version 3.0.36 (32-bit Windows); Spectrum Software Associates: Chapel Hill, NC, 2004.

(57) Graige, M. S.; Paddock, M. L.; Bruce, J. M.; Feher, G.; Okamura, M. Y. *J. Am. Chem. Soc.* **1996**, *118*, 9005.

(58) Lee, I.-S. H.; Chow, K.-H.; Kreevoy, M. M. *J. Am. Chem. Soc.* **2002**, *124*, 7755 and references therein.

(59) Wherland, S. *Coord. Chem. Rev.* **1993**, *123*, 169.

(60) Klinman, J. P. *Biochim Biophys Acta* **2006**, *1757*, 981.

(61) Nelsen, S. F.; Blackstock, S. C.; Kim, Y. *J. Am. Chem. Soc.* **1987**, *109*, 677.

(62) Nelsen, S. F.; Weaver, M. N.; Pladziewicz, J. R.; Ausman, L. K.; Jentzsch, T. L.; O'Konek, J. J.; *J. Phys. Chem. A* **2006**, *110*, 11665.

(63) Wander, M. C. F.; Kubicki, J. D.; Clark, A. E.; Schoonen, M. A. A. *J. Phys. Chem. A* **2009**, *113*, 1020.

(64) Tenderholt, Adam L. *QMForge*, Version 2.1. Stanford University, Stanford, CA, USA.

(65) DeSimone, R. E.; Drago, R. S. *J. Am. Chem. Soc.* **1970,** *92*, 2343.

(66) Ryu, H.-K.; Kim, W.-Y.; Nahm, K. S.; Hahn, Y. B.; Lee, Y. S.; Lee, C. *Synthetic Metals.* **2002**, *128*, 21.

(67) Cottet, F.; Marull, M.; Lefebvre, O.; Schlosser, M. *Eur. J. Org. Chem.* **2003**, 1559.

(68) Z. Otwinowski and W. Minor, "Processing of X-ray Diffraction Data Collected in Oscillation Mode", Methods in Enzymology, Volume 276: Macromolecular Crystallography, part A, p.307-326, 1997,C.W. Carter, Jr. & R. M. Sweet, Eds., Academic Press (New York).

(69) Bruker APEX2 (Version 2.1-4), SAINT (version 7.34A), SADABS (version 2007/4), BrukerAXS Inc, Madison, Wisconsin, USA, 2007.

(70) Altomare A, Cascarano G, Giacovazzo C, Guagliardi A. *J. Appl. Cryst.* **1993**, *26*, 343.

(71) Sheldrick G. M. SHELXL-97, Program for the Refinement of Crystal Structures. University of Göttingen, Germany, 1997.

(72) Mackay, S.; Edwards, C.; Henderson, A.; Gilmore, C.; Stewart, N.; Shankland, K.; Donald, A. *MaXus* University of Glasgow, Scotland, 1997.

(73) Noel, M.; Vase, K. I. *Cyclic Voltammetry and the Frontiers of Electrochemistry*; Aspect: London, 1990; pp. 141-143.

(74) Braga, T. G. ; Wahl, A. C. *J. Phys. Chem.* **1985**, *89*, 5822.

(75) Chan, M. S.; Wahl, A. C. *J. Phys. Chem.* **1978**, *82*, 2542.

(76) Frisch, M. J.; Trucks, G. W.; Schlegel, H. B.; Scuseria, G. E.; Robb, M. A.; Cheeseman, J. R.; Montgomery, Jr., J. A.; Vreven, T. K.; Kudin, N.; Burant, J. C.; Millam, J. M.; Iyengar, S. S.; Tomasi, J.; Barone, V.; Mennucci, B.; Cossi, M.; Scalmani, G.; Rega, N.; Petersson, G. A.; Nakatsuji, H.; Hada, M.; Ehara, M.; Toyota, K. ; Fukuda, R.; Hasegawa, J.; Ishida, M.; Nakajima, T.; Honda, Y.; Kitao, O.; Nakai, H.; Klene, M.; Li, X.; Knox, J. E.; Hratchian, H. P.; Cross, J. B.; Bakken, V.; Jaramillo, C.; Gomperts, R.; Stratmann, R. E.; Yazyev, O.; Austin, A. J.; Cammi, R.; Pomelli, C.; Ochterski, J. W.; Ayala, P. Y.; Morokuma, K.; Voth, G. A.; Salvador, P.; Dannenberg, J. J.; Zakrzewski, V. G.; Dapprich, S.; Daniels, A. D.; Strain, M. C.; Farkas, O., Malick, D. K.; Rabuck, A. D.; Raghavachari, K.; Foresman, J. B.; Ortiz, J. V.; Cui, Q.; Baboul, A. G.; Clifford, S.; Cioslowski, J.; Stefanov, B. B.; Liu, G.; Liashenko, A.; Piskorz, P.; Komaromi, I.; Martin, R. L.; Fox, D. J.; Keith, T.; Al-Laham, M. A.; Peng, C. Y.; Nanayakkara, A.; Challacombe, M.; Gill, P. M. W.; Johnson, B.; Chen, W.; Wong, M. W.; Gonzalez, C.; Pople, J. A. *Gaussian 03*, Revision D.02, Gaussian, Inc., Wallingford CT, 2004.

Chapter 3

Development of a Model System for Studying Concerted Proton-Electron Transfer through a Hydrogen-Bonding Chain

3.1 Introduction

In many biological electron transfer processes, electron transfer is coupled to proton transfer. Often, both the electron transfer and proton transfer take place over significant distances.[1,2] This phenomenon is found in many of the enzymes involved in biological energy storage/release, such as photosystem II,[3,4] the bacterial photosynthetic RC,[5] cytochrome *c* oxidase,[6] and hydrogenase.[7] In these enzymes, electron transfer at the active site is coupled to rapid proton transfer between the active site buried deep within the protein and water at the surface of the protein, distances of nanometers. While electrons may reasonably transfer over distances of greater than 1 nm, proton transfer is limited to much shorter distances because of the larger mass of the proton relative to the electron, and often occur between a hydrogen-bonded donor and acceptor at distances of 3Å or less.[1,2,8] Proton coupled electron transfer (PCET) reactions in enzymes that involve proton transfers over large distances have been proposed to occur through tightly hydrogen-bonded chains of peptide residues or in hydrophobic protein channels through a hydrogen-bonded chain of water molecules.[1,2,5-7,9,10] This type of tightly controlled proton delivery appears to prevent undesired side reactions in these molecules, and is critical to catalysis.[1,2]

In many PCET reactions, proton transfer occurs in a single kinetic step with electron transfer, because in many cases this mechanism avoids high-energy intermediates.[11] A well-known example of this concerted proton-electron transfer (CPET) mechanism is the oxidation of tyrosine-161 in photosystem II.[12,13] Electron transfer from the phenol of this tyrosine residue is coupled to the concerted transfer of the phenolic hydroxyl proton to the hydrogen-bonded imidazolyl nitrogen of histidine-190. It has been proposed recently that these CPET reactions may occur with proton transfer through a hydrogen-bonded channel *i.e.* transfer of one electron coupled to the concerted transfer of multiple protons, such that positive charges do not accumulate on the intervening hydrogen-bonding proton carriers.[14-16] This type of mechanism has even been proposed

for tyrosine-161 oxidation in photosystem II, which may involve proton transfer not just to histidine-190, but though histidine-190 along a series of hydrogen bonds to the exterior of the protein.[17] So far, evidence for CPET though a hydrogen-bonded chain has been largely computational, because of the challenges of studying such a system in the complex environment of a protein,[18] and so the feasibility of this type of process and the effect that multiple proton transfers might have on oxidation kinetics remain unknown. Model complexes for the related process of excited-state multiple proton transfer have been developed, and evidence for concerted proton transfer in these systems has been observed.[19-21] Discussed in this chapter is an attempt to develop a small molecule model system for studying CPET with multiple protons transferring through a chain. The model system is a phenol with a pendent pyridyl methanol group, **1** (Figure 3.1a). This system was developed in collaboration with Dr. Todd Markle, with synthetic assistance provided by Dr. Brian Cochran. Oxidation of this phenol may be coupled to proton transfer from the phenolic proton to the alkyl alcohol and proton transfer from the alkyl hydroxyl to the pyridine (Figure 3.1c). A related system without the alcohol group, **2** (Figure 3.1b), has been extensively studied,[22] and is discussed in Chapter 2. The oxidation of this species occurs with concerted proton transfer to the pendent pyridine. Comparison of these two systems could allow for a direct comparison of the kinetics of oxidation with and without an intervening alcohol. A similar model system has been developed by Costentin and coworkers and studied electrochemically.[23,24] Comparisons to this system are discussed.

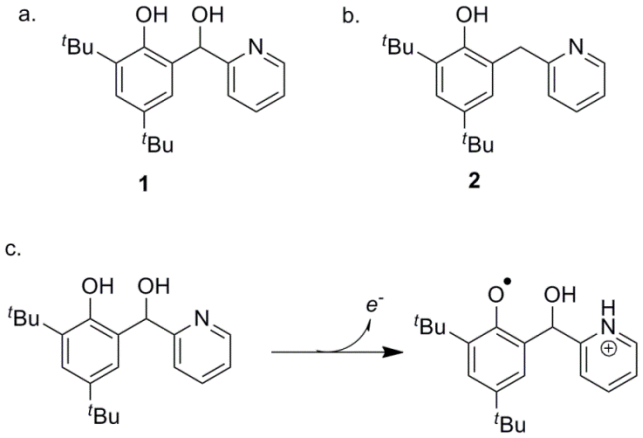

Figure 3.1: Comparison of **1** and **2**, and the oxidation of **1**.

3.2 Results

3.2.1 Synthesis of 1

The model system **1** was synthesized by a modification of the synthetic procedure used to synthesize **2**.[22] The precursor (2-(benzyloxy)-3,5-di-tert-butylphenyl)(pyridin-2-yl)methanol (**3**) was synthesized as reported previously in the synthesis of **2**. The benzyl protecting group was then removed by catalytic hydrogenation with palladium on carbon (Scheme 3.1). This molecule has a chiral center at the carbon bridging the phenol and pyridine. However, this chirality is not expected to affect the oxidation, because the proton transfer coordinate will be the exact mirror image in the opposite enantiomer, and the use of achiral oxidants will prevent the phenol chirality from affecting the electron transfer.

Scheme 3.1: Synthesis of **1** by hydrogenation of **3**.

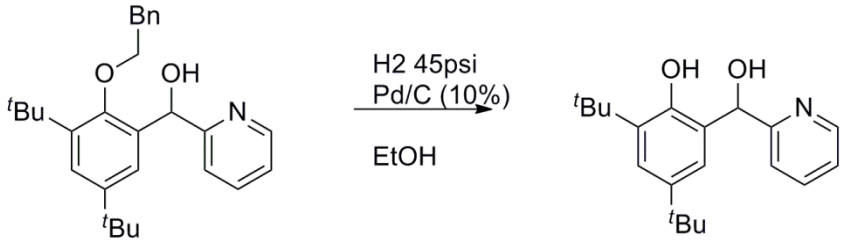

3 **1**

Of greater concern for understanding the proton-coupled oxidation of this model complex is that two possible intramolecular hydrogen-bonding configurations may occur in acetonitrile solution, the conditions in which the oxidation reactions were studied. The configuration desired for studying CPET through a hydrogen bonding chain has the phenol hydroxyl hydrogen bonded to the alkyl hydroxyl, which is itself hydrogen bonded to the pyridine (Figure 3.2, **A**). However, another possible conformation would be a conformation more similar to what is observed for **2**, with a hydrogen bond between the phenolic hydroxyl and the pyridine directly, with the alkyl hydroxyl not involved (Figure 3.2, **B**). Oxidation of this species would likely be mechanistically the same as oxidation of **2**. Gas phase DFT calculations (B3LYP/6-31G(d)) on a single molecule of **1** indicate the desired conformation **A** is lower in energy, but the calculated energy difference was only 0.7 kcal/mol, suggesting that both conformations are energetically accessible. This

small energy difference may be considered within the error of the computational method. These calculations also do not consider the role that a solvent molecule might play in stabilizing conformation **B** by accepting a hydrogen bond from the bridging alkyl hydoxyl.

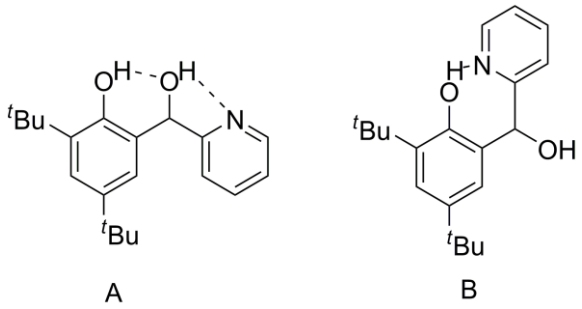

Figure 3.2: Possible hydrogen bonded conformations of **1**.

The X-ray crystal structure obtained for **1** does not resolve which of the two conformations is preferred (Figure 3.3, relevant bond lengths given in Table 3.1). In fact, in the solid state, neither conformation is observed. A hydrogen bond is observed between the two hydroxyl moieties, but neither is hydrogen bonded to the pyridine. This is because in the solid state, the pyridine forms an *inter*molecular hydrogen bond to the alkyl hydroxyl of an adjacent molecule (Figure 3.4). The solid state conformation is likely not relevant to dilute solutions of **1**.

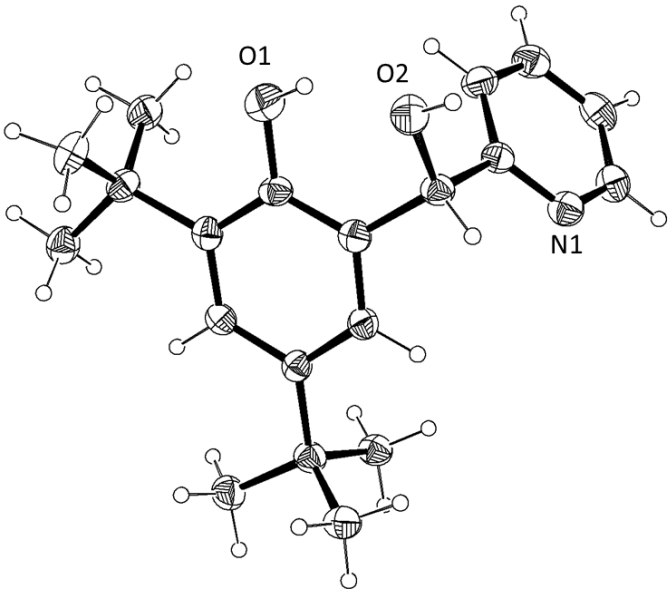

Figure 3.3: ORTEP diagram of **1**, with thermal ellipsoids shown at 30% probability.

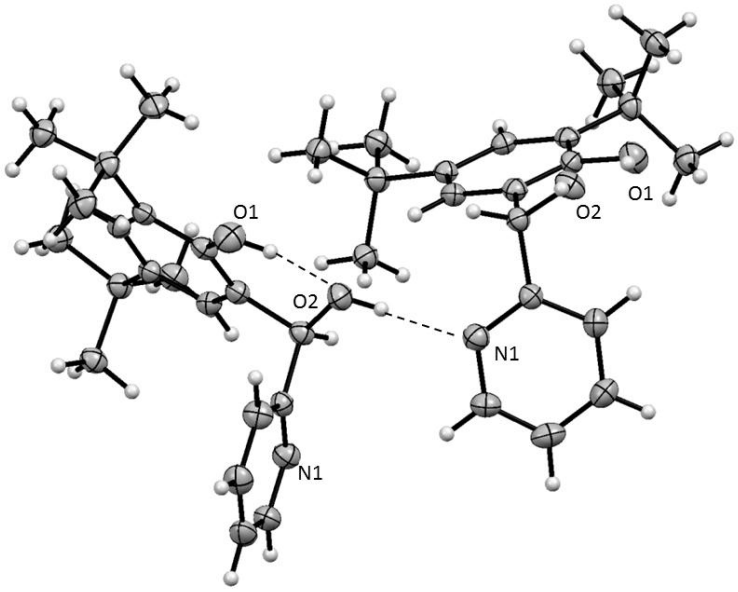

Figure 3.4: ORTEP diagram of two molecules of **1**, showing the intra- and intermolecular hydrogen bonding pattern in the solid state. Hydrogen bonds are indicated by dashed lines. Thermal ellipsoids shown at 30% probability.

Table 3.1: Selected hydrogen bonding distances (Å) for **1**.

Bond	
O1⋯O2	2.563(3)
O2⋯N1	3.551(3)
O2⋯N1’	2.786(3)

Table 3.2: Crystallographic data for **1**

	1
Formula	$C_{20}H_{27}NO_2$
T (K)	130(2)
Wavelength	0.71073 Å
Size (mm)	0.50 x 0.08 x 0.06
Cryst. Syst	Monoclinic
Space group	C 2/c
(Å)	30.671(2)
b (Å)	13.9980(11)
c (Å)	8.3550(7)
α (deg)	90
β (deg)	98.096(3)
γ (deg)	90
V ($Å^3$)	3551.3(5)
Z	8
D_{calc} (g/cm^3)	1.172
Abs. coeff. (mm^{-1})	0.075
Reflections total	6928
Reflections uniq. (R_{int})	3972 [R(int) = 0.0690]
Data/restraints/ parameters	3972 / 0 / 220
GOF	1.000
R1/wR2 [I>2σ(I)]	0.0672 / 0.1404
R1/wR2 (all data)	0.1688 / 0.1665

3.2.2 Spectroscopic Evidence for Hydrogen Bonding in Solution

The conformation of **1** in acetonitrile solution was probed by ^{1}H NMR spectroscopy. If **1** were in the conformation likely to facilitate multiple proton transfer, conformation **A**, both the phenol and alkyl hydroxyl protons would be expected to be in strong hydrogen bonds. Because hydrogen bonding affects the electronic environment of these protons, the chemical shift (δ(OH)) can be used as an approximate measure of the relative strength of the hydrogen bonds these protons are involved in. A stronger hydrogen bond generally results in a more downfield chemical shift, because hydrogen bonding polarizes the O-H bond and deshields the proton.[25] In dry CD_3CN, both OH protons appear as sharp singlets with $\delta(OH)_{phenol}$ = 10.58 ppm and $\delta(OH)_{hydroxyl}$ = 4.30 ppm. The OH resonances were identified by their chemical shifts, as discussed below. The phenolic resonance is significantly downfield of phenols without pendant bases, such as tri-*t*-butyl phenol (δ(OH) = 5.25 ppm in CD_3CN), indicating a strong hydrogen bonding environment. To determine if the hydrogen bonding observed was *inter* rather than *intra*molecular, as in the solid structure, NMR spectra were obtained at several concentrations of **1** ranging from 0.6 mM to 19 mM. No shift was observed in either OH resonance, indicating that hydrogen bonding occurs either *intra*molecularly or to solvent. The phenolic proton in **1** is not as strongly hydrogen bonded as in **2**, $\delta(OH)_{phenol}$ = 11.15 ppm. This difference would be consistent with conformation **A**, but the difference is not large enough to rule out small changes in hydrogen bonding due to inductive effects of the additional OH group, or some small steric effect of the hydroxyl preventing the pyridine from approaching the phenolic proton as closely.

The spectra of the related compounds 2-pyridylmethanol and 2,4-di-tert-butyl-6-(hydroxymethyl)phenol (**3**) were also recorded for comparison, and the relevant resonances are presented in Table 3.3. These two spectra add some support for the presence of conformation **A**, because the alkyl hydroxyl proton appears to be is in a stronger hydrogen bond in **1** than in 2-pyridylmethanol or **4**. However, the chemical shift of the alkyl hydroxyl might also be sensitive to deshielding due to its proximity to both the phenol and pyridine aryl rings.

To determine if the observed spectrum was an average of both conformations **A** and **B**, a spectrum of **1** was taken at 280 K. However, at this temperature no broadening

of the resonances was apparent, which suggests that either only one conformation is present in solution or the conformational change is very fast at these temperatures. Fast exchange seems unlikely since the phenolic proton is clearly in a strongly hydrogen-bonded environment based on the chemical shift. A NOESY spectrum was taken to determine whether the phenolic and alkyl hydroxyl protons were in close proximity. However, no NOE correlation could be observed at this temperature, because OH exchange took place on the timescale of the experiment, evidenced by cross peaks between the phenolic and alkyl hydroxyl protons of the same phase and magnitude as their diagonal peaks. A NOESY experiment at a lower temperature to reduce the effect spin saturation transfer was not attempted, because the conformation of **1** at very low temperature might not be relevant to the conformation at ambient temperature required for kinetics experiments.

Table 3.3: Chemical shifts of phenol and hydroxyl protons for **1** and related compounds in d^3-acetonitrile

	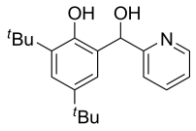 **1**	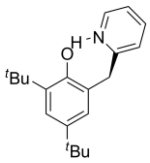 **2**	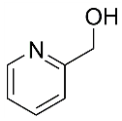 2-pyridylmethanol	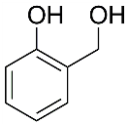 **4**
$\delta(OH)_{phenol}$	10.58	11.15[a]	-	8.13
$\delta(OH)_{hydroxyl}$	4.30	-	3.63	3.90

[a]Ref. 22

Because NMR spectroscopy did not provide conclusive evidence of the conformation of **1** in solution, the IR spectrum of **1** was taken 0.1M in acetonitrile solution (Figure 3.4). IR spectroscopy shows the vibrational modes of all conformations present in solution at a given temperature, rather than an average as observed by NMR. The magnitude of the shift in ν(O-H) from the non-hydrogen bonded frequency to a lower frequency is a measure of the strength of the hydrogen bond.[26] The spectrum of **1** shows two major peaks that are identified as O-H stretching modes, a broad peak centered at

~3500 cm^{-1} and a very broad peak centered at ~2800 cm^{-1}. The very broad feature is also observed in spectrum of **2**,[22] and is assigned to a strongly hydrogen bonded phenol. Broad, low energy ν(O-H) are characteristic of strong hydrogen bonding.[27] The sharper feature at ~3500 cm^{-1} appears to be a weakly hydrogen bonded alkyl hydroxyl, though it could also be weakly hydrogen bonded phenol. Perhaps the strongest evidence of the solution conformation of **1** comes from comparison to the IR spectrum of **4** (Figure 3.5). The spectrum of **4** (0.05M in acetonitrile) has two broad peaks assigned to OH stretches from 3200-3500 cm^{-1}. There is no very broad OH stretch at ~2800 cm^{-1} in the spectrum of **4**, which supports the previous assignment of this ~2800 cm^{-1} stretch to a phenol directly hydrogen bonded to pyridine in **1**. Both spectra have very similar features at ~3500 cm^{-1}, consistent with a weakly hydrogen bonded alkyl hydroxyl in both compounds. The comparison of these spectra provides strong evidence that conformation **B** is present in solution.

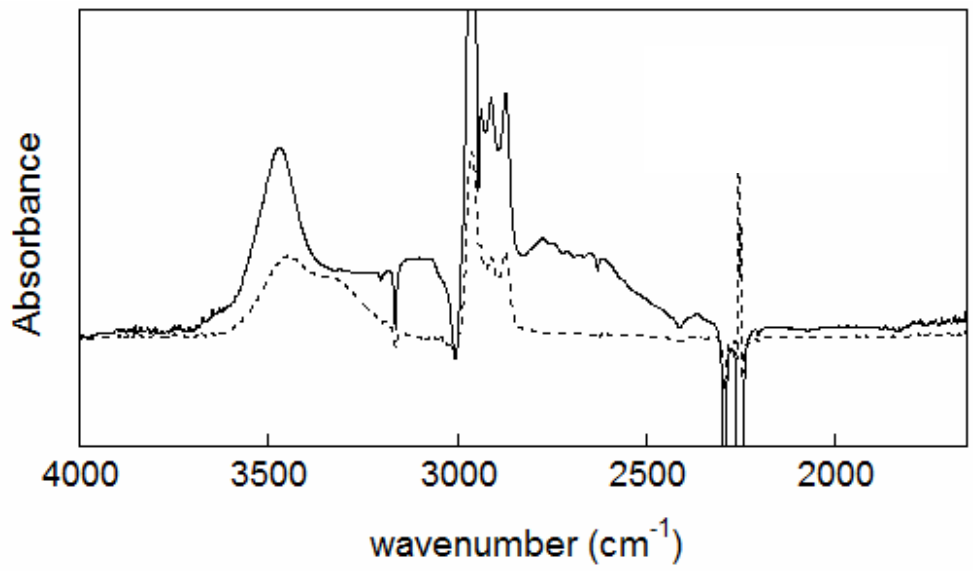

Figure 3.5: IR spectra of **1** 0.1M in acetonitrile (solid line), and **4** 0.05M in acetonitrile (dashed line), showing the O−H stretching region. Absorbances between ~2400 cm^{-1} and ~2200 cm^{-1} are due to incomplete solvent subtraction.

3.2.3 Electrochemical Characterization of 1 Oxidation

The oxidation of **1** was observed by cyclic voltammetry (CV) in acetonitrile solution (0.1 M [*n*-Bu_4N][PF_6]). The CV (Figure 3.6) shows one quasi-reversible oxidation wave with $E_{1/2}$ = +0.47 ± 0.02 V vs. ferrocene. This value is significantly negative of tri-*t*-butyl phenol ($E_{1/2}$ = +1.09 V vs. ferrocene),[28] indicative of the role of the pendent base in accepting the proton and lowering the potential for oxidation. The quasi-reversibility of this wave and large separation between anodic and cathodic peaks also indicate proton transfer to the pendent base.[29] The value of $E_{1/2}$ **1** is only +0.03 V greater than that of **2**.[22] This similarity in $E_{1/2}$ is not unexpected given the structural similarity between the two compounds. The difference between the two is likely due to the small inductive effect of the hydroxyl on the phenol, making **1** slightly more difficult to oxidize.

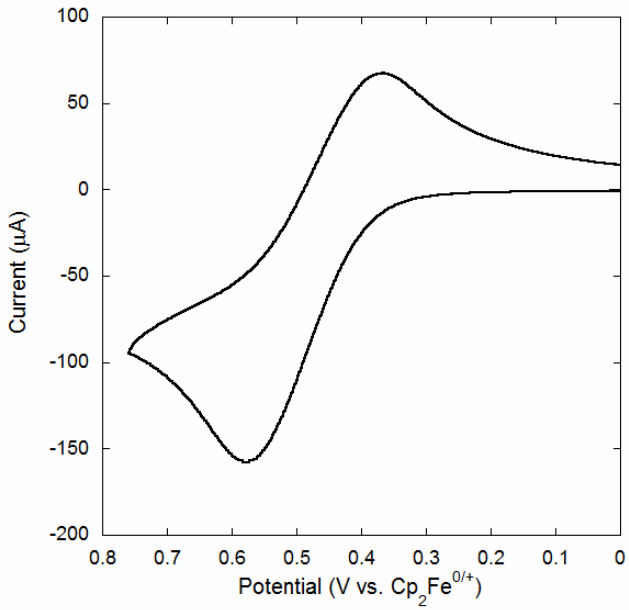

Figure 3.6: Cyclic voltammogram of **1** *ca.* 10 mM in acetonitrile (0.1 M [*n*-Bu_4N][PF_6]), showing quasi-reversible oxidation wave. Scan rate is 0.1 V/s.

3.2.4 Kinetics of 1 Oxidation

The kinetics of CPET oxidation of **1** with chemical oxidants was studied by stopped-flow UV-vis to determine the mechanism of proton transfer in this reaction.

Triarylamminium radical oxidants with substituents at the 4-position of the aryl rings ($[N(C_6H_4X)_3]^{+\bullet}$) were used to vary the thermodynamic driving force of the reaction, and reaction progress was followed by monitoring the disappearance of the blue amminium absorbance. Kinetics data are summarized in Table 3.4. A Brønsted plot of the kinetic data was constructed (Figure 3.7), and shows the slope of $\alpha \approx 0.5$ expected for a CPET process.[29] An overlay of the Brønsted plot for reactions of **2** with $[N(C_6H_4X)_3]^{+\cdot}$ show that reactions with **1** fall just below the trend line for **2**. Slower oxidation of **1** relative to **2** at the same thermodynamic driving force would be consistent with proton transfer being slowed by the movement of two protons rather than one. However, the difference in rate at the same driving force are not large between **1** and **2** (~10%), and small differences like this might also be possible for CPET without the hydroxyl through conformation **B**. These differences could be explained by factors such as slightly poorer overlap of oxidant and phenol electronic wave functions due a steric interaction with the alkyl hydroxyl, or a longer phenol-pyridine proton transfer distance due to a slightly weaker hydrogen bond,[29] which would be consistent with the slight difference in phenol δ(OH) between these two species.

Table 3.4: Kinetic data for reactions of $[N(C_6H_4X)_3]^{+\cdot}$ with **1**

Oxidant	$\Delta E°_{rxn}$ (V)	k_{rxn} (M^{-1} s^{-1})
$[N(C_6H_4Me)_3]^{+\bullet}$	−0.09 ± 0.03	$2.0 \pm 0.2 \times 10^4$
$[N(C_6H_4OMe)(C_6H_4Br)_2]^{+\bullet}$	+0.06 ± 0.03	$1.2 \pm 0.1 \times 10^5$

The H/D kinetic isotope effect (k_H/k_D) for oxidation of **1** with $[N(C_6H_4OMe)(C_6H_4Br)_2]^{+\bullet}$ was measured by deuteration with methanol-d_4 (1 v/v%) in acetonitrile (Figure 3.8). With this large excess excess of MeOD (phenol at *ca.* 0.1 – 1.0 mM), both the phenol and alkyl hydroxyl OH groups are deuterated, as determined by ^{1}H NMR. The k_H/k_D for this reaction was 4.3 ± 0.7. A strikingly similar k_H/k_D of 4.2 ± 0.6 was measured for **2** under identical conditions, supporting the idea that CPET in **1** is analogous to CPET in **2**, with single proton transfer directly from the phenol to the pyridine. Theoretical treatments of CPET invoke proton vibrational wavefunction overlap

between the reactant and product states as one of the terms defining the CPET kinetics, where it appears as a preexponential term in the rate expression.[29,30] This treatment would seem to predict a different and probably large isotope effect if two proton vibrational wave functions must overlap rather than one, although it is impossible to confidently predict the expected behavior without calculating the wavefunctions involved.

A more complete analysis of the number of protons transferring in the rate determining kinetic step of a reaction involves taking a "proton inventory". [31] A proton inventory measures the relationship between the reaction rate and solvent isotopic composition, and is not sensitive to the electronic differences inherent in comparing **1** with **2**. The general formula for this relationship is given by equation 3.1, where *n* is the mole fraction D/(H+D) of exchangeable protons and deuterons in the solvent mixture, and *m* is the number of protons transferring in the rate determining step. The variable φ_i is the partitioning coefficient between the solvent and the proton transfer site *i*, essentially the equilibrium isotope effect at site *i*. The variable σ_i is the kinetic transfer ratio k_D/k_H at site *i*.

$$\frac{k_n}{k_0} = \frac{\prod^m (1-n+\sigma_i \varphi_i n)}{\prod^m (1-n+\varphi_i n)} \qquad (3.1)$$

In this model, k_n, the rate constant at deuterium mole fraction *n*, should vary roughly linearly with *n* for transfer of one-proton, and quadratically with *n* for two-proton transfer. Kinetic experiments were performed in the same manner as described above using $[N(C_6H_4OMe)(C_6H_4Br)_2]^{+\bullet}$ as the oxidant, but with the solution of **1** prepared with 1% v/v (MeOH+d^4-MeOD), varying the ratio of the volume of d^4-MeOD to the total volume of MeOH and d^4-MeOD. The proton inventory plot from these experiments (Figure 3.9) was fit by linear and quadratic models. Values of φ_i were found experimentally, by adding d^4-MeOD to a sample of **1** in acetonitrile and observing the decrease in the integrations of the phenolic and hydroxyl peaks in the ^{1}H-NMR spectrum. The decrease of these two peaks was roughly equal, and there was an approximately 50%

decrease after the addition of two equivalents of d^4-MeOD. From this result, φ_1 and φ_2 were approximated as 1 in the linear and quadratic models.

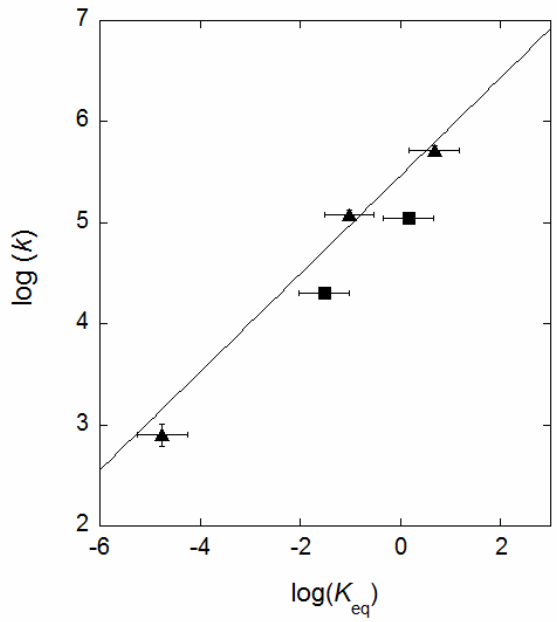

Figure 3.7: Brønsted plot for reactions of $[N(C_6H_4X)_3]^{+\cdot}$ with **2** (▲, Ref. 22) and **1** (■) in acetonitrile. The solid curve is a linear fit data for **2** with $\alpha = 0.49$.

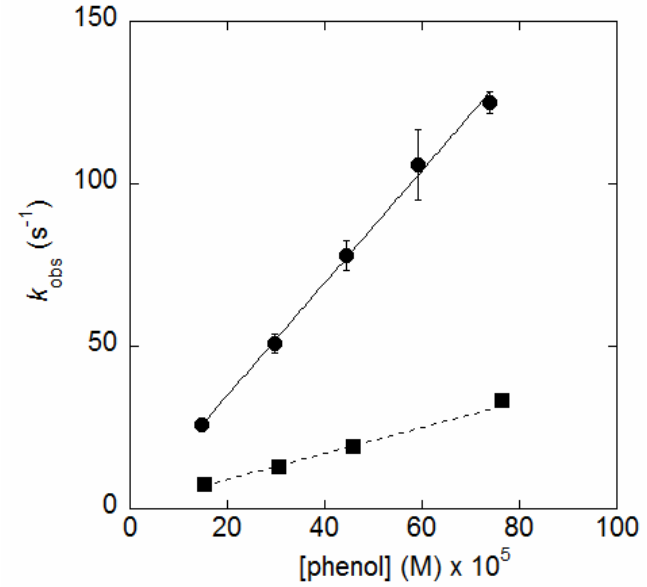

Figure 3.8: Plot of pseudo-first order k_{obs} versus [**1**] for the reaction with $[N(C_6H_4OMe)(C_6H_4Br)_2]^{+\bullet}$ in acetonitrile with 1% MeOH (●) and 1% MeOD (■).

The proton inventory plot can be acceptably fit by both the linear and quadratic models applied, due mainly to the significant error bars at lower deuterium substitution,[32] making it difficult to draw conclusions about mechanism. In a simplified situation in which $\sigma_1 = \sigma_2$, the small kinetic isotope effect measured at $n = 1$ for **1** of $k_H/k_D = 4.3 \pm 0.7$ would be expected to give a maximum deviation from a linear trend for $m = 2$ of only ~10%.[31] This value of 10% is unfortunately less than experimental error, so inconclusiveness of the proton inventory is disappointing, but not entirely unexpected.

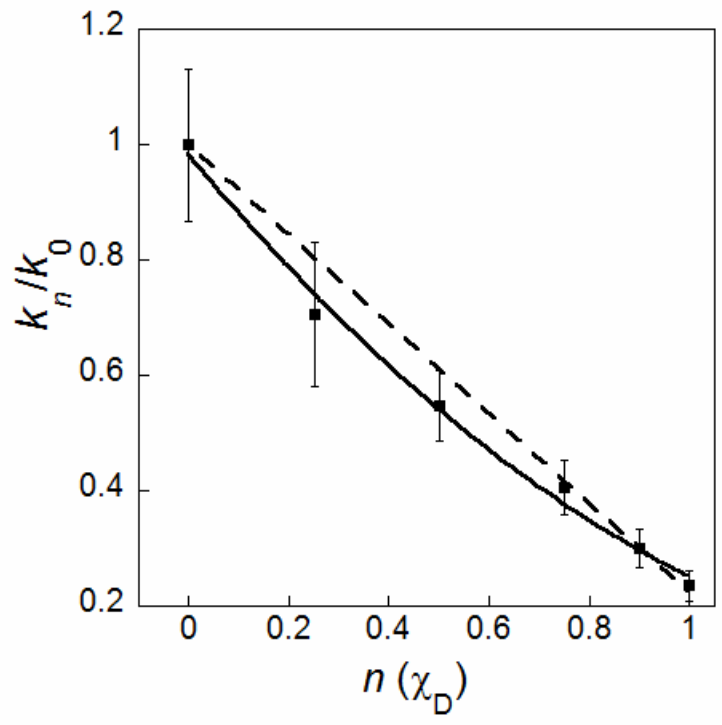

Figure 3.9: Proton inventory data for reaction of **1** with $[N(C_6H_4OMe)(C_6H_4Br)_2]^{+\bullet}$ in acetonitrile with 1% MeOH/MeOD (n = mol fraction deuterated from MeOD/(MeOH + MeOD)). Fits of this data to a linear trend (dashed curve) and a quadratic trend (solid curve) are shown. The quadratic fit shown assumes $\sigma_1 = \sigma_2$.

3.2.5 Attempted Synthesis of Bicyclic System

A model system with a rigid, bicyclic framework was targeted so that the conformation of the hydrogen-bonding chain would be unambiguous (**11** in Scheme 3.2). It was envisioned that this molecule might be synthesized from 1,8-

dihydroxynaphthelene (**5**) by reduction to a ketone followed by Buchwald-Hartwig coupling[33] to pyridine (Scheme 3.2). The first step of the proposed synthesis, reduction to 8-hydroxy-3,4-dihydro-1(2H)-naphthalenone (**6**) was achieved with hydrogen using a Pd/C catalyst. This reaction required that only a stoichiometric amount of hydrogen be used, because the 8-hydroxy-3,4-dihydro-1(2H)-naphthalenone was readily reduced further to the 8-hydroxy-1,2,3,4-tetrahydronaphthalene. Butylation of this ketone to the di-*t*-butyl product (**7**) was then attempted by electrophilic addition with *t*-butanol in a solution of sulfuric acid and methanol. This reaction gave exclusively butylation of the 5 position of the naphthalenone (**8**). Other butylation procedures using catalytic urea or *t*-butyl urea led only to intractable mixtures of products.[34]

Scheme 3.2: Proposed synthesis of bicyclic phenol-amine **11**.

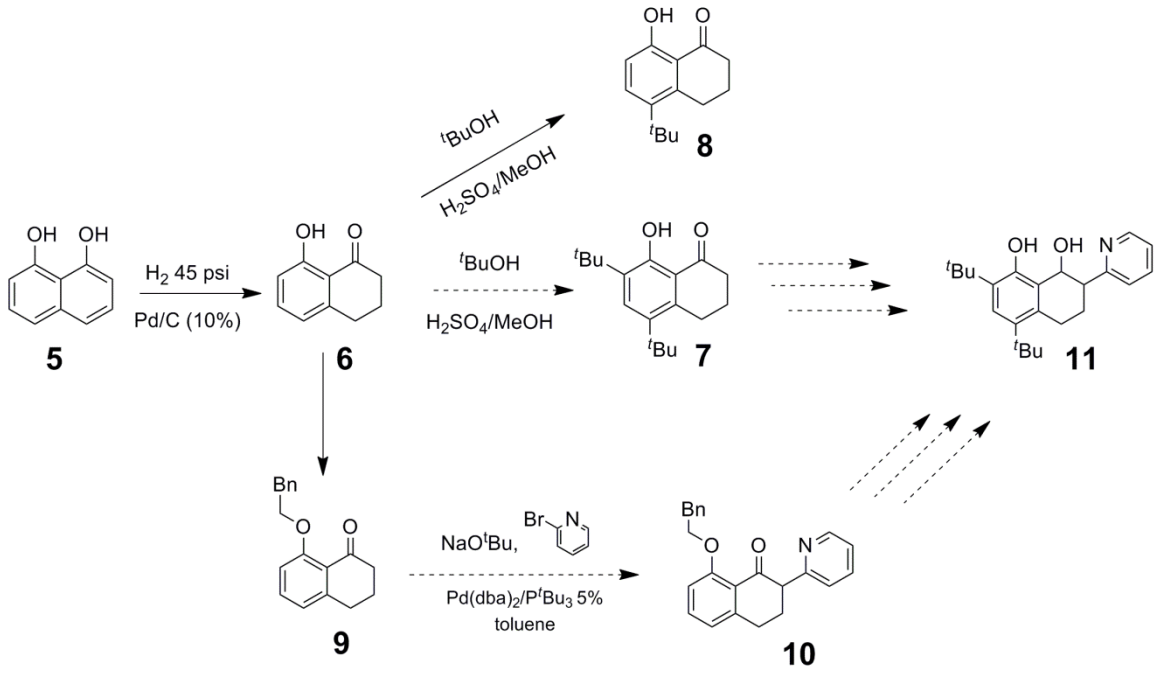

Because butylation of the ketone (**6**) was not successful, it was proposed that butylation might be possible following coupling to pyridine and reduction of the ketone to an alcohol. Prior to coupling to pyridine, the phenol moiety of **6** was benzyl protected by reaction with benzyl bromide to give **9**. Palladium catalyzed coupling of **9** with 2-bromopyridine was then attempted to give **10**, but there was no apparent reaction by the conditions given in Scheme 3.2. A likely explanation for this lack of reactivity is that the

2-bromopyridine binds to the Pd catalyst and makes it inactive, though other reasonable explanations can be given. Because of the challenge of synthesizing the target molecules as well as other rigid bicyclic phenols,[34] this route was not pursued further.

3.3 Discussion

The alcohol bridged phenol-pyridine **1** was selected as a possible model system for observing CPET in which the proton transfers through a hydrogen bonding network, in this case from the phenol to the alkyl hydroxyl and from the alkyl hydroxyl to the pyridine. Unfortunately, it was not possible to determine if this molecule actually formed the desired hydrogen bonding network in solution, because the conformational flexibility of this molecule allowed the pyridine to hydrogen bond directly to the phenol. The presence of a relatively sharp, high energy ν(O-H) in the IR spectrum of **1** was highly suggestive that the alkyl hydroxyl was not involved in hydrogen bonding. A direct phenol to pyridine hydrogen bond might be expected based on the smaller difference in the pK_a values for a phenol and protonated pyridine versus an alkyl alcohol and protonated pyridine.[35] The difference between the pK_a's of phenol and pyridine in organic solvent (DMSO) is 14.6, while the difference between methanol and pyridine is 25.6.[36] The very similar rate constants and deuterium kinetic isotope for oxidations of **1** compared to **2** are certainly consistent with the mechanism of CPET oxidation being the same with these two species.

In order to prevent direct hydrogen bonding between the phenol and the pyridine, a bicyclic system was pursued synthetically that would enforce a rigid hydrogen bonding geometry more similar to what is found in a protein. Unfortunately, synthesis of bicyclic molecules with the necessary functionalizations proved extremely difficult. [37] While this research towards synthesizing these bicyclic molecules was being conducted, Costentin and coworkers published a very similar study of CPET from a phenol to a pendent pyridine through a hydrogen-bonding alkyl alcohol. The differences between the Costentin system and **1** that appear to be key to achieving an intramolecular hydrogen bonding network are the addition of an additional methylene spacer between the phenol and pyridine, lowering the pK_a of the intervening alcohol by functionalization with a $-CF_3$ moeity to increase hydrogen bonding to the pyridine, and addition of a methyl group

to the 6-position of the pyridine to provide a steric impediment to hydrogen bonding with the *t*-butyl functionalized phenol. The X-ray crystal structure of their molecule has the desired conformation, although they do not confirm that it is present in solution. Perhaps the best evidence for the involvement of the alkyl hydroxyl in shuttling protons from phenol to base is that substitution of the $–CF_3$ group for $–CH_3$ or –H leads to essentially irreversible CVs. With this molecule they demonstrate that CPET with the hydrogen-bonding chain has a slower standard rate constant than CPET directly from the phenol to the proton accepting amine. They speculate that this effect is due primarily to poorer overlap of product and reactant proton vibrational wavefunctions in the system with the hydrogen-bonding chain due to poor hydrogen bonding to the alkyl hydroxyl.[24] However, the proton transfer coordinate in solution is not well defined in this system, so it is difficult to draw this conclusion or any stronger conclusions.

3.4 Conclusions

Compound **1** is not a good model for CPET through a hydrogen bonding chain because of its conformational flexibility and low acidity of the alkyl hydroxyl. An ideal model system would enforce a rigid geometry that prevented any hydrogen bonding other than through the expected chain, similar to the proton conducting channels of proteins, but such molecules have proven difficult to synthesize. What factors are critical to understanding and predicting rates of CPET through hydrogen bonding networks remain an open question.

3.5 Experimental

3.5.1 General Considerations

Unless otherwise noted, reagents were purchased from Aldrich, solvents from Fischer, and deuterated solvents from Cambridge Isotope Labs. Acetonitrile was purchased from Burdick and Jackson (low-water brand) and stored in an argon-pressurized stainless steel drum plumbed directly into a glovebox. 2-(hydroxymethyl)phenol (**4**),[38] (2-(benzyloxy)-3,5-di-tert-butylphenyl)(pyridin-2-yl)methanol (**3**),[22] and 1,8-dihydroxynaphthalene (**5**)[39] were synthesized according to literature. Triarylamminium hexafluorophosphate salts were prepared from the

corresponding amines as described previously.[40] ^{1}H NMR spectra were recorded on a Bruker AV300 spectrometer at ambient temperatures; chemical shifts are reported relative to TMS in ppm by referencing to the residual solvent signals. Column chromatography used silica gel as the stationary phase. Infrared spectra were obtained on a Bruker Vector 33 spectrometer in dry acetonitrile in a cell with NaCl windows.

3.5.2 Synthesis

3.5.2.1 2,4-di-*tert*-butyl-6(hydroxyl(pyridin-2-yl)methyl)phenol (1)

A solution of (2-(benzyloxy)-3,5-di-tert-butylphenyl)(pyridin-2-yl)methanol (0.98 g, 2.4 mmol) in EtOH (30 mL) containing Et_3N (0.40 mL, 2.7 mmol) was agitated in a Parr apparatus under H_2 (50 psi) in the presence of Pd(C) (10 mol%). After 24 hr the reaction was filtered through Celite, and volatiles were removed on the rotavap. Column chromatography (3/1 v/v hexanes/ethyl acetate) yielded 2,4-di-*tert*-butyl-6((4-methylpyridin-2-yl)methyl)phenol (0.38 g, 1.2 mmol, 50% yield) as a white solid. ^{1}H NMR (CD_3CN): δ 10.58 (s, 1 H, O*H*), 8.46 (d, *J* = 3 Hz, 1 H, Ar-*H*), 7.85 (t, *J* = 5 Hz, 1 H, Ar-*H*), 7.63 (d, *J* = 5 Hz, 1 H, Ar-*H*), 7.34 (d, *J* = 2 Hz, 1 H, Ar-*H*), 7.29 (t, *J* = 4 Hz, 1 H, Ar-*H*), 7.21 (d, *J* = 2 Hz, 1 H, Ar-*H*), 6.02 (s, 1 H, methylene C*H*), 4.30 (s, 1 H, O*H*), 1.40 (s, 9 H, C(C*H*$_3$)$_3$), 1.26 (s, 9 H, C(C*H*$_3$)$_3$). FTIR: ν(OH) 3500 cm−1 *br*, 2800 cm−1 *vbr*.

3.5.2.2 8-hydroxy-3,4-dihydro-1(2H)-naphthalenone (6)

A solution of 1,8-dihydroxynaphthalene (1.2 g, 7.4 mmol) in 20 mL of ethanol was combined with approximately 1 g of Pd/C (10 wt%) in a 100 mL Parr pressure flask. The flask was evacuated, then charged with H_2 (45 psig, ~ 1.3 equiv.), and shaken for two days. The reaction mixture was then filtered through Celite and dried under vacuum to give a yellow oil. Column chromatography (6:1 hexanes/ethyl acetate) yielded 8-hydroxy-3,4-dihydro-1(2H)-naphthalenone as a colorless liquid (0.76 g, 62% yield). ^{1}H NMR ($CDCl_3$) δ 12.42 (s, 1H, O*H*), 7.40 – 7.31 (m, 1H, Ar-*H*), 6.79 (d, *J* = 8.0 Hz, 1H, Ar-*H*), 6.70 (d, *J* = 7.4 Hz, 1H, Ar-*H*), 2.93 (t, *J* = 6.7 Hz, 2H, C(=O)C*H*$_2$), 2.69 (t, *J* = 7.7 Hz, 2H, ArC*H*$_2$CH$_2$), 2.17 – 2.03 (m, 2H, CH$_2$C*H*$_2$CH$_2$).

3.5.2.2 8-hydroxy-6-*t*-butyl-3,4-dihydro-1(2H)-naphthalenone (8)

To a solution of 8-hydroxy-3,4-dihydro-1(2H)-naphthalenone (0.060 g, 0.37 mmol) in 2 mL of methanol was added *t*-butanol (0.110 g, 1.5 mmol). The solution was cooled to 5°C, and H_2SO_4 (3mL, 56 mmol) was added. The solution was warmed to room temperature and stirred for 12 hours, resulting in the precipitation of a white solid. The reaction mixture was poured onto ice, filtered, and washed with water. The solid was dried under vacuum, but retained a significant amount of water, to give 8-hydroxy-6-*t*-butyl-3,4-dihydro-1(2H)-naphthalenone (0.12 g crude wet solid, ~100% yield). ^{1}H NMR ($CDCl_3$) δ 13.67 (s, 1H, O*H*), 7.74 (d, *J* = 7.9 Hz, 1H, Ar-*H*), 7.00 (d, *J* = 7.9 Hz, 1H, Ar-*H*), 3.26 (t, *J* = 6.1 Hz, 2H, C(=O)CH_2), 3.05 (t, *J* = 6.7 Hz, 2H, ArCH_2CH_2), 2.45 (m, 2H, CH_2CH_2CH_2), 1.91 (s, 9H, *t*Bu-CH_3). MS (EI) 218 (M+).

3.5.2.3 8-benzyloxy-3,4-dihydro-1(2H)-naphthalenone (9)

To a solution of 8-hydroxy-3,4-dihydro-1(2H)-naphthalenone (0.10 g, 0.61 mmol) in 25 mL of acetone was added K_2CO_3 (0.10 g, 0.72 mmol) and benzyl bromide (0.11 g, 0.61 mmol). The reaction mixture was sparged with N_2, then refluxed under N_2 for 12 hours. The reaction mixture was evaporated to dryness, redissolved in diethyl ether, and washed three times with water. The ether extracts were dried over $MgSO_4$ and solvent removed under vacuum to give a yellow oil. Column chromatography (3:1 hexanes/ethyl acetate) gave 8-benzyloxy-3,4-dihydro-1(2H)-naphthalenone as a yellow oil (0.050 g, 32% yield). ^{1}H NMR ($CDCl_3$) δ 7.58 (d, *J* = 7.5 Hz, 2H, Ar-*H*), 7.45 – 7.26 (m, 6H, Ar-*H)*, 6.94 – 6.76 (m, 2H, Ar-*H*), 5.20 (s, 2H, Ph-CH_2), 2.94 (t, *J* = 6.7 Hz, 2H, C(=O)CH_2), 2.66 (t, *J* = 6.8 Hz, 2H, ArCH_2CH_2), 2.08 (m, 2H, CH_2CH_2CH_2).

3.5.3 Electrochemistry

Cyclic voltammograms were recorded on an E2 Epsilon electrochemical analyzer (BASi) at approximately 10 mM substrate in anaerobic 0.1 M [*n*-Bu_4N][PF_6] acetonitrile solution. [*n*-Bu_4N][PF_6] was recrystallized three times from ethanol and dried *in vacuo* for two days at 110 °C prior to use. The electrodes were as follows: working, glassy carbon (3.0 mm dia.); auxiliary, platinum wire; and reference, Ag/$AgNO_3$ (0.01 M) in

electrolyte solution. Ferrocene was used as an internal standard, and potentials are reported vs. the $Cp_2Fe^{+/0}$ couple.

3.5.4 Kinetics

Kinetics experiments were performed on an OLIS RSM-1000 stopped-flow UV-vis spectrometer in anaerobic acetonitrile. The data were analyzed with SpecFit[41] global analysis software. Reactions with $[N(C_6H_4OMe)(C_6H_4Br)_2]^{+\bullet}$ were performed with 1.0×10^{-5} M oxidant and 14-74 equivalents of **1**, and were fit to pseudo-first order kinetics. Reactions with $[N(C_6H_4Me)_3]^{+\bullet}$ were performed with 1.0×10^{-5} M oxidant and 5-25 equivalents of **1**, and were fit to second order kinetics. Typical experiments were performed with the amminium oxidant at a concentration of 1.5×10^{-5} M, and the phenol in excess. Kinetic isotope effect and proton inventory experiments were performed with 1% CH_3OH/D in acetonitrile.

3.5.5 DFT Calculations

All calculations were performed with *Gaussian03*[42] at the B3LYP/6-31G(d) level of theory on isolated molecules in the gas phase. *t*-Butyl groups were replaced with methyl groups to save computational time.

3.5.6 X-ray Crystallography

Crystals were mounted on glass capillaries with Paratone-N oil (Hampton Research) and frozen immediately in a cold nitrogen gas stream. Data were collected on a Enraf-Nonius KappaCCD single crystal X-ray diffractometer with Mo-Kα radiation (λ = 0.71073 Å) utilizing both Φ and Ω scans. Crystal-to-detector distance was 30 mm. The data was integrated and scaled using hkl-2000.[43] Solution by direct methods (SHELXS, SIR97[44,45]) produced a complete heavy atom phasing model consistent with the proposed structure. The structure was completed by difference Fourier synthesis with SHELXL97.[46,47] All hydrogen atoms were placed in geometrically idealized positions and constrained to ride on their parent atoms (a riding model). Isotropic thermal parameters Ueq were fixed such that they were 1.2Ueq of their parent atom Ueq for CH's and OH's, and 1.5Ueq of their parent atom Ueq in case of methyl groups. Hydroxyl protons H1 and H2 could also be

located from the difference map and their positions refined isotropically, increasing the O1-H1 bond length to 1.2 Å, indicating strong hydrogen bonding to O2. However, O-H bond lengths of 1.2 Å are rejected by the IUCr. H1 and H2 thus were included with constrained bond distances. All non-hydrogen atoms were refined anisotropically by full-matrix least-squares.

3.6 Notes to Chapter 3

(1) Dempsey, J. L.; Winkler, J. R.; Gray, H. B. *Chem. Rev.* **2010**, *110*, 7024.

(2) Wraight, C. A. *Biochim. Biophys. Acta* **2006**, *1757*, 886.

(3) Tommos, C. ; Babcock, G. T. *Acc. Chem. Res.* **1998,** *31*, 18.

(4) Meyer, T. J.; Huynh, M. H. V.; Thorp, H. H. *Angew. Chem. Int. Ed.* **2007**, *46*, 5284.

(5) Stowell, M. H. B.; McPhillips, T. M.; Rees, D. C.; Stoltis, S. M.; Abresch, E.; Feher, G. *Science* **1997**, *276*, 812.

(6) Wikström, M.; Verhovsky, M. I.; Hummer, G. *Biochim. Biophys. Acta* **2003**, *1634*, 61.

(7) Nicolet, Y.; Cavazza, C.; Fontecilla-Camps, J. C. *J. Inorg. Biochem.* **2002**, *91*, 1.

(8) Krishtalik, L. I. *Biochim. Biophys. Acta.* **2000**, *1458*, 6.

(9) Yoshikawa, S.; Muramoto, K.; Shinzawa-Itoh, K.; Aoyama, H.; Tsukihara, T.; Shimokata, K.; Katayama, Y.; Shimada, H. *Biochim. Biophys. Acta* **2006**, *1757*, 1110.

(10) Efimov, I.; Badyal, S. K.; Metcalfe, C. L.; Macdonald, I.; Gumiero, A.; Raven, E. L.; Moody, P. C. E. *J. Am. Chem. Soc.* **2011**, *133*, 15376.

(11) Warren, J. J.; Tronic, T. A.; Mayer, J. M. *Chem. Rev.* **2010**, *110*, 6961.

(12) Hammarström, L.; Styring, S. *Energy Environ. Sci.* **2011**, *4*, 2379.

(13) Mayer, J. M.; Rhile, I. J.; Larsen, F. B.; Mader, E. A.; Markle, T. F.; Dipasquale, A. G. *Photosynthesis Res.* **2006**, *87*, 21.

(14) Derat, E.; Shaik, S. *J. Am. Chem. Soc.* **2006**, *128*, 13940.

(15) Siegbahn, P. E. M.; Blomberg, M. R. A.; Crabtree, R. H. *Theor. Chem. Acc.* **1997**, *97*, 289.

(16) Wang, Y.; Hirao, H.; Chen, H.; Onaka, H.; Nagano, S.; Shaik, S. *J. Am. Chem. Soc.* **2008**, *130*, 7170.

(17) Umena, Y.; Kawakami, K,; Shen, J.-R. *Nature* **2011**, *4* 2379.

(18) König, P. H.; Ghosh, N.; Hoffman, M.; Elstner, M.; Tajkhorshid, E.; Frauenheim, T. H.; Cui, Q. *J. Phys. Chem. A* **2006**, *110*, 548.

(19) Tanner, C.; Manca, C.; Leutwyler, S. *Science* **2003**, *302*, 1736.

(20) Kwon, O.-H.; Lee, Y.-S.; Yoo, B. K.; Jang, D.-J. *Angew. Chem. Int. Ed.* **2006**, *45*, 415.

(21) Kang, B.; Ko, K. C.; Park, S.-Y.; Jang, D.-J.; Lee, J. Y. *Phys. Chem. Chem. Phys.* **2011**, *13*, 6332.

(22) Markle, T. F.; Mayer, J. M. *Angew. Chem. Int. Ed.* **2008**, *47*, 738.

(23) Costentin, C.; Robert, M.; Savéant, J.-M.; Tard, C. *Angew. Chem. Int. Ed.* **2010**, *49*, 3803.

(24) Costentin, C.; Robert, M.; Savéant, J.-M.; Tard, C. *Phys. Chem. Chem. Phys.* **2011**, *13*, 5353.

(25) Jeffrey, G. A. in *An Introduction to Hydrogen Bonding* **1997**, (Oxford Univ Press, NewYork), pp 12, 228.

(26) Kuhn, L. P.; Wires, R. A.; Ruoff, W.; Kwart, H. *J. Am. Chem. Soc.* **1969**, *91*, 4790.

(27) Bratos, S.; Leickman, J.-C.; Gallot, G.; Ratajczak, H. in *Ultrafast Hydrogen Bonding Dynamics and Proton Transfer Processes in the Condensed Phase*, eds. Elsaesser, T.; Bakker, H. J. Kluwer Academic, Boston, **2002**, pp 5-30.

(28) Bordwell, F. G.; Cheng, J. P. *J. Am. Chem. Soc.* **1991**, *113*, 1736.

(29) See chapter 2.

(30) Hammes-Schiffer, S.; Stuebrukhov, A. A. *Chem. Rev.* **2010**, *110*, 6939.

(31) Krishtalik, L. I. *Mendeleev Commun.* **1992**, *3*, 66.

(32) Error is approximated as 15% for k_n/k_0, from 10% approximate error on measurements of k_n and k_0. Hence, error is larger at larger values of k_n/k_0, when n is smaller.

(33) Culkin, D. A.; Hartwig, J. F. *Acc. Chem. Res.* **2003**, *36*, 234.

(34) Cochran, B. M. *unpublished results.*

(35) Shan, S.-O.; Loh, S.; Herschlag, D. *Science* **1996**, *272*, 97.

(36) Bordwell, F. G. *Acc. Chem. Res.* **1988**, *21*, 456.

(37) Cochran, B. M. *unpublished results.*

(38) Pérez-Prieto, J.; Galian, R. E.; Burgos, P. O.; Miñana, M. C. M.; Miranda, M. A.; López-Ortiz, F. *Org. Lett.* **2005**, *7*, 3869.

(39) Foti, M. C.; Johnson , E. R.; Vinqvist, M. R.; Wright, J. S.; Barclay, L. R. C.; Ingold, K. U. *J. Org. Chem.* **2002**, *67*, 5190.

(40) Rhile I. J.; Markle T. F.; Nagao H.; DiPasquale A. G.; Lam O. P.; Lockwood M. A.; Rotter K.; Mayer J. M. *J. Am. Chem. Soc.* **2006**, *128*, 6075.

(41) Binstead, R. A.; Zuberbuhler, A. D.; Jung, B (**2004**) *SpecFit* (Spectrum Software Associates, Chapel Hill, NC).

(42) Frisch, M. J.; Trucks, G. W.; Schlegel, H. B.; Scuseria, G. E.; Robb, M. A.; Cheeseman, J. R.; Montgomery, Jr., J. A.; Vreven, T. K.; Kudin, N.; Burant, J. C.; Millam, J. M.; Iyengar, S. S.; Tomasi, J.; Barone, V.; Mennucci, B.; Cossi, M.; Scalmani, G.; Rega, N.; Petersson, G. A.; Nakatsuji, H.; Hada, M.; Ehara, M.; Toyota, K. ; Fukuda, R.; Hasegawa, J.; Ishida, M.; Nakajima, T.; Honda, Y.; Kitao, O.; Nakai, H.; Klene, M.; Li, X.; Knox, J. E.; Hratchian, H. P.; Cross, J. B.; Bakken, V.; Jaramillo, C.; Gomperts, R.; Stratmann, R. E.; Yazyev, O.; Austin, A. J.; Cammi, R.; Pomelli, C.; Ochterski, J. W.; Ayala, P. Y.; Morokuma, K.; Voth, G. A.; Salvador, P.; Dannenberg, J. J.; Zakrzewski, V. G.; Dapprich, S.; Daniels, A. D.; Strain, M. C.; Farkas, O., Malick, D. K.; Rabuck, A. D.; Raghavachari, K.; Foresman, J. B.; Ortiz, J. V.; Cui, Q.; Baboul, A. G.; Clifford, S.; Cioslowski, J.; Stefanov, B. B.; Liu, G.; Liashenko, A.; Piskorz, P.; Komaromi, I.; Martin, R. L.; Fox, D. J.; Keith, T.; Al-Laham, M. A.; Peng, C. Y.; Nanayakkara, A.; Challacombe, M.; Gill, P. M. W.; Johnson, B.; Chen, W.; Wong, M. W.; Gonzalez, C.; Pople, J. A. *Gaussian 03*, Revision D.02, Gaussian, Inc., Wallingford CT, 2004.

(43) Z. Otwinowski and W. Minor, "Processing of X-ray Diffraction Data Collected in Oscillation Mode", Methods in Enzymology, Volume 276: Macromolecular

Crystallography, part A, p.307-326, 1997,C.W. Carter, Jr. & R. M. Sweet, Eds., Academic Press (New York).

(44) Altomare, A.; Burla, C.; Camalli, M.; Cascarano, L.; Giacovazzo, C.; Guagliardi, A.; Moliterni, A. G. G.; Polidori, G.; Spagna, R.; *J. Appl. Cryst*. **1999**, *32*, 115.

(45) Altomare A, Cascarano G, Giacovazzo C, Guagliardi A. *J. Appl. Cryst*. **1993**, *26*, 343.

(46) Sheldrick G. M. SHELXL-97, Program for the Refinement of Crystal Structures. University of Göttingen, Germany, 1997.

(47) Mackay, S.; Edwards, C.; Henderson, A.; Gilmore, C.; Stewart, N.; Shankland, K.; Donald, A. *MaXus* University of Glasgow, Scotland, 1997.

Chapter 4

Towards the Synthesis of Cobalt-cyclam Complexes with Pendent Bases for Catalytic Oxygen Reduction

4.1 Introduction

The efficient electrochemical reduction of dioxygen to water is critical to the development of hydrogen as a clean, renewable source of fuel. The proton-coupled reduction of O_2 to H_2O (equation 4.1), is the cathodic half-reaction in hydrogen polymer electrolyte membrate (PEM) fuel cells.[1,2] The reduction of O_2 requires the movement of four electrons and four protons (a multi proton-coupled electron transfer (PCET) process), through potentially very reactive intermediates.[3] An effective catalyst must stabilize these intermediates and make these PCET reactions kinetically feasible in order to operate at an acceptable overpotential.[4]

$$O_2 + 4e^- + 4H^+ \rightarrow 2H_2O \qquad (4.1)$$

There are many transition metal complexes capable of activating O_2 and catalyzing its reduction. [5-10] However, many of these catalysts either operate at high overpotentials or rely on scarce, expensive platinum-group metals. While considerable effort has gone into understanding and controlling electron delivery in this process, there has been relatively little attention paid to proton delivery. However, in the related PCET process of catalytic proton reduction to hydrogen, a number of research groups, most notably the DuBois group, have demonstrated that incorporating pendent bases into the second coordination sphere of a transition metal catalyst can have a significant impact on improving catalyst turn over frequency and overpotential.[11-24] These pendent bases act as proton relays, shuttling protons to the metal, facilitating PCET.

There are a few examples of oxygen reduction catalysts with pendent non-coordinating bases.[25-28] In these systems, catalysis was more efficient with complexes incorporating proton relays versus the analogous complexes without basic sites in the second coordination sphere. Nocera and coworkers have also demonstrated that the proton relay can drive product selectivity towards H_2O versus H_2O_2 in his "hangman" porphyrin and corrole ligand systems[25,26], and similar selectivity enhancement has been seen with a related iron carboxyphenylporphyrin system.[27] However, the specific role of the proton relay in each of these systems was not well

characterized. We therefore sought to develop a system that would allow for studying in detail the effect of pendent proton relays on O_2 reduction.

The catalytic two-electron reduction of O_2 to H_2O_2 by Co(II) complexes of the tetraazamacrocycles cyclam[29] (1,4,8,11-tetrazacyclotetradecane) and hexamethylcyclam[30] (5,5,7,12,12,14-hexamethyl-1,4,8,11-tetraazacyclotetradecane) has been studied extensively by electrochemical methods. Co(II) cyclam reacts readily with O_2 to form a Co(III)-superoxo species. One-electron reduction in acid produces a Co(III)-hydroperoxo. Further reduction and protonation releases hydrogen peroxide, yielding the starting Co(II) cyclam. Because of this well understood O_2 reduction chemistry, derivatives of Co(II) complexes of cyclam incorporating proton relays were chosen as a potential system for studying the effects of proton relays on this reaction. Although these complexes are only capable of partial O_2 reduction rather than the preferred four-electron reduction, the intermediates in these systems have known potentials, allowing the effect of proton relays on these systems to be observed. Additionally, the cyclam macrocyclic system was chosen because of the high stability of these complexes to acids and oxidants, as well as the perceived ease of synthesis of cyclams relative to tetraaza macrocycles such as porphyrins and corroles.

4.2 Results and Discussion

4.2.1 Attempted Synthesis of Hexaazacyclam Ligands

Initial attempts to introduce pendent bases into cobalt complexes with cyclam ligands focused on synthesis of complexes with amines in the 6 and 13 positions of the cyclam macrocycle (a hexaazacyclam). The synthesis of these ligands has been reported previously by Kang *et al.* by the Ni^{+2} or Cu^{+2} templated condensation reaction of ethylenediamine, formaldehyde, and a primary amine RNH_2 (Scheme 4.1).[31-34] Unfortunately, the synthesis of cobalt complexes of these ligands was not possible. Metal templated synthesis is required to form the macrocyclic ring rather than linear oligomers of amines. Repeating the reported syntheses for R = benzyl,[34] *t*-butyl,[34] or ethylamine[33] gave intractable mixtures of products. A product could be obtained by repeating the Cu^{+2} templated synthesis of the hexaazacyclam with R = methyl that matched literature report of the UV-Vis spectrum.[34] Removal of the Cu^{+2} from this complex to isolate the free ligand was not possible. Methanol solutions of $[Cu(Me_2hexazacyclam)][BF_4]_2$ did not change color when refluxed with excess EDTA or KCN.

The addition of NaHS to [Cu(Me_2-hexazacyclam)][BF_4]$_2$ in methanol did precipitate CuS, but evaporating this solution to dryness after Cu precipitation did not leave behind any organic products. This is likely because the NH-CH_2-NR aminal linkages in the free ligand are unstable, and readily hydrolyze in the strongly basic conditions required to extract the copper. The rapid decomposition of the ligand produces formaldehyde, methyl amine, and ethylenediamine, all of which are evaporated along with the solvent on drying. Kang *et al.* have previously reported that they too were unable to isolate the free ligand for this reason.[31]

Scheme 4.1: Cu^{+2} templated synthesis of R_2-hexaazacyclam.

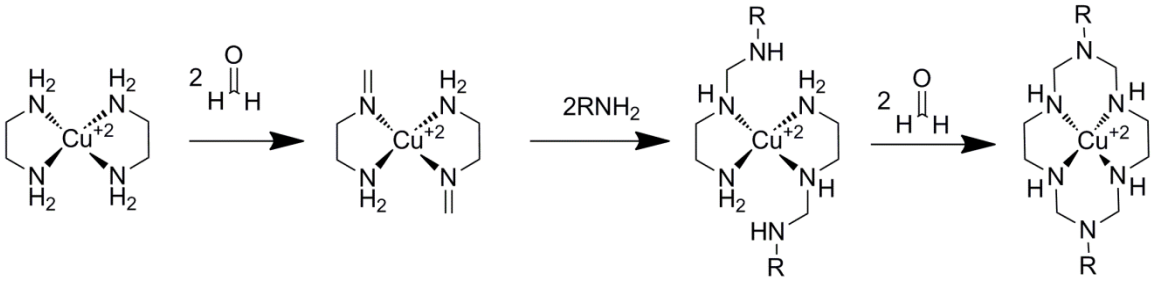

Because it was not possible to remove the metal template at ligand synthesis, synthesis of Me_2-hexaazacyclam with Co^{+2} as the templating metal was attempted, following essentially the same procedure used to obtain the Cu^{+2} complex. Synthesis of a cobalt complex by this method was previously reported by Arjmand *et al*., albeit without any characterization other than CHN compositional analysis.[35,36] Following this procedure, a mixture of blue and green powder was isolated with ^{1}H NMR chemical shifts in the diamagnetic region of the spectrum, suggesting a Co^{+3} product. However, it was not possible to identify this product with the ^{1}H NMR spectrum, and the ESI-MS mass spectrum did not give any peaks consistent with the desired product. Sargeson *et al*. have previously reported the synthesis of sepulchrate complexes of cobalt, in which the cobalt is encapsulated by a bicyclic cyclam-like ligand (Figure 4.1), from nearly identical synthetic conditions, but with a 3:1 rather than 2:1 ethylenediamine to cobalt ratio.[37] It seems likely from the mixture of colors that the product obtained by this method is a mixture of the sepulchrate product and other ethylenediamine and methylamine ligated products. Considering the large number of Ni^{+2} and Cu^{+2} complexes with these ligands as well as the lack of Co^{+2} complexes, it seems clear that it is not possible to obtain a hexaazacyclam by template synthesis on metals such as cobalt(II) that strongly prefer octahedral geometries, and removal of

a hexaazacyclam from a metal such as copper(II) that is stable in square planar geometries leads to destruction of the ligand.

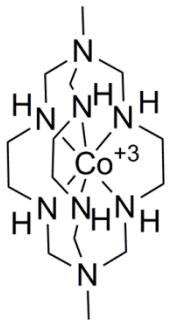

Figure 4.1: Sepulchrate cobalt complex from condensation reaction of ethylenediamine, formaldehyde, and methylamine.

4.2.2 Synthesis of *N*-Functionalized Cyclam Ligands

Cyclam was alkylated at the amines by the method of Royal *et al*. (Scheme 4.2)[38] in order to introduce two pendent bases into an already formed macrocycle and avoid the challenges of metal template reactions. This method uses formaldehyde to first form a bridged bisaminal cyclam (1,4,8,11-tetraazatricyclo[9.3.1.14,8]hexadecane) by an aqueous condensation reaction (Scheme 4.2). The bisaminal cyclam is insoluble in water and precipitates readily as the sole product. This versatile aminal protected cyclam reacts with alkyl halides in acetonitrile solution, precipitating exclusively the *trans*-di-*N*-alkylated product. The aminal bridges are then hydrolyzed in acidic or basic solution. Two cyclam derivatives were synthesized by this method. The first pendent base introduced through this method was a 2-picoline (2-methylpyridine, 2-pic) with a methylene linker between the amine of the cyclam and the pyridyl ring. The (2-pic)$_2$cyclam was readily synthesized from the bisaminal cyclam and 6-methyl-2-bromomethyl pyridine,[39] followed by hydrolysis in aqueous KOH. The *ortho* methyl was employed in an effort to prevent binding of the pendent pyridines to the metal center, as observed in a previously characterized Fe(II) complex without *ortho* methyl groups.[40]

Scheme 4.2: Synthesis of *N*-functionalized cyclams.

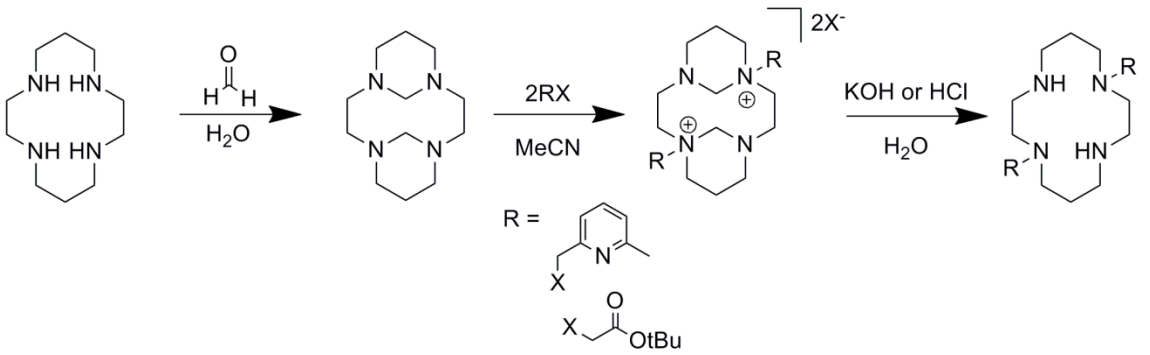

The second pendent base introduced by this method was acetate (Ac), to probe the effect of an anionic rather than neutral base. This $(Ac)_2$cyclam species is short lived as the neutral free ligand. It has been reported to rapidly and irreversibly cyclize to the lactam,[41] even when protected as the ethyl ester.[42] Therefore, the bisaminal protected cyclam was reacted with a *t*-butyl protected bromoacetate to give $(tBu\text{-}Ac)_2$cyclam, by a modification of a recently reported procedure.[43] Deprotection of the bisaminal diammonium salt could not be done with aqueous KOH, as this lead to rapid lactamization, so this was accomplished with ethanolic HCl, which precipitates the aminal-hydrolyzed HCl salt with the esters intact. After neutralization with $NaHCO_{3(aq)}$ and extraction into dichloromethane, the neutral *t*-butyl protected ligand ($(t$BuAc$)_2$cyclam) is obtained. The *t*-butyl protecting group is sufficiently stable to base-catalyzed hydrolysis that this compound is stable to lactamization as a solid at −20°C for weeks, and lasts for days in aqueous solution.

4.2.3 Synthesis and Characterization of $[Co((2\text{-pic})_2cyclam)]^{2+}$

A cobalt complex of the $(2\text{-pic})_2$cyclam ligand was obtained by stirring $CoCl_2 \bullet 6H_2O$ in a methanolic solution of the ligand. Only a slight color change of the red $CoCl_2 \bullet 6H_2O$ solution to a pink solution was observed upon addition of the ligand, and no further change was observed after three hours of reflux. This pink color, which is typical of octahedrally ligated Co^{II} complexes, remained after bubbling the solution with air and refluxing the solution in air, indicating that this species is not sensitive to oxidation by O_2 like the parent $Co(cyclam)Cl_2$. ^{1}H-NMR spectra recorded in methanol-d_4 shows the complete disappearance of the resonances for $(2\text{-pic})_2$cyclam upon the addition of $CoCl_2 \bullet 6H_2O$ from the diamagnetic region of the spectrum

(0-10 ppm), indicating that the ligand is coordinated to a paramagnetic, likely Co^{II}, center. Further evidence of this species' stability to oxidation was obtained by adding an excess of $H_2O_{2(aq)}$ to the methanol solution of $[Co((2\text{-pic})_2cyclam)]^{2+}$, which also did not produce any visible change in the solution.

A solid product could be isolated from solutions of $[Co((2\text{-pic})_2cyclam)]^{2+}$ by adding an excess of $KPF_{6(aq)}$. On standing at 5 °C overnight, a mixture of white crystals precipitated, leaving a nearly colorless solution. The purple crystals were found by X-ray crystallography to be $[Co((2\text{-pic})_2cyclam)][PF_6]_{1.5}[Cl]_{0.5}\bullet 0.15H_2O$, and the white crystals presumed to be KPF_6. These purple crystals are soluble in acetone, but have limited solubility in methanol, DMSO, and acetonitrile, and no appreciable solubility in CH_2Cl_2, THF, ethyl acetate, or water. This low solubility may be the result of the mixture of Cl^- and PF_6^- counterions. No attempt has been made to improve the solubility of this species by anion exchange. The ^{1}H-NMR spectrum of the isolated crystals, like that of the solution they were obtained from, has no resonances in the typical diamagnetic region from 0-20 ppm.

The X-ray structure of $[Co((2\text{-pic})_2cyclam)][PF_6]_{1.5}[Cl]_{0.5}\bullet 0.15H_2O$ shows that the ligand coordinates to the Co center through the picolyl nitrogens as well as the macrocyclic amines (Figure 4.2, bond lengths and angles in Table 4.1), giving the Co a distorted octahedral geometry. Accommodating the coordination of the picolyl nitrogens forces the cyclam into a strained *cis* coordination geometry. This strained geometry may prevent effective electron removal from the Co^{+2}, explaining its oxidative stability. The longest Co−N distances are from the alkylated macrocyclic nitrogens, which are almost 2.3 Å.

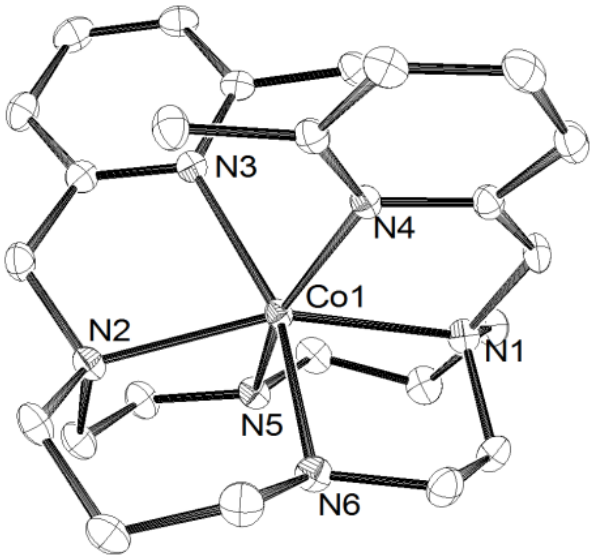

Figure 4.2: ORTEP diagram of $[Co((2\text{-pic})_2cyclam)][PF_6]_{1.5}[Cl]_{0.5}\bullet 0.15H_2O$. For clarity, only the cationic portion is shown, and hydrogen atoms have been omitted. Crystallographic data given in Table 4.3.

Table 4.1: Selected bond lengths (Å) and angles (°) for $[Co((2\text{-pic})_2cyclam)][PF_6]_{1.5}[Cl]_{0.5}\bullet 0.15H_2O$.

Bond		Angle	
Co1−N1	2.2911(14)	N1−Co1−N2	157.96(5)
Co1−N2	2.2982(13)	N5−Co1−N6	95.20(5)
Co1−N3	2.2386(13)	N3−Co1−N4	90.68(5)
Co1−N4	2.2094(13)	N3−Co1−N5	89.67(5)
Co1−N5	2.1470(13)	N1−Co1−N3	118.65(5)
Co1−N6	2.1464(13)	N2−Co1−N3	77.39(5)

The $[Co((2\text{-pic})_2cyclam)]^{2+}$ is not stable in the presence of acid. Additions of aliquots of up to one equivalent of *p*-toluenesulfonic acid to a pink acetone solution of $[Co((2\text{-pic})_2cyclam)][PF_6]_{1.5}[Cl]_{0.5}$ gives a blue solution. By UV-vis spectroscopy, complex, non-isosbestic behavior is observed (Figure 4.3). After one equivalent of acid has been added, a peak at 670 nm persists. This absorbance is nearly identical to $CoCl_2$ in acetone, suggesting complete loss of ligand at one equivalent of strong acid. After the addition of more than 1 equivalent of

tosylic acid, a white precipitate formed that was confirmed by ^{1}H-NMR to be the tosylic acid salt of (2-pic)$_2$cyclam.

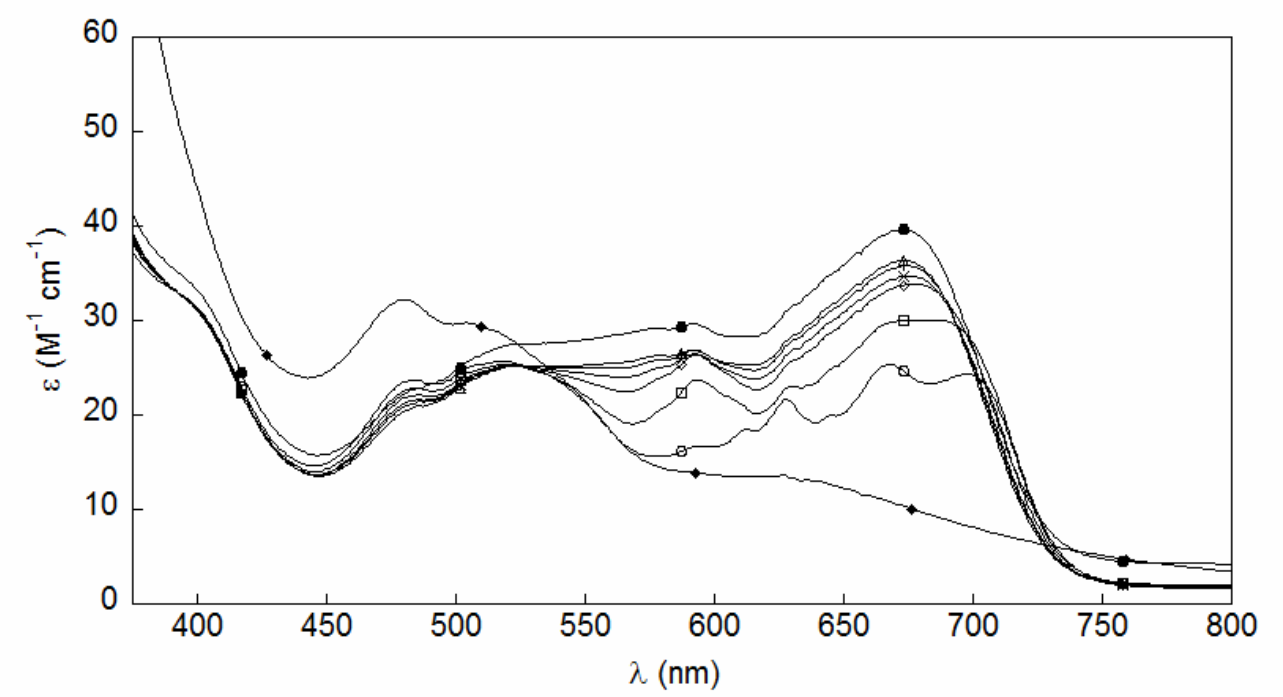

Figure 4.3: UV-Vis spectra of [Co((2-pic)$_2$cyclam)][PF$_6$]$_{1.5}$[Cl]$_{0.5}$ in acetone solution (♦), and with the addition of 0.13 (○), 0.25 (□), 0.38 (◊), 0.50 (x), 0.63 (|), 0.75 (Δ), and 1.0 (●) equivalents of tosylic acid.

The oxidation of [Co((2-pic)$_2$cyclam)]$^{2+}$ was explored by cyclic voltammetry (CV). The CV of [Co((2-pic)$_2$cyclam)]$^{2+}$ in acetonitrile (0.1M [*n*-Bu$_4$N][PF$_6$]) (Figure 4.4) gives one reversible wave, with $E_{1/2}$ of ca. +0.70 V vs. Cp$_2$Fe, which likely corresponds to the Co$^{2+/3+}$ couple. This very high oxidation potential is consistent with the lack of O$_2$ reactivity observed for this complex.

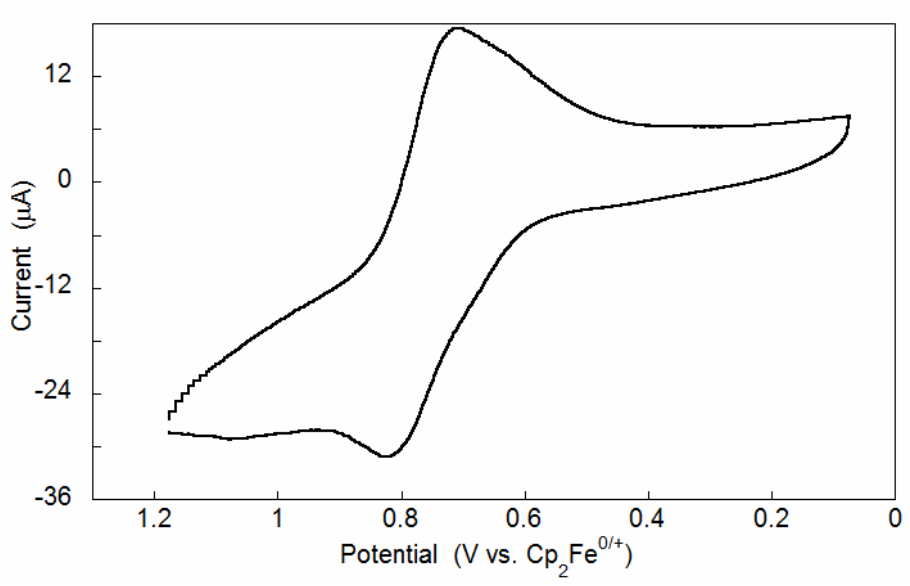

Figure 4.4: Oxidizing cyclic voltammogram of $[Co((2\text{-pic})_2cyclam))][PF_6]_{1.5}[Cl]_{0.5}$ in acetonitrile under N_2. Voltammogram recorded at 0.1 V/s on *ca.* 5 mM solutions of Co complex in acetonitrile (0.1 M [*n*-Bu_4N][PF_6]).

4.2.4 Synthesis and Characterization of $[Co((Ac)_2cyclam)]^+$

A cobalt complex of $(Ac)_2$cyclam was obtained by first deprotecting (*t*BuAc)cyclam with excess LiOH in methanol. The crude reaction mixture was then combined with 1 equivalent of $CoCl_2 \bullet H_2O$ and refluxed open to air. The solution changed from pink to black, consistent with aerobic oxidation to Co^{III}. The solution was neutralized by adding $HPF_{6(conc)}$. On standing overnight at 5 °C, $[Co((Ac)_2cyclam)][PF_6]$ precipitated as a brown solid in very low yield. Red, X-ray quality crystals were obtained by recrystallization from hot water ($\lambda_{max(MeCN)}$ = 453 nm). X-ray crystallography was the only method that used to determine the composition of this material, as no identifiable peaks were present by ESI-MS in acetonitrile, and the ^{1}H-NMR was too complex to be interpreted despite having peaks in the diamagnetic region. Attempts to ligate Co^{+2} prior to cleaving the *t*-butyl esters of the ligand were not successful. Reaction of $CoCl_2 \cdot 6H_2O$ in aerobic methanol with the *t*-butyl protected cyclam followed by precipitation with excess KPF_6 gave a red solid which could not be identified by NMR or ESI-MS.

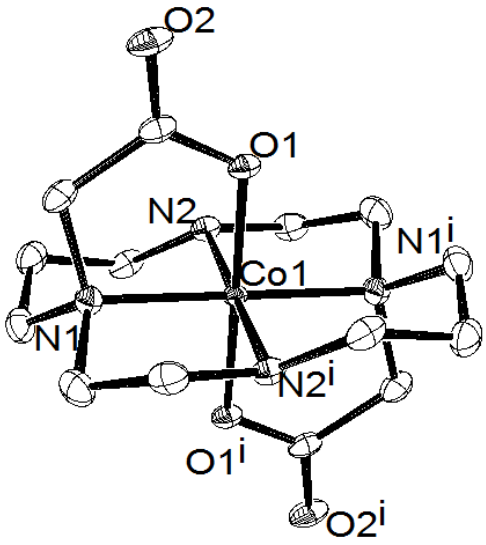

Figure 4.5: ORTEP diagram of [Co((Ac)$_2$cyclam)][PF_6]•MeOH. Thermal ellipsoids shown at 50% probability. For clarity, only the cationic portion is shown, and hydrogen atoms have been omitted. Crystallographic data are given in Table 4.3.

Table 4.2: Selected bond lengths (Å) and angles (°) for [Co((Ac)$_2$cyclam)][PF_6]•MeOH.

Bond		Angle	
Co1−N1	1.975(3)	N1−Co1−N2	92.68(11)
Co1−N2	1.973(3)	N1−Co1−N2^i	87.32(11)
Co1−O1	1.884(2)	O1−Co1−N2^i	89.70(10)
		O1−Co1−N2	90.30(10)

The X-ray structure of [Co((Ac)$_2$cyclam)][PF_6], obtained from these crystals (Figure 4.5, selected bond lengths and angles in Table 4.2) shows that the cyclam macrocycle is bound in the *trans* geometry, and the whole cationic portion is C_{2h} symmetric. The acetate groups are bound axially, giving a the Co^{III} center a nearly octahedral geometry. The single PF_6^- counterion confirms that this is a Co^{III} complex. The Co-N bonding distance are also shorter relative to [Co((2-pic)$_2$cyclam)][PF_6]$_{1.5}$[Cl]$_{0.5}$.

UV-vis acid titration of an acetonitrile solution of [Co((Ac)$_2$cyclam)][PF$_6$] with 2,6-dichloroanilinium tetrafluoroborate (pK_a = 5.1)[44] caused the peak at 453 nm to diminish in intensity until 1 equivalent of acid had been added (Figure 4.6). A very large initial decrease in absorbance is observed upon the addition of 0.02 equivalents of acid, and subsequent acid additions also do not result in monotonic changes in absorbance. This may be due to the solution becoming less cloudy as some species becomes more soluble in the presence of acid. Upon the addition of greater than 1 and up to 8 equivalents of acid, essentially no change was observed in the UV-vis absorbance. Though added acid clearly interacts with [Co((Ac)$_2$cyclam)][PF$_6$], is not clear if this interaction involves protonation and dissociation of one of the acetate arms.

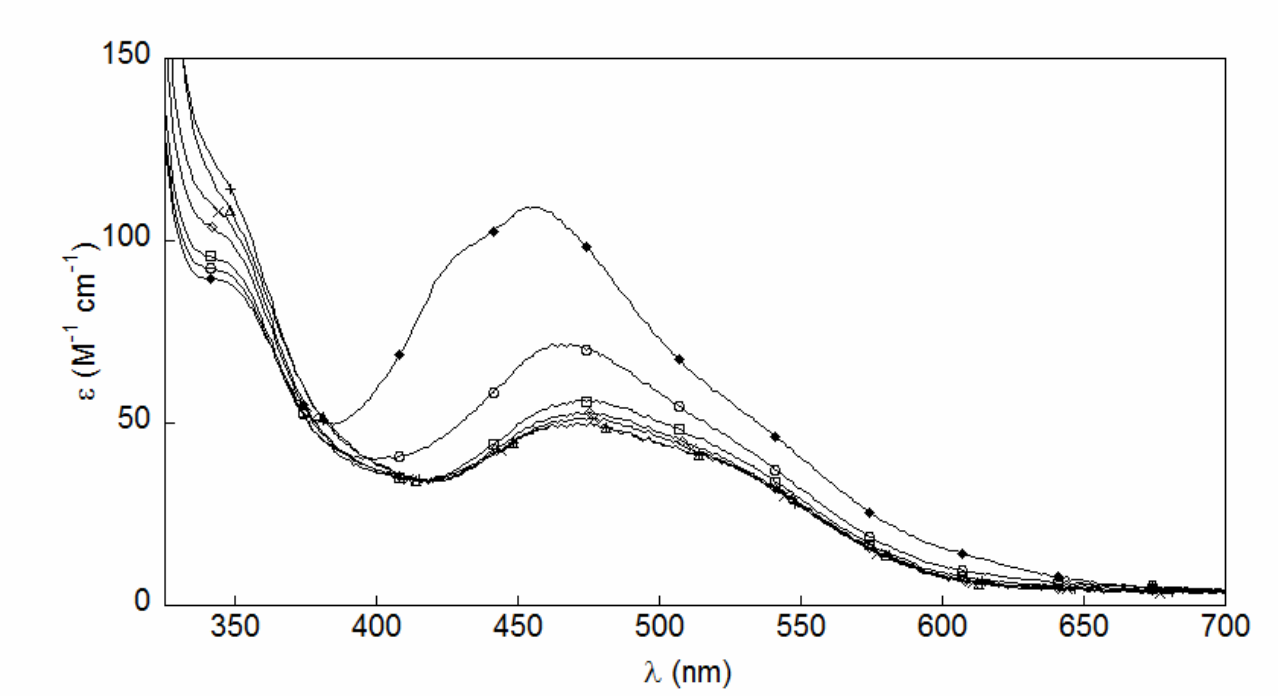

Figure 4.6: UV-Vis spectra of [Co((Ac)$_2$cyclam)][PF$_6$] in acetonitrile solution (♦), and with the addition of 0.02 (○), 0.10 (□), 0.50 (◊), 1.0 (x), 4.0 (+), and 8.0 (Δ) equivalents of 2,6-dichloroanilinium tetrafluoroborate.

Table 4.3: Crystallographic data for cobalt cyclam complexes.

	[Co((2-pic)$_2$cyclam)] [PF$_6$]$_{1.5}$[Cl]$_{0.5}$•0.15H$_2$O	[Co((Ac)$_2$cyclam)][PF$_6$]•MeOH
Formula	$C_{48}H_{76.6}ClCo_2F_{18}N_{12}P_3O_{0.3}$	$C_{15}H_{30}CoO_5N_2F_6P$
T (K)	110(2)	110(2)
Wavelength	0.71073 Å	0.71073 Å
Size (mm)	0.50 x 0.08 x 0.06	0.19 x 0.06 x 0.03
Cryst. Syst	Triclinic	Orthorhombic
Space group	P -1	P n m a
a (Å)	9.8342(3)	15.1730(3)
b (Å)	9.8618(3)	19.2273(3)
c (Å)	15.8737(5)	7.12240(10)
α (deg)	96.027(2)	90
β (deg)	97.162(2)	90
γ (deg)	101.569(2)	90
V (Å^3)	1482.99(8)	2077.86(6)
Z	1	4
D_{calc} (g/cm^3)	1.584	1.759
Abs. coeff. (mm^{-1})	0.789	0.994
Reflections total	57730	21698
Reflections uniq. (R_{int})	9037 [R(int) = 0.0394]	2655 [R(int) = 0.0616]
Data/restraints/ parameters	9037 / 24 / 406	2655 / 0 / 158
GOF	0.904	1.102
R1/wR2 [I>2σ(I)]	0.0337 / 0.0787	0.0468 / 0.1075
R1/wR2 (all data)	0.0525 / 0.0883	0.0720 / 0.1175

4.2.5 Electrochemical Reduction of [Co((Ac)$_2$cyclam)]$^+$

The reduction of [Co((Ac)$_2$cyclam)][PF$_6$] was monitored by CV of a *ca.* 10 mM solution in acetonitrile (0.1M [*n*-Bu$_4$N][PF$_6$]) (Figure 4.7). Under a N_2 atmosphere, a reversible wave was observed at −1.05 V vs. Cp_2Fe. This wave is believed to correspond to the $Co^{III/II}$ couple. This potential is significantly negative of the $Co^{III/II}$ couple for the parent [Co(cyclam)Cl$_2$][Cl] (−0.69 V vs. Cp_2Fe).[45] This difference is presumably due to the chelating acetate arms remaining bound in solution giving the complex a +1 charge, while for [Co(cyclam)Cl$_2$][Cl] the chlorides can dissociate in acetonitrile with 0.1 M electrolyte, giving the complex a +2 or +3 charge. This potential is too close to the potential for reduction of O_2 to $O_2^{-\bullet}$ at the glassy carbon electrode

under these conditions ($E_{1/2} \approx -1.3$ V) to observe reaction of a reduced [Co^{II}((Ac)$_2$cyclam)] species with O_2.

Upon the addition of ~1 equivalent of tosylic acid to an acetonitrile solution of [Co((Ac)$_2$cyclam)][PF_6] under a N_2 atmosphere, a new reductive wave appeared centered at ca. −0.2 V. This new wave may correspond to the protonated species observed by UV-Vis spectroscopy, which might be reduced at a more positive potential than the unprotonated [Co((Ac)$_2$cyclam)][PF_6]. This wave was not reversible, and in fact the current of the reoxidation wave was greater than that of the initial reduction wave. The Co(II/III) couple of the unprotonated species was still observed, with no drop in the peak currents of this wave. The new electrochemical process occurring during this reduction could not be determined, but this new protonated species was tested for possible electrocatalytic O_2 reduction by introducing an air atmosphere and an excess of tosylic acid. Strangely, in the presence of air, the irreversible wave at −0.2 V was no longer observed. Instead, the only wave observed is that of O_2 reduction at the electrode, which in the presence of acid shifts to a more positive potential, with complex, irreversible reduction wave features. Nearly identical waves are seen in CVs without Co complex under identical conditions. Without any understanding of what the acidic [Co((Ac)$_2$cyclam)][PF_6] wave corresponded to or what protonated species was initially present in solution prior to the addition of air, it was impossible to explain this disappearance. However, because no electrocatalytic O_2 reduction involving a cobalt species was observed, further understanding of the electrochemical behavior of [Co((Ac)$_2$cyclam)][PF_6] was not pursued.

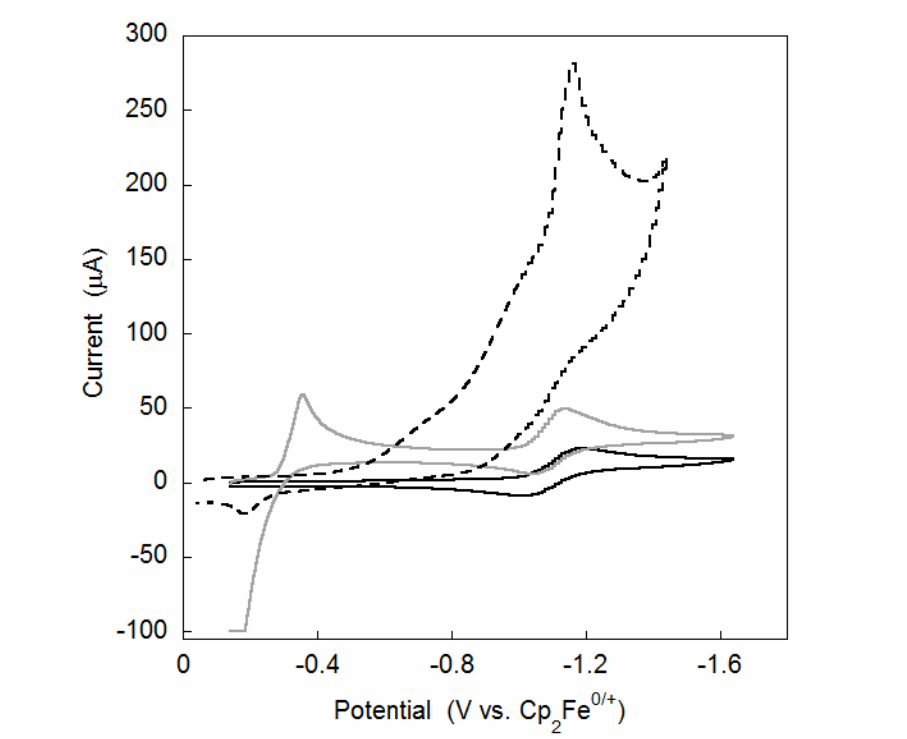

Figure 4.7: Reductive cyclic voltammograms of [Co((Ac)$_2$cyclam)][PF_6] in acetonitrile under N_2 (solid line, black), under N_2 with 1 equiv. tosylic acid (solid line, gray), and under air with 4 equiv. tosylic acid (dashed line, black). Voltammograms recorded at 100 mV/s on *ca.* 10 mM solutions of complex in acetonitrile (0.1 M [*n*-Bu_4N][PF_6]).

4.3 Conclusions

Derivatives of cyclam with pendent bases were explored as ligands for cobalt for studying oxygen reduction. The synthesis of macrocyclic amine ligands with pendent bases is challenging. However, cyclam ligands functionalized with pendent bases attached at the 1 and 7 positions have been successfully synthesized. Cobalt complexes of these ligands could be synthesized. However, both anionic acetate and neutral pyridine bases bind strongly to the cobalt center. This binding appears to prevent reactivity with O_2 under catalytically useful conditions. These studies highlight a key challenge in developing catalysts with pendent bases as proton relays, that pendent bases that bind protons can also bind to the metal. To overcome this, it is necessary to design ligands in which the ligands that bind in the first coordination sphere can bind much more strongly than the pendent bases, and pendent bases must be held rigidly away from binding to the metal to leave a coordination site available to the substrate. Attempts to use

such a ligand type for oxygen reduction, 1,5-diaza-3,7-diphosphacyclooctane ligands developed by the DuBois group,[11] are described in Chapters 5 and 6.

4.4 Experimental

4.4.1 General Considerations

All reagents were purchased from Aldrich, solvents from Fisher, and deuterated solvents from Cambridge Isotope Labs unless otherwise noted. 1,4,8,11-tetraazatricyclo[9.3.1.14,8]hexadecane was prepared according to literature,[38] using cyclam purchased from Strem. NMR spectra were recorded on a Bruker AV300 spectrometer; chemical shifts are reported relative to TMS in ppm by referencing to the residual solvent signals. Mass spectrometry was performed on a Bruker Esquire Ion Trap Mass Spectrometer using electrospray ionization. UV-Vis spectra were recorded in glass cuvettes using a Hewlett-Packard 8453 diode array spectrophotometer.

4.4.2 Synthesis

4.4.2.1 Typical synthetic procedure for attempted synthesis of R_2-hexaazacyclam To a solution of $MCl_2 \cdot xH_2O$ (M = Co, Cu, Ni) (30 mmol) in 50 mL of methanol was added ethylenediamine (60 mmol) dropwise. This solution was stirred for 30 minutes. The amine RNH_2 was added (60 mmol), and the solution was brought to reflux. Once the solution was refluxing, aqueous formaldehyde (37 wt %, 120 mmol) was added dropwise over 20 minutes. The reaction mixture was refluxed overnight, and then cooled to room temperature. The mixture was acidified with aqueous $HClO_4$ (72%) or HBF_4 (50%) to a pH of ~1, and then cooled to 5 °C and stored overnight. *Caution: Perchlorate salts are explosive, and perchloric acid solutions may explode if the perchlorate concentration exceeds 72%. Manipulations of these materials, especially drying/concentrating, should only be performed on a small scale and with extreme caution. Addition of perchloric acid in this case was performed by dividing the reaction into batches of ~20% of the total reaction mixture volume and acidifying each batch individually.* On standing a sticky solid formed that was collected by filtration and washed with ice-cold ethanol/ether. In most cases, $HClO_4$ gave significantly higher yields of solid than HBF_4, but the materials obtained with both acids were qualitatively the same by UV-Vis spectroscopy.

4.4.2.2 (2-pic)$_2$cyclam A solution of 1,4,8,11-tetraazatricyclo[9.3.1.14,8]hexadecane (1.0 g, 4.5 mmol) in 50 mL of acetonitrile was combined with with a solution of 6-methyl-2-bromomethylpyridine (3.3 g, 18 mmol) in 20 mL of acetonitrile. The red solution was stirred for 2 days, forming a white precipitate. The precipitate was separated by filtration and washed with several small portions of ice-cold acetonitrile to remove some remaining pink color from the precipitate. The precipitate was then dried under vacuum for several hours. The dried precipitate was dissolved in 50 mL of 2M aqueous KOH, and stirred for 30 minutes. The solution was then extracted 3 times with 50 mL of chloroform. The chloroform extracts were dried over $MgSO_4$ and vacuum dried to yellow oil. Repeated trituration with hexanes and vacuum drying gave (2-pic)$_2$cyclam as a white solid (0.71 g, 39% yield). NMR($CDCl_3$) ^{1}H: δ 7.47 (t, *J* = 7.7 Hz, 2H, Ar-*H*), 7.23 (d, *J* = 7.7 Hz, 2H, Ar-*H*), 6.95 (d, *J* = 7.6 Hz, 2H, Ar-*H*), 3.78 (s, 4H, pic-C*H*$_2$-NH), 2.93 – 2.51 (br m, 18H, NC*H*$_2$ and N*H*), 2.51 (s, 6H, pic-C*H*$_3$), 1.84 (m, 4H, $NCH_2CH_2CH_2N$).

4.4.2.3 (tBu-Ac)$_2$cyclam To a solution of 1,4,8,11-tetraazatricyclo[9.3.1.14,8]hexadecane (3.2 g, 14 mmol) in 50 mL of acetonitrile was added *t*-butylbromacetate (8.3 mL, 32 mmol). The solution was stirred for 1 day, forming a white precipitate. The precipitate was separated by filtration, washed with ice-cold acetonitrile, and dried under vacuum to give hydrochloride salt as a white powder. The hydrochloride salt was suspended in 150 mL of ethanol to which approximately 15 mL of concentrated HCl was added quickly dropwise until the white solid was completely dissolved, giving a clear colorless solution. Stirring for 15 minutes caused the precipitation of the hydrochloride salt of (tBu-Ac)$_2$cyclam, which was separated by filtration and washed with cold ethanol. The hydrochloride salt was dissolved in a sufficient volume of saturated aqueous Na_2CO_3 such that the pH of the solution was ~10, and then extracted five times with an equal volume of chloroform. The chloroform extracts were dried over $MgSO_4$ and vacuum dried to yellow oil. Repeated trituration with hexanes and vacuum drying gave neutral (tBu-Ac)$_2$cyclam as a white solid (1.35 g, 22% yield). This compound decomposes over a period of days on the benchtop, but is stable for a few weeks at −20 °C. NMR($CDCl_3$) ^{1}H: δ 3.34 (s, 4H, NC*H*$_2$C=O), 2.72-2.63 (br m, 18 H, NC*H*$_2$ and N*H*), 1.74 (m, 4H, $NCH_2CH_2CH_2N$), 1.44 (s, 18H, *t*Bu-C*H*$_3$).

4.4.2.4 $[Co((2\text{-pic})_2cyclam)][PF_6]_{1.5}[Cl]_{0.5}\bullet 0.15H_2O$ To a solution of $(2\text{-pic})_2$cyclam (0.21 g, 0.51 mmol) in 20 mL of methanol was added solid $CoCl_2\bullet 6H_2O$ (0.12g, 0.50 mmol). The pink solution was reflux for 3 hours, cooled to room temperature, and excess KPF_6 (1.0 g) in 15 mL H_2O was added. The solution was stored at 5°C for 12 hours, affording purple crystals of $[Co((2\text{-pic})_2cyclam)][PF_6]_{1.5}[Cl]_{0.5}\bullet 0.15H_2O$, as well as some crystals of KPF_6 (*ca.*10-15% of material) (0.40 g of total material, 0.36 g expected for 100% yield with no KPF_6). λ_{max} (acetone) = 480 nm.

4.4.2.5 $[Co((Ac)_2cyclam)][PF_6]\bullet MeOH$ To a solution of $(tBu\text{-}Ac)_2$cyclam (1.2 g, 2.8 mmol) in 40 mL of methanol was added LiOH (0.59 g, 24.6 mmol). This solution was refluxed overnight, then vacuum dried to a white solid. The solid was redissolved in 30 mL of methanol, and then $CoCl_2\bullet 6H_2O$ (0.65g, 2.7 mmol) in 5 mL of methanol was added. The reaction mixture was refluxed in air for 4 hours, with the pink color of the solution changing to a deep brown over the course of the reaction. To the reaction mixture was added concentrated aqueous HPF_6 until the pH was ~7, followed by excess LiPF6 (4 g). The reaction mixture was stored at 5°C overnight, giving a brown precipitate. Recrystallization from hot water gave red crystals of $[Co((Ac)_2cyclam)][PF_6]\bullet MeOH$ (0.11 g, 7% yield). λ_{max} (acetonitrile) = 453 nm.

4.4.3 X-ray Crystallography

Crystals were mounted on glass capillaries with Paratone-N oil (Hampton Research) and frozen immediately in a cold nitrogen gas stream. Data were collected on a Bruker APEX II single crystal X-ray diffractometer with Mo-Kα radiation (λ = 0.71073 Å) utilizing both Φ and Ω scans. Crystal-to-detector distance was 40 mm. The data was integrated and scaled using SAINT, SADABS within the APEX2 software package by Bruker.[46] Solution by direct methods (SHELXS, SIR97[47,48]) produced a complete heavy atom phasing model consistent with the proposed structure. The structure was completed by difference Fourier synthesis with SHELXL97.[49,50] Scattering factors are from Waasmair and Kirfel[51]. All hydrogen atoms were placed in geometrically idealized positions and constrained to ride on their parent atoms with C-H and N-H distances in the range 0.95-1.00 Angstrom (a riding model). Isotropic thermal parameters Ueq were fixed such that they were 1.2Ueq of their parent atom Ueq for CH's and

NH's, and 1.5Ueq of their parent atom Ueq in case of methyl groups. All non-hydrogen atoms were refined anisotropically by full-matrix least-squares.

4.4.4 Electrochemistry

Cyclic voltammetry (CV) was performed under N_2 using a E2 Epsilon electrochemical apparatus (BASi) equipped with glassy carbon (3.0 mm dia.) working electrode, platinum wire auxiliary electrode, and $Ag/Ag(NO)_3$ (0.01 M in acetonitrile) reference electrode. CV was carried out in acetonitrile with 0.1 M $[^nBu_4N][PF_6]$ as supporting electrolyte. $[^nBu_4N][PF_6]$ was recrystallized three times from ethanol and dried under vacuum at 110°C prior to use. Ferrocene was added as an internal standard, and all potentials are reported vs. the $Cp_2Fe^{+/0}$ couple.

4.5 Notes to Chapter 4

(1) Winter, M.; Broad, R. J. *Chem. Rev.* **2004**, *104*, 4245.

(2) Borup, R.; Meyers, J.; Pivovar, B.; Kim, Y. S.; Mukundan, R.; Garland, N.; Myers, D.; Wilson, M.; Garzon, F.; Wood, D.; Zelenay, P.; More, K.; Stroh, K.; Zawodzinski, T.; Boncella, J.; McGrath, J. E.; Inaba, M.; Miyatake, K.; Hori, M.; Ota, K.; Ogumi, Z.; Miyata, S.; Nishikata, A.; Siroma, Z.; Uchimoto, Y.; Yasuda, K.; Kimijima, K.-I.; Iwishita, N. *Chem. Rev.* **2007**, 107, 3904.

(3) Warren, J. J.; Tronic, T. A.; Mayer, J. M. *Chem. Rev.* **2010**, *110*, 6961.

(4) Savéant, J-M. *Chem. Rev.* **2008**, *108*, 2348.

(5) Bezerra, C. W. B.; Zhang, L.; Lee, K.; Liu, H.; Marques, A. L. B.; Marques, E. P.; Wang, H.; Zhang, J. *Electrochim. Acta.* **2008**, *53*, 4937.

(6) Anson, F. C., Shi, C.; Steiger, B. *Acc. Chem. Res.* **1997**, *30*, 437.

(7) Durand Jr., R. R.; Anson, F. J. *J. Electroanal. Chem.* **1982**, *134*, 273.

(8) Durand Jr., R. R.; Bencosme, C. S.; Collman, J. P.; Anson, F. C. *J. Am. Chem. Soc.* **1983**, *105*, 2710.

(9) Chang, C. J.; Loh, Z-H.; Shi, C.; Anson, F. C.; Nocera, D. G. *J. Am. Chem. Soc.* **2004**, *126*, 10013.

(10) Volpe, M.; Hartnett, H.; Leeland, J. W.; Wills, K.; Ogunshun, M.; Duncombe, B. J.; Wilson, C.; Blake, A. J.; McMaster, J.; Love, J. B. *Inorg. Chem.* **2009**, *48*, 5195.

(11) DuBois, M. R.; DuBois, D. L. *Chem. Soc. Rev.* **2009**, *38*, 62.

(12) Small, Y. A.; DuBois, D. L.; Fujita, E.; Muckerman, J. T. *Energy Environ. Sci.* **2011**, *4*, 3008.

(13) Liu, T.; Chen, S.; O'Hagan, M. J., DuBois, M. R.; Bullock, R. M.; DuBois, D. L. *J. Am. Chem. Soc.* **2012**, ASAP.

(14) Lounissi, S.; Capon, J.-F.; Gloaguen, F.; Matoussi, F.; Pétillon, F. Y.; Schollhammer, P.; Talarmin, J. *Chem. Commun.* **2011**, *47*, 878.

(15) Camara, J. M.; Rauchfuss, T. B. *Nature Chemistry* **2012**, *4*, 26.

(16) Helm. M. L.; Stewart, M. P.; Bullock, R. M.; DuBois, M. R.; DuBois, D. L. *Science* **2011**, *333*, 863.

(17) Wiese, S.; Kilgore, U. J.; DuBois, D. L.; Bullock, R. M. *ACS Catal.* **2012**, *2*, 720.

(18) Wilson, A. D.; Shoemaker, R. K.; Miedaner, A.; Muckerman, J. T.; DuBois, D. L.; DuBois, M. R. *Proc. Natl. Acad. Sci. U.S.A.* **2007**, *104*, 6951.

(19) Kilgore, U. J.; Stewart, M. P.; Helm, M. L.; Dougherty, W. G.; Kassel, W. S.; DuBois, M. R.; DuBois, D. L.; Bullock, R. M. *Inorg. Chem.* **2011**, *50*, 10908.

(20) Fraze, K.; Wilson, A. D.; Appel, A. M.; DuBois, M. R.; Dubois, D. L. *Organometallics* **2007**, *26*, 3918.

(21) Kilgore, U. J.; Roberts, J. A. S.; Pool, D. H.; Appel, A. M.; Stewart, M. P.; DuBois, M. R.; Dougherty, W. G.; Kassel, W. S.; Bullock, R. M.; DuBois, D. L. *J. Am. Chem. Soc.* **2011**, *133*, 5861.

(22) Yang, J. Y.; Chen. S.; Dougherty, W. G.; Kassel, W. S.; Bullock, R. M.; DuBois, D. L.; Raugei, S.; Rousseau, R.; Dupuis, M.; DuBois, M. R. *Chem. Commun.* **2010**, *46*, 8618.

(23) Lee, C. H.; Dogutan, D. K.; Nocera, D. G. *J. Am. Chem. Soc.* **2011**, *133*, 8775.

(24) Jacobsen, G. M.; Yang, J. Y.; Twamley, B.; Wilson, A. D.; Bullock, R. M.; DuBois, M. R.; DuBois, D. L. *Energy Environ. Sci.* **2008**, *1*, 167.

(25) McGuire, R.; Dogutan, D. K.; Teets, T. S.; Sutivich, J.; Shao-Horn, Y.; Nocera, D. G. *Chem. Sci.* **2010**, *1*, 411.

(26) Dogutan, D.; Stoian, S. A.; McGuire, R.; Schwalbe, M.; Teets, T. S.; Nocera, D. G. *J. Am. Chem. Soc.* **2011**, *133*, 131.

(27) Carver, C. T.; Matson, B. D.; Mayer, J. M. *J. Am. Chem. Soc.* **2012**, *134*, 5444.

(28) Yang, J. Y.; Bullock, R. M.; Dougherty, W. G.; Kassel, W. S.; Twamley, B.; DuBois, D. L.; Rakowski Dubois, M. *Dalton Trans.* **2010**, *39*, 3001.

(29) Geiger, T.; Anson, F. C. *Inorg. Chem.* **1981**, *103*, 7489.

(30) Kang, C.; Anson, F. C. *Inorg. Chem.* **1995**, *34*, 2771.

(31) Suh, M. P.; Kang, S-G. *Inorg. Chem.* **1988**, *27*, 2544.

(32) Kang, S-G.; Ryu, K.; Jung, S-K.; Kim, C-S. *Bull. Korean Chem. Soc.* **1996**, *17*, 331.

(33) Kang, S-G.; Ryu, K.; Jung, S-K.; Kim, J. *Inorg. Chim. Acta* **1999**, *293*, 140.

(34) Jung, S-K.; Kang, S-G., Suh, M. P. *Bull. Korean Chem. Soc.* **1989**, *10*, 363.

(35) Tabassum, S.; Parveen, S.; Arjmand, F. *Indian J. Chem., Sec. A* **2004**, *43*, 270.

(36) Tabassum, S.; Parveen, S.; Arjmand, F. *Trans. Met. Chem.* **2005**, *30*, 196.

(37) Geue, R. J.; Hambley, T. W.; Harrowfield, J. M.; Sargeson, A. M.; Snow, M. R. *J. Am. Chem. Soc.* **1984**, *106*, 5478.

(38) Royal, G.; Dauaoui-Gindrey, V; Dahaoui, S.; Tabard, A.; Guilard, R.; Pullumbi, P.; Lecomte, C. *Eur. J. Org. Chem.* **1998**, 1971.

(39) Feig, A. L.; Becker, M.; Schindler, S.; van Eldik; R.; Lippard, S. J. *Inorg. Chem.* **1996**, *35*, 2590.

(40) Hajj, F. E.; Sebki, G.; Patinec, V.; Marchivie, M.; Triki, S.; Handel, H.; Yefsah, S.; Tripier, R.; Gómez-García, C. J.; Coronado, E. *Inorg. Chem.* **2009**, *48*, 10416.

(41) Helps, I. M.; Parker, D.; Chapman, J.; Ferguson, G. *J. Chem. Soc. Chem. Commun.* **1988**, 1094.

(42) Helps, I. M.; Parker, D.; Murphy, J. R. Chapman, J. *Tetrahedron* **1989**, *45*, 219.

(43) Pandya, D. N.; Kim, J. Y.; Park, J. C.; Lee, H.; Phapale, P. B.; Kwak, W.; Choi, T. H.; Cheon, G. J.; Yoon, Y-R.; Yoo, J. *Chem. Commun.* **2010**, *46*, 3517.

(44) Kaljurand, I., Kütt, A., Sooväli, L., Rodima, T.; Mäemets, V.; Leito, I.; Koppel, I. A. *J. Org. Chem.* **2005**, *70*, 1019.

(45) Matsuoka, S.; Yamamoto, K.; Ogata, T.; Kusaba, M.; Nakshima, N.; Fujita, E.; Yanagida, S. *J. Am. Chem. Soc.* **1993**, *115*, 601.

(46) Bruker APEX2 (Version 2.1-4), SAINT (version 7.34A), SADABS (version 2007/4), BrukerAXS Inc, Madison, Wisconsin, USA, 2007.

(47) Altomare, A.; Burla, C.; Camalli, M.; Cascarano, L.; Giacovazzo, C.; Guagliardi, A.; Moliterni, A. G. G.; Polidori, G.; Spagna, R.; *J. Appl. Cryst*. **1999**, *32*, 115.

(48) Altomare A, Cascarano G, Giacovazzo C, Guagliardi A. *J. Appl. Cryst*. **1993**, *26*, 343.

(49) Sheldrick G. M. SHELXL-97, Program for the Refinement of Crystal Structures. University of Göttingen, Germany, 1997.

(50) Mackay, S.; Edwards, C.; Henderson, A.; Gilmore, C.; Stewart, N.; Shankland, K.; Donald, A. *MaXus* University of Glasgow, Scotland, 1997.

(51) Waasmaier, D.; Kirfel, A. *Acta Cryst. A*, **1995**, *51*, 416.

Chapter 5

Directing Protons to the Dioxygen Ligand of a Ruthenium(II) Complex with Pendent Amines in the Second Coordination Sphere[1]

5.1 Introduction

The activation and reduction of dioxygen (O_2) by transition metal centers are key to a variety of biochemical[2-5] and industrial processes.[6-8] Efficient reduction of dioxygen to water is also important in the operation of fuel cells.[9] These processes are typically proton-coupled electron transfer (PCET) reactions, requiring the coordinated movement of multiple protons and electrons.[10,11] In biological systems, it is known that initial dioxygen bonding is facilitated by hydrogen bonding and proton delivery.[12-15] A few recent synthetic transition-metal catalysts for oxygen reduction have utilized directed proton delivery from the metal's second coordination sphere.[16-19] Nocera and coworkers have pioneered using a single pendent carboxylic acid group to improve O_2 reduction catalysts by cobalt porphyrin[16] or corrole complexes.[17] Yang *et al.* found a more dramatic acceleration on including non-coordinating amines as 'proton relays' in nickel(II) bis-diphosphine O_2 reduction catalysis.[18] The origin of this catalytic acceleration is not well established. There are few well characterized catalytic intermediates that show the interaction of a proton relay with a dioxygen intermediate. Chapter 3 describes efforts to better understand these intermediates with cobalt complexes of tetraazamacrocylic ligands with pendent pyridine and acetate bases. These pendent bases were found to bind to the metal center rather than act as proton relays because the ligand backbone was not sufficiently rigid to prevent binding. To address this issue, we have used the more rigid bis-diphosphine ligands used by Yang *et al*.[18] Reported here are ruthenium-O_2 complexes with protonated and deprotonated amine proton relays, showing that the relay positions protons to form a hydrogen bond with the bound O_2.

5.2 Results and Discussion

5.2.1 Synthesis of $[Cp^*Ru(P_2N_2)(O_2)]^+$

$[Cp^*Ru(phosphine)_2]^+$ complexes form stable η^2-O_2 species with a variety of phosphine ligands (Cp^* = η^5-C_5Me_5).[20-25] This study used a 1,5-diaza-3,7-diphosphacyclooctane ligand with *t*-butyl substituents on the phosphines and benzyl groups on the amines (P_2N_2),[26] similar to those used by Yang *et al*.[18] Adding this ligand to $[Cp^*RuCl]_4$ yielded $[Cp^*Ru(P_2N_2)Cl]$ (Scheme 5.1). The X-ray crystal structure (Figure 4.1, selected bond lengths and angles in Table 5.1) and the ^1H and $^{31}P\{^1H\}$ NMR spectra confirm formation of a single Ru complex, with binding of the P_2N_2 ligand through the phosphines.

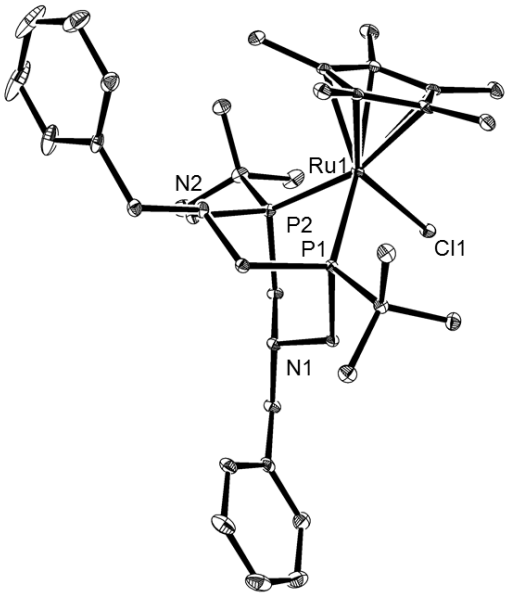

Figure 5.1: ORTEP diagram of $Cp^*Ru(P_2N_2)Cl$. Thermal ellipsoids shown at 50% probability. For clarity, hydrogen atoms have been omitted, and only one of the two independent molecules within the unit cell is shown. Crystallographic data are given in Table 5.2.

Table 5.1: Selected bond lengths and angles for Cp*Ru(P_2N_2)Cl[a].

	Cp*Ru(P_2N_2)Cl[b]
P1-Ru1	2.3125(5), 2.3120(5)
P2-Ru1	2.3049(5), 2.3071(5)
Cl1-Ru1	2.4418(4), 2.4443(4)
P1-Ru1-P2	78.118(17), 77.924(16)

[a] Distances are in Å, angles are in degrees. [b] Values are given for each independent molecule within the unit cell.

Table 5.2: Crystallographic data for Cp*Ru(P_2N_2)Cl.

	Cp*Ru(P_2N_2)Cl
Emp. formula	$C_{36}H_{55}ClN_2P_2Ru$
T (K)	100(2)
Wavelength	0.71073 Å
Size (mm)	0.59 x 0.07 x 0.02
Cryst. Syst	Triclinic
Space group	P $\bar{1}$ (No.2)
a (Å)	12.3107(6)
b (Å)	16.6690(7)
c (Å)	19.2249(9)
α (deg)	64.997(2)
β (deg)	86.345(3)
γ (deg)	89.404(2)
V ($Å^3$)	3567.5(3)
Z	4
D_{calc} (g/cm^3)	1.330
Abs. coeff. (mm^{-1})	0.631
Reflections total	35355
Reflections uniq. (R_{int})	17733 [R(int) = 0.0258]
Data/restraints/ parameters	17733 / 0 / 779
GOF	1.055
R1/wR2 [I>2σ(I)]	0.0296 / 0.0663
R1/wR2 (all data)	0.0419 / 0.0698

The chloride complex was converted to the η^2-dioxygen compounds $[Cp^*Ru(P_2N_2)(O_2)][X]$ (X = PF_6^-, BPh_4^-) by chloride abstraction with $TlPF_6$ or $NaBPh_4$ in air-saturated acetone or ethanol, respectively (Scheme 5.1). The ^1H and $^{31}P\{^1H\}$ NMR spectra of the PF_6^- and BPh_4^- salts in CD_2Cl_2 are identical, except for those peaks assigned to the anion, and are representative of this class of compounds.

Scheme 5.1: Synthesis of $[Cp^*Ru(P_2N_2)(O_2)][X]$ (X = PF_6^-, BPh_4^-).

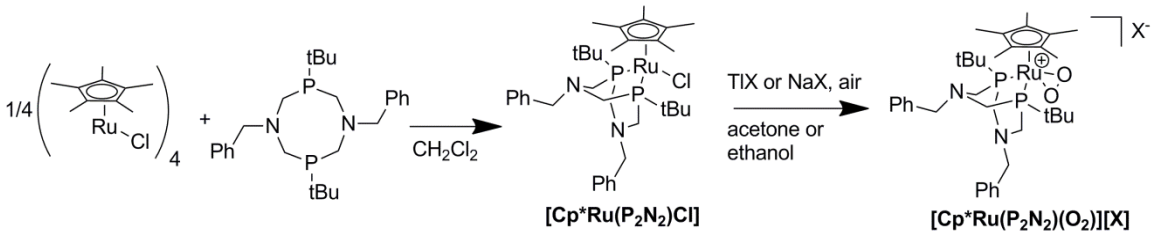

The X-ray crystal structure of $[Cp^*Ru(P_2N_2)(O_2)][BPh_4]$ (Figure 5.2, selected bond lengths and angles in Table 5.3) confirms the assignment. The O_2 ligand is bound essentially symmetrically η^2 to the Ru center, with Ru−O bond distances of 2.019(1) and 2.023(1) Å. The O−O bond length of 1.401(1) Å is within the range of *ca.* 1.36 – 1.40 Å observed for other $[Cp^*Ru(phosphine)_2(O_2)]^+$ complexes,[20-25] and is in between the O–O distances in superoxide (KO_2, 1.28 Å)[27] and hydrogen peroxide (1.46 Å).[28] IR spectra show $\nu_{O\text{-}O}$ = 935 cm^{-1} ($\nu_{^{18}O\text{-}^{18}O}$ = 880 cm^{-1}) (Figure 5.3), consistent with an η^2-O_2 complex with this O−O bond length.[29] This complex thus could be formally described as a Ru^{IV}-peroxo complex.

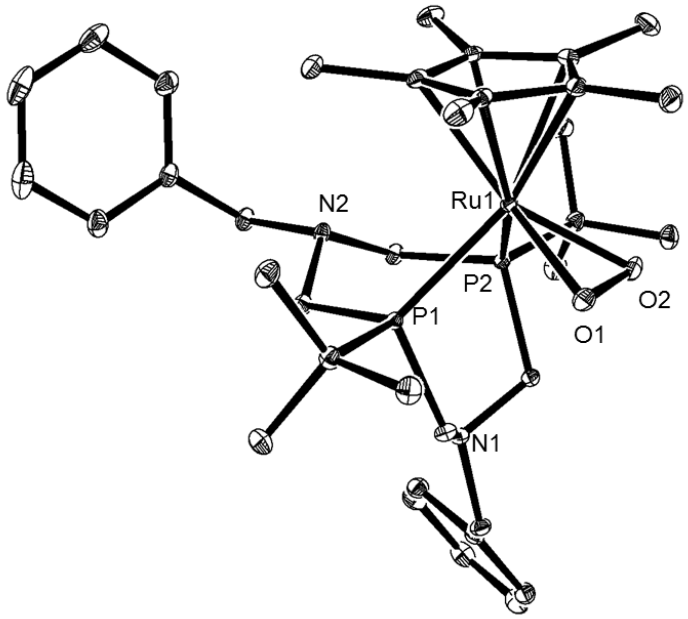

Figure 5.2: ORTEP diagram of $[Cp^*Ru(P_2N_2)(O_2)][BPh_4]$. Thermal ellipsoids shown at 50% probability. For clarity, the BPh_4^- anion and the hydrogen atoms have been omitted. Crystallographic data are given in Table 5.4.

Table 5.3: Relevant bond lengths (Å) from X-ray crystal structures of $[Cp^*Ru(P_2N_2)(O_2)][BPh_4]$ and $[Cp^*Ru(P_2N_2H)(O_2)][PF_6]_2$ forms **A** and **B**.

Bond	$[Cp^*Ru(P_2N_2)(O_2)][BPh_4]$	$[Cp^*Ru(P_2N_2H)(O_2)][PF_6]_2$	
		Form **A**	Form **B**
Ru−O1	2.0229(7)	2.0393(14)	2.0260(11)
Ru−O2	2.0190(7)	2.0362(14)	2.0350(11)
O1−O2	1.4009(11)	1.405(2)	1.4161(17)
N1···O1	3.959(1)	2.846(2)	2.905(2)
N1···O2	3.978(1)	2.934(2)	2.746(2)

Table 5.4: Crystallographic data for of $[Cp^*Ru(P_2N_2)(O_2)][BPh_4]$.

	$[Cp^*Ru(P_2N_2)(O_2)][BPh_4]$
Emp. formula	$C_{60}H_{75}BN_2O_2P_2Ru$
T (K)	110(2)
Wavelength	0.71073 Å
Size (mm)	0.16 x 0.14 x 0.13
Cryst. Syst	Orthorhombic
Space group	P c a 2_1
a (Å)	20.9684(10)
b (Å)	10.6178(5)
c (Å)	23.3629(11)
α (deg)	90
β (deg)	90
γ (deg)	90
V ($Å^3$)	5201.5(4)
Z	4
D_{calc} (g/cm^3)	1.315
Abs. coeff. (mm^{-1})	0.408
Reflections total	223510
Reflections uniq. (R_{int})	19951 [R(int) = 0.0333]
Data/restraints/ parameters	19951 / 1 / 624
GOF	1.040
R1/wR2 [I>2σ(I)]	0.0205 / 0.0489
R1/wR2 (all data)	0.0225 / 0.0499

$[Cp^*Ru(P_2N_2)(O_2)]^+$ and $[Cp^*Ru(P_2N_2)Cl]$ have similar ^1H and $^{31}P\{^1H\}$ NMR spectra, suggesting that the changes in electronic structure on replacing Cl^- by O_2 are not very extensive. The Cp* and *t*-butyl resonances are slightly more downfield in the O_2 complex, by *ca.* 0.1 ppm, and the ^{31}P resonance is 10.6 ppm upfield. The $[Cp^*Ru(P_2N_2)(O_2)]^+$ salts are stable under vacuum and CH_2Cl_2 solutions are stable to sparging with N_2 or freeze-pump-thawing, indicating that the binding of O_2 is not reversible. The O_2 and chloride structures both have the P_2N_2 ligand bound to the metal center only through the phosphorus atoms. As found in P_2N_2 complexes with other metals, the ligand structure discourages the amines from chelating the metal center, as this would form strained four-membered rings.[30] The uncoordinated amines are therefore potentially able to act as second-coordination sphere proton relays, although the chair

conformation of the proximal side of the P_2N_2 ligand orients N1 away from the O_2 ligand. The other amine nitrogen, N2, is on the opposite side of the ruthenium center and cannot interact with the O_2 ligand.

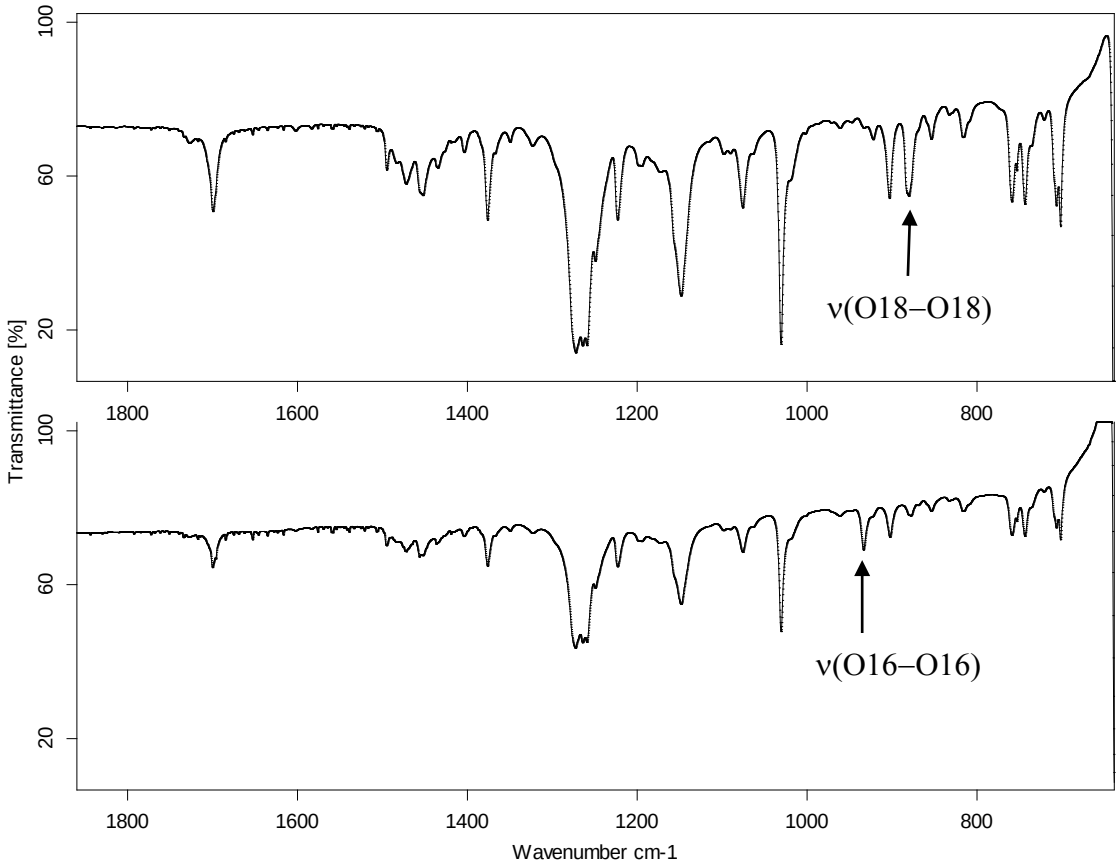

Figure 5.3: IR spectra of [Cp*Ru(P_2N_2)($^{18}O_2$)][OTf] (top) and [Cp*Ru(P_2N_2)($^{16}O_2$)][OTf] (bottom).

5.2.2 Protonation of [Cp*Ru(P_2N_2)(O_2)]$^+$

Treatment of [Cp*Ru(P_2N_2)Cl] with excess $LiPF_6$ and tosylic acid in aerobic methanol yielded yellow-brown crystals. NMR spectra and an X-ray crystal structure showed these to be the protonated derivative, [Cp*Ru(P_2N_2H)(O_2)][PF_6]$_2$ (Figure 5.3). In the absence of tosylic acid the same compound is formed (determined by NMR), but in much lower yields. Crystals were obtained from the tosylic acid reaction which contained one water of crystallization for every four cations (structure **A**); similar crystals from a reaction without added acid were the 0.5 methanol solvate (structure **B**; Figure 5.4, Table

5.3). $[Cp^*Ru(P_2N_2H)(O_2)]^{2+}$ can also be generated *in situ* in CD_2Cl_2 and observed by NMR spectroscopy, using ~1 equiv. of 2,6-dimethoxypyridine·HPF_6 (equation 5.1).

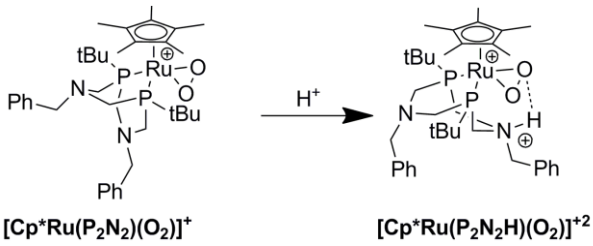

(5.1)

Structures **A** and **B**, and the NMR spectra, show that this compound has a protonated amine group. There are two PF_6^- anions per Ru center, indicating that the metal complex has a 2+ charge consistent with a protonated species. The two structures have somewhat different metrical parameters, apparently because the methanol or water molecules of crystallization are involved in different hydrogen bonding networks with the PF_6^- anions. In neither structure is the solvent interacting with the protonated or unprotonated amines, or with the O_2 ligand. In both structures, the conformation of the proximal amine is inverted relative to the structures of $[Cp^*Ru(P_2N_2)Cl]$ and $[Cp^*Ru(P_2N_2)(O_2)][BPh_4]$, bringing N1 into close proximity with the O_2 ligand. The shorter of the N···O distances in each structure, 2.846(2) Å in **A** and 2.746(2) Å in **B** (Table 5.3), are indicative of substantial hydrogen bonding interactions.[31,32] The protonated nitrogen is somewhat farther from the other oxygen of the O_2 ligand (2.934(2), 2.905(2) Å in **A** and **B**, respectively. In each of these structures, the η^2 binding mode of the O_2 ligand is retained. The O−O bond is essentially unchanged in form **A** ($d_{O1\text{-}O2}$ = 1.405(2) Å, within error of $[Cp^*Ru(P_2N_2)(O_2)][BPh_4]$), but is lengthened slightly in form **B** to 1.4161(17) Å (Δ = 0.152(20) Å). The O−O bond distance in structure **B** is, to our knowledge, longer than in any previously reported $[Cp^*Ru(phosphine)_2O_2]^+$ complex.[20-25] It seems likely that the longer O–O distance in structure **B** is related to the shorter N···O hydrogen bond in that structure. Though the structural changes are slight, the perturbation of the O_2 ligand on protonation is also indicated by the shift in $\nu_{O\text{-}O}$ to 905 cm^{-1} ($\nu_{^{18}O\text{-}^{18}O}$ = 840) cm^{-1} (Figure 5.5).

^{1}H NMR spectra of [Cp*Ru(P_2N_2H)(O_2)][PF_6]$_2$ in CD_2Cl_2 show sharp resonances that are consistent with the crystal structures. Half of the benzylic C*H*$_2$ and PC*H*$_2$N resonances are shifted downfield by *ca.* 1 ppm relative to [Cp*Ru(P_2N_2)(O_2)][PF_6], consistent with protonation of one of the two amine nitrogens. Additionally, the downfield benzylic C*H*$_2$ is split into a doublet (J_{HH} = 3 Hz) due to coupling with the N*H*, while the upfield benzyl resonance is a singlet (as in the spectra of the unprotonated complexes). The ^{31}P{^{1}H} spectrum shows a broad resonance, rather than the sharp singlet observed for [Cp*Ru(P_2N_2)(O_2)][PF_6] (Figure 5.6). Lowering the temperature to −60 °C causes decoalescence into two signals. The rate constant for this process was estimated from variable temperature NMR data and the equation $k_C = 2.22\Delta\nu$,[33] where k_C is the rate

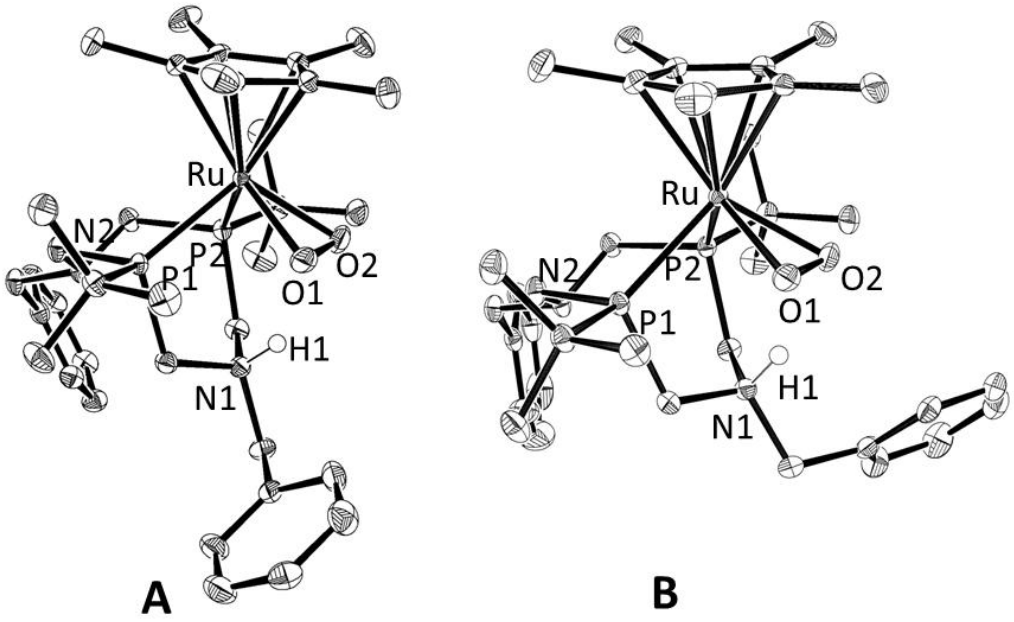

Figure 5.4: ORTEP diagrams of two different structures of [Cp*Ru(P_2N_2H)(O_2)][PF_6]$_2$: **A** (•$^{1}/_{4}$ H_2O), left, and **B** (•½ MeOH), right, with thermal ellipsoids shown at 50% probability. For clarity, the solvent molecules, counterions, and hydrogen atoms except for the hydrogen bonding H1, have been omitted. Crystallographic data are given in Table 5.5.

constant at the coalescence temperature and Δν is the peak separation in Hz of the two decoalesced peaks. The coalescence temperature is taken to be ~ −20°C and Δν =2700Hz, giving a barrier of ~10 kcal mol^{-1}. This process is not exchange between protonated and unprotonated species, as NMR spectra of $[Cp^*Ru(P_2N_2)(O_2)][PF_6]$ with less than 1 equiv of dimethoxypyridine·HPF_6 show both this broad resonance and the sharp resonance of $[Cp^*Ru(P_2N_2)(O_2)][PF_6]$. These spectra may reflect a fluxional process in which the protonated amine exchanges between hydrogen bonding to O1 and O2, as suggested by the asymmetric structures in the solid state.

Table 5.5: Crystallographic data for of $[Cp^*Ru(P_2N_2H)(O_2)][PF_6]_2$: **A** (•¼ H_2O), left, and **B** (•½ MeOH).

	$[Cp^*Ru(P_2N_2H)(O_2)][PF_6]_2$ •¼ H_2O	$[Cp^*Ru(P_2N_2H)(O_2)][PF_6]_2$ •½ MeOH
Emp. formula	$C_{144}H_{226}F_{48}N_8O_9P_{16}Ru_4$	$C_{73}H_{116}F_{24}N_4O_5P_8Ru_2$
T (K)	100(2)	100(2)
Wavelength	0.71073 Å	0.71073 Å
Size (mm)	0.60 x 0.20 x 0.15	0.17 x 0.16 x 0.15
Cryst. Syst	Monoclinic	Triclinic
Space group	C 2/c	P $\bar{1}$ (No.2)
a (Å)	42.530(4)	11.3774(4)
b (Å)	11.3512(9)	11.4514(4)
c (Å)	17.9636(13)	17.5208(5)
α (deg)	90	72.6030(10)
β (deg)	97.631(6)	84.111(2)
γ (deg)	90	87.532(2)
V ($Å^3$)	8595.4(12)	2166.63(12)
Z	2	1
D_{calc} (g/cm^3)	1.555	1.560
Abs. coeff. (mm^{-1})	0.601	0.598
Reflections total	229245	103581
Reflections uniq. (R_{int})	13110 [R(int) = 0.0292]	10831 [R(int) = 0.0303]
Data/restraints/ parameters	13110 / 0 / 551	10831 / 33 / 573
GOF	1.124	1.040
R1/wR2 [I>2σ(I)]	0.0351 / 0.0801	0.0264 / 0.0681
R1/wR2 (all data)	0.0401 / 0.0831	0.0287 / 0.0701

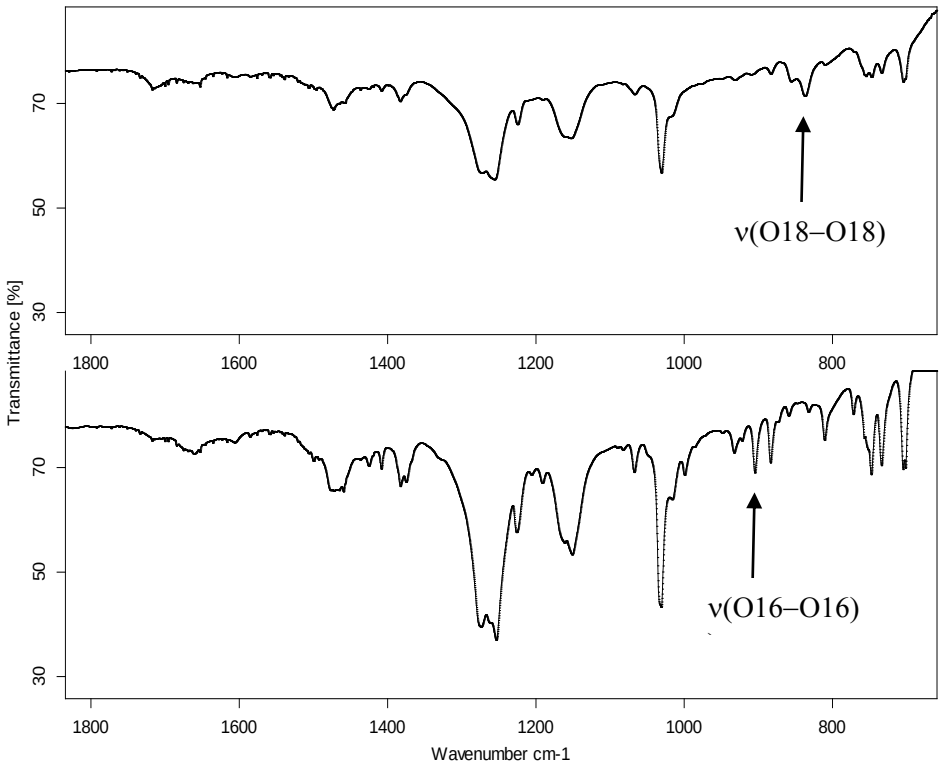

Figure 5.5: IR spectra of $[Cp^*Ru(P_2N_2H)(^{18}O_2)][OTf]_2$ (top) and $[Cp^*Ru(P_2N_2H)(^{16}O_2)][OTf]_2$ (bottom).

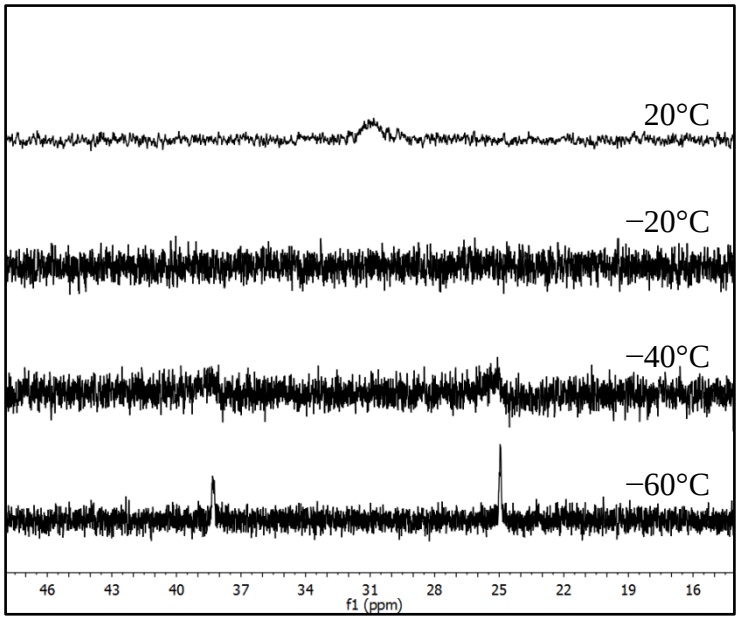

Figure 5.6: Variable temperature $^{31}P\{^1H\}$ NMR spectra of $[Cp^*Ru(P_2N_2H)O_2][PF_6]_2$ in CD_2Cl_2.

The location of the proton on the amine has been further confirmed by ^{1}H-^{15}N NMR spectra in CH_2Cl_2 of the ^{15}N labeled compound. The 1-D heteronuclear single quantum coherence (HSQC) spectrum of $[Cp^*Ru(P_2{}^{15}N_2H)(O_2)][PF_6]_2$ has a single peak at 7.6 ppm and the $J_{1H\text{-}15N}$ of 76 Hz shows the presence of an N–H bond (Figure 5.7). The downfield ^{1}H NMR chemical shift is suggestive of a hydrogen bonding environment.[32] The chemical shift and coupling constant are also consistent with the proton being located on one benzylamine rather than bridged between two benzylamines. Such benzylamine-bridged species have previously been determined to have chemical shifts of ~15 ppm and $J_{1H\text{-}15N} \approx 30$ Hz.[34]

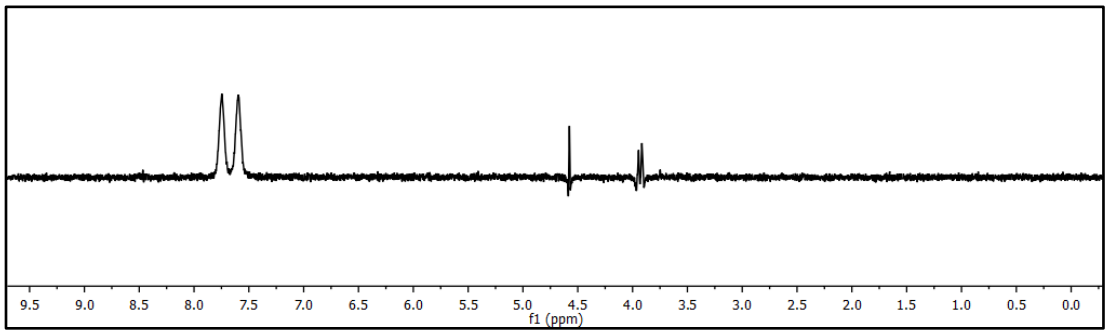

Figure 5.7: ^{1}H-^{15}N HSQC of $[Cp^*Ru(P_2{}^{15}N_2H)(O_2)][PF_6]_2$ in CD_2Cl_2 without ^{15}N decoupling.

Density functional theory calculations were performed to further support the proposed protonated structure. Gas-phase calculations (BP86/6-31G**(SDD)) were performed with Gaussian09.[35] Optimizations of $[Cp^*Ru(P_2N_2)(O_2)]^{+}$ and $[Cp^*Ru(P_2N_2H)(O_2)]^{+2}$ gave structures very similar to those found in the crystal structures. In the latter, the protonated amine nitrogen N1 is calculated to form a short hydrogen bond to O1 ($d_{N1\text{-}O1}$ = 2.65 Å), with a considerably longer distance to the other oxygen ($d_{N1\text{-}O2}$ = 3.00 Å), as in the crystal structures. The calculated $d_{O1\text{-}O2}$ lengthens upon protonation, by 0.015 Å, consistent with the change observed crystallographically. The use of other functionals or larger basis sets gave similar geometries, and consistently showed a change in $d_{O1\text{-}O2}$ of ca. 0.015 Å (Table 5.6), suggesting that the change in $d_{O1\text{-}}$

$_{O2}$, though relatively small, is due to the presence of the proton. The calculated $\nu_{^{16}O-^{16}O}$ is shifted from 976 cm^{-1} to 951 cm^{-1} with protonation, consistent with the ca. 30 cm^{-1} shift observed experimentally.

Another minimum was located with the proton bound to N2, on the opposite side of the ruthenium from the O_2 ligand. However, the energy of this species is calculated to be 23 kcal mol^{-1} above the isomer with N1 protonated. In the N2-protonated structure, and in the unprotonated O_2 structure, the N1···O distances are both long, *ca.* 3.1 Å. Furthermore, the calculated O−O in the N2-protonated form is actually 0.008 Å shorter than in the calculated structure of $[Cp^*Ru(P_2N_2)(O_2)]^+$. Additionally, the calculated d_{O1-O2} in $[Cp^*Ru(P_2N_2)(O_2)]^+$ is not affected by the P_2N_2 conformation, since the same bond distance is found in an alternative higher energy minimized structure obtained by optimization starting from the ligand geometry of $[Cp^*Ru(P_2N_2H)(O_2)]^{+2}$, but without including the acidic proton. In sum, locating the proton in positions other than N1 did not lead to good agreement with the crystal structures, and therefore the DFT calculations support the structure of $[Cp^*Ru(P_2N_2H)(O_2)]^{2+}$ as N1-protonated and that this protonation lengthens the O–O bond.

Table 5.6: Calculated O-O bond length (d(O-O)) in Å for the optimized geometries of $[Cp^*Ru(P_2N_2)(O_2)]^+$ and $[Cp^*Ru(P_2N_2H)(O_2)]^{2+}$ at different levels of theory, and the difference (Δd(O-O)) between d(O-O) for the optimized geometries of $[Cp^*Ru(P_2N_2)(O_2)]^+$ and $[Cp^*Ru(P_2N_2H)(O_2)]^{2+}$ at that level of theory.

Method	d(O-O) $[Cp^*Ru(P_2N_2)O_2]^+$	d(O-O) $[Cp^*Ru(P_2N_2H)O_2]^{+2}$	Δd(O-O)
BP86/6-31G** (SDD) [a]	1.404	1.419	+0.015
B3LYP/6-31G** (LANL2DZ) [b]	1.380	1.395	+0.015
B3LYP/6-31G** (SDD) [a]	1.387	1.401	+0.014
B3LYP/6-311G(2d,p) (LANL2DZ) [c]	1.377	1.391	+0.014
B3LYP/6-31G** (6-311++G(3df, 3pd) (LANL2TZ-f) [d]	1.377	1.390	+0.013
BP86/6-31G** (LANL2DZ) [b]	1.397	1.413	+0.016
B3P86/6-31G** (6-311++G(3df, 3pd) (LANL2TZ-f) [d]	1.364	1.377	+0.013
M06/6-31G** (6-311++G(3df, 3pd) (LANL2TZ-f) [d]	1.352	1.367	+0.015

[a] 6-31G** basis set for all atoms except Ru, SDD basis set and ECP for Ru. [b] 6-31G** basis set for all atoms except Ru, LANL2DZ basis set and ECP for Ru. [c] 6-311G(2d,p) basis set for all atoms except Ru, LANL2DZ basis set and ECP for Ru. [d] 6-31G** basis set for C, H, N, 6-311++G(3df, 3pd) basis set for O, P, and LANL2TZ-f basis set and ECP for Ru.

5.2.3 Reduction of $[Cp^*Ru(P_2N_2H)(O_2)]^{2+}$

The presence of the proton on the amine makes reduction of the dioxygen complex significantly more facile. A cyclic voltammogram (CV) of $[Cp^*Ru(P_2N_2)(O_2)][PF_6]$ in CH_2Cl_2 (0.1 M $[^nBu_4N][PF_6]$) has an irreversible reduction wave with a peak at −1.47 V vs. $Cp_2Fe^{+/0}$ (Figure 5.8). Upon the addition of triflic acid, a new irreversible reduction wave appears, shifted by +0.67 V. An identical peak is seen in the CV of isolated $[Cp^*Ru(P_2N_2H)(O_2)][PF_6]_2$. Work examining the products of these reductions is discussed in Chapter 6.

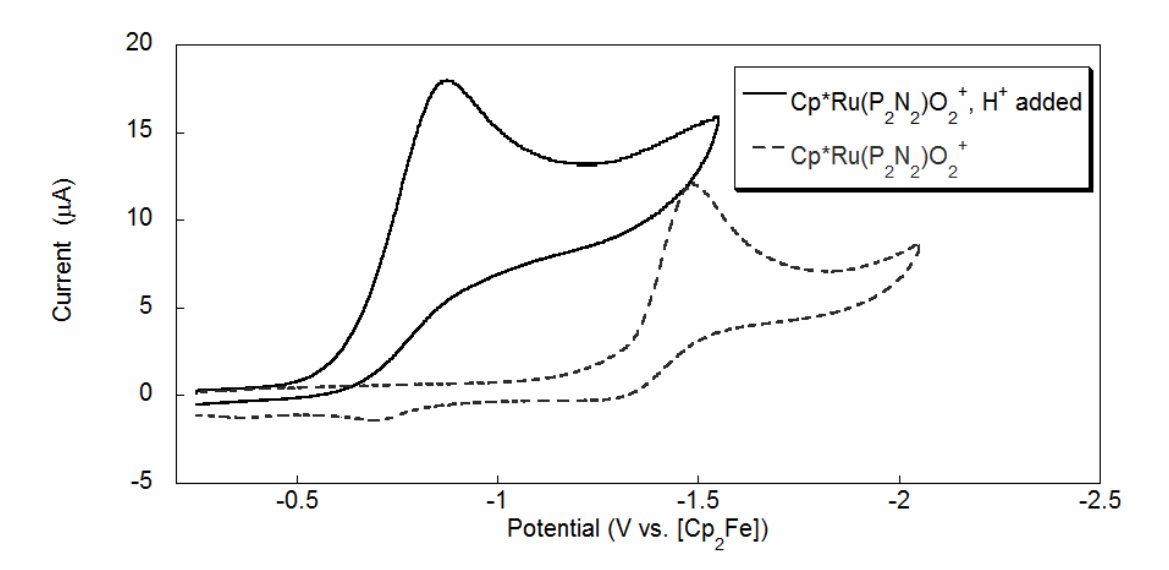

Figure 5.8: Cyclic voltammograms of $[Cp^*Ru(P_2N_2)(O_2)][PF_6]$ (1.2 mM) (gray, dashed line) and $[Cp^*Ru(P_2N_2)(O_2)][PF_6]$ with HOTf added (black, solid line) in CH_2Cl_2, 0.1 M $[^nBu_4N][PF_6]$, scan rate 0.1 V/s.

The complexes $[Cp^*Ru(P_2N_2)(O_2)][PF_6]$ and $[Cp^*Ru(P_2N_2H)(O_2)][PF_6]_2$ were also tested as oxidants with a variety of substrates.[36] It was anticipated that the greater extent of O-O bond activation of $[Cp^*Ru(P_2N_2H)(O_2)][PF_6]_2$ might make this a more potent oxidant. Test reactions were carried out in CD_2Cl_2 on ca. 5 mM solutions of ruthenium complex with 1-5 equivalents of substrate, and followed by ^1H and ^{31}P NMR spectroscopy. Reactions were performed with both nucleophilic and electrophilic substrates, and results are summarized in Table 5.7. No reduction of either species was observed with the substrates tested over several days, with the exception of the reaction of $[Cp^*Ru(P_2N_2)(O_2)][PF_6]$ with PCy_3, which did produce a small quantity of the phosphine oxide. A color change was observed in the reaction of $[Cp^*Ru(P_2N_2)(O_2)][PF_6]$ with tetracyanoethylene to a cyan color. By NMR spectroscopy, there was little evidence of reaction, so this blue species was likely a minor but deeply colored product. With basic phosphines, deprotonation of $[Cp^*Ru(P_2N_2H)(O_2)][PF_6]_2$ was observed. A lack of oxidation reactivity is not unexpected for Ru(II) peroxo complexes.[37,38]

Table 5.7: Results of oxidation test reactions with $[Cp^*Ru(P_2N_2)(O_2)][PF_6]$ and $[Cp^*Ru(P_2N_2H)(O_2)][PF_6]_2$.

Substrate	$[Cp^*Ru(P_2N_2)(O_2)][PF_6]$	$[Cp^*Ru(P_2N_2H)(O_2)][PF_6]_2$
Tricyclohexylphosphine	$O=PCy_3$, starting material	Deprotonation
Methyldiphenylphosphine	NR	Deprotonation
Triphenylphosphine	NR	NR
Thioanisole	NR	NR
Cyclohexene	NR	NR
2-Cyclohexen-1-one	NR	-
Tetracyanoethylene	Unknown blue species forms	-

NR = no reaction; - = reaction not performed

5.3 Conclusions

In summary, a ruthenium η^2-O_2 complex has been synthesized with a pendent amine in the second coordination sphere of the metal. The crystal structures, NMR and IR data indicate that the pendent amine can bind a proton, and that the resulting ammonium ion forms a hydrogen bond with the O_2 ligand, slightly lengthening the O-O bond. Experiments further elucidate how the relays affect the ability of this complex to act as a catalyst for O_2 reduction are discussed in Chapter 6.

5.4 Experimental

5.4.1 General considerations

All manipulations were carried out under a nitrogen atmosphere using standard glove box and Schlenk techniques unless otherwise specified. Solvents and reagents were purchased from Aldrich. Dichloromethane was dried over CaH_2 prior to use. Deuterated dichloromethane was purchased from Cambridge Isotope Labs and dried over CaH_2 prior to use. $[Cp^*RuCl]_4$ was purchased from Aldrich or Strem Chemicals and used as received. IR spectra were recorded using a Bruker Optics Tensor27 FTIR spectrometer at

room temperature as KBr pellets. $^{18}O_2$ gas (97 atom% ^{18}O) was purchased from Cambridge Isotope Labs. NMR spectra were recorded at 298 K (unless otherwise noted) on Bruker AV300, AV500, or DRX500 spectrometers. ^{1}H-NMR chemical shifts are reported versus TMS and referenced to residual solvent. ^{31}P-NMR chemical shifts are reported relative to an 85% $H_3PO_{4\ (aq)}$ external standard. 2,6-dimethoxypyridine·HPF_6 was synthesized by slow addition of HPF_6 (60% aqueous) to a diethyl ether solution of 2,6-dimethoxypyridine in an ice bath. The white precipitate was filtered and dried under vacuum, and its purity confirmed by ^{1}H NMR.

5.4.2 Synthesis

5.4.2.1 [Cp*Ru(P_2N_2)Cl] The ligand 3,7-dibenzylamino-1,5-di-tert-butyl-phosphinocyclooctane (P_2N_2) was prepared as reported previously.[39] P_2N_2 (0.476 g, 1.1 mmol) was dissolved in 25 mL of deoxygenated CH_2Cl_2. To this solution, a slurry of $[Cp^*RuCl]_4$ (0.293 g, 0.025 equiv.) in 10 mL CH_2Cl_2 was added dropwise with stirring over 10 minutes. The remaining solid $[Cp^*RuCl]_4$ was washed into the reaction mixture with an additional 5 mL of CH_2Cl_2. The resulting deep red solution was stirred for two hours. The solution was then filtered in air to remove a small amount of black solid, and vacuum dried to an orange-brown solid. This solid was suspended in 10 mL of diethyl ether and filtered to remove remaining free ligand. The orange solid was then dissolved in a minimum of toluene (~2 mL), layered with n-hexane (~4 mL), and stored at −20°C overnight. The resulting orange precipitate was collected by filtration, giving [Cp*Ru(P_2N_2)Cl] as an orange powder (0.236 g, 30% yield). X-ray quality crystals were obtained by slow evaporation of acetonitrile solvent. NMR(CD_2Cl_2): 1H: δ = 7.34-7.18 (m, 10H, Ar-H), 3.73 (s, 2H, benzyl CH_2), 3.50 (s, 2H, benzyl CH_2), 3.42 (m, 2H, PCH_2N), 2.69 (m, 2H, PCH_2N), 2.57 (m, 2H, PCH_2N), 2.46 (m, 2H, PCH_2N), 1.62 (s, 15H, Cp* CH_3), 1.05 (3-line pattern, 18H, *t*Bu CH_3) 31P: δ = 40.0 (s) Anal. calc. (Found): C, 60.53 (60.53); H, 7.76 (7.74); N, 3.92 (3.87).

5.4.2.2 [Cp*Ru(P_2N_2)(O_2)][PF_6] [Cp*Ru(P_2N_2)Cl] (0.10 g, 0.14 mmol) was dissolved in 15 mL of aerobic acetone. A solution of $TlPF_6$ (0.048g, 1 equiv.) in 5 mL of acetone was added at once. The solution was stirred overnight and then filtered through Celite to

remove TlCl. The resulting yellow-brown solution was dried under vacuum to give [Cp*Ru(P_2N_2)(O_2)][PF_6] as a yellow brown solid (0.098 g, 82% yield). NMR(CD_2Cl_2): 1H: δ = 7.44-7.12 (m, 10H, Ar-H), 3.83 (s, 2H, benzyl CH_2), 3.52 (s, 2H, benzyl CH_2), 2.83-2.50 (m, 8H, PCH_2N), 1.72 (s, 15H, Cp* CH_3), 1.17 (3-line pattern, 18H, *t*Bu CH_3) 31P: δ = 29.4 (s), -144.0 (m, $J_{19F\text{-}31P}$ = 720 Hz). Anal. calc. (Found): C, 50.52 (50.87); H, 6.48 (6.77); N, 3.27 (3.22). Because of the strong absorbance of PF_6^- in the region of interest, IR spectra were obtained using the trifluoromethanesulfonate ([OTf^-]) counterion, with the complex being obtained by analogous methods using TlOTf. [Cp*Ru(P_2N_2)(O_2)][OTf] is identical to [Cp*Ru(P_2N_2)(O_2)][PF_6] by ^{1}H NMR spectroscopy. Isotopic labeling was achieved by repeating the synthesis under an atmosphere of $^{18}O_2$. IR (KBr) ν(^{16}O–^{16}O) = 935 cm^{-1}, ν(^{18}O–^{18}O) = 880 cm^{-1}.

5.4.2.3 [Cp*Ru(P_2N_2)(O_2)][BPh_4] [Cp*Ru(P_2N_2)Cl] (0.056 g, 0.08 mmol) was dissolved in 20 mL of aerobic ethanol. A solution of $NaBPh_4$ (0.027 g, 1 equiv.) in 5 mL ethanol was added, and the solution stirred in air for 2 hours, resulting in the precipitation of a yellow solid. The solution was concentrated under vacuum to a volume of 10 mL, and the yellow solid was collected by filtration to give [Cp*Ru(P_2N_2)(O_2)][BPh_4] (0.068 g, 83% yield). X-ray quality crystals were grown by slow evaporation of acetone/diethyl ether solvent. NMR(CD_2Cl_2): 1H: δ = 7.44-6.87 (m, 10H, Ar-H), 3.83 (s, 2H, benzyl CH_2), 3.52 (s, 2H, benzyl CH_2), 2.83-2.50 (m, 8H, PCH_2N), 1.72 (s, 15H, Cp* CH_3), 1.16 (3-line pattern, 18H, *t*Bu CH_3) 31P: δ = 29.4 (s). Anal. calc. (Found): C, 69.96 (69.34); H, 7.34 (7.33); N, 2.72 (2.89).

5.4.2.4 [Cp*Ru(P_2N_2H)(O_2)][PF_6]$_2$ [Cp*Ru(P_2N_2)Cl] (0.010 g) was dissolved in 3 mL of aerobic methanol. To this was added a solution of anhydrous tosylic acid (0.019 g) and $LiPF_6$ (0.130 mg) in 2 mL of methanol. The orange solution was allowed to stand open to air for 2 days, during which time the solution became faintly yellow and red-brown crystals formed. The solution was decanted, and the crystals of [Cp*Ru(P_2N_2H)(O_2)][PF_6]$_2$ were dried under a stream of N_2 (0.08 g, 55% yield). The crystals obtained by this method were of X-ray quality and contained 0.25 molecules of water per ruthenium complex (called structure **A**). Multiple crystallizations by this

method have yielded samples of $[Cp^*Ru(P_2N_2H)(O_2)][PF_6]_2$ that are identical by NMR. Structure **B**, the 0.5 methanol solvate, was obtained by the same procedure but in the absence of added acid, where it crystallized as a minor species in sufficient concentration that it could be observed in the bulk material by ^{1}H-NMR (the major species by NMR was $[Cp^*Ru(P_2N_2)(O_2)][PF_6]$). Presumably the proton in this case comes from methanol or water. The ^{15}N labeled analogue was synthesized by an analogous method from ^{15}N-labeled $[Cp^*Ru(P_2N_2)Cl]$, which in turn was prepared from $P_2{}^{15}N_2$ using ^{15}N benzylamine: NMR(CD_2Cl_2): 1H: δ = 7.68 (s, 1H, NH), 7.64-7.40 (m, 10H, Ar-H), 4.54 (d, J = 3 Hz, 2H, benzyl CH_2), 3.85 (s, 2H, benzyl CH_2), 3.85(m, 2H, PCH_2N), 3.70 (m, 2H, PCH_2N), 3.15 (m, 2H, PCH_2N), 2.80 (m, 2H, PCH_2N), 1.81 (s, 15H, Cp* CH_3), 1.10 3-line pattern, 18H, *t*Bu CH_3) 31P: δ = 30.3 (br s), -144.0 (m, $J_{19F\text{-}31P}$ = 720 Hz). At -60°C the peak at 30.3 decoalesceces to give two peaks at 38.3 and 24.9 ppm. Anal. calc. (Found): C, 43.16 (43.03); H, 5.63 (5.62); N, 2.80 (2.84). Because of the strong absorbance of PF_6^- in the region of the $\nu(^{16}O–^{16}O)$, IR spectra of the protonated complex were obtained by the addition of 1 equivalent of trifluoromethanesulfonic acid to a solution of $[Cp^*Ru(P_2N_2)(O_2)][OTf]$, followed by evaporation of the solvent. IR (KBr) (Figure S11 below): $\nu(^{16}O–^{16}O)$ = 905 cm^{-1}, $\nu(^{18}O–^{18}O)$ = 840 cm^{-1}. The ν(N−H) could not be assigned. Broad ν(N−H) peaks that may overlap with the ν(C−H) region are typical of N-H's involved in hydrogen bonds of the strength suggested by the crystallographic N•••O distance.[40]

5.4.3 Crystallographic Details

Crystals were mounted on glass capillaries with Paratone-N oil (Hampton Research) and frozen immediately in a cold nitrogen gas stream. Data were collected on a Bruker APEX II single crystal X-ray diffractometer with Mo-Kα radiation (λ = 0.71073 Å) utilizing both Φ and Ω scans. Crystal-to-detector distance was 40 mm. X-ray diffraction data were collected on a Bruker APEXII single crystal diffractometer coupled to a Bruker APEXII CCD detector with graphite-monochromated Mo Kα radiation (λ = 0.71073 Å). The data was integrated and scaled using SAINT, SADABS within the APEX2 software package by Bruker.[41] Solution by direct methods (SHELXS, SIR97[4243]) produced a complete heavy atom phasing model consistent with the proposed structure. The structure was

completed by difference Fourier synthesis with SHELXL97.[44,45] Scattering factors are from Waasmair and Kirfel[46]. All hydrogen atoms inlcuding acidic N-H's were placed in geometrically idealized positions and constrained to ride on their parent atoms with C-H and N-H distances in the range 0.95-1.00 Angstrom (a riding model). Isotropic thermal parameters Ueq were fixed such that they were 1.2Ueq of their parent atom Ueq for CH's and NH's, and 1.5Ueq of their parent atom Ueq in case of methyl groups. All non-hydrogen atoms were refined anisotropically by full-matrix least-squares.

Further data can be obtained free of charge from the Cambridge Crystallographic Data Centre via www.ccdc.cam.ac.uk/data_request/cif under deposit codes CCDC 826157, 832828, 826159, and 826160.

The raw data for [Cp*Ru(P_2N_2)Cl] appeared twinned. Using CELL_NOW,[47] a 180^o twin rotation about [100] was found which, if unresolved, would have caused considerable overlap of diffraction peak intensities from different domains of the sample. Multi-domain integration with SAINT within the APEX2 software package by Bruker[48] and absorption correction with twinabs[49] removed the overlap.

5.4.4 Electrochemistry

Cyclic voltammetry (CV) was performed under N_2 using a CH Instruments 600D apparatus equipped with glassy carbon (3.0 mm dia.) working electrode, platinum wire auxiliary electrode, and $Ag/Ag(NO)_3$ (0.01 M in acetonitrile) reference electrode. CV was carried out in dichloromethane with 0.1 M [^{n}Bu$_4$N][PF_6] as supporting electrolyte. Ferrocene was added as an internal standard and all potentials are reported vs. the $Cp_2Fe^{+/0}$ couple.

5.4.5 Oxidation Test Reactions

Typical oxidation test reactions were performed in Teflon capped NMR tubes in CD_2Cl_2 solutions of 5 mM Ru complex. Substrates were added (1-5 equivalents) under an N_2 atmosphere, and reactions were monitored via ^{1}H and ^{31}P NMR overa period of 3 days.

5.5 Notes to Chapter 5

(1) This work published as Tronic, T. A.; DuBois, M. R.; Kaminsky, W.; Coggins, M. K.; Liu, T.; Mayer, J. M. *Angew. Chem. Int. Ed.* **2011**, *50*, 10936 except as noted.

(2) Kaila, V. R. I.; Verkhovsky, M. I.; Wikström, M. *Chem. Rev.* **2010,** *110*, 7062.

(3) Solomon, E. I.; Chen, P.; Metz, M.; Lee, S.-K.; Palmer, A. E. *Angew. Chem. Int. Ed.* **2001,** *40*, 4570.

(4) Denisov, I. G.; Makris, T. M.; Sligar, S. G.; Schlichting, I. *Chem. Rev.* **2005,** *105*, 2253.

(5) Sono, M.; Roach, M. P.; Coulter, E. D.; Dawson, J. H. *Chem. Rev.* **1996,** *96*, 2841.

(6) Matlack, A. S., *Introduction to Green Chemistry*. Marcel Dekker: 2001.

(7) Stahl, S. S. *Angew. Chem. Int. Ed.* **2004,** *43*, 3400.

(8) Stahl, S. S. *Science* **2005,** *309*, 1824.

(9) Winter, M.; Brodd, R. J. *Chem. Rev.* **2004,** *104*, 4245.

(10) Warren, J. J.; Tronic, T. A.; Mayer, J. M. *Chem. Rev.* **2010,** *110*, 6961.

(11) Savéant, J.-M. *Chem. Rev.* **2008,** *108*, 2348.

(12) Rodriguez-Lopez, J. N.; Smith, A. T.; Thorneley, R. N. F. *J. Biol. Chem.* **1997,** *272*, 389.

(13) Proshlyakov, D. A.; Pressler, M. A.; Babcock, G. T. *Proc. Nat. Acad. Sci. USA* **1998,** *95*, 8020.

(14) Hamdane, D.; Zhang, H.; Hollenberg, P. *Photosynth. Res.* **2008,** *98*, 657.

(15) Song, W. J.; McCormick, M. S.; Behan, R. K.; Sazinsky, M. H.; Jiang, W.; Lin, J.; Krebs, C.; Lippard, S. J. *J. Am. Chem. Soc.* **2010,** *132*, 13582.

(16) McGuire Jr, R.; Dogutan, D. K.; Teets, T. S.; Suntivich, J.; Shao-Horn, Y.; Nocera, D. G. *Chem. Sci.* **2010,** *1*, 411.

(17) Dogutan, D. K.; Stoian, S. A.; McGuire, R.; Schwalbe, M.; Teets, T. S.; Nocera, D. G. *J. Am. Chem. Soc.* **2010,** *133*, 131.

(18) Yang, J. Y.; Bullock, R. M.; Dougherty, W. G.; Kassel, W. S.; Twamley, B.; DuBois, D. L.; Rakowski DuBois, M. *Dalton Trans.* **2010,** *39*, 3001.

(19) Shook, R. L.; Peterson, S. M.; Greaves, J.; Moore, C.; Rheingold, A. L.; Borovik, A. S. *J. Am. Chem. Soc.* **2011,** *133*, 5810.

(20) Kirchner, K.; Mauthner, K.; Mereiter, K.; Schmid, R. *J. Chem. Soc., Chem. Comm.* **1993**, 892.

(21) Mauthner, K.; Mereiter, K.; Schmid, R.; Kirchner, K. *Inorg. Chim. Acta* **1995,** *236*, 95.

(22) Sato, M.; Asai, M. *J. Organomet. Chem.* **1996,** *508*, 121.

(23) Lindner, E.; Haustein, M.; Fawzi, R.; Steimann, M.; Wegner, P. *Organometallics* **1994,** *13*, 5021.

(24) Jia, G.; Ng, W. S.; Chu, H. S.; Wong, W.-T.; Yu, N.-T.; Williams, I. D. *Organometallics* **1999,** *18*, 3597.

(25) de los Ríos, I.; Jiménez Tenorio, M.; Padilla, J.; Puerta, M. C.; Valerga, P. *Organometallics* **1996,** *15*, 4565.

(26) Wiedner, E. S.; Yang, J. Y.; Dougherty, W. G.; Kassel, W. S.; Bullock, R. M.; Rakowski DuBois, M.; DuBois, D. L. *Organometallics* **2010,** *29*, 5390.

(27) Valentine, J. S. *Chem. Rev.* **1973,** *73*, 235.

(28) Savariault, J. M.; Lehmann, M. S. *J. Am. Chem. Soc.* **1980,** *102*, 1298.

(29) Cramer, C. J.; Tolman, W. B.; Theopold, K. H.; Rheingold, A. L. *Proc. Nat. Acad. Sci. USA* **2003,** *100*, 3635.

(30) Rakowski DuBois, M.; DuBois, D. L. *Chem. Soc. Rev* **2009,** *38*, 62.

(31) Steiner, T. *Angew. Chem. Int. Ed.* **2002,** *41*, 48.

(32) Jeffrey, G. A., *An Introduction to Hydrogen Bonding*. Oxford University Press: 1997.

(33) Friebolin, H. *Basic One- and Two-Dimensional NMR Spectroscopy, vol 4*. VCH, Weinheim, **2005**, pp 311-313.

(34) Wilson, A. D.; Shoemaker, R. K.; Miedaner, A.; Muckerman, J. T.; DuBois, D. L.; Rakowski DuBois, M. *Proc. Nat. Acad. Sci. USA* **2007,** *104*, 6951.

(35) Gaussian 09, Revision B.1, Frisch, M. J.; Trucks, G. W.; Schlegel, H. B.; Scuseria, G. E.; Robb, M. A.; Cheeseman, J. R.; Scalmani, G.; Barone, V.; Mennucci, B.; Petersson, G. A.; Nakatsuji, H.; Caricato, M.; Li, X.; Hratchian, H.

P.; Izmaylov, A. F.; Bloino, J.; Zheng, G.; Sonnenberg, J. L.; Hada, M.; Ehara, M.; Toyota, K.; Fukuda, R.; Hasegawa, J.; Ishida, M.; Nakajima, T.; Honda, Y.; Kitao, O.; Nakai, H.; Vreven, T.; Montgomery, Jr., J. A.; Peralta, J. E.; Ogliaro, F.; Bearpark, M.; Heyd, J. J.; Brothers, E.; Kudin, K. N.; Staroverov, V. N.; Kobayashi, R.; Normand, J.; Raghavachari, K.; Rendell, A.; Burant, J. C.; Iyengar, S. S.; Tomasi, J.; Cossi, M.; Rega, N.; Millam, N. J.; Klene, M.; Knox, J. E.; Cross, J. B.; Bakken, V.; Adamo, C.; Jaramillo, J.; Gomperts, R.; Stratmann, R. E.; Yazyev, O.; Austin, A. J.; Cammi, R.; Pomelli, C.; Ochterski, J. W.; Martin, R. L.; Morokuma, K.; Zakrzewski, V. G.; Voth, G. A.; Salvador, P.; Dannenberg, J. J.; Dapprich, S.; Daniels, A. D.; Farkas, Ö.; Foresman, J. B.; Ortiz, J. V.; Cioslowski, J.; Fox, D. J. Gaussian, Inc., Wallingford CT, 2009.

(36) This section has not been previously published.

(37) Sisemore, M. F.; Selke, M.; Burstyn, J. N.; Valentine, J. S. *Inorg. Chem.* **1997**, *36*, 979.

(38) Martelletti, A.; Gramlich, V.; Zürcher, F.; Mezzetti, A. *New J. Chem.* **1999**, 199.

(39) Wiedner, E. S.; Yang, J. Y.; Dougherty, W. G.; Kassel, W. S.; Bullock, R. M.; DuBois, M. R.; DuBois, D. L. *Organometallics* **2010**, *29*, 5390-5401.

(40) Bratos, S.; Leicknam, J-C.; Gallot, G.; Ratajczak, H. In *Ultrafast Hydrogen Bonding Dynamics and Proton Transfer Processes in the Condensed Phase.* Elsaesser, T. and Bakkar, H. J., Eds. Kluwer Academic Publishers: Netherlands, 2002.

(41) Bruker APEX2 (Version 2.1-4), SAINT (version 7.34A), SADABS (version 2007/4), BrukerAXS Inc, Madison, Wisconsin, USA, 2007.

(42) Altomare, A.; Burla, C.; Camalli, M.; Cascarano, L.; Giacovazzo, C.; Guagliardi, A.; Moliterni, A. G. G.; Polidori, G.; Spagna, R.; *J. Appl. Cryst*. **1999**, *32*, 115.

(43) Altomare A, Cascarano G, Giacovazzo C, Guagliardi A. *J. Appl. Cryst*. **1993**, *26*, 343.

(44) Sheldrick G. M. SHELXL-97, Program for the Refinement of Crystal Structures. University of Göttingen, Germany, 1997.

(45) Mackay, S.; Edwards, C.; Henderson, A.; Gilmore, C.; Stewart, N.; Shankland, K.; Donald, A. *MaXus* University of Glasgow, Scotland, 1997.

(46) Waasmaier, D.; Kirfel, A. *Acta Cryst. A*, **1995**, *51*, 416.

(47) Sheldrick, G. M. (2005). CELL_NOW. University of Goettingen, Germany.

(48) Bruker (2007) APEX2 (Version 2.1-4), SAINT (version 7.34A), SADABS

(49) Sheldrick, G. M. (2007). TWINABS. University of Goettingen, Germany.

Chapter 6

Synthesis, Protonation, and Reduction of $Ru(O_2)$ Complexes with Pendent Nitrogen Bases

6.1 Introduction

The efficient reduction of dioxygen to water is critical to the development of hydrogen as a fuel source, as this is the cathodic half-reaction in a polymer electrolyte membrane (PEM) fuel cell.[1-3] This reaction, termed the oxygen reduction reaction (ORR) is a proton-coupled electron transfer (PCET) process, requiring the coordinated movement of four electrons and four protons per molecule of O_2. An ideal catalyst would control the delivery of these electrons and protons and would stabilize the many intermediates in this process.[4,5] The extensive research in this area has primarily focused on using redox-active transition metal complexes to control the electron delivery. Much progress has been made by studying iron,[68] cobalt,[9-11] and copper[12-15] complexes with primary coordination spheres that resemble the active sites of biological oxidase enzymes.[16-18] In one recent elegant example, Collman, Chidsey and coworkers have attached ORR catalysts to a gold electrode via a self-assembled monolayer (SAM), and length of the SAM was varied to control the rate of electron transfer to the catalyst.[19] In contrast to the considerable progress that has been made in controlling electron delivery, only recently have complexes been developed that attempt to control the delivery of protons.[20-25] This report focuses on developing an understanding of the design requirements for a catalyst to control the delivery of protons to O_2-derived substrates, using amine bases in the second coordination sphere that can act as proton relays.[26,27]

The utility of positioned proton relays in molecular, transition metal-catalyzed redox transformations of small molecules has been extensively demonstrated for H_2 oxidation/H^+ reduction with complexes of Fe,[28-30] Ni,[26,31-37] and Co.[38-40] In particular, 1,5-diaza-3,7-diphosphacyclooctane ($P^R_2N^{R'}_2$) ligands have emerged as powerful ligands for H_2 oxidation/H^+ reduction catalysts,[26,29,32-34,39,40] in part because they bind to the metal center preferentially through the phosphines, and their semi-rigid cyclooctane structure prevents amine binding to the metal center but positions the amines near the site of H_2

binding/formation. Additionally, substitution of the R and R' groups of these ligands is relatively synthetically facile and allows for tuning of the metal's redox properties and pendent amine basicity. The $P^{R}_2N^{R'}_2$ ligands have been shown to dramatically improve catalyst overpotential and turnover frequency in these systems. Recently, there has been considerable interest in extending the utility of these ligands to proton-coupled redox transformations of other small molecules including CO_2/HCOOH[41,42] and N_2/NH_3.[43,44]

The utility of acidic proton relays in O_2 reduction has been explored previously with carboxylic acids rather than amines as proton relays. Nocera and coworkers have pioneered the use of proton relays with their "hangman" porphyrinoid complexes, which position a carboxylic acid rigidly above the metal center.[22,23] They have shown with a cobalt "hangman" porphyrin complex, selectivity for H_2O production can be increased from 48% to 71% in electronically similar complexes.[22] We have built on this work, showing that with a series of iron (*meso*-tetra(carboxyphenyl))porphine catalysts, positioning carboxylic acids near the oxygen binding site of the complex dramatically improves catalyst stability and product selectivity.[25] While changes to the electronic structure of these catalysts have been explored, no systematic study of the pK_a of the proton relay has been performed, nor has the mechanistic role of the proton relay been elucidated in these systems. We and others have begun exploring the use of $P^{R}_2N^{R'}_2$ ligands for O_2 reduction, motivated in part by the relative synthetic ease with which the pendent base may be modified without significant changes to ligand structure. Yang *et al.* have demonstrated that Ni($P^{R}_2N^{R'}_2$) complexes can reduce O_2 to H_2O if a sufficiently basic pendent amine is used.[45] However, this system was not stable under catalytic conditions, and no mechanistic data could be obtained. To address this lack of mechanistic information, we have explored Ru complexes with $P^{R}_2N^{R'}_2$ ligands as potentially more stable systems, and recently we have reported the synthesis and protonation of a $[Cp^*Ru(P^{R}_2N^{R'}_2)]^+$ ($Cp^* = \eta^5$-C_5Me_5) complex that binds O_2.[46]

The previously reported complex $[Cp^*Ru(P^{tBu}_2N^{Bn}_2)]^+$ (tBu = *t*-butyl, Bn = benzyl) reacts with O_2 to make an η^2-peroxo complex.[46] In the presence of acid, $[Cp^*Ru(P^{tBu}_2N^{Bn}_2)(O_2)]^+$ is protonated at a pendent amine, forming a hydrogen bond with the O_2 ligand. Both the protonated and unprotonated species could be characterized by X-

ray crystallography, allowing the interaction between the protonated pendent amine and the O_2 to be visualized. This species demonstrated a proton dependent reduction potential, suggestive that the pendent amine may be able to relay protons to the O_2, but the reduction mechanism could not be determined.

We have sought better mechanistic understanding of the ability of these complexes to direct protons to O_2 during reduction by studying the effects of variations in the ligands. Presented herein are the synthesis, protonation, and reduction of new $[Cp^{R"}Ru(P^{R}{}_2N^{R'}{}_2)(O_2)]^+$ complexes with systematic variation in the ligands from the previously studied $P^{tBu}{}_2N^{Bn}{}_2$ complex. A less basic pendent amine has been tested by synthesizing a complex with a $P^{tBu}{}_2N^{Ph}{}_2$ ligand (Ph = phenyl), and a less electron donating phosphine has been tested by synthesizing a complex with a $P^{Ph}{}_2N^{Bn}{}_2$ ligand. Additionally, the role of the Cp* has been tested by substituting this for a Cp ligand (Cp = η^5-C_5H_5). The effect of each of these changes on the basicity and reduction potential of the complex has been probed. These studies have shown that these complexes decompose during reduction, likely due to oxidation of the phosphines, highlighting the limitations of applying $P^{R}{}_2N^{R'}{}_2$ ligands to O_2 reduction. However, these studies have also shown that the potential for reduction of these species can be controlled via the acidity of the pendent amine, highlighting the important role that proton relays can play in improving O_2 reduction catalysts.

6.2 Results

6.2.1 Synthesis of Cp*Ru($P^{R}{}_2N^{R'}{}_2$)Cl and Related Complexes.

New complexes of Cp*Ru(II) with 1,5-diaza-3,7-diphosphacyclooctane ($P^{R}{}_2N^{R'}{}_2$) ligands were synthesized by reaction of $Cp^*Ru^{II}Cl$ precursors with the appropriate $P^{R}{}_2N^{R'}{}_2$ ligand (Scheme 6.1), similar to the previously reported Cp*Ru($P^{tBu}{}_2N^{Bn}{}_2$)Cl. Cp*Ru($P^{tBu}{}_2N^{Ph}{}_2$)Cl was prepared by the room temperature reaction of $[Cp^*RuCl]_4$ with $P^{tBu}{}_2N^{Ph}{}_2$ in THF. The reaction is slow, due to the low solubility of $P^{tBu}{}_2N^{Ph}{}_2$ in THF, but after three days affords the desired product in modest yield as an orange powder. The same synthetic procedure with $P^{Ph}{}_2N^{Bn}{}_2$ gave a mixture of Cp*Ru($P^{Ph}{}_2N^{Bn}{}_2$)Cl and other products, as determined by NMR, that could not be separated by recrystallization or

column chromatography. These side products may contain diphosphine ligands that bridge multiple Ru centers, as has been observed in the synthesis of Cp*Ru(dppm)Cl.[47] In this case, phosphine ligand exchange is a better procedure: refluxing $Cp^*Ru(PPh_3)_2Cl$ with $P^{Ph}{}_2N^{Bn}{}_2$ in toluene for two days gave $Cp^*Ru(P^{Ph}{}_2N^{Bn}{}_2)Cl$ as a yellow powder in modest yield.

The $Cp^*Ru(P^R{}_2N^{R'}{}_2)Cl$ compounds have been characterized by ^1H and ^{31}P NMR spectroscopy and X-ray crystallography. Their ^{31}P NMR spectra contain only one sharp singlet corresponding to the two equivalent phosphines (see Table 6.2 below). The X-ray crystal structures show that the $P^R{}_2N^{R'}{}_2$ ligands bind only through the phosphines, with the third leg of the piano stool occupied by a bound Cl^- (Figure 6.1a and 6.1b; the structure of $Cp^*Ru(P^{tBu}{}_2N^{Bn}{}_2)Cl$ is reported in Ref. 46). The nitrogen bases in each complex are positioned in the second coordination sphere of the metal. The lone pair of the nitrogen closest to the Cl^- (N1) points away from electron-rich Cl^-, and the lone pair of N2 points away from the lone pair of N1. The binding of the phosphine ligands is essentially the same in $Cp^*Ru(P^{tBu}{}_2N^{Bn}{}_2)Cl$[46] and $Cp^*Ru(P^{tBu}{}_2N^{Ph}{}_2)Cl$, with average Ru-P distances of 2.309 ± 0.004Å and 2.304 ± 0.009Å and average P-Ru-P angles of 78.0 ± 0.1 ° and 78.4 ± 0.1°, respectively (avg. of two independent molecules in each unit cell). With a phenyl substituent on the phosphine ($Cp^*Ru(P^{Ph}{}_2N^{Bn}{}_2)Cl$), the average Ru-P bond distance is shortened by 0.063 ± 0.005Å (see Table 6.3 below).

The Cp derivative $CpRu(P^{tBu}{}_2N^{Bn}{}_2)Cl$ was obtained in good yield by refluxing $CpRu(PPh_3)_2Cl$ with $P^{tBu}{}_2N^{Bn}{}_2$ in toluene for two days. Its ^1H NMR spectrum closely resembles that of $Cp^*Ru(P^{tBu}{}_2N^{Bn}{}_2)Cl$, and it has a $^{31}P\{^1H\}$ NMR singlet resonance that is 11.8 ppm downfield from that of $Cp^*Ru(P^{tBu}{}_2N^{Bn}{}_2)Cl$. $CpRu(P^{tBu}{}_2N^{Bn}{}_2)Cl$ did not form crystals suitable for X-ray diffraction. However, an X-ray structure was obtained for a related complex with acetonitrile in place of chloride, $[CpRu(P^{tBu}{}_2N^{Bn}{}_2)(MeCN)][PF_6]$, synthesized by chloride abstraction with $TlPF_6$ in the presence of acetonitrile. The geometry of the phosphine ligand of this acetonitrile complex closely resembles that of the $Cp^*Ru(P^R{}_2N^{R'}{}_2)Cl$ complexes (Figure 6.1c).

Scheme 6.1: Synthesis of $Cp^{R''}Ru(P^{R}_{2}N^{R'}_{2})Cl$ compounds.

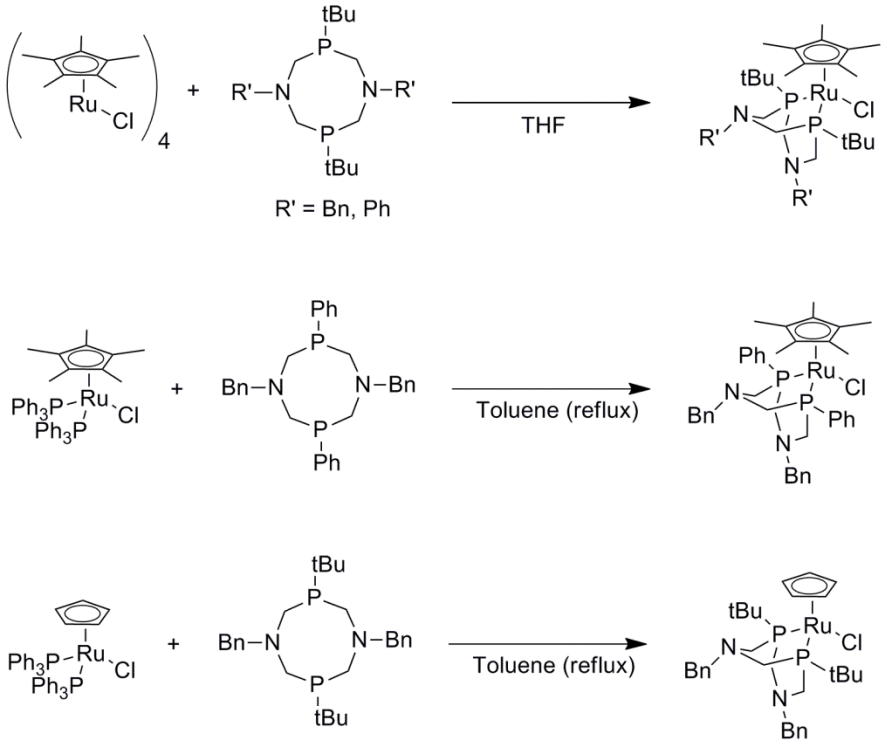

A closely related Cp*Ru complex without a pendent amine, Cp*Ru(dippp)Cl (dippp = 1,3-bis(diisopropylphosphino)propane), was synthesized for comparison with the ($P^{R}_{2}N^{R'}_{2}$) derivatives. Its X-ray crystal structure (Figure 6.1d) shows that the bulky isopropyl substituents and trimethylene backbone of dippp resemble the *t*-butyl substituents and three-atom backbone of $P^{tBu}_{2}N^{Bn}_{2}$. Although the crystallographically observed Ru-P bond lengths and bite angle are slightly larger in Cp*Ru(dippp)Cl, this complex appears to be a good all-alkyl analogue of than $Cp^{*}Ru(P^{tBu}_{2}N^{Bn}_{2})Cl$ based on the reactivity and redox potentials presented below.

$Cp^{*}Ru(P^{tBu}_{2}N^{Bn}_{2})Cl$ can be protonated, as observed by NMR spectroscopy. Upon addition of 1 equivalent of protonated dimethylformamide triflate ($[H^{+}DMF][OTf]$, pK_a in acetonitrile of 6.1),[48] a solution of $Cp^{*}Ru(P^{tBu}_{2}N^{Bn}_{2})Cl$ in CD_2Cl_2 showed concomitant formation of a new species by ^{1}H and ^{31}P NMR spectroscopy. In the ^{1}H NMR spectrum of $Cp^{*}Ru(P^{tBu}_{2}N^{Bn}_{2})Cl$ + $[H^{+}DMF][OTf]$, one of the benzyl CH_2 resonances is shifted downfield and split into a doublet ($J_{H\text{-}H}$ = 5.5 Hz) due to its proximity to the acidic N*H*.

The N*H* proton appears as a broad singlet at 11.1 ppm. The ^{1}H NMR spectrum of this solution closely resembles that of the protonated O_2 complex [Cp*Ru($P^{tBu}_2N^{Bn}_2H$)(O_2)][PF_6].[46] This suggests that protonation of the chloride species in CD_2Cl_2 is similar to protonation of the O_2 species, with the acidic proton located on the pendent amine (see below).

6.2.2 Chloride abstraction reactions

Reaction of Cp*Ru($P^{R}_2N^{R'}_2$)Cl with TlX (X = OTf^- or PF_6^-) in CH_2Cl_2 or acetone solution under an N_2 atmosphere led to the precipitation of TlCl and the formation of a deep red solution. The deep red color of these chloride abstracted species was unexpected. Related Cp*Ru(phosphine)$_2^+$ complexes without a fourth ligand are often deep blue in color,[49,50] and Cp*Ru(phosphine)$_2^+$ complexes with bound dinitrogen or other L type ligands as the fourth ligand are faintly yellow.[51] Room temperature ^{1}H and ^{31}P NMR spectra of these chloride abstraction reactions are broadened and have several resonances, possibly indicating a fluxional process. The control complex without the pendent amine, Cp*Ru(dippp)Cl, is deeply blue colored following chloride abstraction.

A chloride abstracted compound was crystallized by reaction of Cp*Ru($P^{tBu}_2N^{Ph}_2$)Cl with Na[BArF'] in CH_2Cl_2 (BArF' = tetrakis[3,5-bis(trifluoromethyl)phenyl]borate). Filtration of the NaCl from the reaction mixture gave a deep red solution identical to reactions with Tl^+ by ^{31}P NMR. On standing at −35°C for weeks, yellow crystals were isolated that were identified by X-ray crystallography as the dinitrogen-bound complex, [Cp*Ru($P^{tBu}_2N^{Ph}_2$)(N_2)][BArF'], (Figure 6.2, selected bond lengths given in Table 6.1). The dinitrogen ligand is essentially unactivated from free dinitrogen (d(N-N) =1.0975 Å),[52] which is typical of Ru(II)-N_2 complexes.[51,53] Interestingly, in the solid state, the lone pair of the pendent amine nearest the bound N_2 is pointed towards N_2. This is the opposite of what would be expected based on the solid-state structures of other N_2 complexes of Cr, Mo, and W with $P^{R}_2N^{R'}_2$ ligands,[43,44] which have electron-rich N_2 ligands that repel the amine lone pair. This difference may be due a combination of less electron donation to the N_2 from the Ru(II) and a favorable intermolecular π-stacking interaction between pendent anilines in the solid state.

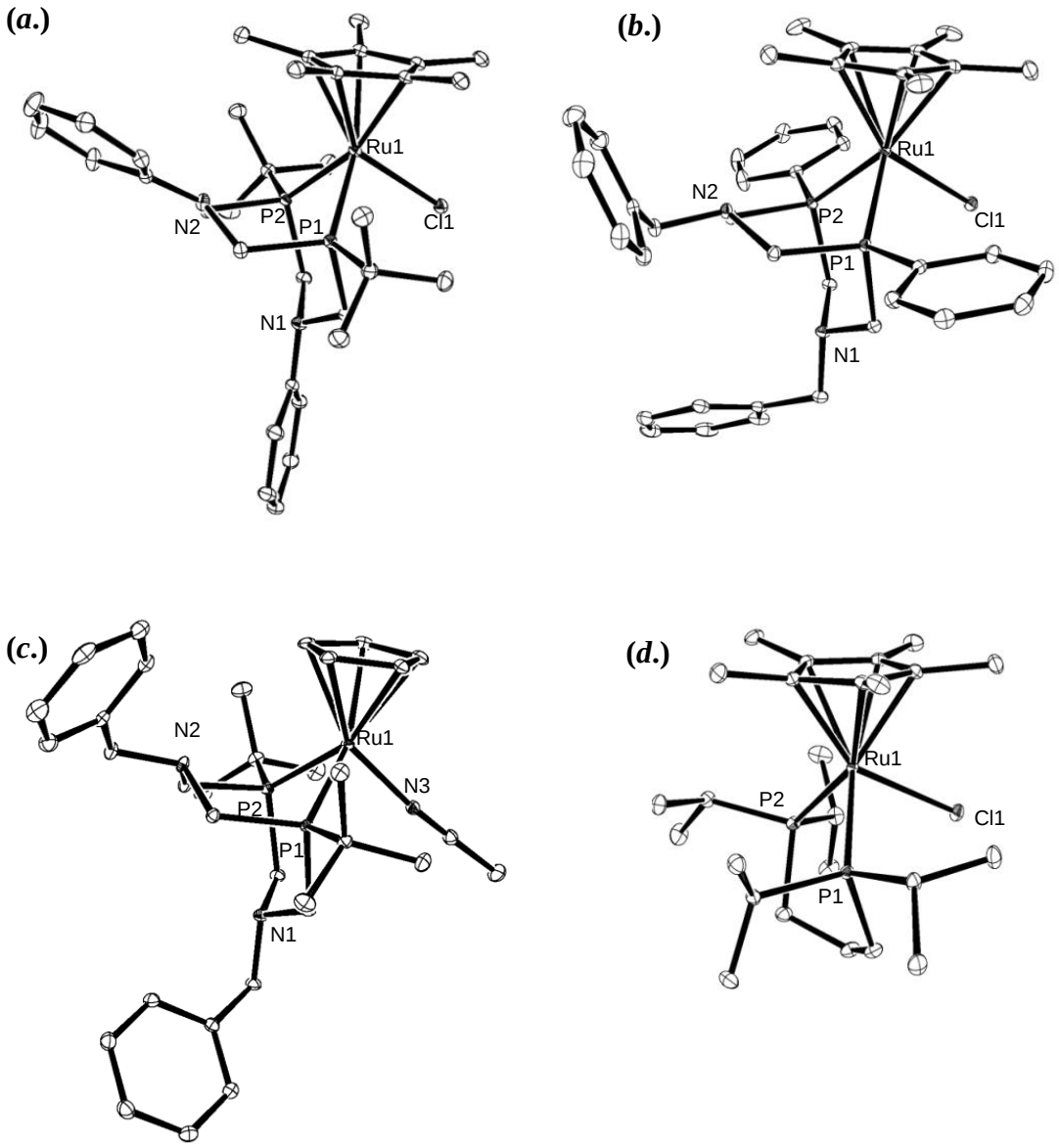

Figure 6.1: ORTEPs of (*a.*) Cp*Ru($P^{tBu}_2N^{Ph}_2$)Cl, (*b.*) Cp*Ru($P^{Ph}_2N^{Bn}_2$)Cl, (*c.*) [CpRu($P^{tBu}_2N^{Bn}_2$)(MeCN)][PF_6], and (*d.*) Cp*Ru(dippp)Cl. Thermal ellipsoids are shown at 50% probability. Hydrogen atoms and solvent molecules have been omitted for clarity. Only the cationic portion of [CpRu($P^{tBu}_2N^{Bn}_2$)(MeCN)][PF_6] and only one of the two independent molecules of Cp*Ru($P^{tBu}_2N^{Ph}_2$)Cl in the unit cell are shown.

Because of the difference in color between the crystals and the solution as well as the broadened NMR spectrum, it seems unlikely that the solid-state structure corresponds to what is present in solution at room temperature. Indeed, variable temperature UV-vis spectroscopy on a CH_2Cl_2 solution of Cp*Ru($P^{tBu}_2N^{Ph}_2$)Cl + Na[BArF'] indicates that as the temperature of the solution is lowered, the broad visible absorbance between ~400 nm and 500 nm is lost and shoulder at ~330 nm grows in isosbestically (Figure 6.3). The yellow color of the solution at low temperature is similar to the color of the crystals of [Cp*Ru($P^{tBu}_2N^{Ph}_2$)(N_2)][BArF']. It is possible that the dinitrogen is weakly bound or not bound at all at room temperature, and the N_2 ligated species is only present in high concentration only at low temperature or in the solid state. The red color might then be due a mixture of yellow N_2 ligated and unligated complex, or possibly to weak binding of the pendent amine. Interaction of the pendent amine could explain why this color has not been previously observed for these types of complexes without pendent amines. More experiments such are needed to confirm this hypothesis.

Table 6.1: Selected lengths for [Cp*Ru($P^{tBu}_2N^{Ph}_2$)(N_2)][BArF'][a]

	[Cp*Ru($P^{tBu}_2N^{Ph}_2$)(N_2)][BArF']
N3-N4	1.102(3)
N1⋯N3	2.860(2)
Ru-N3	1.9917(19)
Ru⋯N1	3.522(2)
Ru-P1	2.3409(8)
Ru-P2	2.3297(10)

[a] Distances are in Å.

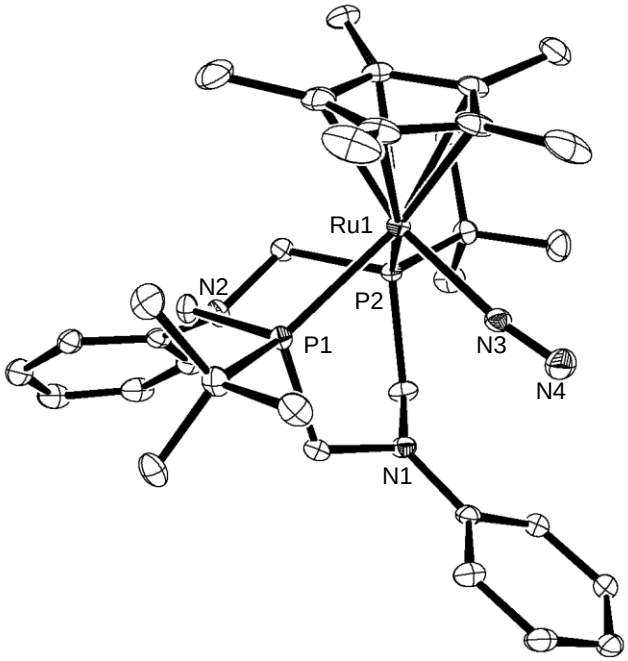

Figure 6.2: ORTEP of [Cp*Ru($P^{tBu}_2N^{Ph}_2$)(N_2)][BArF']. Thermal ellipsoids shown at 50% probability. For clarity, hydrogen atoms and $[BArF']^-$ anion have been omitted.

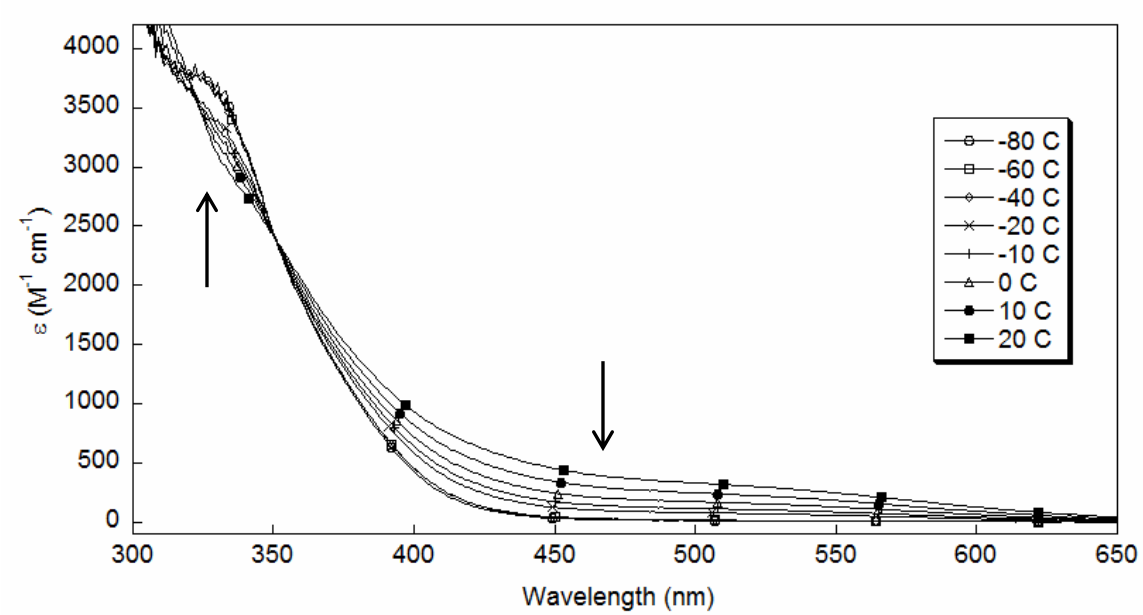

Figure 6.3: UV-vis spectra of Cp*Ru($P^{tBu}_2N^{Ph}_2$)Cl + Na[BArF'] (5 mM) in CH_2Cl_2 under N_2 with temperatures ranging from 20°C to −80°C. Arrows indicate changes in absorbance with decreasing temperature.

6.2.3 Synthesis of Dioxygen Complexes.

Dioxygen-bound complexes are obtained by chloride abstraction from Cp*Ru($P^R_2N^{R'}_2$)Cl with TlX (X = OTf^- or PF_6^-) in CH_2Cl_2 or acetone solutions that are exposed to air (eq. 6.1). These reactions parallel well-known analogues with simple bis(phosphine) ligands,[54-59] and the chemistry of the dippp complexes is very similar. The O_2 complexes are stable species, and removal of the solvent under vacuum yields [Cp*Ru($P^R_2N^{R'}_2$)(O_2)][X] or [Cp*Ru(dippp)(O_2)][X] as brown solids in high yield. Additionally, [Cp*Ru($P^{tBu}_2N^{Ph}_2$)(O_2)]$^+$ and [Cp*Ru(dippp)(O_2)]$^+$ may be obtained as tetraphenylborate (BPh_4^-) salts by stirring the respective Cl^- complex with $NaBPh_4$ in aerated ethanol. The complexes have been characterized by X-ray crystallography, IR spectroscopy, and by their sharp ^1H and ^{31}P spectra. One sharp singlet is observed in the $^{31}P\{^1H\}$ spectra due to the equivalent phosphines of the $P^R_2N^{R'}_2$ ligand, shifted ~10 ppm upfield of the singlet observed for the chloride precursors (Table 6.2). These O_2 complexes appear to be indefinitely stable in the solid state, and stable for several days in CH_2Cl_2 solution before any decomposition is evident by NMR. In solution they do not lose their O_2 ligand under vacuum or under a nitrogen atmosphere, though the O_2 is displaced by solvent in acetonitrile solution.

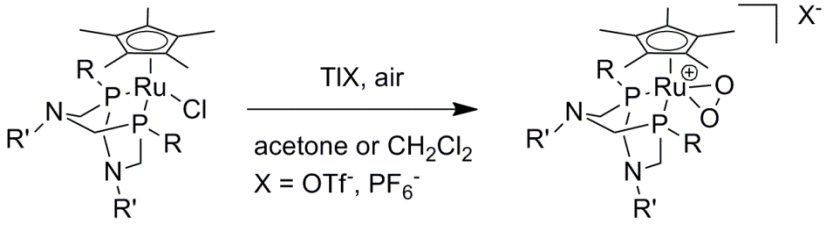

(6.1)

The X-ray crystal structures of the [Cp*Ru($P^R_2N^{R'}_2$)(O_2)]$^+$ and [Cp*Ru(dippp)(O_2)]$^+$ complexes show that the O_2 ligand is bound in an η^2–fashion (Figure 6.4), with O–O bond distances of 1.400 – 1.406 Å (Table 6.3). The O–O stretching frequencies were obtained from spectra of KBr pellets and confirmed by $^{18}O_2$-labelling (Table 6.2), for instance a value of 930 cm^{-1} ($\nu_{18O-18O}$ = 880 cm^{-1}) is observed for the $P^{tBu}_2N^{Ph}_2$ derivative. These values are in the typical range for [Cp*Ru(diphosphine)(O_2)]$^+$ complexes,[54-59] and make these species formally Ru(IV)-

peroxo complexes. Interestingly, all of the O–O stretching frequencies are within 9 cm^{-1} and the O–O bond distances are the same within error (Table 6.3). From these data it can be concluded that there is very little difference in the binding of O_2 with changes in the ligand. The conformation of the $P^R{}_2N^{R'}{}_2$ ligands in the peroxo species is identical to that in the chloride complexes, with the amine adjacent to the O_2 ligand positioned with its lone electron pair pointed away from the O_2 ligand.

The dioxygen complex of the Cp derivative, $[CpRu(P^{tBu}{}_2N^{Bn}{}_2)(O_2)]^+$, was obtained by reaction of $[CpRu(P^{tBu}{}_2N^{Bn}{}_2)]^+$ with air but is not stable and could be isolated only in sufficient yield to obtain a crystal structure. Formation of the O_2 complex was observed on stirring a CD_2Cl_2 solution of $[CpRu(P^{tBu}{}_2N^{Bn}{}_2)][OTf]$, generated *in situ* from $CpRu(P^{tBu}{}_2N^{Bn}{}_2)Cl$ and TlOTf, in air, forming a yellow solution in minutes. The formation of the O_2 complex was observed by NMR by the appearance of a singlet in the $^{31}P\{^1H\}$ NMR spectrum at 45.9 ppm, characteristically shifted upfield from the $CpRu(P^{tBu}{}_2N^{Bn}{}_2)Cl$ resonance (51.8 ppm). This O_2 complex decomposes completely over 1-2 hours to an unidentified brown oil, and some decomposition is apparent even in the time required to prepare an NMR sample. Only one complex of the type $[CpRu(phosphine)_2(O_2)]^+$ has been reported previously,[60] so instability is characteristic of these complexes. The high stability of the related Cl^- and MeCN complexes suggests that the O_2 ligand plays a role in the decomposition. Quickly layering a CH_2Cl_2 solution of $[CpRu(P^{tBu}{}_2N^{Bn}{}_2)(O_2)][OTf]$ with hexanes, followed by storing the solution at −20°C for weeks afforded a few X-ray quality crystals from which a structure was obtained. NMR spectra of these crystals were identical to the spectra of the compound prepared *in situ*. The X-ray crystal structure of $[CpRu(P^{tBu}{}_2N^{Bn}{}_2)(O_2)][OTf]$, to our knowledge the only crystal structure of a Cp ligated Ru-O_2 complex, is very similar to that of the Cp* complexes (Figure 6.4c, Table 6.3). The O_2 is bound η^2 with *d*(O1-O2) = 1.404(4) Å. While the esd on this distance is large, the similarity to the O–O bond distances of the Cp* derivatives is nonetheless striking considering the differences in the stability of these species and electron donating character of Cp* versus Cp (see electrochemical data and Table 6.5 below). From a simplistic perspective, a more electron donating Cp* ligand would be expected to give more peroxo character and a longer O–O distance, but this

simple approach is clearly not adequate.[61,62] The O_2 ligand is hydrogen bonded to a water molecule with *d*(O2-O3) = 2.898(4) Å, which may impart stability to this structure and explain why it was able to be isolated despite the instability of solutions of this compound.

Table 6.2: Selected ^{1}H and $^{31}P\{^{1}H\}$ NMR resonances and ν(O–O).[a]

	$^{31}P\{^{1}H\}$	$^{1}H(C_5CH_3)_5$	$^{1}H(NH^{+})$	ν(O–O) [$^{18}O_2$]	*d*(O-O)
Cp*Ru($P^{tBu}_2N^{Bn}_2$)Cl [b]	40.0	1.62	-	-	-
Cp*Ru($P^{Ph}_2N^{Bn}_2$)Cl	31.0	1.29	-	-	-
Cp*Ru($P^{tBu}_2N^{Ph}_2$)Cl	44.0	1.68	-	-	-
CpRu($P^{tBu}_2N^{Bn}_2$)Cl	51.8	4.64 (C_5H_5)	-	-	-
Cp*Ru(dippp)Cl	32.5	1.63	-	-	-
[Cp*Ru($P^{tBu}_2N^{Bn}_2$)(O_2)][PF_6] [b]	29.4	1.72	-	935 [880]	1.4009(11)
[Cp*Ru($P^{Ph}_2N^{Bn}_2$)(O_2)][OTf]	22.0	1.25	-	926 [879]	1.400(3)
[Cp*Ru($P^{tBu}_2N^{Ph}_2$)(O_2)][OTf]	30.2	1.82	-	930 [880]	1.4063(13)
[CpRu($P^{tBu}_2N^{Bn}_2$)(O_2)][OTf]	45.9	5.83 (C_5H_5)	-	- [d]	1.404(4)
[Cp*Ru(dippp)(O_2)][PF_6]	23.3	1.77	-	- [d]	1.4003(12), 1.4064(12)
[Cp*Ru($P^{tBu}_2N^{Bn}_2H$)(O_2)][PF_6]$_2$ [b]	30.3[c]	1.81	7.68	905 [840]	1.405(2), 1.4161(17)
[Cp*Ru($P^{Ph}_2N^{Bn}_2H$)(O_2)][PF_6]$_2$	16.6	1.24	8.29	- [d]	1.414(4)
[Cp*Ru($P^{tBu}_2N^{Ph}_2H$)(O_2)][PF_6]$_2$	41.6	2.01	9.98	~910[e] [857]	-

[a] Chemical shifts in δ (ppm); ν(O–O) in cm^{-1}, *d*(O-O) in Å. [b] Data from ref. 46. [c] Resonance is broad at room temperature. [d] ν(O–O) not assigned. [e] ν(O–O) is obscured by absorbance of the CH_2Cl_2 solvent. An approximate value based on the ν(^{18}O–^{18}O) value is provided, assuming harmonic oscillator behavior for the O–O bond (see text).

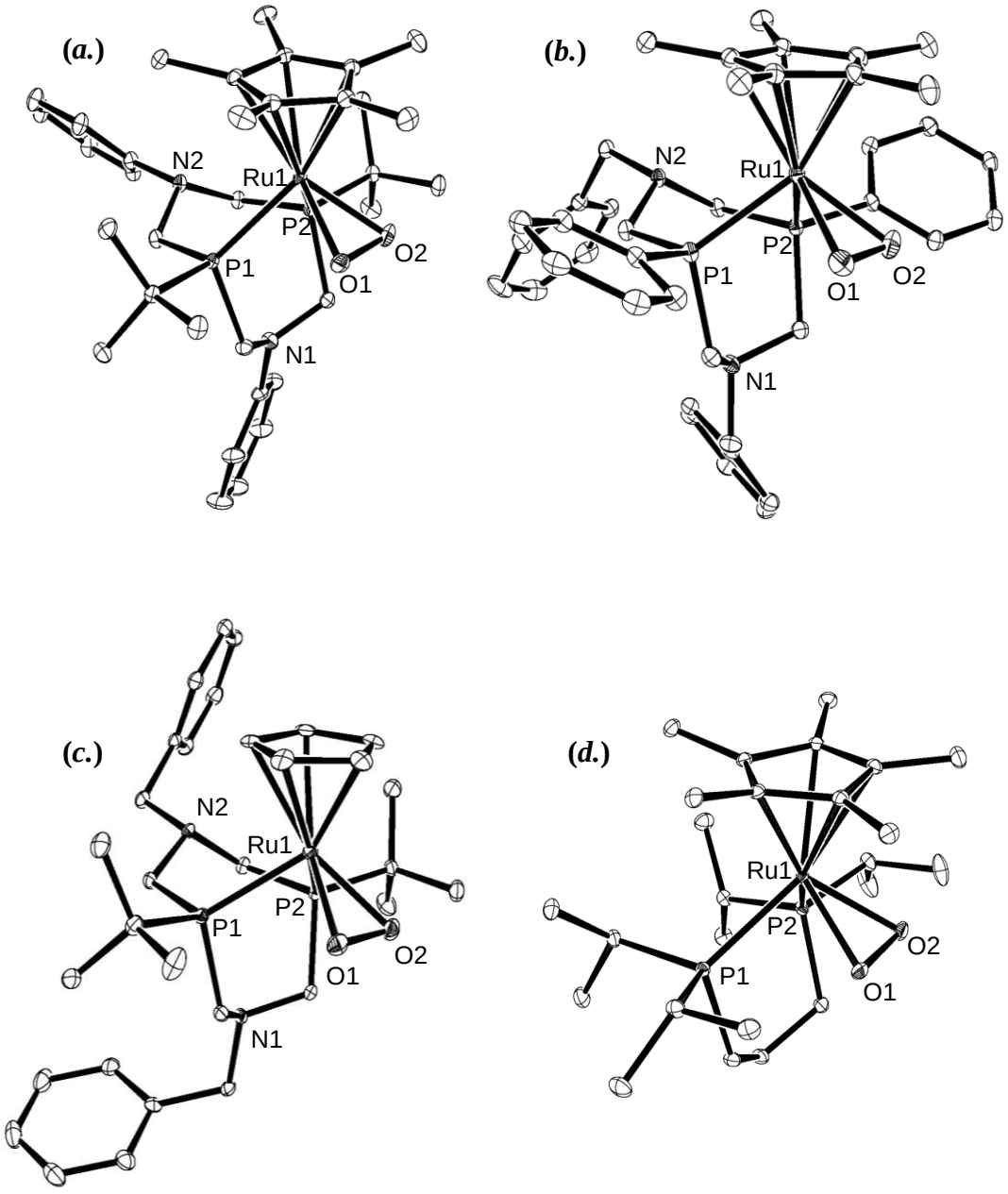

Figure 6.4: ORTEPs of (a.) [Cp*Ru($P^{tBu}_2N^{Ph}_2$)(O_2)][BPh_4], (b.) [Cp*Ru($P^{Ph}_2N^{Bn}_2$)(O_2)][OTf], (c.) [CpRu($P^{tBu}_2N^{Bn}_2$)(O_2)][OTf], and (d.) [Cp*Ru(dippp)(O_2)][PF_6]. Thermal ellipsoids are shown at 50% probability. Hydrogen atoms, counteranions, and solvent molecules have been omitted for clarity. Only one of the two independent molecules of [Cp*Ru(dippp)(O_2)][PF_6] in the unit cell are shown.

Table 6.3: Selected bond lengths and angles of chloride, acetonitrile, and dioxygen ligated complexes.[a]

	P1-Ru1	P2-Ru1	Cl1-Ru1	O1-Ru1	O2-Ru1	O1-O2	P1-Ru1-P2
Cp*Ru($P^{tBu}_2N^{Ph}_2$)Cl [b]	2.3077(4), 2.3043(4)	2.3001(4), 2.3134(4)	2.4597(4), 2.4550(4)	–	–	–	78.272(15), 78.375(15)
Cp*Ru($P^{Ph}_2N^{Bn}_2$)Cl	2.2492(4)	2.2435(4)	2.4412(3)	–	–	–	77.780(12)
[CpRu($P^{tBu}_2N^{Bn}_2$)(MeCN)][PF_6]	2.2868(4)	2.2914(4)	–	–	–	–	79.643(12)
Cp*Ru(dippp)Cl	2.3271(3)	2.3271(3)	2.4608(3)	–	–	–	88.045(10)
[Cp*Ru($P^{tBu}_2N^{Bn}_2$)(O_2)][BPh_4] [c]	2.3591(3)	2.3668(3)	–	2.0229(7)	2.0190(7)	1.4009(11)	76.572(9)
[Cp*Ru($P^{tBu}_2N^{Ph}_2$)(O_2)][BPh_4]	2.3660(3)	2.3774(3)	–	2.0280(8)	2.0227(8)	1.4063(13)	76.957(10)
[Cp*Ru($P^{Ph}_2N^{Bn}_2$)(O_2)][OTf]	2.3053(8)	2.3022(8)	–	2.028(2)	2.027(2)	1.400(3)	76.83(3)
[CpRu($P^{tBu}_2N^{Bn}_2$)(O_2)][OTf]	2.3264(9)	2.3286(9)	–	2.027(2)	2.025(3)	1.404(4)	78.59(3)
[Cp*Ru(dippp)(O_2)][PF_6] [b]	2.3777(3), 2.3865(3)	2.3812(3), 2.3920(3)	–	2.0244(10), 2.0312(9)	2.0294(8), 2.0245(8)	1.4003(12), 1.4064(12)	85.524(11), 85.030(10)
[Cp*Ru($P^{tBu}_2N^{Bn}_2H$)(O_2)][PF_6]$_2$ [c, d]	2.3574(5), 2.3580(4)	2.3674(5), 2.3744(4)	–	2.0393(14), 2.0260(11)	2.0362(14), 2.0350(11)	1.405(2), 1.4161(17)	78.412(16), 78.093(14)
[Cp*Ru($P^{Ph}_2N^{Bn}_2H$)(O_2)][OTf]$_2$	2.2974(9)	2.3224(9)	–	2.025(2)	2.041(2)	1.414(4)	78.46(4)
[Cp*Ru($P^{tBu}_2N^{Ph}_2$)Cl][PF_6] [b]	2.3758(6), 2.3674(6)	2.3658(5), 2.3759(6)	2.3221(5), 2.3326(5)	–	–	–	77.388(18), 77.511(19)

[a] Distances are in Å, angles are in degrees. [b] Values are given for each independent molecule within the unit cell. [c] Ref 46.
[d] Values are given for the two different crystal structures obtained of this material (See Ref. 46).

6.2.4 Protonation of Dioxygen Complexes

6.2.4.1 Effect of Phosphine Substituent on Protonation

The ability of the pendent amines to direct protons to the O_2 ligand has been tested by adding acid to solutions of $[Cp^*Ru(P^R{}_2N^{R'}{}_2)(O_2)]^+$. We have reported previously (see Chapter 5) that the *t*-butyl/benzyl derivative can be protonated at the pendent amine forming a stable complex $[Cp^*Ru(P^{tBu}{}_2N^{Bn}{}_2H)(O_2)]^+$ in which there is an intramolecular hydrogen bond between the protonated amine and the O_2 ligand.[46] Protonation of $[Cp^*Ru(P^{Ph}{}_2N^{Bn}{}_2)(O_2)]^+$, which differs only in having a phenyl substituent at the phosphine, is very similar. Addition of 1 equivalent of $[H^+DMF][OTf]$ to a CD_2Cl_2 solution of $[Cp^*Ru(P^{Ph}{}_2N^{Bn}{}_2)(O_2)][OTf]$ gives $[Cp^*Ru(P^{Ph}{}_2N^{Bn}{}_2H)(O_2)][OTf]_2$ by ^1H and ^{31}P NMR spectroscopy (eq. 6.2). One benzylic resonance and the PCH_2N resonances of the ligand are shifted downfield and a new, slightly broad singlet appears at 8.29 ppm in the ^1H NMR spectrum, consistent with protonation of one of the benzylamine ligands. Assignment of this new resonance at 8.29 ppm as the acidic benzylammonium proton is supported by the signal dropping in intensity when deuterium-labeled $[D^+DMF][OTf]$ is used to protonate $[Cp^*Ru(P^{Ph}{}_2N^{Bn}{}_2)(O_2)][OTf]$. The chemical shift of this benzylammonium is similar to the chemical shift of 7.68 ppm observed for protonated $[Cp^*Ru(P^{tBu}{}_2N^{Bn}{}_2)(O_2)]^+$, evidence that the environment of the acidic proton is similar between these two complexes. This chemical shift is inconsistent with the proton bridging the two benzylamine groups of the $P^{tBu}{}_2N^{Bn}{}_2$ ligand, behavior that has been observed previously in the protonation of nickel-$P^R{}_2N^{Bn}{}_2$ complexes.[33] Such benzylamine-bridging protons have chemical shifts of *ca.* 15 ppm. In the $^{31}P\{^1H\}$ NMR spectrum, a new sharp singlet resonance appears, shifted upfield by 5.4 ppm (Table 6.2). This upfield shift contrasts with the slight downfield shift and substantial broadening observed in $^{31}P\{^1H\}$ spectra upon protonation of $[Cp^*Ru(P^{tBu}{}_2N^{Bn}{}_2)(O_2)]^+$.[46]

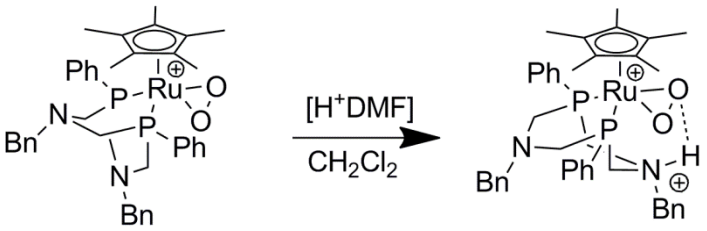

(6.2)

$[Cp^*Ru(P^{Ph}{}_2N^{Bn}{}_2H)(O_2)]^{+2}$ is stable for days in solution and may be isolated as a red solid, similar to $[Cp^*Ru(P^{tBu}{}_2N^{Bn}{}_2H)(O_2)]^{+2}$. Red, X-ray quality crystals of $[Cp^*Ru(P^{Ph}{}_2N^{Bn}{}_2H)(O_2)][OTf]_2$ were obtained from an acetone solution of $[Cp^*Ru(P^{Ph}{}_2N^{Bn}{}_2)(O_2)][OTf]$ and $[H^+DMF][OTf]$ stored at −20°C for one week. The X-ray structure obtained from these crystals suffers from multiply disordered triflate anions and acetone solvent, and is disordered in the position of the benzyl arms of the ligand (Figure 6.5). The thermal parameters of the disordered phenyl rings were restrained to be similar within each pair. However, no restraints were imposed that would have affected the structure of the complex other than the phenyl rings. The atomic positions of the core of the cationic portion of the molecule show clear evidence of protonation at the amine nearest the O_2 ligand, and there are strong similarities with the structure of $[Cp^*Ru(P^{tBu}{}_2N^{Bn}{}_2H)(O_2)]^+$.[46] Both amines are inverted from their orientation in the unprotonated molecule, bringing nitrogen N1 within less than 2.9 Å from oxygen O2. This is characteristic of an NH···O hydrogen bond, and bringing the lone pair of an amine within such a short distance of the lone pair of an O_2 ligand would be unlikely without protonation at the amine. The NH···O_2 interaction is asymmetric, with the protonated amine substantially closer to one oxygen atom than the other, d(N1···O2) = 2.716(4) Å, d(N1···O1) = 2.934(4) Å (Table 6.3).

The effect of varying the phosphine substituent on the basicity of $[Cp^*Ru(P^R{}_2N^{R'}{}_2)(O_2)]^+$ was tested by combining a CD_2Cl_2 solution of the protonated *t*-butylphosphine complex $[Cp^*Ru(P^{tBu}{}_2N^{Bn}{}_2H)(O_2)][PF_6]_2$ with an equimolar quantity of the unprotonated phenylphosphine compound $[Cp^*Ru(P^{Ph}{}_2N^{Bn}{}_2)(O_2)][OTf]$. ^1H and ^{31}P NMR spectra show distinct resonances of the both the protonated and unprotonated forms of both the *t*-butyl- and phenyl-substituted complexes (eq. 6.3, Figure 6.6). Thus proton exchange between the complexes is slow on the NMR timescale, and the equilibrium constant K_{eq} for this reaction is ~0.04 (based on integration of the *t*-butyl and Cp* resonances in the ^1H NMR or from integration of the $^{31}P\{^1H\}$ resonances). From this it can be seen that the phosphine substituent, despite its distance from the amine in the $P^R{}_2N^{R'}{}_2$ ligand, exerts a measurable effect on the basicity of the complex, a difference in pK_a of ~1.4.

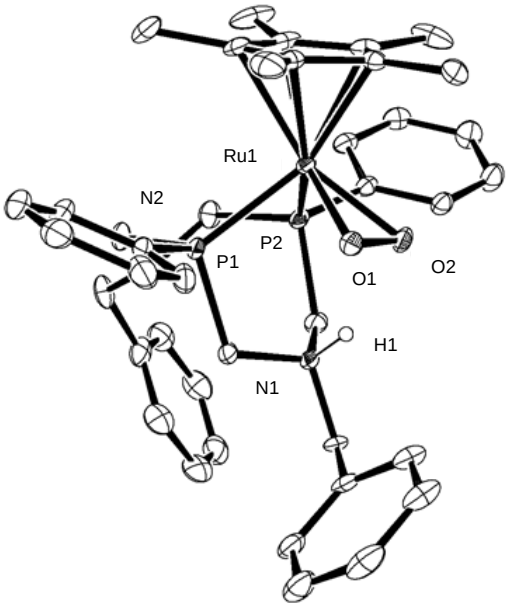

Figure 6.5: ORTEP of $[Cp^*Ru(P^{Ph}{}_2N^{Bn}{}_2H)(O_2)][OTf]_2\cdot$(acetone). Thermal ellipsoids are shown at 50% probability. Hydrogen atoms except for the acidic N-H, counteranions, and solvent molecules have been omitted for clarity. The acidic hydrogen was not located in the difference map, and was placed in a geometrically idealized position (a riding model).

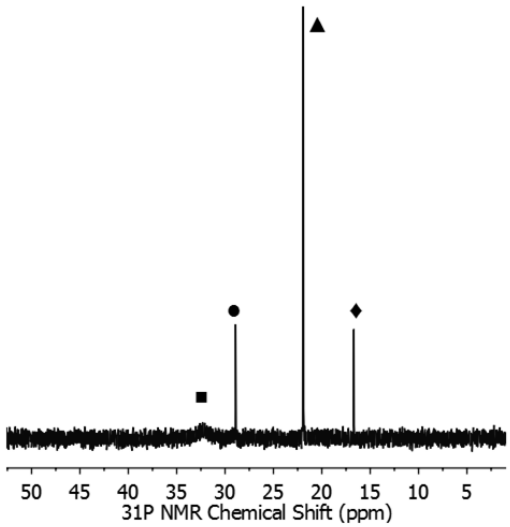

Figure 6.6: $^{31}P\{^1H\}$ NMR spectrum of the reaction of $[Cp^*Ru(P^{tBu}{}_2N^{Bn}{}_2H)(O_2)]^{+2}$ (■) with $[Cp^*Ru(P^{Ph}{}_2N^{Bn}{}_2)(O_2)]^+$ (▲) to form $[Cp^*Ru(P^{Ph}{}_2N^{Bn}{}_2H)(O_2)]^{+2}$ (♦) and $[Cp^*Ru(P^{tBu}{}_2N^{Bn}{}_2)(O_2)]^+$ (●) in CD_2Cl_2.

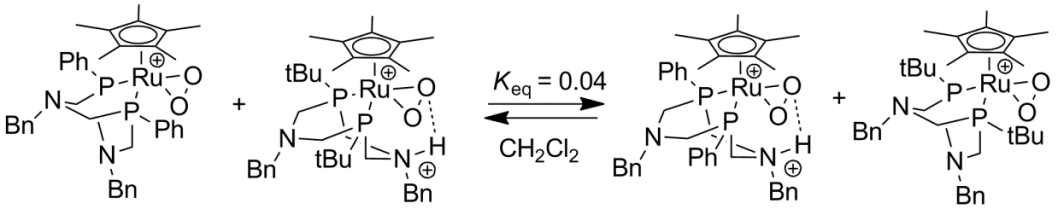

(6.3)

6.2.4.2 Effect of Amine Substituent on Protonation

Protonation of the *N*-phenyl derivative [Cp*Ru($P^{tBu}_2N^{Ph}_2$)(O_2)][OTf] with 1 equivalent of [H^+DMF][OTf] to a CD_2Cl_2 solution also forms a protonated species. The NMR spectra of this complex indicate that protonation occurs at one pendent amine, likely the amine near the O_2, as for the complexes with pendent benzylamines. The sharp singlet in the $^{31}P\{^1H\}$ NMR spectrum of the unprotonated complex at δ = 30.2 ppm is shifted downfield by 11.5 ppm upon protonation. ^1H NMR spectra show a downfield shift of two of the PC*H*$_2$N and the aryl resonances, as well as the appearance of a broad singlet integrating to 1H at 9.98 ppm. This new broad singlet has been identified as a protonated pendent aniline by ^1H-^{15}N correlated NMR spectroscopy of isotopically labeled [Cp*Ru($P^{tBu}_2{}^{15}N^{Ph}_2$)(O_2)][OTf]. The 1D ^1H-^{15}N HSQC spectrum of [Cp*Ru($P^{tBu}_2{}^{15}N^{Ph}_2$)(O_2)][OTf] with 1 equivalent of [H^+DMF][OTf] has one resonance at δ = 9.98 ppm, with a typical one-bond coupling constant, $J_{1H\text{-}15N}$ = 75 Hz. These data demonstrate protonation of the NPh group, and show that the proton does not bridge two anilines.[63,64]

Solutions of [Cp*Ru($P^{tBu}_2N^{Ph}_2H$)(O_2)]$^{+2}$ showed multiple decomposition products by NMR spectroscopy within a day. The stability of the protonated complexes is thus greatly reduced on decreasing the basicity of the pendent amine, since solutions of [Cp*Ru($P^{tBu}_2N^{Bn}_2H$)(O_2)]$^{+2}$ and [Cp*Ru($P^{Ph}_2N^{Bn}_2H$)(O_2)]$^{+2}$ showed no such signs of decomposition after several days at room temperature. While crystals of [Cp*Ru($P^{tBu}_2N^{Ph}_2H$)(O_2)]$^{+2}$ could not be obtained, IR spectra provide clear evidence for hydrogen bonding between the protonated pendent amine and the O_2 ligand. IR spectra of CH_2Cl_2 solutions of [Cp*Ru($P^{tBu}_2N^{Ph}_2$)(O_2)]$^+$ have an O–O stretch at 930 cm^{-1}

($\nu(^{18}O-^{18}O)$ = 880 cm^{-1}). Upon addition of 1 equivalent of [H^+DMF][OTf], this stretch is no longer present but no new band is observed (see Supporting Information). Protonation of the $^{18}O_2$-labelled material shows a new band at 857 cm^{-1}, shifted −23 cm^{-1} from the band in the unprotonated material. A similar shift for the $^{16}O_2$ compound would place the stretch underneath a solvent absorption, explaining why the band was not observed. A ν(O−O) of ~910 cm^{-1} is predicted for the $^{16}O_2$ compound by a harmonic oscillator approximation, or a shift of *ca.* −20 cm^{-1} upon protonation. This shift in ν(O−O) is a little smaller than the −30 cm^{-1} observed on protonation of the related *N*-benzyl derivative [Cp*Ru($P^{tBu}{}_2N^{Bn}{}_2H$)(O_2)][OTf]$_2$.[46]

Density functional theory (DFT) calculations were performed to demonstrate that protonation at the aniline and hydrogen bonding to O_2 is a reasonable structure for this compound. Gas-phase geometry optimization of the unprotonated, cationic [Cp*Ru($P^{tBu}{}_2N^{Ph}{}_2$)(O_2)]$^+$ was performed at the BP86/6-31G** (C, H, N, O, P) SDD (Ru) level of theory using *Gaussian09*.[65] This level of theory was chosen because of its previously demonstrated ability to reproduce the geometries of [Cp*Ru($P^{tBu}{}_2N^{Bn}{}_2$)(O_2)]$^+$and [Cp*Ru($P^{tBu}{}_2N^{Bn}{}_2H$)(O_2)]$^{+2}$.[46] The DFT optimized geometry of [Cp*Ru($P^{tBu}{}_2N^{Ph}{}_2$)(O_2)]$^+$ agrees well with the X-ray structure (see Table 6.4). A gas-phase optimization was also performed on the protonated [Cp*Ru($P^{tBu}{}_2N^{Ph}{}_2H$)(O_2)]$^{+2}$, which gave a minimum with the proton hydrogen bonding to the O_2 (Figure 6.7). The hydrogen bonding is asymmetric, with *d*(N1-O2) = 2.638 Å and *d*(N1-O1) = 2.998 Å. The calculated O−O stretching frequency is reduced on protonation by 20 cm^{-1}, which is quite consistent with experiment.

The change in the basicity of the complex on changing the pendent base was tested by NMR. A CD_2Cl_2 solution of the protonated *N*-phenyl complex, prepared *in situ* from [Cp*Ru($P^{tBu}{}_2N^{Ph}{}_2$)(O_2)][OTf] and *ca.* 1 equivalent of [H^+DMF][OTf], was treated with *ca.* 1 equivalent of [Cp*Ru($P^{tBu}{}_2N^{Bn}{}_2$)(O_2)][OTf]. Complete deprotonation of the aniline complex and formation of protonated benzylamine complex [Cp*Ru($P^{tBu}{}_2N^{Bn}{}_2H$)(O_2)][OTf]$_2$ was observed by ^{1}H and ^{31}P NMR. The relative integrations of the species in the product NMR spectra implies a difference in pK_a of at

least ~3. The large difference is not surprising, given that the pK_a of aniline in acetonitrile is 6.3 pK_a units less than that of benzylamine.[66]

Table 6.4: Selected DFT-calculated bond lengths and O−O stretching frequencies for $[Cp^*Ru(P^{tBu}{}_2N^{Ph}{}_2)(O_2)]^+$ and $[Cp^*Ru(P^{tBu}{}_2N^{Ph}{}_2H)(O_2)]^{+2}$.[a]

	$[Cp^*Ru(P^{tBu}{}_2N^{Ph}{}_2)(O_2)]^+$ (difference from experiment)	$[Cp^*Ru(P^{tBu}{}_2N^{Ph}{}_2H)(O_2)]^{+2}$
d(Ru-P)$_{avg}$ (Å)	2.411 (+0.039)	2.419
d(Ru-O1) (Å)	2.043 (+0.015)	2.044
d(Ru-O2) (Å)	2.050 (+0.027)	2.085
d(O1-O2) (Å)	1.404 (−0.002)	1.418
ν(O−O) (cm^{-1})	976 (+46)	956

[a] DFT calculations at the BP86/6-31G** (C, H, N, O, P) SDD (Ru) level of theory.

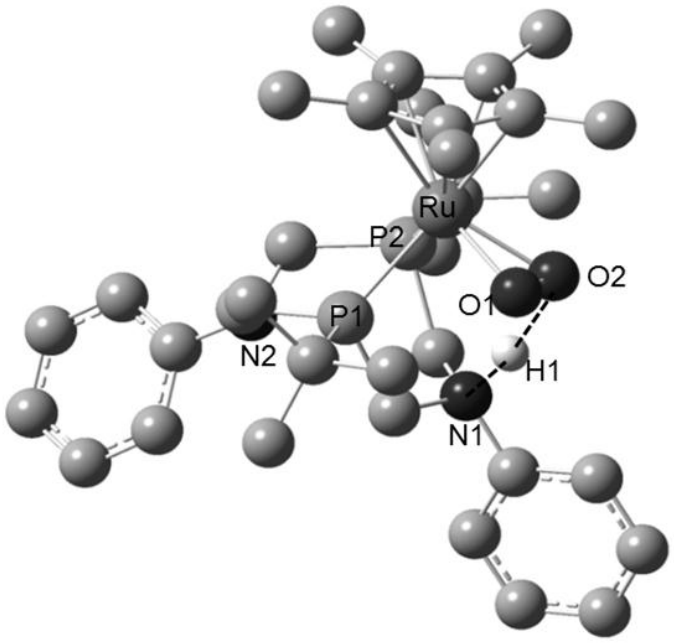

Figure 6.7: DFT (BP86/6-31G** (C, H, N, O, P) SDD (Ru)) optimized geometry of $[Cp^*Ru(P^{tBu}{}_2N^{Bn}{}_2H)(O_2)]^{+2}$. Hydrogen atoms except the acidic hydrogen have been omitted for clarity. Hydrogen bonding N1−H1···O2 interaction indicated by dashed line.

The complex [Cp*Ru(dippp)(O_2)][PF_6], without a pendent amine, does not protonate under the conditions tested. A CD_2Cl_2 solution showed no change in its NMR spectrum when 1 equivalent of [H^+DMF][OTf] was added. The O_2 ligand in this complex, despite being formally reduced to a peroxide, is still less basic than dimethylformamide.

6.2.5 Electrochemical Characterization

6.2.5.1 Oxidation of Chloride Complexes

Cyclic voltammograms (CVs) of all of the chloride complexes show a reversible oxidation wave between −0.1 V and −0.4 V versus Cp_2Fe, with typical peak separations of 0.12 – 0.15 V in CH_2Cl_2 with 0.1 M tetra-*n*-butylammonium hexafluorophosphate ($TBAPF_6$). The $E_{1/2}$ potentials are given in Table 6.5, and CVs are shown in Figure 6.9. The potentials show only modest differences with ligand, with all Cp* derivatives being within 0.1 V. The oxidation waves are attributed to $Ru^{II} \rightarrow Ru^{III}$ oxidation. To confirm this assignment, Cp*Ru($P^{tBu}{}_2N^{Bn}{}_2$)Cl was chemically oxidized by one equivalent of [Cp_2Fe^+][PF_6^-] in CH_2Cl_2, yielding dark green crystals. The X-ray crystal structure (Figure 6.8) confirms the composition as the Ru(III) complex [Cp*Ru($P^{tBu}{}_2N^{Bn}{}_2$)Cl][PF_6] with no ligand oxidation. The Ru–Cl bond length (average of two independent molecules in the unit cell) is 0.115 ± 0.005 Å shorter in the Ru^{III} species than the parent Ru^{II} complex (Table 6.3).

CV was also performed on a solution of Cp*Ru($P^{tBu}{}_2N^{Bn}{}_2$)Cl in the presence of 1 equivalent of [H^+DMF][OTf]. With the complex protonated, the wave corresponding to neutral Cp*Ru($P^{tBu}{}_2N^{Bn}{}_2$)Cl oxidation is no longer present. Instead, a new reversible wave is observed, which is shifted from the complex in the absence of acid by +0.60 V (Figure 6.10).

Table 6.5: Half-wave ($E_{1/2}$) potentials for $1e^-$ oxidation of chloride complexes from CV in CH_2Cl_2 (0.1M $TBAPF_6$).

	$E_{1/2}$ vs Cp_2Fe (V)[a]
Cp*Ru($P^{tBu}_2N^{Bn}_2$)Cl	−0.38
Cp*Ru($P^{Ph}_2N^{Bn}_2$)Cl	−0.38
Cp*Ru($P^{tBu}_2N^{Ph}_2$)Cl	−0.30
CpRu($P^{tBu}_2N^{Bn}_2$)Cl	−0.12
Cp*Ru(dippp)Cl	−0.40
Cp*Ru($P^{tBu}_2N^{Bn}_2$)Cl + H^+DMF	+0.22

[a] Estimated error in $E_{1/2}$ is ± 0.01 V.

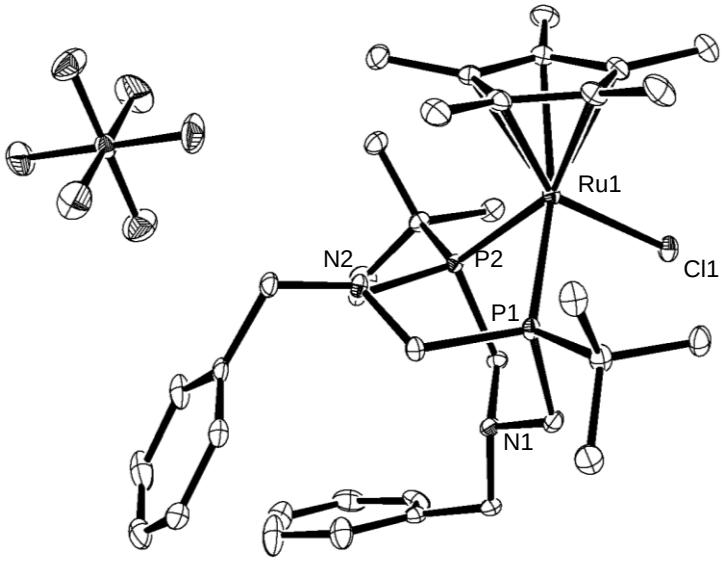

Figure 6.8: ORTEP of [Cp*Ru($P^{tBu}_2N^{Bn}_2$)Cl][PF_6]. Ellipsoids are shown at 50% probability. For clarity, one crystallographically independent [Cp*Ru($P^{tBu}_2N^{Bn}_2$)Cl][PF_6] unit, hydrogen atoms, and an acetone of crystallization are not shown.

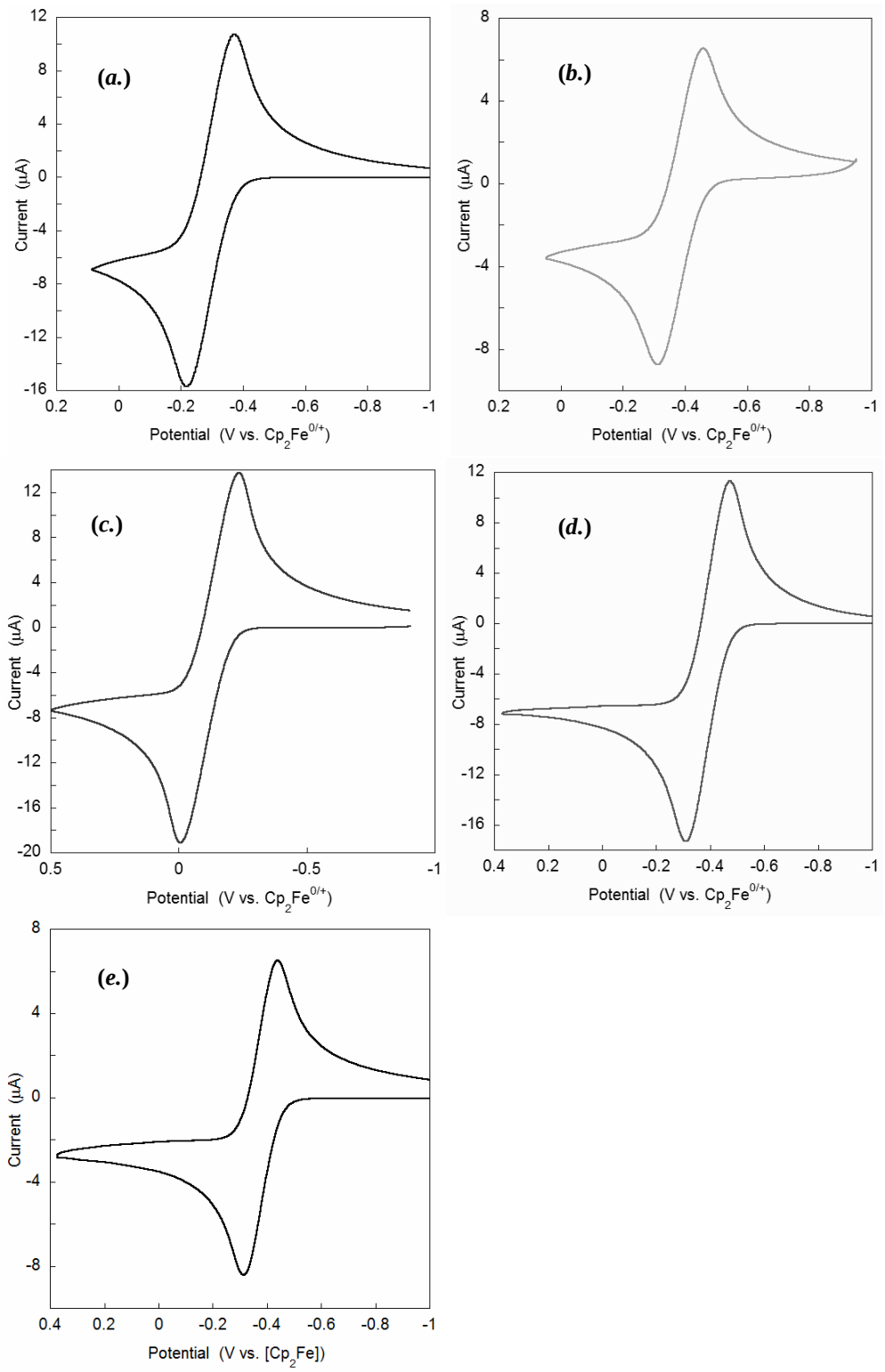

Figure 6.9: Cyclic voltammograms of (*a.*) Cp*Ru($P^{tBu}_2N^{Ph}_2$)Cl, (*b.*) Cp*Ru($P^{Ph}_2N^{Bn}_2$)Cl, (*c.*) CpRu($P^{tBu}_2N^{Bn}_2$)Cl, (*d.*) Cp*Ru(dippp)Cl, and (*e.*) Cp*Ru($P^{tBu}_2N^{Bn}_2$)Cl. Complexes are *ca.* 1-2 mM in CH_2Cl_2 (0.1M $TBAPF_6$) under N_2. Scan rate is 0.1 V/s.

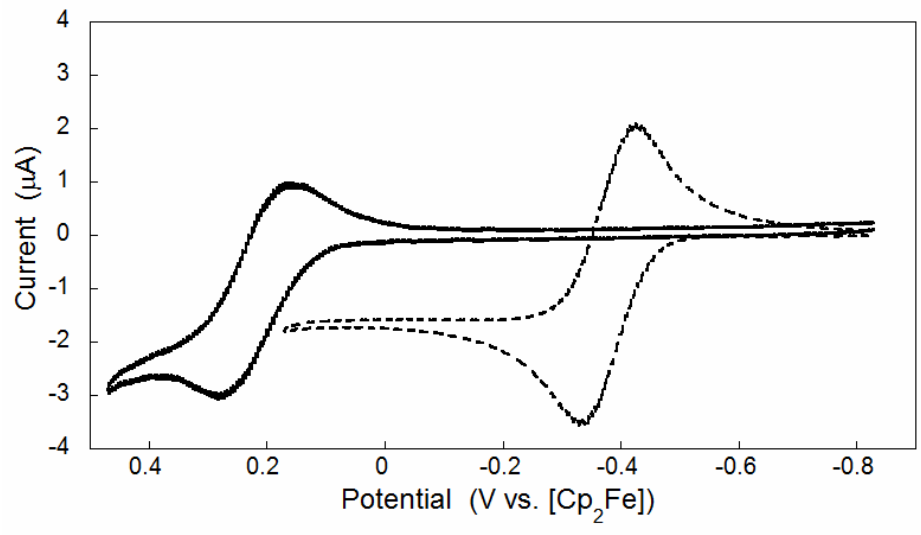

Figure 6.10: Overlay plot of cyclic voltammograms of Cp*Ru($P^{tBu}_2N^{Ph}_2$)Cl (*ca*. 0.5 mM) in the absence (dashed) and presence (solid) of 1 eq. of [H^+DMF][OTf] in CH_2Cl_2 (0.1M $TBAPF_6$) under N_2. Scan rate is 0.1 V/s.

6.2.5.2 Reduction of Dioxygen Complexes

Cyclic voltammograms of the dioxygen complexes [Cp*Ru($P^R_2N^{R'}_2$)(O_2)]$^+$ and [Cp*Ru(dippp)(O_2)]$^+$ in CH_2Cl_2 (*ca*. 1.5 mM, 0.1 M $TBAPF_6$) show one completely irreversible reduction wave at potentials negative of −1 V vs. Cp_2Fe (Figure 6.11), as previously shown for [Cp*Ru($P^{tBu}_2N^{Bn}_2$)(O_2)]$^+$.[46] CVs were recorded in CH_2Cl_2 rather than acetonitrile or other more polar solvents that are typically used for CV because the O_2 ligand is displaced in coordinating solvents like acetonitrile. The potentials of the peak cathodic currents (E_{pc}) depend on the ligand, with a span of 0.23 V.

In the presence of 1 equivalent of [H^+DMF][OTf], a new irreversible reduction wave is observed for all [Cp*Ru($P^R_2N^{R'}_2$)(O_2)]$^+$, with a positive shift in E_{pc} (Figure 6.12, Table 6.6). This wave does not shift in potential with the addition of up to 10 equivalents of [H^+DMF][OTf]. The magnitude of the shift, ΔE_{pc} (Table 6.6), is approximately +0.7 V for all three cations.

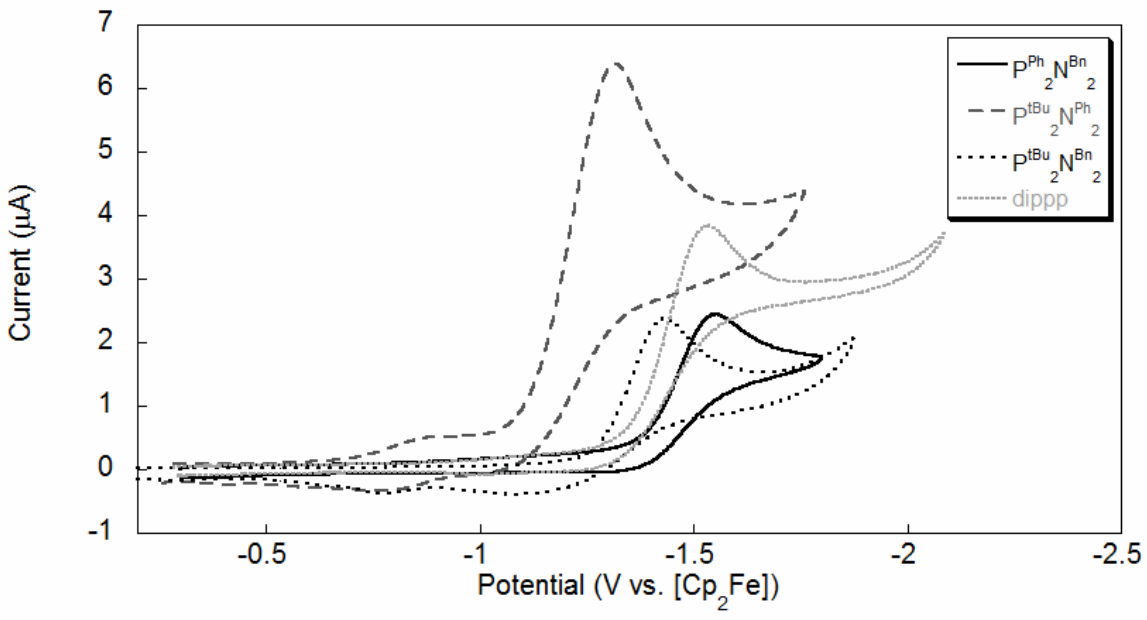

Figure 6.11: Overlay plot of cyclic voltammograms of [Cp*Ru($P^{tBu}_2N^{Ph}_2$)(O_2)][OTf] (gray, dashed line), [Cp*Ru($P^{Ph}_2N^{Bn}_2$)(O_2)][OTf] (black, solid line), [Cp*Ru($P^{tBu}_2N^{Bn}_2$)(O_2)][OTf] (black, short dashed line), and [Cp*Ru(dippp)(O_2)][PF_6] (gray, dotted line). Complexes are *ca.* 1.5 mM in CH_2Cl_2 (0.1M $TBAPF_6$) under N_2. Scan rate is 0.1 V/s.

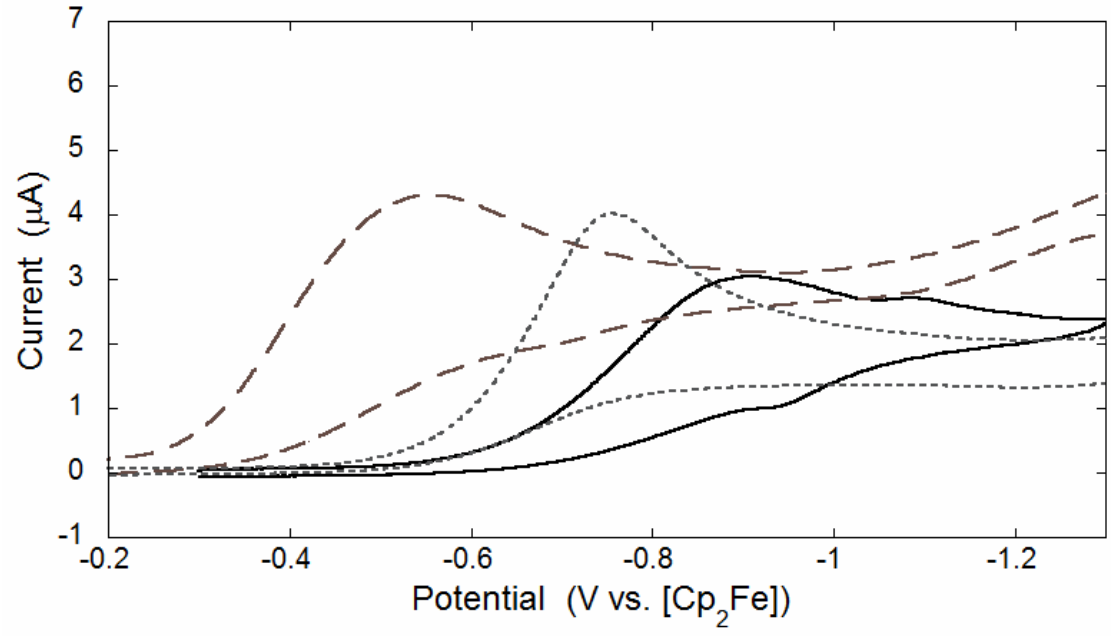

Figure 6.12: Overlay plot of reductive cyclic voltammograms of *ca.* 1.5 mM [Cp*Ru($P^{tBu}_2N^{Bn}_2$)(O_2)][OTf] (short dashes), [Cp*Ru($P^{tBu}_2N^{Ph}_2$)(O_2)][OTf] (long dashes), and [Cp*Ru($P^{tPh}_2N^{Bn}_2$)(O_2)][OTf] (solid) in CH_2Cl_2 (0.1 M $TBAPF_6$) in the presence of 1 equivalent of [H^+DMF][OTf]. Scan rate is 0.1 V/s.

Table 6.6: Peak irreversible reduction potentials (E_{pc}, V) from cyclic voltammograms of $[Cp^*Ru(diphosphine)(O_2)]^+$ in CH_2Cl_2 with and without acid.[a]

	E_{pc}	E_{pc} with 1 equiv. $[H^+DMF][OTf]$	ΔE_{pc} (V)
$[Cp^*Ru(P^{tBu}{}_2N^{Bn}{}_2)(O_2)]^+$	−1.44	−0.77	+0.67
$[Cp^*Ru(P^{Ph}{}_2N^{Bn}{}_2)(O_2)]^+$	−1.55	−0.90	+0.65
$[Cp^*Ru(P^{tBu}{}_2N^{Ph}{}_2)(O_2)]^+$	−1.32	−0.56	+0.76
$[Cp^*Ru(dippp)(O_2)]^+$	−1.45	−1.22	+0.23

[a] CVs with *ca.* 1.5 mM complex in CH_2Cl_2 with 0.1 M [*n*-Bu_4N][PF_6]. Potentials referenced to $Cp_2Fe^{+/0}$, with estimated errors ± 0.02 V.

CVs of $[Cp^*Ru(dippp)(O_2)][PF_6]$, which lacks a pendent amine, also show an irreversible reduction wave in the presence of 1 equiv. of $[H^+DMF][OTf]$ (Figure 6.13) that does change with up to 10 equiv. of acid. Even though $[Cp^*Ru(dippp)(O_2)][PF_6]$ doesn't react with $[H^+DMF][OTf]$ (see above), this wave is shifted positive of the wave in the absence of acid. However, the magnitude of this shift (+0.23 V) is significantly smaller than for pendent amine complexes, suggesting that the pendent amine does play a role in facilitating reduction. The CV of $[Cp^*Ru(dippp)(O_2)][OTf]$ with $[H^+DMF][OTf]$ does appear to be qualitatively somewhat different than for the $P^R{}_2N^{R'}{}_2$ complexes, with a much greater potential difference between the onset of cathodic current and the peak cathodic current E_{pc}, so this conclusion must be treated with some caution.

Cyclic voltammograms of $[Cp^*Ru(P^R{}_2N^{R'}{}_2)(O_2)]^+$ under an O_2 atmosphere in the presence of acid were also performed in order to test for O_2 reduction catalysis. Large catalytic currents were observed under these conditions. Unfortunately, these currents were also present at similar potentials in control experiments performed under identical conditions but in the absence of ruthenium complex. Thus most of the current observed likely corresponded to direct O_2 reduction by the glassy carbon electrode at these very negative potentials.

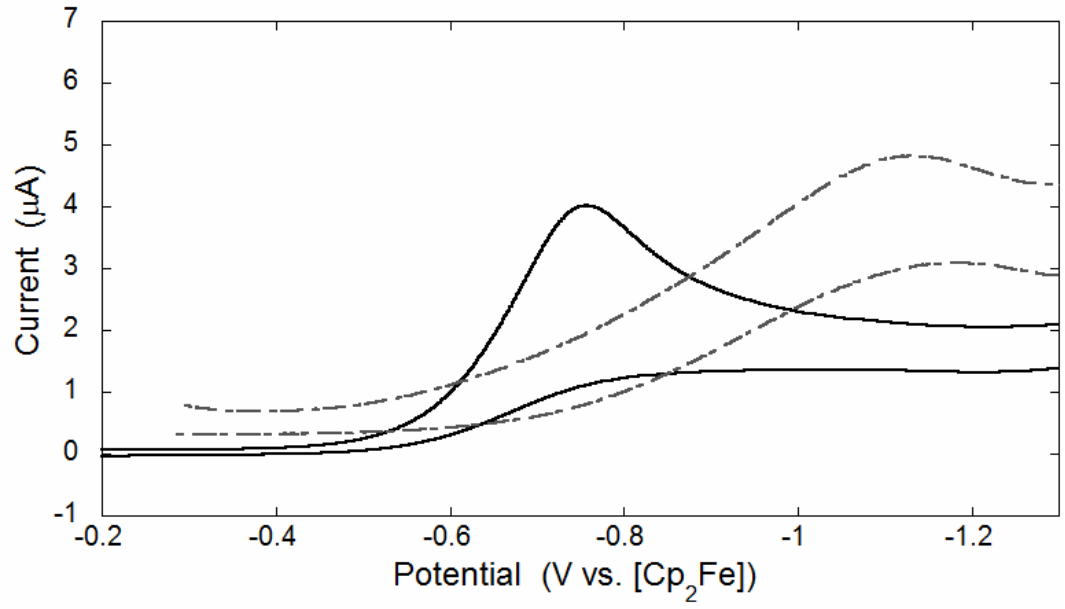

Figure 6.13: Overlay plot of reductive cyclic voltammograms of *ca.* 1.5 mM [Cp*Ru($P^{tBu}_2N^{Bn}_2$)(O_2)][OTf] (black, solid) and [CpRu(dippp)(O_2)][PF_6] in CH_2Cl_2 (0.1 M $TBAPF_6$) in the presence of 1 equivalent of [H^+DMF][OTf].

To investigate the chemical process occurring during reduction of the O_2 ligated complexes [Cp*Ru($P^R_2N^{R'}_2$)(O_2)]$^+$, reactions of these complexes with four equivalents of Cp^*_2Fe ($E_{1/2}$ = −0.53 V vs. Cp_2Fe)[67] were followed by NMR. Consistent with the E_{pc} potentials observed by CV, no reaction was observed between in the absence of acid. Addition of 4 equivalents of [H^+DMF][OTf] to solutions of [Cp*Ru($P^R_2N^{R'}_2$)(O_2)]$^+$ and Cp^*_2Fe caused a rapid color change to bright green, indicating the formation of [Cp^*_2Fe]$^+$. The ^{1}H and ^{31}P NMRs of these reaction solutions contain a large number of peaks, none of which can be identified with certainty, but which suggest decomposition of the complex. With all the complexes, downfield ^{31}P resonances in the +50 − +80 ppm range suggestive of phosphine oxide formation were observed, as well as resonances in the −50 – –20 ppm range suggestive of unbound or decomposed phosphine ligands. For instance, free $P^{tBu}_2N^{Bn}_2$ has a broad ^{31}P resonance in CD_2Cl_2 at *ca.* –45 ppm, and the oxidized ligand (obtained from reaction in CD_2Cl_2 with excess $H_2O_{2(aq)}$) has a sharp resonance at +57 ppm, though there are no peaks at these exact frequencies in the spectrum of the Cp^*_2Fe reduction reaction. Similar spectra have been obtained on addition of excess aqueous H_2O_2 to CD_2Cl_2 solutions of Cp*Ru($P^R_2N^{R'}_2$)Cl.

6.2.6 Oxidation Test Reactions

The protonated complex $[Cp^*Ru(P^{tBu}{}_2N^{Ph}{}_2H)(O_2)][OTf]_2$, generated *in situ* by addition of 1 equiv. of $[H^+DMF][OTf]$ to a CH_2Cl_2 solution of $[Cp^*Ru(P^{tBu}{}_2N^{Ph}{}_2)(O_2)][OTf]$, was tested as an oxidant with a variety of substrates. These reactions essentially paralleled the reactions in reported in Chapter 5 with $[Cp^*Ru(P^{tBu}{}_2N^{Bn}{}_2H)(O_2)]$, although the substrates tested differed slightly. Test reactions were carried out in CD_2Cl_2 on ca. 5 mM solutions of ruthenium complex with 1-5 equivalents of substrate, and followed by ^1H and ^{31}P NMR. The results of these reactions are summarized in Table 6.7. No reaction was observed with any of the substrates tested, with the exception of triphenylphosphine, which completely deprotonated the complex.

Table 6.7: Results of oxidation test reactions with $[Cp^*Ru(P^{tBu}{}_2N^{Ph}{}_2H)(O_2)]^{+2}$ and $[Cp^*Ru(P^{tBu}{}_2N^{Bn}{}_2H)(O2)]^{+2}$.

Substrate	$[Cp^*Ru(P^{tBu}{}_2N^{Ph}{}_2H)(O_2)]^{+2}$	$[Cp^*Ru(P^{tBu}{}_2N^{Bn}{}_2H)(O_2)]^{+2}$ [a]
Tricyclohexylphosphine	-	Deprotonation
Methyldiphenylphosphine	-	Deprotonation
Triphenylphosphine	Deprotonation	NR
Triphenylarsine	NR	-
Tetrahydrothiophene	NR	-
Thioanisole	NR	NR
Norbornylene	NR	-
Cyclohexene	-	NR

NR = no reaction; - = reaction not performed [a] Results for $[Cp^*Ru(P^{tBu}{}_2N^{Bn}{}_2H)(O_2)]^{+2}$ from Chapter 5

6.3 Discussion

Proton relays have been shown to be very valuable components of catalysts for the hydrogenase reaction, $2H^+ + 2e^- \rightleftharpoons H_2$, and are receiving increasing attention for other multielectron, multiproton processes.[22-46] While there has been much study of different $P^R{}_2N^{R'}{}_2$ ligands in nickel hydrogenase catalysis, the key parameters and design

criteria for these ligands are only beginning to be understood. In this work, we have examined the effects of systematic variations in the of $[Cp^*Ru(P^R_2N^{R'}_2)]^+$ framework in the context of dioxygen reduction. Holding the other groups the same, the phosphorus substituent has been varied from *t*-butyl to phenyl, the nitrogen substitutent has been changed from benzyl to phenyl, and the Cp* ligand has been replaced with Cp.

Substituting phenyl for *t*-butyl at the phosphine was expected to make the complexes less electron rich and therefore easier to reduce, due to the more electron-withdrawing character of the phenyl group. In previously studied $Ni(P^R_2N^{Ph}_2)$ complexes, substitution of phenyl for *n*-butyl resulted in changes in reduction potetntial ($\Delta E_{1/2}$'s) in acetonitrile of +0.09 V and +0.21 V for the Ni(II/I) and Ni(I/0) couples, respectively.[34] However, no difference was observed in CVs of $Cp^*Ru(P^{tBu}_2N^{Bn}_2)Cl$ and $Cp^*Ru(P^{Ph}_2N^{Bn}_2)Cl$, and the *t*-butyl-peroxo complex $[Cp^*Ru(P^{tBu}_2N^{Bn}_2)(O_2)]^+$ is actually 0.11 V easier to reduce than the phenyl analogue (Tables 6.5 and 6.6). This may be due to a steric effect of the Cp* ring interacting with the *t*-butyl phosphines, hampering their ability to bind and donate to the Ru, as is reflected in the somewhat longer P-Ru bond distance for $Cp^*Ru(P^{tBu}_2N^{Bn}_2)Cl$ relative to $Cp^*Ru(P^{Ph}_2N^{Bn}_2)Cl$ (Table 6.3). A larger effect is observed upon substitution Cp for Cp*, with an increase in $E_{1/2}$ of +0.26 V. This value is exactly the same as the difference between ferrocene and pentamethylferrocene (CpCp*Fe) under similar conditions ($\Delta E_{1/2}$ = +0.259(3)[67]).

Surprisingly, the effect of changing the amine substituent in the second coordination sphere from R' = Bn to Ph is larger than that of changing the phosphine substituent directly bonded to the metal on the oxidation potential of the chloride ligated species. $Cp^*Ru(P^{tBu}_2N^{Bn}_2)Cl$ is 0.08 V easier to oxidize than $Cp^*Ru(P^{tBu}_2N^{Ph}_2)Cl$ (Table 6.5). A dependence of the redox potential of the metal center on the basicity of the pendent amine with $P^R_2N^{R'}_2$ has previously been demonstrated for $Ni(P^R_2N^{R'}_2)^{+2}$ complexes,[36] with $\Delta E_{1/2}$'s for R' = *t*-butyl versus phenyl of +0.10 V and +0.17 V for the Ni(II/I) and Ni(I/0) couples, respectively, of $Ni(P^{Ph}_2N^{R'}_2)^{+2}$ in acetonitrile.[35] Still, it is surprising that the amine substituent four bonds from the Ru could have a larger effect than the phosphine substituent two bonds from the Ru, especially considering the crystallographic similarity in phosphine binding between these *t*-butyl phosphine

complexes. The oxidation potential of Cp*Ru(dippp)Cl, without a relay, is within error of those of the *N*-benzyl derivatives Cp*Ru($P^{tBu}_2N^{Bn}_2$)Cl and Cp*Ru($P^{Ph}_2N^{Bn}_2$)Cl, supporting the suggestion that this complex is a good analogue electronically to the $P^R_2N^{R'}_2$ complexes.

Not only do the amine substituents affect the ruthenium redox potential, but also the phosphine substituents significantly affect the amine basicity. $[Cp^*Ru(P^{Ph}_2N^{Bn}_2)(O_2)]^+$ is 1.4 pK_a units less basic than $[Cp^*Ru(P^{tBu}_2N^{Bn}_2)(O_2)]^+$ despite having a more negative reduction potential. This may be due to an electron withdrawing effect of the phenyl phosphine on the pendent benzylamine. The aniline-derived proton relay is substantially less basic than the benzylamine relay, as expected. However, as observed with other $P^R_2N^{R'}_2$ complexes,[35] this change in basicity by several pK_a units was coupled to a change in redox potential of the complex of *ca.* 0.1 V (Table 6.6). These results show that the metal and its first coordination sphere are significantly coupled to the proton relays in the second coordination sphere. It is difficult to independently tune properties of a complex and its pendent proton relays.

The nature of the peroxo compounds $[Cp^*Ru(P^R_2N^{R'}_2)(O_2)]^+$ do not appear to be significantly affected by changes in the phosphine, aniline, or Cp groups, based on the structural and spectroscopic parameters. This is surprising, as it might be expected based on the electrochemical data obtained for the Cl^- and O_2 complexes that $[Cp^*Ru(P^{tBu}_2N^{Ph}_2)(O_2)][BPh_4]$ would be more easily reduced than $[Cp^*Ru(P^{tBu}_2N^{Bn}_2)(O_2)][BPh_4]$, and therefore would not donate as much electron density to the bound O_2, resulting in a shorter O–O bond. Substituting Cp for Cp* produced a complex with much lower stability but this does not appear to be due to changes in Ru–O_2 bonding given the similarity of the X-ray structures. The reduced stability could be a steric effect, perhaps involving intermolecular reactions between Cp complexes that are not possible with the less accessible Cp* complexes.

Interestingly, despite the large differences in the basicities of the pendent amines and in the overall complexes, protonation of the peroxo complexes $[Cp^*Ru(P^R_2N^{R'}_2)(O_2)]^+$ proceeds in essentially the same manner for all the compounds tested. The proton is located on the amine near the O_2 ligand, forming a hydrogen bond to

one of the O atoms in the O_2. The hydrogen bond should be stronger to a protonated pendent aniline versus a protonated pendent benzylamine because of the better pK_a matching between the aniline and the bound O_2. This is observed in the O···H−N hydrogen bonding distances predicted by DFT, with *d*(O2···N1) calculated to be 0.016 Å shorter for the aniline compound (Table 6.4). The hydrogen bond in $[Cp^*Ru(P^R{}_2N^{R'}{}_2H)(O_2)]^+$ imparts a small amount of η^1-hydroperoxo character to the bound O_2 ligand, as can be seen by X-ray and in the DFT structures in the lengthening of the Ru−O bond to the hydrogen bonded O atom relative to the other Ru−O bond. Bonding to the positively charged H^+ pulls some electron density out of the Ru and onto the O_2. The additional electron density from Ru is donated to the O_2 π^* orbital, slightly weakening the O−O π bond. This is reflected in lower energy O−O bond stretching frequencies and longer bond lengths on protonation. It is therefore somewhat unexpected that the complex with the pendent aniline has a smaller shift in O−O stretching frequency upon protonation (~20 cm^{-1} versus 30 cm^{-1} for the benzylamine complex (Table 6.2)), despite forming an apparently stronger hydrogen bond. DFT calculations agree with this experimentally observed difference in O−O stretching frequency, predicting a shift of 20 cm^{-1} for the aniline complex versus 25 cm^{-1} for the benzylamine complex.[46] These calculations show that the O−O stretching vibration of the protonated species also involves motion of the $P^R{}_2N^{R'}{}_2$ ligand. Differences in the rigidity of the pendent aniline versus the pendent benzylamine may explain the differences in the shift in stretching frequency. Despite the apparent hydroperoxo character of the protonated complexes, they are incapable of oxidizing electron-rich substrates such as triphenylarsine and thioanisole.

Protonation of the pendent amine substantially facilitates reduction of the peroxo complexes $[Cp^*Ru(P^R{}_2N^{R'}{}_2)(O_2)]^+$, as the cathodic peak potentials E_{pc} shift by 0.65-0.76 V (Table 6.6). The waves in the CVs are irreversible, which complicates the interpretation of these values. Still, the similarity between the complexes studied suggests that the ΔE_{pc} values may be reasonably compared. Some of the shift in E_{pc} is due to the additional positive charge on the complex, but this alone is unlikely to account for all of the ~0.7 V shift. The shift in the $Ru^{II/III}$ couple of $Cp^*Ru(P^{tBu}{}_2N^{Bn}{}_2)Cl$ in the presence and

absence of acid of +0.60 V gives an approximate of value for how the potential might shift due purely to the additional charge of the proton. This is not a perfect model because different electrochemical processes are being compared. However, each electrochemical process involves the interconversion of a monocation with a dication in the presence of protons, so the comparison is not unreasonable. The Coulombic effect of a proton at the pendent amine on the Ru center should be quite similar between the Cl^- and O_2 complexes. From this comparison it may be concluded that roughly +0.6 V of the shift for the O_2 complexes is due to the additional charge of the proton, and +0.1 V can be attributed to the reductions being proton-coupled processes.

It is probable that the first electron transferred occurs with proton transfer, producing a Ru(III) hydroperoxo complex. The protonated formally Ru(IV) η^2-peroxo complexes appear structurally primed to form such $Ru^{III}OOH$ species. The dependence of ΔE_{pc} on the nature of the pendent amine is consistent with this proposal. ΔE_{pc} is 0.09 V larger for the aniline complex than for the related benzyl-amine complex because aniline is the weaker base, making proton transfer from aniline to the peroxide ligand more thermodynamically favorable in the aniline complex. Still, this shift is smaller than would have been expected, since 0.09 V is equivalent to a change in K_{eq} for electron transfer (ET) of $10^{1.5}$ while aniline is $10^{6.3}$ less basic than benzylamine (6.3 pK_a units in MeCN[66]).

The importance of the proton relays is indicated by comparing the peak reduction potentials for the $[Cp^*Ru(P^R{}_2N^{R'}{}_2)(O_2)]^+$ complexes *vs.* that of $[Cp^*Ru(dippp)(O_2)]^+$, which does not contain a pendent amine. Protons do facilitate this reduction, but give a ΔE_{pc} of only 0.23 V, only about a third of the shift for the compounds with the proton relays. It is interesting that $[H^+DMF][OTf]$ does not protonate the O_2 ligand in the dippp complex (since the NMR spectra are unaffected by this acid). The O_2 ligand has very low basicity, suggesting that the Ru–O_2 interaction is quite covalent, so an ionic Ru(IV)-peroxide picture of these species is not accurate. From another perspective, the lack of protonation indicates that the dicationic Ru(IV) hydroperoxide is a high energy species. This analysis also illustrates the value of the proton relays, in holding protons close to a ligand with low basicity.

Despite the favorable interaction between the protonated pendent amine and the O_2, these complexes are not effective catalysts for O_2 reduction. Reduction of the peroxo complexes, both protonated and not, is completely irreversible and the nature of the chemical processes occurring upon reduction is not known. The lack of anodic current in the CVs suggests a rapid loss of ligand, either O_2 or phosphine, or rapid decomposition. The control complex $[Cp^*Ru(dippp)(O_2)][PF_6]$ shows a similar irreversible wave at a similar potential, so the relays are not key to this decomposition. Unfortunately, we have been unable to identify any of the products of reduction of $[Cp^*Ru(P^R{}_2N^{R'}{}_2)(O_2)]^+$ with acid, but ^{31}P NMR spectra of reductions with $Cp^*{}_2Fe$ are highly suggestive of phosphine oxidation. The proposed Ru^{III}-OOH intermediate could undergo many undesirable reactions, including intramolecular O atom insertion into a Ru-P bond to form a phosphine oxide, which is a known reaction for these types of complexes.[58,68] The stabilization of this possible hydroperoxo intermediate by the pendent amine does not appear to be strong enough to prevent this phosphine oxidation reaction from occurring. Phosphine oxidation has been observed previously in O_2 reduction with $Ni(P^R{}_2N^{R'}{}_2)^{+2}$ complexes,[45] and remains a significant challenge for the use of $P^R{}_2N^{R'}{}_2$ ligands even for these relatively substitutionally inert complexes in the presence of oxidizing species.

6.4 Conclusions

A series of Cp*Ru complexes with $P^R{}_2N^{R'}{}_2$ ligands has been prepared. All of the $[Cp^*Ru(P^R{}_2N^{R'}{}_2)]^+$ complexes tightly bind O_2, partially reducing O_2 to give formally a peroxide ligand. The $[Cp^*Ru(P^R{}_2N^{R'}{}_2)(O_2)]^+$ complexes bind protons at the amine near the O_2 ligand, directing the proton to the O_2 ligand through a hydrogen bonding interaction. The same proton directing is seen despite large differences in the basicity of the pendent amines. These compounds thus allow a clear visualization of one potentially key role of second-sphere proton relays in the oxygen reduction reaction. The series of compounds were made in order to adjust the properties of the metal center – by varying the phosphine and Cp substituents – and independently the properties of the relays, by varying the amine substituents. However, it was found that the properties of the metal center and the relays are intertwined, with changes in phosphine substituents affecting the

amine basicity and change in amine substituent affecting the Ru redox potential. The species formed upon reduction of the peroxo complexes are unstable, and decomposition prevents these complexes from acting as oxygen reduction catalysts. However, cyclic voltammetry has shown that the positioned protons significantly facilitate reduction of the peroxo complexes, perhaps by protonating the O_2 ligand upon reduction.

6.5 Experimental

6.5.1 General considerations:

All manipulations were carried out under a nitrogen atmosphere using standard glove box and Schlenk techniques unless otherwise specified. Solvents and reagents, including ^{15}N-labeled aniline and $^{18}O_2$ gas (97 atom% ^{18}O), were purchased from Aldrich unless otherwise noted. 1,3-bis(diisopropylphosphino)propane (dippp) was purchased from Strem. CD_2Cl_2 was purchased from Cambridge Isotope Labs and dried over CaH_2 prior to use. $RuCl_3 \cdot 3H_2O$ was purchased from Pressure Chemical Company. $[Cp^*RuCl]_4$,[69] $Cp^*Ru(PPh_3)_2Cl$,[70] $CpRu(PPh_3)_2Cl$,[71] $[H^+DMF][OTf]$[72], and the ligands $P^{tBu}{}_2N^{Ph}{}_2$[40] and $P^{Ph}{}_2N^{Bn}{}_2$[35] were prepared following literature procedures. $Cp^*Ru(P^{tBu}{}_2N^{Bn}{}_2)Cl$, $[Cp^*Ru(P^{tBu}{}_2N^{Bn}{}_2)(O_2)][PF_6]$, and $[Cp^*Ru(P^{tBu}{}_2N^{Bn}{}_2H)(O_2)][PF_6]_2$ were prepared as reported previously.[46] IR spectra were recorded using a Bruker Optics Tensor27 FTIR spectrometer at room temperature as KBr pellets or in CH_2Cl_2 solution between NaCl plates as indicated. NMR spectra were recorded at 298 K on Bruker AV300, AV500, or DRX500 spectrometers. ^{1}H NMR chemical shifts are reported versus TMS and referenced to residual solvent. ^{31}P NMR chemical shifts are reported relative to an 85% $H_3PO_{4\,(aq)}$ external standard. Mass spectra were recorded on a Bruker Autoflex II MALDI-TOF. Elemental analysis was performed by Atlantic Microlabs. Optical spectroscopy measurements were taken on a Hewlett-Packard 8453 diode array spectrophotometer equipped with a Unisoku sample holder with a temperature controller.

6.5.2 Synthesis

6.5.2.1 Cp*Ru($P^{tBu}_2N^{Ph}_2$)Cl

The ligand $P^{tBu}_2N^{Ph}_2$ (0.223 g, 0.54 mmol) was suspended in 30 mL of THF. A slurry of $[Cp^*RuCl]_4$ (0.145 g, 0.13 mmol) in 10 mL of THF was added over a period of 5 minutes. The dark orange solution was stirred at room temperature for 2 days. The solution was evaporated to dryness. The orange solid was redissolved in 3 mL of toluene, filtered through Celite, and stored at −20°C for 2 days to give dark orange X-ray quality crystals of Cp*Ru($P^{tBu}_2N^{Ph}_2$)Cl•(toluene). The toluene was removed under vacuum to give Cp*Ru($P^{tBu}_2N^{Ph}_2$)Cl as an orange powder (0.200 g, 53% yield). NMR(CD_2Cl_2) ^{1}H: 7.21 (m, 4H, Ar-*H*), 6.94 (m, 4H, Ar-*H*), 6.76 (m, 2H, Ph-*H*), 4.36 (m, 2H, PCH_2N), 3.81 (m, 2H, PCH_2N), 3.51 (m, 2H, PCH_2N), 3.00 (m, 2H, PCH_2N), 1.68 (s, 15H, CpCH_3), 1.39 (3-line pattern, 18H, tBu-CH_3); ^{31}P{^{1}H}: 44.0 (s). Anal. (Calc.) C: 59.72 (59.51) H: 7.54 (7.49) N: 4.10 (4.08).

6.5.2.2 Cp*Ru($P^{Ph}_2N^{Bn}_2$)Cl

The ligand $P^{Ph}_2N^{Bn}_2$ (0.483 g, 1.0 mmol) was suspended in 30 mL of toluene. To this suspension was added Cp*Ru(PPh_3)Cl (0.796 g, 0.98 mmol) slurried in 30 mL of toluene. This mixture was refluxed for 10 minutes, at which time an orange solution was formed. The orange solution was further refluxed for 36 hours. It was then cooled to room temperature and vacuum dried to give an orange oil. The orange oil was triturated with hexanes and vacuum dried three times to give a yellow-orange powder. This powder was collected by filtration and washed once with 10 mL acetone and then five times with 5 mL hexanes. The yellow-orange powder was dried under vacuum to give Cp*Ru($P^{Ph}_2N^{Bn}_2$)Cl (0.408 g, 55% yield). X-ray quality crystals were obtained from CH_2Cl_2 layered with hexanes at −20°C. NMR(CD_2Cl_2) ^{1}H: 7.60-6.93 (m, 20H, Ph-*H*), 4.06 (s, 2H, PhCH_2N), 3.63 (m, 2H, PCH_2N), 3.43 (m, 2H, PCH_2N), 3.42 6 (s, 2H, PhCH_2N), 3.10 (m, 2H, PCH_2N), 2.37 (m, 2H, PCH_2N), 1.29 (s, 15H, CpCH_3); ^{31}P{^{1}H}: 31.0 (s). Anal. (Calc.) C: 64.27 (63.69) H: 6.44 (6.28) N: 3.71 (3.71).

6.5.2.3 CpRu($P^{tBu}_2N^{Bn}_2$)Cl

The ligand $P^{tBu}_2N^{Bn}_2$ (0.500 g, 1.1 mmol) was dissolved in 30 mL of toluene. To this was added CpRu(PPh_3)Cl (0.730 g, 0.98 mmol) slurried in 30 mL of toluene. This mixture was refluxed for 10 minutes, at which time an orange solution was formed. The orange solution was further refluxed for 36 hours. It was then cooled to room temperature and vacuum dried to give an orange oil. The orange oil was triturated with hexanes and vacuum dried three times to give a yellow-orange powder. This powder was collected by filtration and washed three times with 10 mL hexanes. The yellow-orange powder was dissolved in 5 mL of toluene, layered with 8 mL of hexanes, and stored at −20°C for two days, forming a yellow solid. This solid was collected by filtration and dried under vacuum to give CpRu($P^{tBu}_2N^{Bn}_2$)Cl (0.452 g, 72% yield). NMR(CD_2Cl_2) ^{1}H: 7.32-7.18 (m, 10H, Ph-*H*), 4.64 (s, 5H, Cp-*H*), 3.68 (s, 2H, PhCH_2N), 3.61 (s, 2H, PhCH_2N), 3.37 (m, 2H, PCH_2N), 2.68 (m, 2H, PCH_2N), 2.53 (m, 2H, PCH_2N), 2.42 (m, 2H, PCH_2N), 1.03 (3-line pattern, 18H, tBu-CH_3); ^{31}P{^{1}H}: 51.8 (Calc.) C: 58.09 (57.80) H: 7.04 (7.16) N: 4.31 (4.35).

6.5.2.4 Cp*Ru(dippp)Cl

To a solution of 1,3-bis(diisopropylphosphino)propane (dippp) (0.250 g, 0.90 mmol) in 15 mL THF was added $[Cp^*RuCl]_4$ (0.245 g, 0.23 mmol) slurried in 10 mL THF. The mixture was stirred overnight, forming an orange solution. This solution was passed through a Celite plug while open to air to remove a small amount of dark, insoluble material, and then dried under vacuum to give a light orange powder. The orange powder was dissolved in 3 mL of toluene, layered with 5 mL of hexanes, and stored at −20°C. On standing overnight, red crystals formed, as well as a small amount of black oil. The red crystals of Cp*Ru(dippp)Cl of were isolated by filtration, with the black oil remaining on the glassware, and washed with hexanes, giving (0.120 g, 24% yield) of Cp*Ru(dippp)Cl. NMR(CD_2Cl_2): The proton NMR spectrum is complex due to ^{1}H and ^{31}P coupling and has not been fully assigned. ^{1}H: 2.59 (m, 2H), 2.18 (m, 3H), 2.05 (m, 2H) 1.80 (m, 2H), 1.63, (s, 15H, CpCH_3), 1.57 (m, 1H), 1.24-1.18 (m, 24H, CH(CH_3)$_2$); ^{31}P{^{1}H}: 32.5 (s). Anal. (Calc.) C: 54.99 (54.78) H: 9.01 (8.93).

6.5.2.5 [CpRu($P^{tBu}_2N^{Bn}_2$)(MeCN)][PF_6]

To a solution of Cp*Ru($P^{Ph}_2N^{Bn}_2$)Cl (0.020 g, 0.03 mmol) in 2mL CH_2Cl_2 was added $TlPF_6$ (0.11 g, 0.03 mmol) in 2 mL CH_2Cl_2. After 30 minutes, the solution was passed through Celite to remove TlCl, leaving a red solution. To this solution was added an excess (approximately) 5μL of acetonitrile, resulting in an immediate color change to yellow. This solution was dried to a yellow oil under vacuum, redissolved in acetonitrile, and layered with diethyl ether. On standing for several days at −35°C, large yellow crystals of [CpRu($P^{tBu}_2N^{Bn}_2$)(MeCN)][PF_6]•(ether) were obtained. The ether could be removed under vacuum to give [CpRu($P^{tBu}_2N^{Bn}_2$)(MeCN)][PF_6] (0.008 g, 32% yield). NMR(CD_2Cl_2): ^{1}H: 7.32-7.27 (m, 8H, Ph-*H*), 7.16 (d, 2H, Ph-*H*), 4.84 (s, 5H, Cp-*H*), 3.70 (s, 4H, PhCH_2N), 3.06 (m, 2H, PCH_2N), 2.58-2.50 (m, 6H, PCH_2N), 2.24 (s, 3H, NCCH_3), 1.04 (3-line pattern, 18H, tBu-CH_3) ^{31}P{^{1}H}: 52.6 (s) −144.0 (m, $J_{19F\text{-}31P}$ = 720 Hz). Anal. (Calc.) C: 49.85 (49.87) H: 6.23 (6.09) N: 5.33 (5.29).

6.5.2.6 [Cp*Ru($P^{tBu}_2N^{Bn}_2$)Cl][PF_6]

To a solution of Cp*Ru($P^{tBu}_2N^{Bn}_2$)Cl (0.100 g, 0.14 mmol) in 3 mL of CH_2Cl_2 was added a solution of ferrocenium hexafluorophosphate (0.046 g, 0.14 mmol) in 8 mL of CH_2Cl_2. The solution turned greenish-brown upon addition, and was stirred for an additional 20 minutes. The solution was vacuum dried to a dark oil which was then triturated with 5 mL of toluene and filtered through paper, separating the dark green solid from the orange, ferrocene-containing filtrate. The green solid was then washed through the paper with 5 mL of acetone. The green liquid was layered with 5 mL of hexane and stored at −20°C overnight, affording large green crystals of [Cp*Ru($P^{tBu}_2N^{Bn}_2$)Cl][PF_6] (0.105 g, 87%). MS: (MALDI-TOF, pyrene matrix) 714.2 [M^+], 679.2 [M^+−Cl]. Anal. (Calc.) C: 50.49 (50.38) H: 6.52 (6.34) N: 3.32 (3.26).

6.5.2.7 [Cp*Ru($P^{tBu}_2N^{Ph}_2$)(O_2)][OTf]

To an aerobic solution of Cp*Ru($P^{tBu}_2N^{Ph}_2$)Cl (0.053 g, 0.08 mmol) in 10 mL acetone was added a solution of TlOTf (0.027 g, 0.08 mmol) in 5 mL acetone. The yellow-orange solution immediately turned yellow-brown, and white TlCl precipitated.

The solution was stirred for an additional 2 hours, and then the TlCl was removed by filtration through a plug of Celite. The solution was dried to a brown oil under vacuum, triturated with hexanes, and dried again under vacuum to give [Cp*Ru($P^{tBu}_2N^{Ph}_2$)(O_2)][OTf] as a yellow-brown powder (0.059 g, 93%). X-ray quality crystals were obtained by evaporation of acetone solvent. NMR(CD_2Cl_2): ^{1}H: 7.34 (m, 4H, Ar-*H*), 7.00 (m, 6H, Ar-*H*), 3.80 (m, 2H, PC*H*$_2$N), 3.74 (m, 2H, PC*H*$_2$N), 3.57 (m, 2H, PC*H*$_2$N), 3.24 (m, 2H, PC*H*$_2$N), 1.82 (s, 15H, CpC*H*$_3$), 1.48 (3-line pattern, 18H, tBu-*CH*$_3$); ^{31}P{^{1}H}: 30.2 (s). IR(KBr) ν(O-O) = 930 cm^{-1} [^{18}O = 880 cm^{-1}]. Anal. (Calc.) C: 50.20 (50.47) H: 6.20 (6.29) N: 3.49 (3.36).

6.5.2.8 [Cp*Ru($P^{Ph}_2N^{Bn}_2$)(O_2)][OTf]

To an aerobic solution of Cp*Ru($P^{Ph}_2N^{Bn}_2$)Cl (0.070 g, 0.09 mmol) in 10 mL acetone was added a solution of TlOTf (0.033 g, 0.09 mmol) in 5 mL acetone. The yellow-orange solution immediately turned yellow-brown, and white TlCl precipitated. The solution was stirred for an additional 2 hours, and then the TlCl was removed by filtration through a plug of Celite. The solution was dried to a brown oil under vacuum. This oil was recrystallized from acetone/hexanes at −20°C for several days to give after filtration [Cp*Ru($P^{Ph}_2N^{Bn}_2$)(O_2)][OTf]·(acetone) as a yellow-brown microcrystalline powder. The acetone could be removed *in vacuo* to give [Cp*Ru($P^{Ph}_2N^{Bn}_2$)(O_2)][OTf] (0.065 g, 80%). X-ray quality crystals were obtained from CH_2Cl_2 layered with hexanes at −20°C. NMR(CD_2Cl_2): ^{1}H: 7.79 (m, 4H, Ph-*H*), 7.59-7.43 (m, 12H, Ph-*H*), 6.93-6.85 (m, 4H, Ph-*H*), 4.06 (s, 2H, PhC*H*$_2$N), 3.63 (m, 2H, PC*H*$_2$N), 3.43 (m, 2H, PC*H*$_2$N), 3.42 6 (s, 2H, PhC*H*$_2$N), 3.10 (m, 2H, PC*H*$_2$N), 2.37 (m, 2H, PC*H*$_2$N), 1.29 (s, 15H, CpC*H*$_3$); ^{31}P{^{1}H}: 22.0 (s). IR(KBr) ν(O-O) = 926 cm^{-1} [^{18}O = 879 cm^{-1}]. Anal. (Calc.) for [Cp*Ru($P^{Ph}_2N^{Bn}_2$)(O_2)][OTf]·(acetone) C: 55.38 (55.11) H: 5.62 (5.68) N: 3.00 (2.92).

6.5.2.9 [Cp*Ru(dippp)(O_2)][PF_6]

To an aerobic solution of Cp*Ru(dippp)Cl (0.075 g, 0.14 mmol) in 10 mL acetone was added a solution of $TlPF_6$ (0.051 g, 0.15 mmol) in 5 mL acetone. The solution orange solution immediately turned deep blue, and white TlCl precipitated. After 5 minutes of

stirring open to air, the blue color changed to a light yellow, indicating formation of the O_2 complex. The solution was stirred for an additional 2 hours, and then the TlCl was removed by filtration through a plug of Celite. The solution was dried to a brown oil under vacuum, triturated with hexanes, and dried again under vacuum to give [Cp*Ru(dippp)(O_2)][PF_6] as a brown powder (0.090 g, 93%). X-ray quality crystals were obtained from CH_2Cl_2 layered with hexanes at −20°C. NMR(CD_2Cl_2) The proton NMR spectrum is complex due to ^{1}H and ^{31}P coupling and has not been fully assigned. ^{1}H: 2.55 (m, 2H), 2.48 (m, 1H), 1.96-1.89 (m, 6H), 1.77 (s, 15H, CpC*H*$_3$), 1.69 (m, 1H) 1.35 (m, 24H, CHC*H*$_3$); ^{31}P{^{1}H}: 23.5 (s), −144.0 (m, $J_{19F\text{-}31P}$ = 720 Hz). Anal. (Calc.) C: 43.75 (43.54) H: 7.35 (7.16).

6.5.3 Electrochemistry

Cyclic voltammetry (CV) was performed under N_2 using a CH Instruments 600D apparatus equipped with glassy carbon (1.0 mm dia.) working electrode, glassy carbon rod auxiliary electrode, and Ag/Ag(NO)$_3$ (0.01 M in acetonitrile) reference electrode. CV was carried out in dichloromethane with 0.1 M [^{n}Bu$_4$N][PF_6] as supporting electrolyte. [^{n}Bu$_4$N][PF_6] was recrystallized three times from ethanol and dried under vacuum prior to use. Ferrocene or decamethylferrocene were added as internal standards, and all potentials are reported vs. the $Cp_2Fe^{+/0}$ couple. In all cases, solutions were *ca.* 1-2 mM in concentration of Ru complex.

6.5.4 DFT Calculations

Density functional theory calculations were performed with *Gaussian09.*[65] Geometry optimizations were performed in the gas phase on only the cationic portions of [Cp*Ru($P^{tBu}_2N^{Ph}_2H$)(O_2)]$^{+2}$ and [Cp*Ru($P^{tBu}_2N^{Ph}_2$)(O_2)]$^+$. Calculations were performed with the BP86 functional, with the SDD basis set and effective core potential for Ru, and the 6-31G** basis set for all other atoms. Optimization of [Cp*Ru($P^{tBu}_2N^{Ph}_2$)(O_2)]$^+$ was performed starting for the geometry of the crystal structure. All geometries were confirmed to be minima by vibrational analysis (NImag = 0).

6.5.5 X-ray Crystallographic Data

X-ray diffraction data were collected on a Bruker APEXII single crystal diffractometer coupled to a Bruker APEXII CCD detector with graphite-monochromated Mo Kα radiation (λ = 0.71073 Å). The data was integrated and scaled using SAINT, SADABS within the APEX2 software package by Bruker.[73] Solution by direct methods (SHELXS, SIR97[74,75]) produced a complete heavy atom phasing model consistent with the proposed structure. The structure was completed by difference Fourier synthesis with SHELXL97.[76,77] Scattering factors are from Waasmair and Kirfel[78]. All hydrogen atoms, including the hydrogen-bonding N-H protons, were placed in geometrically idealized positions and constrained to ride on their parent atoms with C-H and N-H distances in the range 0.90-1.00 Angstrom (a riding model). Isotropic thermal parameters Ueq were fixed such that they were 1.2Ueq of their parent atom Ueq for CH's and NH's, and 1.5Ueq of their parent atom Ueq in case of methyl groups. All non-hydrogen atoms were refined anisotropically by full-matrix least-squares. Collection and refinement data are presented in Tables 6.8 – 6.14. In the structure of [Cp*Ru($P^{tBu}_2N^{Ph}_2$)(N_2)][BArF'], numerous restraints were placed on the positions of the $[BArF']^-$ fluorine atoms. The structures of Cp*Ru($P^{tBu}_2N^{Ph}_2$)Cl•(toluene) and [Cp*Ru($P^{Ph}_2N^{Bn}_2$) (O_2)][OTf]•(hexane)$_{1/3}$•(CH_2Cl_2)$_{2/3}$ required restraints on the solvent molecules. The structure of [Cp*Ru($P^{tBu}_2N^{Bn}_2$)Cl][PF_6] •(acetone)$_{1/2}$ and [CpRu($P^{tBu}_2N^{Bn}_2$)(O_2)][OTf]•(CH_2Cl_2)$_2$•(H_2O) required restraints on the fluorines of the anions. The restraints used to fit the structure of [Cp*Ru($P^{Ph}_2N^{Bn}_2$H)(O_2)][OTf]$_2$•(acetone) are described in the text.

Table 6.8: Collection and refinement data for Cp*Ru($P^{tBu}_2N^{Ph}_2$)Cl and Cp*Ru($P^{Ph}_2N^{Bn}_2$)Cl.

	Cp*Ru($P^{tBu}_2N^{Ph}_2$)Cl •(toluene)	Cp*Ru($P^{Ph}_2N^{Bn}_2$)Cl
Emp. formula	$C_{41}H_{59}ClN_2P_2Ru$	$C_{40}H_{47}Cl\ N_2P_2Ru$
T (K)	100(2)	100(2)
Wavelength	0.71073 Å	0.71073 Å
Size (mm)	0.17 x 0.14 x 0.12	0.30 x 0.26 x 0.15
Cryst. Syst	Triclinic	Tetragonal
Space group	P $\bar{1}$	P 42/n
a (Å)	11.8320(5)	21.5703(7)
b (Å)	17.2336(6)	21.5703(7)
c (Å)	20.2054(8)	15.5860(8)
α (deg)	93.416(2)	90
β (deg)	102.043(2)	90
γ (deg)	106.753(2)	90
V ($Å^3$)	3826.7(3)	7251.8(5)
Z	4	8
D_{calc} (g/cm^3)	1.351	1.382
Abs. coeff. (mm^{-1})	0.594	0.625
Reflections total	158277	259709
Reflections uniq. (R_{int})	23413 [R(int) = 0.0358]	9088 [R(int) = 0.0408]
Data/restraints/ parameters	23413 / 42 / 924	9088 / 0 / 420
GOF	1.054	1.061
R1/wR2 [I>2σ(I)]	0.0312 / 0.0666	0.0213 / 0.0508
R1/wR2 (all data)	0.0429 / 0.0723	0.0285 / 0.0557

Table 6.9: Collection and refinement data for [CpRu($P^{tBu}_2N^{Bn}_2$)(MeCN)][PF_6] and Cp*Ru(dippp)Cl.

	[CpRu($P^{tBu}_2N^{Bn}_2$)(MeCN)][PF_6] •(diethyl ether)	Cp*Ru(dippp)Cl
Emp. formula	$C_{37}H_{58}F_6N_3P_3ORu$	$C_{25}H_{49}ClP_2Ru$
T (K)	100(2)	100(2)
Wavelength	0.71073 Å	0.71073 Å
Size (mm)	0.21 x 0.18 x 0.10	0.15 x 0.09 x 0.08
Cryst. Syst	Orthorhombic	Monoclinic
Space group	P 2_1 2_1 2_1	C 2/c
a (Å)	10.2885(2)	33.8620(14)
b (Å)	18.7620(5)	8.3781(3)
c (Å)	20.8913(5)	19.8445(8)
α (deg)	90	90
β (deg)	90	110.850(4)
γ (deg)	90	90
V ($Å^3$)	4032.71(16)	5261.2(4)
Z	4	8
D_{calc} (g/cm^3)	1.431	1.384
Abs. coeff. (mm^{-1})	0.569	0.830
Reflections total	121656	121843
Reflections uniq. (R_{int})	10156 [R(int) = 0.0361]	10289 [R(int) = 0.0407]
Data/restraints/ parameters	10156 / 0 / 469	10289 / 0 / 275
GOF	1.070	1.050
R1/wR2 [I>2σ(I)]	0.0188 / 0.0465	0.0213 / 0.0472
R1/wR2 (all data)	0.0210 / 0.0475	0.0277 / 0.0500

Table 6.10: Collection and refinement data for $[Cp^*Ru(P^{tBu}{}_2N^{Bn}{}_2)Cl][PF_6]$

	$[Cp^*Ru(P^{tBu}{}_2N^{Bn}{}_2)Cl][PF_6]\cdot(acetone)_{1/2}$
Emp. formula	$C_{75}H_{116}F_{12}N_4OP_6Ru_2Cl$
T (K)	100(2)
Wavelength	0.71073 Å
Size (mm)	0.45 x 0.30 x 0.02
Cryst. Syst	Triclinic
Space group	P -1
a (Å)	12.7960(12)
b (Å)	17.3536(17)
c (Å)	19.7893(17)
α (deg)	78.400(4)
β (deg)	78.472(4)
γ (deg)	72.842(5)
V ($Å^3$)	4066.4(7)
Z	2
D_{calc} (g/cm^3)	1.451
Abs. coeff. (mm^{-1})	0.628
Reflections total	160936
Reflections uniq. (R_{int})	20221 [R(int) = 0.0364]
Data/restraints/parameters	20221 / 69 / 1007
GOF	1.028
R1/wR2 [I>2σ(I)]	0.0304 / 0.0685
R1/wR2 (all data)	0.0434 / 0.0757

Table 6.11: Collection and refinement data for [Cp*Ru($P^{tBu}_2N^{Ph}_2$)(N_2)][BArF’]

	[Cp*Ru($P^{tBu}_2N^{Ph}_2$)(N_2)][BArF’]
Emp. formula	$C_{66}H_{63}BF_{24}N_4P_2Ru$
T (K)	100(2)
Wavelength	0.71073 Å
Size (mm)	0.20 x 0.10 x 0.05
Cryst. Syst	Monoclinic
Space group	C 2/c
a (Å)	35.810(12)
b (Å)	13.787(4)
c (Å)	28.311(11)
α (deg)	90
β (deg)	104.256(18)
γ (deg)	90
V ($Å^3$)	13548(8)
Z	8
D_{calc} (g/cm^3)	1.512
Abs. coeff. (mm^{-1})	0.389
Reflections total	151104
Reflections uniq. (R_{int})	16839 [R(int) = 0.0404]
Data/restraints/parameters	16839 / 545 / 1075
GOF	1.020
R1/wR2 [I>2σ(I)]	0.0343 / 0.0742
R1/wR2 (all data)	0.0494 / 0.0812

Table 6.12: Collection and refinement data for [Cp*Ru($P^{tBu}_2N^{Ph}_2$)(O_2)][BPh_4] and [Cp*Ru($P^{Ph}_2N^{Bn}_2$) (O_2)][OTf].

	[Cp*Ru($P^{tBu}_2N^{Ph}_2$)(O_2)][BPh_4] •(acetone)	[Cp*Ru($P^{Ph}_2N^{Bn}_2$) (O_2)][OTf] •(hexane)$_{1/3}$•(CH_2Cl_2)$_{2/3}$
Emp. formula	$C_{61}H_{77}BN_2P_2Ru$	$C_{43.65}H_{52.96}Cl_{1.34}F_3N_2O_5P_2RuS$
T (K)	100(2)	100(2)
Wavelength	0.71073 Å	0.71073 Å
Size (mm)	0.29 x 0.16 x 0.13	0.17 x 0.10 x 0.10
Cryst. Syst	Monoclinic	Monoclinic
Space group	P 1 2_1/m 1	C 2/c
a (Å)	15.0443(9)	25.413(3)
b (Å)	20.1203(12)	13.9781(10)
c (Å)	18.3601(11)	25.488(2)
α (deg)	90	90
β (deg)	94.960(3)	96.688(8)
γ (deg)	90	90
V (Å^3)	5536.7(6)	8992.5(13)
Z	4	8
D_{calc} (g/cm^3)	1.272	1.455
Abs. coeff. (mm^{-1})	0.387	0.604
Reflections total	305341	141832
Reflections uniq. (R_{int})	22253 [R_{int} = 0.0345]	11462 [R_{int} = 0.0765]
Data/restraints/ parameters	22253 / 0 / 644	11462 / 11 / 547
GOF	1.052	1.029
R1/wR2 [I>2σ(I)]	0.0270 / 0.0645	0.0423 / 0.0903
R1/wR2 (all data)	0.0388 / 0.0722	0.0725 / 0.1041

Table 6.13: Collection and refinement data for [CpRu($P^{tBu}_2N^{Bn}_2$)(O_2)][OTf] and [Cp*Ru(dippp)(O_2)][PF_6].

	[CpRu($P^{tBu}_2N^{Bn}_2$)(O_2)][OTf] •(CH_2Cl_2)$_2$•(H_2O)	[Cp*Ru(dippp)(O_2)][PF_6]
Emp. formula	$C_{34}H_{51}Cl_4F_3N_2O_6P_2RuS$	$C_{25}H_{49}F_6O_2P_3Ru$
T (K)	100(2)	100(2)
Wavelength	0.71073 Å	0.71073 Å
Size (mm)	0.45 x 0.15 x 0.05	0.40 x 0.15 x 0.12
Cryst. Syst	Monoclinic	Monoclinic
Space group	P 2_1	P c
a (Å)	10.9690(8)	9.9055(6)
b (Å)	17.1250(13)	19.7003(12)
c (Å)	11.8410(8)	15.1944(10)
α (deg)	90	90
β (deg)	105.713(4)	92.242(3)
γ (deg)	90	90
V (Å^3)	2141.1(3)	2962.8(3)
Z	2	4
D_{calc} (g/cm^3)	1.516	1.546
Abs. coeff. (mm^{-1})	0.795	0.751
Reflections total	86557	140981
Reflections uniq. (R_{int})	10613 [R_{int} = 0.0648]	22623 [R_{int} = 0.0266]
Data/restraints/ parameters	10613 / 13 / 484	22623 / 2 / 693
GOF	1.023	1.014
R1/wR2 [I>2σ(I)]	0.0390 / 0.0827	0.0167 / 0.0387
R1/wR2 (all data)	0.0520 / 0.0885	0.0181 / 0.0393

Table 6.14: Collection and refinement data for $Cp^*Ru(P^{Ph}{}_2N^{Bn}{}_2H)(O_2)][OTf]_2 \cdot$(acetone)

	$[Cp^*Ru(P^{Ph}{}_2N^{Bn}{}_2H)(O_2)][OTf]_2$ •(acetone)
Emp. formula	$C_{45}H_{54}F_6N_2O_9P_2RuS_2$
T (K)	100(2)
Wavelength	0.71073 Å
Size (mm)	0.45 x 0.30 x 0.15
Cryst. Syst	Monoclinic
Space group	P 2_1/n
a (Å)	14.7040(10)
b (Å)	19.2540(14)
c (Å)	16.9090(12)
α (deg)	90
β (deg)	99.200(3)
γ (deg)	90
V ($Å^3$)	4725.5(6)
Z	4
D_{calc} (g/cm^3)	1.557
Abs. coeff. (mm^{-1})	0.568
Reflections total	164099
Reflections unique (R_{int})	16104 [R_{int} = 0.0630]
Data/restraints/ parameters	16104 / 506 / 937
GOF	1.138
R1/wR2 [I>2σ(I)]	0.0636 / 0.1225
R1/wR2 (all data)	0.0884 / 0.1394

6.6 Notes to Chapter 6

(1) Winter, M.; Brodd, R. J. *Chem. Rev.* **2004,** *104*, 4245.

(2) Borup, R.; Meyers, J.; Pivovar, B.; Kim, Y. S.; Mukundan, R.; Garland, N.; Myers, D.; Wilson, M.; Garzon, F.; Wood, D.; Zelenay, P.; More, K.; Stroh, K.; Zawodzinski, T.; Boncella, J.; McGrath, J. E.; Inaba, M.; Miyatake, K.; Hori, M.; Ota, K.; Ogumi, Z.; Miyata, S.; Nishikata, A.; Siroma, Z.; Uchimoto, Y.; Yasuda, K.; Kimijima, K.-I.; Iwishita, N. *Chem. Rev.* **2007**, 107, 3904.

(3) Gewirth, A. A.; Thorum, M. S. *Inorg. Chem.* **2010**, *49*, 3557.

(4) Warren, J. J.; Tronic, T. A.; Mayer, J. M. *Chem. Rev.* **2010**, *110*, 6961.

(5) Savéant, J.-M. *Chem. Rev.* **2008**, *108*, 2348.

(6) Collman, J. P.; Boulatov, R.; Sunderland, C. J.; Fu, L. *Chem. Rev.* **2004**, *104*, 561.

(7) Shigehara, K; Anson F. C. *J. Phys. Chem.* **1982**, *86*, 2776.

(8) Fukuzumi, S.; Okamoto, K.; Gros, C. P.; Guilard, R. *J. Am. Chem. Soc.* **2004**, *126*, 10441.

(9) Wisener, K.; Ohms, D.; Neumann, V.; Franke, R. *Mater. Chem. Phys.* **1989**, *22*, 457.

(10) Chang, C. J.; Deng, Y.; Shi, C.; Chang, C. K.; Anson, F. C.; Nocera, D. G. *Chem. Commun.* **2000**, 1355.

(11) Chang, C. J.; Loh, Z.-H.; Shi, C.; Anson, F. C.; Nocera, D. G. *J. Am. Chem. Soc.* **2004**, *126*, 10013.

(12) McCrory, C. C. L.; Ottenwaelder, X.; Stack, T. D. P.; Chidsey, C. E. D. *J. Phys. Chem. A* **2007**, *111*, 12641.

(13) McCrory, C. C. L.; Devadoss, A.; Ottenwaelder, X.; Lowe, R. D.; Stack, T. D. P.; Chidsey, C. E. D. *J. Am. Chem. Soc.* **2011**, *133*, 3696.

(14) Ward, A. L.; Elbaz, L.; Kerr, J. B.; Arnold, J. *Inorg. Chem.* **2012**, *51*, 4694.

(15) Fukuzumi, S.; Kotani, H.; Lucas, H. R.; Doi, K.; Suenobu, T.; Peterson, R. L.; Karlin, K. D. *J. Am. Chem. Soc.* **2010**, *132*, 6874.

(16) Kaila, V. R. I.; Verkhovsky, M. I.; Wikström, M. *Chem. Rev.* **2010**, *110*, 7062.

(17) Meunier, B.; de Visser, S. P.; Shaik, S. *Chem. Rev.* **2004**, *104*, 3947.

(18) Solomon, E. I.; Chen, P.; Metz. M.; Lee, S.-K.; Palmer, A. E. *Angew. Chem. Int. Ed.* **2001**, *40*, 4570.

(19) Collman, J. P.; Devaraj, N. K.; Decréau, R. A.; Yang, Y.; Yan, Y.-L., Ebina, W.; Eberspacher, T. A.; Chidsey, C. E. D. *Science* **2007**, *315*, 1565.

(20) Shook, R. L.; Borovik, A. S. *Inorg. Chem.* **2010**, *49*, 3646.

(21) Collman, J. P.; Decréau, R. A.; Zhang, C. *J. Am. Chem. Soc.* **2004**, *69*, 3546.

(22) McGuire, R.; Dogutan, D. K.; Teets, T. S.; Suntivich, J.; Shao-Horn, Y.; Nocera, D. G. *Chem. Sci.* **2010**, *1*, 411.

(23) Dogutan, D. K.; Stoian, S. A.; McGuire, R.; Schwalbe, M.; Teets, T. S.; Nocera, D. G. *J. Am. Chem. Soc.* **2011**, *133*, 131.

(24) Shook, R. L.; Peterson, S. M.; Greaves, J.; Moore, C.; Rheingold, A. L.; Borovik, A. S. *J. Am. Chem. Soc.* **2011**, *133*, 5810.

(25) Carver, C. T.; Matson, B. D.; Mayer, J. M. *J. Am. Chem. Soc.* **2012**, *134*, 5444.

(26) DuBois, M. R.; DuBois, D. L. *Chem. Soc. Rev.* **2009**, *38*, 62.

(27) Small, Y. A.; DuBois, D. L.; Fujita, E.; Muckerman, J. T. *Energy Environ. Sci.* **2011**, *4*, 3008.

(28) Liu, T.; Chen, S.; O'Hagan, M. J., DuBois, M. R.; Bullock, R. M.; DuBois, D. L. *J. Am. Chem. Soc.* **2012**, *134*, 6257.

(29) Lounissi, S.; Capon, J.-F.; Gloaguen, F.; Matoussi, F.; Pétillon, F. Y.; Schollhammer, P.; Talarmin, J. *Chem. Commun.* **2011**, *47*, 878.

(30) Camara, J. M.; Rauchfuss, T. B. *Nature Chemistry* **2012**, *4*, 26.

(31) Helm. M. L.; Stewart, M. P.; Bullock, R. M.; DuBois, M. R.; DuBois, D. L. *Science* **2011**, *333*, 863.

(32) Wiese, S.; Kilgore, U. J.; DuBois, D. L.; Bullock, R. M. *ACS Catal.* **2012**, *2*, 720.

(33) Wilson, A. D.; Shoemaker, R. K.; Miedaner, A.; Muckerman, J. T.; DuBois, D. L.; DuBois, M. R. *Proc. Natl. Acad. Sci. U.S.A.* **2007**, *104*, 6951.

(34) Kilgore, U. J.; Stewart, M. P.; Helm, M. L.; Dougherty, W. G.; Kassel, W. S.; DuBois, M. R.; DuBois, D. L.; Bullock, R. M. *Inorg. Chem.* **2011**, *50*, 10908.

(35) Fraze, K.; Wilson, A. D.; Appel, A. M.; DuBois, M. R.; Dubois, D. L. *Organometallics* **2007**, *26*, 3918.

(36) Kilgore, U. J.; Roberts, J. A. S.; Pool, D. H.; Appel, A. M.; Stewart, M. P.; DuBois, M. R.; Dougherty, W. G.; Kassel, W. S.; Bullock, R. M.; DuBois, D. L. *J. Am. Chem. Soc.* **2011**, *133*, 5861.

(37) Yang, J. Y.; Chen. S.; Dougherty, W. G.; Kassel, W. S.; Bullock, R. M.; DuBois, D. L.; Raugei, S.; Rousseau, R.; Dupuis, M.; DuBois, M. R. *Chem. Commun.* **2010**, *46*, 8618.

(38) Lee, C. H.; Dogutan, D. K.; Nocera, D. G. *J. Am. Chem. Soc.* **2011**, *133*, 8775.

(39) Jacobsen, G. M.; Yang, J. Y.; Twamley, B.; Wilson, A. D.; Bullock, R. M.; DuBois, M. R.; DuBois, D. L. *Energy Environ. Sci.* **2008**, *1*, 167.

(40) Wiedner, E. S.; Yang, J. Y.; Dougherty, W. G.; Kassel, W. S.; Bullock, R. M.; DuBois, M. R.; DuBois, D. L. *Organometallics* **2010**, *29*, 5390.

(41) Galan, B. R.; Schöffel, J.; Linehan, J. C.; Seu, C.; Appel, A. M.; Roberts, J. A. S.; Helm, M. L.; Kilgore, U. J.; Yang, J. Y.; DuBois, D. L.; Kubiak, C. P. *J. Am. Chem. Soc.* **2011**, *133*, 12767.

(42) Seu, C. S.; Appel, A. M.; Doud, M. D.; DuBois, D. L.; Kubiak, C. P. *Energy Environ. Sci.* **2012**, *5*, 6480.

(43) Weiss, C. J.; Groves, A. N.; Mock. M. T.; Dogherty, W. G.; Kassel, S. K.; Helm, M. L.; DuBois, D. L.; Bullock, M. R. *Dalton Trans.* **2012**, *41*, 4517.

(44) Mock, M. T.; Chen, S.; Rouseau, R.; O'Hagan, M. J.; Dougherty, W. G.; Kassel, W. S.; DuBois, D. L.; Bullock, R. M. *Chem. Commun.* **2011**, *47*, 12212.

(45) Yang, J. Y.; Bullock, R. M.; Dougherty, W. G.; Kassel, W. S.; Twamley, B.; DuBois, D. L.; DuBois, M. R. *Dalton Trans.* **2010**, *39*, 3001.

(46) Tronic, T. A.; DuBois, M. R.; Kaminsky, W.; Coggins, M. K.; Liu, T.; Mayer, J. M. *Angew. Chem. Int. Ed.* **2011**, *50*, 10936.

(47) Lin, W.; Wilson, S. R.; Girolami, G. S. *Organometallics* **1996**, *16*, 2987.

(48) Izutsu, K. *Acid–Base Dissociation Constants in Dipolar Aprotic Solvents*; Blackwell: Oxford, **1990.**

(49) Jiménez-Tenorio, M.; Mereiter, K.; Puerta, M. C.; Valerga, P. *J. Am. Chem. Soc.* **2000**, *122*, 11230.

(50) Aneetha, H.; Jiménez-Tenorio, M.; Puerta, M. C.; Valerga, P.; Sapunov, V. N.; Schmid, R.; Kirchner, K.; Mereiter, K. *Organometallics* **2002**, *21*, 5334.

(51) Aneetha, H.; Jiménez-Tenorio, M.; Puerta, M. C.; Valerga, P. *Organometallics* **2003**, *22*, 1779.

(52) Wilkinson, P. G.; Houk, N. B. *J. Chem. Phys.* **1956**, *24*, 128.

(53) Trimmel, G.; Slugovc, C.; Wiede, P.; Mereiter, K.; Sapunov, V. N.; Schmid, R.; Kirchner, K. *Inorg. Chem.* **1997**, *36*, 1076.

(54) Kirchner, K.; Mauthner, K.; Mereiter, K.; Schmid, R. *J. Chem.Soc., Chem. Comm.* **1993**, 892.

(55) Mauthner, K. ; Mereiter, K. ; Schmid, R.; Kirchner, K. *Inorg. Chim. Acta* **1995**, *236*, 95.

(56) Sato, M.; Asai, M. *J. Organomet. Chem.* **1996**, *508*, 121.

(57) Lindner, E.; Haustein, M.; Fawzi, R.; Steimann, M.; Wegner, P. *Organometallics* **1994**, *13*, 5021.

(58) Jia, G.; Ng, W. S.; Chu, H. S.; Wong, W.-T.; Yu, N.-T.; Williams, I. D. *Organometallics* **1999**, *18*, 3597.

(59) de los Ríos, I.; Jiménez Tenorio, M.; Padilla, J.; M. Puerta, C.; Valerga, P. *Organometallics* **1996**, *15*, 4565.

(60) Palacios, M. D.; Puerta, M. C.; Valerga, P.; Lledós, A.; Veilly, E. *Inorg. Chem.* **2007**, *46*, 6958.

(61) Praetorius, J. M.; Allen, D. P.; Wang, R.; Webb, J. D.; Grein, F.; Kennepohl, P.; Crudden, C. M. *J. Am. Chem. Soc.* **2008**, *130*, 3724.

(62) Covelli, D. "Probing the Electronic Structure of Dioxygen as a Ligand: Using X-Ray Absorption Spectroscopy to Quantify Backbonding." Ph.D. Thesis, University of British Columbia, Vancouver, British Columbia, Canada, **2011**.

(63) Piertzak, M.; Stefaniak, L.; Pozharskii, A. F.; Ozeryanskii, V. A.; Nowicka-Scheibe, J.; Grech, E.; Webb, G. A. *J. Phys. Org. Chem.* **2000**, *13*, 35.

(64) Axenrod, T.; Pregosin, P. S.; Wieder, M. J.; Becker, E. D.; Bradley, R. B.; Milne, G. W. A. *J. Am. Chem. Soc.* **1971**, *93*, 6536.

(65) Gaussian 09, Revision B.1, Frisch, M. J.; Trucks, G. W.; Schlegel, H. B.; Scuseria, G. E.; Robb, M. A.; Cheeseman, J. R.; Scalmani, G.; Barone, V.; Mennucci, B.; Petersson, G. A.; Nakatsuji, H.; Caricato, M.; Li, X.; Hratchian, H. P.; Izmaylov, A. F.; Bloino, J.; Zheng, G.; Sonnenberg, J. L.; Hada, M.; Ehara, M.; Toyota, K.; Fukuda, R.; Hasegawa, J.; Ishida, M.; Nakajima, T.; Honda, Y.; Kitao, O.; Nakai, H.; Vreven, T.; Montgomery, Jr., J. A.; Peralta, J. E.; Ogliaro, F.; Bearpark, M.; Heyd, J. J.; Brothers, E.; Kudin, K. N.; Staroverov, V. N.; Kobayashi, R.; Normand, J.; Raghavachari, K.; Rendell, A.; Burant, J. C.; Iyengar, S. S.; Tomasi, J.; Cossi, M.; Rega, N.; Millam, N. J.; Klene, M.; Knox, J. E.; Cross, J. B.; Bakken, V.; Adamo, C.; Jaramillo, J.; Gomperts, R.; Stratmann, R. E.; Yazyev, O.; Austin, A. J.; Cammi, R.; Pomelli, C.; Ochterski, J. W.; Martin, R. L.; Morokuma, K.; Zakrzewski, V. G.; Voth, G. A.; Salvador, P.; Dannenberg, J. J.; Dapprich, S.; Daniels, A. D.; Farkas, Ö.; Foresman, J. B.; Ortiz, J. V.; Cioslowski, J.; Fox, D. J. Gaussian, Inc., Wallingford CT, 2009.

(66) Kaljurand, I.; Kütt, A.; Sooväli, L.; Rodima, T.; Mäemets, V.; Leito, I.; Koppel, I. A. *J. Org. Chem.* **2005**, *70*, 1019.

(67) Noviandri, I.; Brown, K. N.; Fleming, D. S.; Gulyas, P. T.; Lay, P. A.; Masters, A. F.; Phillips, L. *J. Phys. Chem. B* **1999**, *103*, 6713.

(68) Man, L. M.; Zhu, J.; Ng, S. M.; Zhou, Z.; Yin, C.; Lin, Z.; Lau, C. P. *Organometallics* **2004**, *23*, 6214.

(69) Fagan, P. J.; Ward, M. D.; Calabrese, J. C. *J. Am. Chem. Soc.* **1989**, *111*, 1698.

(70) Boren. B. C.; Narayan, S.; Rasmussen, L. K.; Zhang, L.; Zhao, H.; Lin, Z.; Jia, G.; Fokin, V. V. *J. Am. Chem. Soc.* **2008**, *130*, 9823.

(71) Bruce, M. I.; Hameister, C.; Swincer, A. G.; Wallis, R. C. *Inorg. Synth.* **1982**, 21, 78.

(72) Faviera, I.; Duñach, E. *Tetrahedron Lett.* **2004**, *45*, 3393.

(73) Bruker APEX2 (Version 2.1-4), SAINT (version 7.34A), SADABS (version 2007/4), BrukerAXS Inc, Madison, Wisconsin, USA, 2007.

(74) Altomare, A.; Burla, C.; Camalli, M.; Cascarano, L.; Giacovazzo, C.; Guagliardi, A.; Moliterni, A. G. G.; Polidori, G.; Spagna, R.; *J. Appl. Cryst*. **1999**, *32*, 115.

(75) Altomare A, Cascarano G, Giacovazzo C, Guagliardi A. *J. Appl. Cryst*. **1993**, *26*, 343.

(76) Sheldrick G. M. SHELXL-97, Program for the Refinement of Crystal Structures. University of Göttingen, Germany, 1997.

(77) Mackay, S.; Edwards, C.; Henderson, A.; Gilmore, C.; Stewart, N.; Shankland, K.; Donald, A. *MaXus* University of Glasgow, Scotland, 1997.

(78) Waasmaier, D.; Kirfel, A. *Acta Cryst. A*, **1995**, *51*, 416.

BIBLIOGRAPHY

Altomare, A.; Burla, C.; Camalli, M.; Cascarano, L.; Giacovazzo, C.; Guagliardi, A.; Moliterni, A. G. G.; Polidori, G.; Spagna, R.; *J. Appl. Cryst*. **1999**, *32*, 115.

Altomare, A.; Cascarano, G.; Giacovazzo, C.; Guagliardi, A. *J. Appl. Cryst*. **1993**, *26*, 343.

Aneetha, H.; Jiménez-Tenorio, M.; Puerta, M. C.; Valerga, P. *Organometallics* **2003**, *22*, 1779.

Aneetha, H.; Jiménez-Tenorio, M.; Puerta, M. C.; Valerga, P.; Sapunov, V. N.; Schmid, R.; Kirchner, K.; Mereiter, K. *Organometallics* **2002**, *21*, 5334.

Anson, F. C., Shi, C.; Steiger, B. *Acc. Chem. Res.* **1997**, *30*, 437.

Augustin-Nowacka, D.; Chmurzyñski, L. *Anal. Chim. Acta* **1999**, *381*, 215.

Axenrod, T.; Pregosin, P. S.; Wieder, M. J.; Becker, E. D.; Bradley, R. B.; Milne, G. W. A. *J. Am. Chem. Soc.* **1971**, *93*, 6536.

Barbara, P. F.; Meyer, T. J.; Ratner, M. A. *J. Phys. Chem.* **1996**, *100*, 13148.

Bíczók, L.; Gupta, N.; Linschitz, H. *J. Am. Chem. Soc.* **1997**, *119*, 12601.

Bíczók, L.; Linschitz, H. *J. Phys. Chem.* **1995**, *99*, 1843–1845.

Bordwell, F. G. *Acc. Chem. Res.* **1988**, *21*, 456.

Bordwell, F. G.; Cheng, J. P. *J. Am. Chem. Soc.* **1991**, *113*, 1736.

Boren. B. C.; Narayan, S.; Rasmussen, L. K.; Zhang, L.; Zhao, H.; Lin, Z.; Jia, G.; Fokin, V. V. *J. Am. Chem. Soc.* **2008**, *130*, 9823.

Borup, R.; Meyers, J.; Pivovar, B.; Kim, Y. S.; Mukundan, R.; Garland, N.; Myers, D.; Wilson, M.; Garzon, F.; Wood, D.; Zelenay, P.; More, K.; Stroh, K.; Zawodzinski, T.; Boncella, J.; McGrath, J. E.; Inaba, M.; Miyatake, K.; Hori, M.; Ota, K.; Ogumi, Z.; Miyata, S.; Nishikata, A.; Siroma, Z.; Uchimoto, Y.; Yasuda, K.; Kimijima, K.-I.; Iwishita, N. *Chem. Rev.* **2007**, 107, 3904.

Braga, T. G. ; Wahl, A. C. *J. Phys. Chem.* **1985**, *89*, 5822.

Bratos, S.; Leickman, J.-C.; Gallot, G.; Ratajczak, H. in *Ultrafast Hydrogen Bonding Dynamics and Proton Transfer Processes in the Condensed Phase*, eds. Elsaesser, T.; Bakker, H. J. Kluwer Academic, Boston, 2002.

Bruce, M. I.; Hameister, C.; Swincer, A. G.; Wallis, R. C. *Inorg. Synth.* **1982**, 21, 78.

Carver, C. T.; Matson, B. D.; Mayer, J. M. *J. Am. Chem. Soc.* **2012**, *134*, 5444.

Camara, J. M.; Rauchfuss, T. B. *Nature Chemistry* **2012**, *4*, 26.

Chan, M. S.; Wahl, A. C. *J. Phys. Chem.* **1978**, *82*, 2542.

Chang, C. J.; Deng, Y.; Shi, C.; Chang, C. K.; Anson, F. C.; Nocera, D. G. *Chem. Commun.* **2000**, 1355.

Chang, C. J.; Loh, Z.-H.; Shi, C.; Anson, F. C.; Nocera, D. G. *J. Am. Chem. Soc.* **2004**, *126*, 10013.

Chrystiuk, E.; Williams, A. *J. Am. Chem. Soc.* **1987**, *109*, 3040.

Collman, J. P.; Boulatov, R.; Sunderland, C. J.; Fu, L. *Chem. Rev.* **2004**, *104*, 561.

Collman, J. P.; Decréau, R. A.; Zhang, C. *J. Am. Chem. Soc.* **2004**, *69*, 3546.

Collman, J. P.; Devaraj, N. K.; Decréau, R. A.; Yang, Y.; Yan, Y.-L., Ebina, W.; Eberspacher, T. A.; Chidsey, C. E. D. *Science* **2007**, *315*, 1565.

Costentin, C. *Chem. Rev.* **2008**, *108*, 2145-2179.

Costentin, C.; Robert, M.; Savéant, J. -M. *J. Am. Chem. Soc.* **2007**, *129*, 5870.

Costentin, C.; Robert, M.; Savéant, J. -M. *J. Am. Chem. Soc.* **2007**, *129*, 9953.

Costentin, C.; Robert, M.; Savéant, J.-M.; Tard, C. *Angew. Chem. Int. Ed.* **2010**, *49*, 3803.

Costentin, C.; Robert, M.; Savéant, J.-M.; Tard, C. *Phys. Chem. Chem. Phys.* **2011**, *13*, 5353.

Cottet, F.; Marull, M.; Lefebvre, O.; Schlosser, M. *Eur. J. Org. Chem.* **2003**, 1559.

Covelli, D. "Probing the Electronic Structure of Dioxygen as a Ligand: Using X-Ray Absorption Spectroscopy to Quantify Backbonding." Ph.D. Thesis, University of British Columbia, Vancouver, British Columbia, Canada, **2011**.

Cramer, C. J.; Tolman, W. B.; Theopold, K. H.; Rheingold, A. L. *Proc. Nat. Acad. Sci. USA* **2003,** *100*, 3635.

Cukier, R. I. *J. Phys. Chem. B* **2002**, *106*, 1746.

Cukier, R. I.; Nocera, D. G. *Annu. Rev. Phys. Chem.* **1998**, *49*, 337.

Culkin, D. A.; Hartwig, J. F. *Acc. Chem. Res.* **2003**, *36*, 234.

de los Ríos, I.; Jiménez Tenorio, M.; Padilla, J.; Puerta, M. C.; Valerga, P. *Organometallics* **1996,** *15*, 4565.

Dempsey, J. L.; Winkler, J. R.; Gray, H. B. *Chem. Rev.* **2010**, *110*, 7024.

Denisov, I. G.; Makris, T. M.; Sligar, S. G.; Schlichting, I. *Chem. Rev.* **2005,** *105*, 2253.

Derat, E.; Shaik, S. *J. Am. Chem. Soc.* **2006**, *128*, 13940.

DeSimone, R. E.; Drago, R. S. *J. Am. Chem. Soc.* **1970,** *92*, 2343.

Dogutan, D. K.; Stoian, S. A.; McGuire, R.; Schwalbe, M.; Teets, T. S.; Nocera, D. G. *J. Am. Chem. Soc.* **2011**, *133*, 131.

DuBois, M. R.; DuBois, D. L. *Chem. Soc. Rev.* **2009**, *38*, 62.

Durand Jr., R. R.; Anson, F. J. *J. Electroanal. Chem.* **1982**, *134*, 273.

Durand Jr., R. R.; Bencosme, C. S.; Collman, J. P.; Anson, F. C. *J. Am. Chem. Soc.* **1983**, *105*, 2710.

Efimov, I.; Badyal, S. K.; Metcalfe, C. L.; Macdonald, I.; Gumiero, A.; Raven, E. L.; Moody, P. C. E. *J. Am. Chem. Soc.* **2011**, *133*, 15376.

Fagan, P. J.; Ward, M. D.; Calabrese, J. C. *J. Am. Chem. Soc.* **1989**, *111*, 1698.

Faviera, I.; Duñach, E. *Tetrahedron Lett.* **2004**, *45*, 3393.

Fecenko, C. J.; Thorp, H. H.; Meyer, T. J. *J. Am. Chem. Soc.* **2007**, *129*, 15098.

Feig, A. L.; Becker, M.; Schindler, S.; van Eldik; R.; Lippard, S. J. *Inorg. Chem.* **1996**, *35*, 2590.

Foti, M. C.; Johnson , E. R.; Vinqvist, M. R.; Wright, J. S.; Barclay, L. R. C.; Ingold, K. U. *J. Org. Chem.* **2002**, *67*, 5190.

Fraze, K.; Wilson, A. D.; Appel, A. M.; DuBois, M. R.; Dubois, D. L. *Organometallics* **2007**, *26*, 3918.

Friebolin, H. *Basic One- and Two-Dimensional NMR Spectroscopy, vol 4*. VCH, Weinheim, **2005**.

Fukuzumi, S.; Kotani, H.; Lucas, H. R.; Doi, K.; Suenobu, T.; Peterson, R. L.; Karlin, K. D. *J. Am. Chem. Soc.* **2010**, *132*, 6874.

Fukuzumi, S.; Okamoto, K.; Gros, C. P.; Guilard, R. *J. Am. Chem. Soc.* **2004**, *126*, 10441.

Galan, B. R.; Schöffel, J.; Linehan, J. C.; Seu, C.; Appel, A. M.; Roberts, J. A. S.; Helm, M. L.; Kilgore, U. J.; Yang, J. Y.; DuBois, D. L.; Kubiak, C. P. *J. Am. Chem. Soc.* **2011**, *133*, 12767.

Geiger, T.; Anson, F. C. *Inorg. Chem.* **1981**, *103*, 7489.

Geue, R. J.; Hambley, T. W.; Harrowfield, J. M.; Sargeson, A. M.; Snow, M. R. *J. Am. Chem. Soc.* **1984**, *106*, 5478.

Gewirth, A. A.; Thorum, M. S. *Inorg. Chem.* **2010**, *49*, 3557.

Graige, M. S.; Paddock, M. L.; Bruce, J. M.; Feher, G.; Okamura, M. Y. *J. Am. Chem. Soc.* **1996**, *118*, 9005.

Hajj, F. E.; Sebki, G.; Patinec, V.; Marchivie, M.; Triki, S.; Handel, H.; Yefsah, S.; Tripier, R.; Gómez-García, C. J.; Coronado, E. *Inorg. Chem.* **2009**, *48*, 10416.

Hamdane, D.; Zhang, H.; Hollenberg, P. *Photosynth. Res.* **2008,** *98*, 657.

Hammarström, L.; Styring, S. *Energy Environ. Sci.* **2011**, *4*, 2379.

Hammes-Schiffer, S. *Acc. Chem. Res.* **2001**, *34*, 273.

Hammes-Schiffer, S. *Chem. Rev.* **2010**, *110*, 6937.

Hammes-Schiffer, S.; Stuchebrukhov, A. A. *Chem. Rev.* **2010**, *110*, 6939.

Hays, A-M. A.; Vassiliev, I. R.; Golbeck, J. H.; Debus, R. J. *Biochemistry* **1998**, *37*, 11352.

Helm. M. L.; Stewart, M. P.; Bullock, R. M.; DuBois, M. R.; DuBois, D. L. *Science* **2011**, *333*, 863.

Helps, I. M.; Parker, D.; Chapman, J.; Ferguson, G. *J. Chem. Soc. Chem. Commun.* **1988**, 1094.

Helps, I. M.; Parker, D.; Murphy, J. R. Chapman, J. *Tetrahedron* **1989**, *45*, 219.

Hodgkiss, J. M.; Rosenthal, J.; Nocera, D. G.; In *Hydrogen Transfer Reactions*, Hynes, J. T.; Klinman, J. P.; Limbach, H. -H.; Schowen, R. L., Eds.; Wiley-VCH: Weinheim, 2007.

Huynh, M. H. V.; Meyer, T. J. *Chem. Rev.* **2007**, *107*, 5004.

Irebo, T.; Johansson, O.; Hammarström, L. *J. Am. Chem. Soc.* **2008**, *130*, 9194.

Irebo T.; Reece S. Y.; Sjödin M.; Nocera D.G.; Hammarström L. *J. Am. Chem. Soc.* **2007,** *129*, 15462.

Ishikita, H.; Soudackov, A. V.; Hammes-Schiffer, S. *J. Am. Chem. Soc.* **2007**, *129*, 11146.

Izutsu, K. *Acid-Base Dissociation Constants in Dipolar Aprotic Solvents*, IUPAC Chemical Data Series No. 35; Blackwell Scientific Publications: Boston, MA, 1990.

Jacobsen, G. M.; Yang, J. Y.; Twamley, B.; Wilson, A. D.; Bullock, R. M.; DuBois, M. R.; DuBois, D. L. *Energy Environ. Sci.* **2008**, *1*, 167.

Jeffrey, G. A. in *An Introduction to Hydrogen Bonding*; Oxford Univ Press: NewYork, 1997.

Jia, G.; Ng, W. S.; Chu, H. S.; Wong, W.-T.; Yu, N.-T.; Williams, I. D. *Organometallics* **1999,** *18*, 3597.

Jiménez-Tenorio, M.; Mereiter, K.; Puerta, M. C.; Valerga, P. *J. Am. Chem. Soc.* **2000**, *122*, 11230.

Jung, S-K.; Kang, S-G., Suh, M. P. *Bull. Korean Chem. Soc.* **1989**, *10*, 363.

Kaila, V. R. I.; Verkhovsky, M. I.; Wikström, M. *Chem. Rev.* **2010,** *110*, 7062.

Kaljurand, K.; Kütt, A.; Sooväli, L.; Rodima, T.; Mäemets, V.; Leito, I.; Koppel, I. A. *J. Org. Chem.* **2005**, *70*, 1019.

Kang, B.; Ko, K. C.; Park, S.-Y.; Jang, D.-J.; Lee, J. Y. *Phys. Chem. Chem. Phys.* **2011**, *13*, 6332.

Kang, C.; Anson, F. C. *Inorg. Chem.* **1995**, *34*, 2771.

Kang, S-G.; Ryu, K.; Jung, S-K.; Kim, C-S. *Bull. Korean Chem. Soc.* **1996**, *17*, 331.

Kang, S-G.; Ryu, K.; Jung, S-K.; Kim, J. *Inorg. Chim. Acta* **1999**, *293*, 140.

Kilgore, U. J.; Roberts, J. A. S.; Pool, D. H.; Appel, A. M.; Stewart, M. P.; DuBois, M. R.; Dougherty, W. G.; Kassel, W. S.; Bullock, R. M.; DuBois, D. L. *J. Am. Chem. Soc.* **2011**, *133*, 5861.

Kilgore, U. J.; Stewart, M. P.; Helm, M. L.; Dougherty, W. G.; Kassel, W. S.; DuBois, M. R.; DuBois, D. L.; Bullock, R. M. *Inorg. Chem.* **2011**, *50*, 10908.

Kirchner, K.; Mauthner, K.; Mereiter, K.; Schmid, R. *J. Chem. Soc., Chem. Comm.* **1993**, 892.

Klinman, J. P. *Biochim Biophys Acta* **2006**, *1757*, 981.

König, P. H.; Ghosh, N.; Hoffman, M.; Elstner, M.; Tajkhorshid, E.; Frauenheim, T. H.; Cui, Q. *J. Phys. Chem. A* **2006**, *110*, 548.

Krishtalik, L. I. *Biochim. Biophys. Acta.* **2000**, *1458*, 6.

Krishtalik, L. I. *Mendeleev Commun.* **1992**, *3*, 66.

Kuhn, L. P.; Wires, R. A.; Ruoff, W.; Kwart, H. *J. Am. Chem. Soc.* **1969**, *91*, 4790.

Kuhne, H. ; Brudvig, G. W. *J. Phys. Chem. B* **2002**, *106*, 8189.

Kuznetsov, A. M.; Ulstrup, J. *Can. J. Chem.* **1999**, *77*, 1085.

Kwon, O.-H.; Lee, Y.-S.; Yoo, B. K.; Jang, D.-J. *Angew. Chem. Int. Ed.* **2006**, *45*, 415.

Lee, C. H.; Dogutan, D. K.; Nocera, D. G. *J. Am. Chem. Soc.* **2011**, *133*, 8775.

Lee, I.-S. H.; Chow, K.-H.; Kreevoy, M. M. *J. Am. Chem. Soc.* **2002**, *124*, 7755.

Lin, W.; Wilson, S. R.; Girolami, G. S. *Organometallics* **1996**, *16*, 2987.

Lindner, E.; Haustein, M.; Fawzi, R.; Steimann, M.; Wegner, P. *Organometallics* **1994,** *13*, 5021.

Liu, T.; Chen, S.; O'Hagan, M. J., DuBois, M. R.; Bullock, R. M.; DuBois, D. L. *J. Am. Chem. Soc.* **2012**, *134*, 6257.

Lounissi, S.; Capon, J.-F.; Gloaguen, F.; Matoussi, F.; Pétillon, F. Y.; Schollhammer, P.; Talarmin, J. *Chem. Commun.* **2011**, *47*, 878.

Man, L. M.; Zhu, J.; Ng, S. M.; Zhou, Z.; Yin, C.; Lin, Z.; Lau, C. P. *Organometallics* **2004**, *23*, 6214.

Marcus, R. A.; Sutin, N. *Biochim. Biophys. Acta* **1985**, *811*, 265.

Markle, T. F. *Concerted Proton-Electron Transfers in the Oxidation of Hydrogen Bonded Phenol-Base Compounds* Ph.D. Thesis, University of Washington, Seattle, Washington, **2009**.

Markle, T. F.; Mayer, J. M. *Angew. Chem. Int. Ed.* **2008**, *47*, 738.

Markle, T. F.; Rhile, I. J.; Mayer, J. M. *J. Am. Chem. Soc.* **2011**, *133*, 17341.

Markle, T. F.; Rhile, I. J.; Mayer, J. M.; DiPasquale, A. G. *Proc. Nat. Acad. Sci. USA* **2008**, *105*, 8185.

Markle, T. F.; Tenderholt, A. L.; Mayer. J. M. *J. Phys. Chem. B* **2012**, *116*, 571.

Martelletti, A.; Gramlich, V.; Zürcher, F.; Mezzetti, A. *New J. Chem.* **1999**, 199.

Matlack, A. S., *Introduction to Green Chemistry*. Marcel Dekker: 2001.

Matsuoka, S.; Yamamoto, K.; Ogata, T.; Kusaba, M.; Nakshima, N.; Fujita, E.; Yanagida, S. *J. Am. Chem. Soc.* **1993**, *115*, 601.

Mauthner, K. ; Mereiter, K. ; Schmid, R.; Kirchner, K. *Inorg. Chim. Acta* **1995**, *236*, 95.

Mayer, J. M. *Acc. Chem. Res.* **2011**, *44*, 36.

Mayer, J. M. *Annu. Rev. Phys. Chem.* **2004**, *55*, 363

Mayer, J. M.; Rhile, I. J.; Larsen, F. B.; Mader, E. A.; Markle, T. F.; Dipasquale, A. G. *Photosynthesis Res.* **2006**, *87*, 21.

McCrory, C. C. L.; Devadoss, A.; Ottenwaelder, X.; Lowe, R. D.; Stack, T. D. P.; Chidsey, C. E. D. *J. Am. Chem. Soc.* **2011**, *133*, 3696.

McCrory, C. C. L.; Ottenwaelder, X.; Stack, T. D. P.; Chidsey, C. E. D. *J. Phys. Chem. A* **2007**, *111*, 12641.

McEvoy, J. P.; Brudvig, G. W. *Chem. Rev.* **2006**, *106*, 4455.

McGuire, R.; Dogutan, D. K.; Teets, T. S.; Suntivich, J.; Shao-Horn, Y.; Nocera, D. G. *Chem. Sci.* **2010**, *1*, 411.

Meunier, B.; de Visser, S. P.; Shaik, S. *Chem. Rev.* **2004**, *104*, 3947.

Meyer, T. J.; Huynh, M. H. V.; Thorp, H. H. *Angew. Chem. Int. Ed.* **2007**, *46*, 5284.

Mock, M. T.; Chen, S.; Rouseau, R.; O'Hagan, M. J.; Dougherty, W. G.; Kassel, W. S.; DuBois, D. L.; Bullock, R. M. *Chem. Commun.* **2011**, *47*, 12212.

Nelsen, S. F.; Blackstock, S. C.; Kim, Y. *J. Am. Chem. Soc.* **1987**, *109*, 677.

Nelsen, S. F.; Weaver, M. N.; Pladziewicz, J. R.; Ausman, L. K.; Jentzsch, T. L.; O'Konek, J. J.; *J. Phys. Chem. A* **2006**, *110*, 11665.

Nicolet, Y.; Cavazza, C.; Fontecilla-Camps, J. C. *J. Inorg. Biochem.* **2002**, *91*, 1.

Noel, M.; Vase, K. I. *Cyclic Voltammetry and the Frontiers of Electrochemistry*; Aspect: London, 1990.

Noviandri, I.; Brown, K. N.; Fleming, D. S.; Gulyas, P. T.; Lay, P. A.; Masters, A. F.; Phillips, L. *J. Phys. Chem. B* **1999**, *103*, 6713.

Otwinowski, Z.; Minor, W. "Processing of X-ray Diffraction Data Collected in Oscillation Mode", *Methods in Enzymology*, *Volume 276: Macromolecular Crystallography, part A*, p.307-326,C.W. Carter, Jr. & R. M. Sweet, Eds., Academic Press (New York), 1997.

Palacios, M. D.; Puerta, M. C.; Valerga, P.; Lledós, A.; Veilly, E. *Inorg. Chem.* **2007**, *46*, 6958.

Pandya, D. N.; Kim, J. Y.; Park, J. C.; Lee, H.; Phapale, P. B.; Kwak, W.; Choi, T. H.; Cheon, G. J.; Yoon, Y-R.; Yoo, J. *Chem. Commun.* **2010**, *46*, 3517.

Pérez-Prieto, J.; Galian, R. E.; Burgos, P. O.; Miñana, M. C. M.; Miranda, M. A.; López-Ortiz, F. *Org. Lett.* **2005**, *7*, 3869.

Perrin, D. D. *Dissociation Constants of Organic Bases in Aqueous Solution.* Butterworths: London, 1965.

Perrin, D. D.; Dempsey, B.; Serjeant, E. P. *pKa Prediction for Organic Acids and Bases.* Chapman and Hall: New York, 1981.

Pesavento, R. P.; van der Donk, W. A. *Adv. Prot. Chem.* **2001**, *58*, 317.

Piertzak, M.; Stefaniak, L.; Pozharskii, A. F.; Ozeryanskii, V. A.; Nowicka-Scheibe, J.; Grech, E.; Webb, G. A. *J. Phys. Org. Chem.* **2000**, *13*, 35.

Praetorius, J. M.; Allen, D. P.; Wang, R.; Webb, J. D.; Grein, F.; Kennepohl, P.; Crudden, C. M. *J. Am. Chem. Soc.* **2008**, *130*, 3724.

Proshlyakov, D. A.; Pressler, M. A.; Babcock, G. T. *Proc. Nat. Acad. Sci. USA* **1998,** *95*, 8020.

Rakowski DuBois, M.; DuBois, D. L. *Chem. Soc. Rev* **2009,** *38*, 62.

Reece, S. Y.; Nocera, D. G. *J. Am. Chem. Soc.* **2005**, *127*, 9448.

Renger, G. *Biochim. Biophys. Acta* **2012** DOI: 10.1016/j.bbabio.2012.02.005

Rhile I. J.; Markle T. F.; Nagao H.; DiPasquale A. G.; Lam O. P.; Lockwood M. A.; Rotter K.; Mayer J. M. *J. Am. Chem. Soc.* **2006**, *128*, 6075.

Rodriguez-Lopez, J. N.; Smith, A. T.; Thorneley, R. N. F. *J. Biol. Chem.* **1997,** *272*, 389.

Royal, G.; Dauaoui-Gindrey, V; Dahaoui, S.; Tabard, A.; Guilard, R.; Pullumbi, P.; Lecomte, C. *Eur. J. Org. Chem.* **1998**, 1971.

Ryu, H.-K.; Kim, W.-Y.; Nahm, K. S.; Hahn, Y. B.; Lee, Y. S.; Lee, C. *Synthetic Metals.* **2002**, *128*, 21.

Sato, M.; Asai, M. *J. Organomet. Chem.* **1996,** *508*, 121.

Savariault, J. M.; Lehmann, M. S. *J. Am. Chem. Soc.* **1980,** *102*, 1298.

Savéant, J-M. *Chem. Rev.* **2008**, *108*, 2348.

Schrauben, J. N.; Cattaneo, M.; Day, T. C.; Tenderholdt, A. L.; Mayer, J. M. *unpublished results.*

Seu, C. S.; Appel, A. M.; Doud, M. D.; DuBois, D. L.; Kubiak, C. P. *Energy Environ. Sci.* **2012**, *5*, 6480.

Shan, S.-O.; Loh, S.; Herschlag, D. *Science* **1996**, *272*, 97.

Shigehara, K; Anson F. C. *J. Phys. Chem.* **1982**, *86*, 2776.

Shook, R. L.; Borovik, A. S. *Inorg. Chem.* **2010**, *49*, 3646.

Shook, R. L.; Peterson, S. M.; Greaves, J.; Moore, C.; Rheingold, A. L.; Borovik, A. S. *J. Am. Chem. Soc.* **2011,** *133*, 5810.

Siegbahn, P. E. M.; Blomberg, M. R. A.; Crabtree, R. H. *Theor. Chem. Acc.* **1997**, *97*, 289.

Sisemore, M. F.; Selke, M.; Burstyn, J. N.; Valentine, J. S. *Inorg. Chem.* **1997**, *36*, 979.

Sjödin, M.; Irebo, T.; Utlas, T. E.; Lind, J.; Merényi, G.; Åkermark, B.; Hammarström, L. *J. Am. Chem. Soc.* **2006**, *128*, 13076.

Sjödin, M.; Styring, S.; Wolpher, H.; Xu, Y.; Sun, L.; Hammarström, L. *J. Am. Chem. Soc.* **2005**, *127*, 3855.

Small, Y. A.; DuBois, D. L.; Fujita, E.; Muckerman, J. T. *Energy Environ. Sci.* **2011**, *4*, 3008.

Solomon, E. I.; Chen, P.; Metz, M.; Lee, S.-K.; Palmer, A. E. *Angew. Chem. Int. Ed.* **2001,** *40*, 4570.

Song, C.; Zhang, J. in *PEM Fuel Cell Electrocatalysts and Catalyst Layers Fundamentals and Applications* Zhang, J. (ed.) **2008**, *12*, 110-114.

Song, N.; Stanbury, D. M. *Inorg. Chem.* **2008**, *47*, 11458.

Song, S.; Zhang, H.; Ma, X.; Shao, Z.; Baker, R. T.; Yi, B. *Int. J. Hydrogen Energy* **2008**, *33*, 4955.

Song, W. J.; McCormick, M. S.; Behan, R. K.; Sazinsky, M. H.; Jiang, W.; Lin, J.; Krebs, C.; Lippard, S. J. *J. Am. Chem. Soc.* **2010,** *132*, 13582.

Sono, M.; Roach, M. P.; Coulter, E. D.; Dawson, J. H. *Chem. Rev.* **1996,** *96*, 2841.

Stahl, S. S. *Angew. Chem. Int. Ed.* **2004,** *43*, 3400.

Stahl, S. S. *Science* **2005,** *309*, 1824.

Steiner, T. *Angew. Chem. Int. Ed.* **2002,** *41*, 48.

Stowell, M. H. B.; McPhillips, T. M.; Rees, D. C.; Stoltis, S. M.; Abresch, E.; Feher, G. *Science* **1997**, *276*, 812.

Stubbe, J.; van der Donk, W. *Chem. Rev.* **1998,** *98*, 705.

Stuchebrukhov, A. A. “Electron transfer reactions coupled to proton translocation in proteins. Computational studies or redox driven proton pumps, cytochrome c oxidase, and biological energy transduction,” in: *Energy, Heat and Signal Flows in Proteins*, D. Leitner and J. Straub Eds., Taylor and Francis/CRC Press, 2009, Chapter 4, 71-106.

Suh, M. P.; Kang, S-G. *Inorg. Chem.* **1988**, *27*, 2544.

Tabassum, S.; Parveen, S.; Arjmand, F. *Indian J. Chem., Sec. A* **2004**, *43*, 270.

Tabassum, S.; Parveen, S.; Arjmand, F. *Trans. Met. Chem.* **2005**, *30*, 196.

Tanner, C.; Manca, C.; Leutwyler, S. *Science* **2003**, *302*, 1736.

Tishchenko, O.; Truhlar, D. G.; Ceulemans, A.; Nguyen, M. T. *J. Am. Chem. Soc.* **2008**, *130*, 7000.

Tommos, C. ; Babcock, G. T. *Acc. Chem. Res.* **1998,** *31*, 18.

Trimmel, G.; Slugovc, C.; Wiede, P.; Mereiter, K.; Sapunov, V. N.; Schmid, R.; Kirchner, K. *Inorg. Chem.* **1997**, *36*, 1076.

Tronic, T. A.; DuBois, M. R.; Kaminsky, W.; Coggins, M. K.; Liu, T.; Mayer, J. M. *Angew. Chem. Int. Ed.* **2011**, *50*, 10936.

Umena, Y.; Kawakami, K,; Shen, J.-R. *Nature* **2011**, *4* 2379.

Umena, Y.; Kawakami, K.; Shen, J.-R.; Kamiya, N. *Nature* **2011**, *473*, 55.

Valentine, J. S. *Chem. Rev.* **1973,** *73*, 235.

Volpe, M.; Hartnett, H.; Leeland, J. W.; Wills, K.; Ogunshun, M.; Duncombe, B. J.; Wilson, C.; Blake, A. J.; McMaster, J.; Love, J. B. *Inorg. Chem.* **2009**, *48*, 5195.

Waasmaier, D.; Kirfel, A. *Acta Cryst. A*, **1995**, *51*, 416.

Wander, M. C. F.; Kubicki, J. D.; Clark, A. E.; Schoonen, M. A. A. *J. Phys. Chem. A* **2009**, *113*, 1020.

Wang, Y.; Hirao, H.; Chen, H.; Onaka, H.; Nagano, S.; Shaik, S. *J. Am. Chem. Soc.* **2008**, *130*, 7170.

Wang, X.; Luo, H.; Yang, H.; Sebastian, P. J.; Gamboa, S. A. *Int. J. Hydrogen Energy* **2004**, *29*, 967.

Ward, A. L.; Elbaz, L.; Kerr, J. B.; Arnold, J. *Inorg. Chem.* **2012**, *51*, 4694.

Warren, J. J.; Tronic, T. A.; Mayer, J. M. *Chem. Rev.* **2010**, *110*, 6961.

Weiss, C. J.; Groves, A. N.; Mock. M. T.; Dogherty, W. G.; Kassel, S. K.; Helm, M. L.; DuBois, D. L.; Bullock, M. R. *Dalton Trans.* **2012**, *41*, 4517.

Wherland, S. *Coord. Chem. Rev.* **1993**, *123*, 169.

Wiedner, E. S.; Yang, J. Y.; Dougherty, W. G.; Kassel, W. S.; Bullock, R. M.; Rakowski DuBois, M.; DuBois, D. L. *Organometallics* **2010,** *29*, 5390.

Wiese, S.; Kilgore, U. J.; DuBois, D. L.; Bullock, R. M. *ACS Catal.* **2012**, *2*, 720.

Wikström, M.; Verhovsky, M. I.; Hummer, G. *Biochim. Biophys. Acta* **2003**, *1634*, 61.

Wilkinson, P. G.; Houk, N. B. *J. Chem. Phys.* **1956**, *24*, 128.

Wilson, A. D.; Shoemaker, R. K.; Miedaner, A.; Muckerman, J. T.; DuBois, D. L.; DuBois, M. R. *Proc. Natl. Acad. Sci. U.S.A.* **2007**, *104*, 6951.

Winter, M.; Broad, R. J. *Chem. Rev.* **2004**, *104*, 4245.

Wisener, K.; Ohms, D.; Neumann, V.; Franke, R. *Mater. Chem. Phys.* **1989**, *22*, 457.

Wraight, C. A. *Biochim. Biophys. Acta* **2006**, *1757*, 886.

Yang, J. Y.; Bullock, R. M.; Dougherty, W. G.; Kassel, W. S.; Twamley, B.; DuBois, D. L.; Rakowski Dubois, M. *Dalton Trans.* **2010**, *39*, 3001.

Yang, J. Y.; Chen. S.; Dougherty, W. G.; Kassel, W. S.; Bullock, R. M.; DuBois, D. L.; Raugei, S.; Rousseau, R.; Dupuis, M.; DuBois, M. R. *Chem. Commun.* **2010**, *46*, 8618.

Yoshikawa, S.; Muramoto, K.; Shinzawa-Itoh, K.; Aoyama, H.; Tsukihara, T.; Shimokata, K.; Katayama, Y.; Shimada, H. *Biochim. Biophys. Acta* **2006**, *1757*, 1110.

VITA

Tristan Tronic was born and raised in Annandale, Virginia. He earned his B.S. in Chemistry in 2007 from the College of William and Mary, where he performed research in the lab of Prof. Robert Pike. He began graduate school at the University of Washington in 2007. He performed his graduate work with Prof. James Mayer, earning his Ph.D. in Chemistry in 2012.